Doctoral Dissertation
Doctoral Program in Material Science and Technology (33rd Cycle)

Advanced phosphate glasses for photonics: from materials to applications

Duccio Gallichi Nottiani

* * * * * *

Supervisor
Prof. Davide Luca Janner

Doctoral Examination Committee:
Prof. Matthieu Lancry, ICMMO, Université Paris-Saclay (Orsay, France)
Prof. Maurizio Ferrari, CSMFO, IFN – CNR (Trento, Italy)

Politecnico di Torino
2021

I hereby declare that the contents and organisation of this dissertation constitute my own original work and does not compromise in any way the rights of third parties, including those relating to the security of personal data.

Duccio Gallichi Nottiani
20th March 2021

Abstract

Phosphate glasses are excellent candidates for several advanced photonics applications, thanks to their tailorable properties. During the present research, different compositions of phosphate glasses have been synthesised and successfully employed either in active, bioresorbable, or antibacterial optical applications. These materials can be drawn in fibre form, which provides enhanced potentialities in the photonics sector. A customised extrusion technique is here proposed to reshape the glasses into preforms, that are subsequently drawn into standard 125-μm fibres. This technique has been seldom used for glass processing but offers several advantages for the production of high-quality optical fibres, related to the possibility of varying the preform design, reaching also non-symmetrical configurations, to the adaptability to different glass compositions and various shapes, and also to the enhanced surface quality of the results that averts time-consuming polishing procedures. These favourable features promote high design flexibility. The drawbacks of the glass extrusion technique, associated with preform distortions, are addressed during the current work. Solutions are proposed by using a simulation-aided approach along with several experimental strategies, allowing for an effective minimisation of the disturbances and optimisation of the results.

Three case studies are presented within the current thesis. The first is related to active fibre: phosphate glasses doped with active lanthanides are employed as optical fibre amplifiers systems to obtain compact high-power lasers. The extrusion technique was here applied for the production of the active fibre preform. The target device is a LIDAR system that can be mounted on a small flying drone and used for environmental monitoring applications. This part of the study was performed in collaboration with several international academic institutions. The second case study is related to bioresorbable microstructured phosphate glass fibres, employed as sensors or as light/drug delivery systems in biomedicine. Two separate fibres are studied, a solid-core hollow-cladding microstructure and an asymmetric double-channel design. These optical systems are thoroughly described along with the technique adopted for their optimisation. Computational fluid dynamics resulted as a powerful tool to study the behaviour of glass during extrusion of a complex-shaped preform. Finally, the third case study is related to antibacterial glasses, synthesised by adding several antimicrobial ions to a bioresorbable phosphate glass composition. The thermo-mechanical and optical properties are analysed together with preliminary tests of antibacterial and cytotoxicity assays performed on a Cu-doped glass. External partners were involved in the biological tests. The interesting results achieved so far encourage further studies in this field.

Acknowledgements

I would like to express my gratitude to my supervisor, Prof. Davide Janner, for the consistent support and guidance during these years. I would like to thank Dr Diego Pugliese, for his constant help in the glass making. I would like to thank my colleague Elisa Muzi for the time we spent together when we were sitting in front of each other as well as when we were living in different countries, by sharing not only the desk, but also books, thoughts, hopes, and alternative scenarios. I would also like to thank Dr Nadia Boetti, for hosting me at LINKS Foundation Laboratories and Prof. Daniel Milanese for being a reference for the whole research group in photonic glasses. Furthermore, I acknowledge prof. Monica Ferraris and the whole GLANCE group for the help they gave me throughout this research.

At Politecnico, during the last years, I spent a great time and I would like to thank all the people who shared great moments with me. I will not personally mention each of them since they already know how grateful I am for all the nice time we spent together.

Finally, I would also like to thank my partner and my whole family for their patient and constant support.

Contents

Chapter 1.

Introduction

1.1 Aims and motivation

Photonics is a wide discipline embracing several aspects of physics and offering great possibilities of research. Studies in the field of photonics, as the present, are deeply linked with their target applications. Indeed, the course of the research in this sector is often driven by requirements related to the specific application. This calls for a multidisciplinary way of thinking, that starts from the development of new and more performing materials for innovative applications. In particular, glass-based photonics is the key element for the development of new materials as well as innovative processing technologies for fibre optics research. In this context, the present work is focused on the synthesis of phosphate glasses employed as optical materials and their use in glass extrusion for the production of optical fibres. This approach has produced interesting results and found applications in areas such as: light amplifiers for LIDARs, bioresorbable optical fibres for light and drug delivery, and antibacterial/antiviral applications. To achieve these goals, we combined knowledge of the following different disciplines:

(i) glass manufacturing and characterisation;
(ii) technological expertise, aimed at either designing and controlling customised laboratory equipment, handling different materials especially at high temperature, developing technical solutions to optimise the performances of complex systems, etc.;
(iii) development of structural models to study and optimise the behaviour of dynamic systems such as the glass extruder;
(iv) computational fluid dynamics studies of a high viscosity fluid (i.e. softened glass);
(v) optical fibres production and characterisation along with their applications in different environments.

The effective synergy between all these disciplines has been supported by a deep investigation into the scientific literature of different research fields.

In the following sections, an overview of soft glasses fabrication and preform extrusions will be given and, finally, the structure of the chapter will be presented.

1.2 Soft glasses fabrication

The concept of *soft glasses* is employed to describe many different types of glasses. The term *soft* is related to the low *softening* temperature which is a special feature of these glasses compared to silica glass. The actual definition of soft glasses is not unique since some authors prefer to include also the standard soda-lime-silicate glass [1], [2], while others consider soft glasses only the glasses with a lower softening point than soda-lime-silicate [3]. Yet, this expression is often used in scientific papers to refer to glasses that show lower processing temperature and often also lower mechanical properties than pure silica [4]–[7]. These glasses may belong to different families, among which it is possible to cite lead-silicate, chalcogenide, tellurite, phosphate, borate, and fluoride glasses. The composition, as well as the chosen processing technique, may cause a variation of several orders of magnitude in the properties of the materials.

Among the different soft glasses, the present thesis focuses on phosphate glasses. These glasses have potential use in a huge number of applications given the vast range of permitted compositions. In the following pages, we will demonstrate the possibility of synthesising, on the one hand, chemically inert active phosphate glasses employed as lasing media and on the other hand soluble glasses that are designed to easily dissolve inside the human body. These bioresorbable glasses can also release specific ions such as antibacterial or therapeutic agents, that may inhibit the proliferation of unhealthy microorganisms.

All these glasses are obtained by melt-quenching starting from powder reagents and, during casting, they can be formed into the most diverse shapes. Forming these materials into bulk substrates can be used to directly produce the glass for the final application (as for antibacterial surfaces) or can be the starting point for preform fabrication for the production of fibre optics.

1.3 Extrusion of preforms for optical fibres

In several industries, extrusion is a well-consolidated technique. From the processing of aluminium components to ceramic brick production, from thermoplastic polymers to long-shaped reinforced composite profiles, extruded products are present almost everywhere. Yet, glass extrusion is still at a research stage and strong research interest is present either about the choice of the right material or the development and consolidation of the production process, or about the characterisation of the properties associated with extruded glass products. The development of extruders to process glass is carried out by a few research groups. At the moment, our extruder is the only example of a glass extrusion system in Italy.

The process consists of forcing a softened glass to pass through a specifically designed hole. To reach the softening point the glass must be heated to the right temperature. After passing through the extrusion die, the temperature is lowered so that the extrudate is frozen with its new shape. A big advantage of extrusion, compared to other preform-production techniques, is that the same extruder may be employed to produce preforms with various shapes by simply substituting the extrusion die. The die is the core of the extruder and its design can present different issues depending on the desired extrudate's shape. The present work is partly dedicated to understanding the physical aspects of the extrusion process and offering solutions to some of the problems that may be encountered during the extrusion of a soft-glass fibre preform. The complexity of the system arises from the fact that the average working temperature is usually above 500 °C which leads to a glass viscosity in the order of $10^7 - 10^8$ Pa·s, processed under an applied load of a few kN. Distortions of the extrudate may occur and must be addressed. Also, at these temperatures, the firmness of the whole system must be ensured. Furthermore, the stability of the glass against crystallisation, or *devitrification*, is mandatory for optical applications.

Several aspects have to be considered with a systemic approach, to reach a better knowledge of this process. Due to its high scalability, advancements in this topic may lead to substantial progress in the field of glass manufacturing. The present work focuses on the main aspects of soft glass extrusion to achieve flexible solutions that may be employed to overcome the limitation of such technique making it easier to adopt it as a widespread tool for advanced and complex fibre drawing. This could open up new possibilities letting the fibre research advance steadily in many novel applications.

1.4 Structure of the chapters

The thesis can be divided into two parts: a theoretical introduction and the experimental section dedicated to three main applications. The former is covered by Chapters 2 and 3, while the latter is reported in Chapters 4, 5, and 6. In more detail, we can say that Chapter 2 is focused on Material Science and deals with the phosphate glass formation and the control and measure of the glass properties. Chapter 3 is dedicated to Material Technology: the glass processing techniques are reviewed with a specific focus on soft glass extrusion and fibre drawing. After these introductory chapters, Chapter 4 focuses on the synthesis of phosphate glasses used in the production of active fibre amplifiers and lasers. These glasses are characterised and processed using the extrusion technique to obtain both single- and multi-mode fibres. Chapter 5 is dedicated to the design and production of microstructured bioresorbable fibres. The bioresorbable glass fibres described in Chapter 5 are obtained by processing custom phosphate glasses with the extrusion technique followed by fibre drawing. Furthermore, we investigated the use of the extrusion to produce complex microstructured fibres and we proposed innovative solutions by adopting a simulation-aided approach. In this framework, we developed a double-channel preform that can be used in the production of bioresorbable glass fibres for simultaneous drug delivery and light propagation. Chapter 6 describes another feature of the bioresorbable glass: the ability to carry and release into the body therapeutic agents such as antibacterial ions. We synthesised new phosphate glass compositions, by doping a bioresorbable glass with several antibacterial ions. The properties of these bioresorbable glasses are investigated and the preliminary results of antibacterial and cytotoxicity tests are presented. Finally, in Chapter 7, we draw conclusions on the thesis work and we present further perspectives.

References

[1] N. P. Bansal and R. H. Doremus, *Handbook of Glass Properties*, Academic Press Inc. London, UK, 1986.

[2] G. W. Morey, *The Properties of Glass*, 2nd ed. New York, NY: Reinhold Publishing Inc., 1954.

[3] J. E. Shelby, *Introduction to Glass Science and Technology*, 2nd ed. London, UK: Royal Society of Chemistry, 2015.

[4] J. Lousteau, G. Jose, D. Furniss, A. B. Seddon, T. M. Benson, and A. Jha, ‘A novel approach for the fabrication of planar waveguides from heavy metal oxide glasses’, *Journal of Non-Crystalline Solids*, vol. 355, no. 37–42, pp. 1973–1979, 2009, doi: 10.1016/j.jnoncrysol.2009.01.058.

[5] H. Ebendorff-Heidepriem and T. M. Monro, ‘Analysis of glass flow during extrusion of optical fiber preforms’, *Optical Materials Express*, vol. 2, no. 3, p. 304, 2012, doi: 10.1364/OME.2.000304.

[6] G. Tao, S. Shabahang, S. Dai, and A. F. Abouraddy, ‘Multimaterial disc-to-fiber approach to efficiently produce robust infrared fibers’, *Optical Materials Express*, vol. 4, no. 10, p. 2143, 2014, doi: 10.1364/OME.4.002143.

[7] D. Gallichi-Nottiani, D. Pugliese, N. Giovanna Boetti, D. Milanese, and D. Janner, ‘Toward the fabrication of extruded microstructured bioresorbable phosphate glass optical fibers’, *International Journal of Applied Glass Science*, no. June, pp. 1–9, 2019, doi: 10.1111/ijag.14652.

Chapter 2.

Phosphate glasses

2.1 Introduction

2.1.1 Glassy state, soft glasses, oxide glasses

History of glass

Fig. 2.1. Examples of natural glasses and ancient glass products: (a) fragment of obsidian glass; (b) Globular obsidian Jar of King Merneferre Aya, Egypt, 1700 –1676 B.C.E. (Metropolitan Museum of Art, New York, NY, USA); (c) Roman glass bowl found in Steinfort, Luxembourg, 400 C.E., (Metropolitan Museum of Modern Art, New York, NY, USA); (d) Stained glass window in the choir of Chartres cathedral, France, 1100-1200 C.E. Images available under Creative Commons CC0 1.0 Universal Public Domain Dedication.

Natural glasses have existed since the oldest ages of planet Earth. Because of volcanic eruptions, rocks rich in quartz, alkali feldspar, and iron oxide can melt and solidify in the form of obsidian glass (Fig. 2.1a). These glasses, at the early stage of human development, were worked to form the first knives well before the Iron Age [1]. Archaeological evidence of obsidian cutting tools, plates, and other wares like mirrors was found in each continent (an example, although not so ancient is visible in Fig. 2.1b). The actual discovery of *modern* glass-making may be attributed to different populations and with great uncertainty on the time.

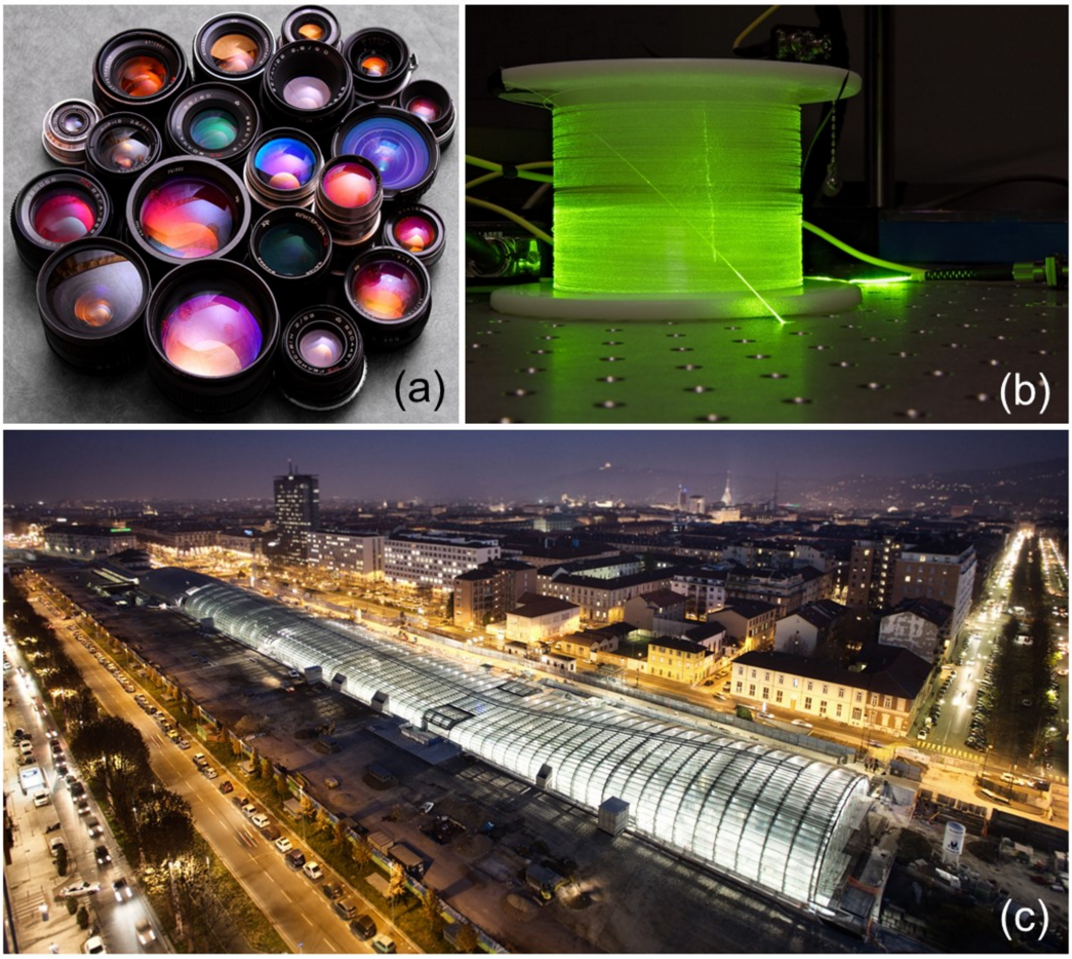

Fig. 2.2. Examples of modern glass products: (a) camera lenses with different coatings [author: Victor Gorelov] ; (b) single-mode glass optical erbium-doped fibre being illuminated by green laser light (the coil contains about 30m of fibre) [author: Ximeg]; (c) examples of usage of architectural glass in the Torino Porta Susa train station [author: Michele D'Ottavio]. Images adapted and reproduced under the Creative Commons Attribution-Share Alike 3.0 Unported license.

According to the Roman author Pliny the Elder, the first glass manufacturing can be dated back to 5000 B.C.E., when Phoenician merchants accidentally discovered how to produce glass by melting nitrate stones with silica sand [2]. However, historians do not agree about this rather fascinating legend, and some evidence shows even more ancient glass products, like small statues or amulets, belonging to the Badarian Age in Egypt, around 12000 B.C.E. [3]. Nevertheless, all the sources agree that since around 1500 B.C.E., several ancient populations, like Egyptians, Greeks, and Romans, learned how to manipulate glass for the production of vessels or jewellery. Even the invention of glass blowing dates back to the beginning of the Christian Era (a Roman glass bowl is shown in Fig. 2.1c). During the Middle Age, the first evidence of a deeper knowledge of the glass-manufacturing technique started to be visible due to the usage of different raw materials. This allowed to control the colour of glasses; great examples can be found in several cathedrals (see, for example, Fig. 2.1d) [1].

In the subsequent centuries, the technical approach to glass science and production allowed for the creation of complex handcrafts with various colours, and even with full transparency. Since the discovery of transparent glass, according to some authors [4], humankind has entered a new epoch: the *Glass Age*. Transparent glass has led to the diffusion of windows, spectacles, lenses for telescopes and microscopes, mirrors, urban building and skyscrapers, photography, motion picture, television, optical fibres, smartphones, and so on (some of these are shown in Fig. 2.2). A popular science journalist even argued that “A world without glass would strike at the foundation of modern progress” [5]. Despite this fascinating but also simplistic approach, there is no doubt that the discovery of glass allowed huge steps forward in human knowledge.

Definition of “glass”

An intriguing point about glass, despite its evolution during all these centuries, is that a fully accepted answer to the rather simple question “what *is* glass?” has not been given yet. The intuitive idea of what the word *glass* means can be understood by most people (and a schematic representation is given in Fig. 2.3) but the common meaning is often incomplete, not to say misleading. To get a quick comprehension, surfing the internet it is possible to find several definitions of glass:

- A hard, brittle substance, typically transparent or translucent, made by fusing sand with soda, lime, and sometimes other ingredients and cooling rapidly. It is used to make windows, drinking containers, and other articles[1].
- Any of the various amorphous materials formed from a melt by cooling to rigidity without crystallization[2].
- A hard, brittle, non-crystalline, more or less transparent substance produced by fusion[3].

---

[1] https://www.lexico.com/definition/glass

[2] https://www.merriam-webster.com/dictionary/glass

[3] https://www.dictionary.com/browse/glass

- The standard definition of a glass (or vitreous solid) is a solid formed by rapid melt quenching. However, the term "glass" is often defined in a broader sense, to describe any non-crystalline (amorphous) solid that exhibits a glass transition when heated towards the liquid state[4].

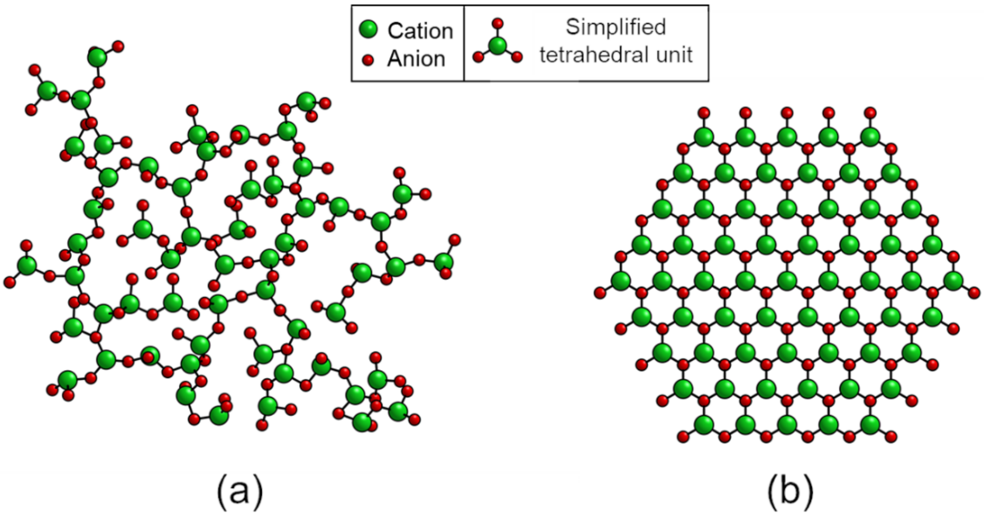

Fig. 2.3. Schematic examples of (a) the random network of glass and (b) the regular network of a crystalline solid.

This quick review gives a hint that the concept of glass is rather difficult to define. Besides, most of the definition listed above carry also misleading or inappropriate meanings. In fact, during the 20th century, the scientific debate has overcome several obstacles to reach an accepted definition of glass. The *modern* scientific discussion has begun in 1932 with a paper by Zachariasen. He stated that “It must be frankly admitted that we know practically nothing about the atomic arrangement in glasses” [6]. At that time the glass-network theory, which will be illustrated in a while, was being formulated. One of the first contributions related to a proper definition of glass was given by Tamman in 1933, who asserted that “glasses are undercooled solidified melts” [7]. This definition appears today to be inadequate, because it neglects all the non-melted glasses, such as the ones obtained via the sol-gel method or vapour deposition techniques. However, it was accepted until 1973, when Doremus proposed a similar definition: “a material formed by cooling from the normal liquid state which has shown no discontinuous change in properties at any temperature, but has become more or less rigid through a progressive increase in its viscosity” [8]. Almost at that time, Cooper & Gupta tried to give a technical explanation, by affirming that “Glass is an isotropic material with relaxation time $\gg 10^3$ s and $\chi \sim 1$”, where χ is a normalized correlation range, which is zero for a dilute gas and close to 1 for a normal liquid or a glass [9]. While this definition is formally correct, it could be hard to grasp its full significance, especially for a non-scientific reader. Because of this, the sentence of

---

[4] https://en.wikipedia.org/wiki/Glass

Doremus was further extended by Wong and Angell in 1976 who started to consider the concept of crystallinity, claiming that “Glass is an X-ray amorphous material that exhibits the glass transition. This being defined as that phenomenon in which a solid amorphous phase exhibits with changing temperature (heating) a more or less sudden change in its derivative thermodynamic properties such as heat capacity and expansion coefficient, from crystal-like to liquid-like values” [10] In the same year a similar sentence, but more compact, was suggested by Mari, who defined glasses as “Amorphous solids that are obtained by fast cooling a molten mass averting its crystallization” [11]. During the ‘80s and ‘90s some scientist started to distinguish between glasses and amorphous solids. In fact, Zarzycki in 1982 defined the glass as “A non-crystalline solid that presents the phenomenon of glass transition” [12] and Gupta in 1996 clarified this distinction by considering that a non-crystalline solid (NCS) must satisfy two main rules derived from the Zachariasen’s conditions for glass formation [6]: a system is a good NCS former if *(i)* the short-range order (SRO) of the crystal is indistinguishable from the SRO of NCS and if *(ii)* it is topologically disordered. Among all the material that satisfy these two rules, i.e. all the NCS, only the ones that satisfy a third rule can be properly called *glasses*: *(iii)* a glass must show the same SRO at the solid state and after melting. If this latter condition is not satisfied, the corresponding material should be simply considered as an *amorphous solid* [13].

Scientists and researchers kept trying to find a compact and simple definition and, in 2002, Rao claimed that glass is “A solid obtained by supercooling a liquid and that is X-ray amorphous” [14]. This sentence distinguishes the general concept of *amorphous solid* from *X-Ray amorphous material*, also avoiding the usage of the concept of glass transition which should be therefore defined. It is worth noting that, although glass products have been present all over our lives for centuries, the glass definition was still debatable even in the last twenty years. Shelby, in 2005, tried to overcome the issue by splitting the definition into two sentences: a glass is “An amorphous solid completely lacking in long-range order, periodic atomic structure, and exhibiting a region of glass transformation behaviour”, or, in other words, “Any material, inorganic, organic, or metallic, formed by any technique, which exhibits glass transformation behaviour” [15]. However, while some authors still tried to take advantages of complex concepts arguing that “Glasses are thermodynamically non-equilibrium kinetically stabilized amorphous solids, in which the molecular disorder and the thermodynamic properties corresponding to the state of the respective under-cooled melt at a [generic] temperature T* are frozen-in.” [16], others revert the point of view by affirming that “Glass is a solid having a non-crystalline structure, which continuously converts to a liquid upon heating” [17].

This latter definition, published in 2010 and adopted also since the second edition of the book “Fundamentals of Inorganic Glasses” by Varshneya [18], was fully accepted until 2017 when Zanotto & Mauro further extended the debate by giving two definitions: a simpler one for the general public: “Glass is a nonequilibrium, non-crystalline state of matter that appears solid on a short time scale but continuously relaxes towards the liquid state”; and a more complex one for the scientific community: “Glass is a nonequilibrium, non-crystalline condensed state of matter that exhibits a glass transition. The structure of glasses is similar to that of their parent supercooled liquids (SCL), and they spontaneously relax toward the SCL state. Their ultimate fate, in the limit of infinite time, is to crystallize” [19]. This latter concept of instability was a subject of a fervent discussion published in the *Journal of Non-Crystalline Solids*. In particular, Popov proposed a less radical definition of a *metastable state of matter* [20], while Zanotto & Mauro confirmed their hypothesis which considers glass as *an unstable material* [21]. The two sentences of Zanotto & Mauro appear to be the most detailed, complete, and comprehensible definitions of glass available to date. At the same time, these phrases also leave the implicit idea that even though glass can be seen as a solid and *immutable* material, it is not more than a liquid, if looked through a long (almost infinite) timescale. For the sake of completeness, in 2019 the last definition, to date, was proposed by Rajaramakrishna & Kaewkhao, who argued that “Glass is an amorphous solid which exhibits glass transition temperature by arresting the kinetics below supercooled liquid region when bypassed crystallization” [22]. However, this latter definition neglects the consideration of the unstable nature of glass matter and introduces concepts that should be explained to a non-scientific reader. For this reason, the definition of Zanotto & Mauro is still preferred and has been also included in the third edition of the book from Varshneya, published in 2019, with Mauro as co-author [23].

Glass chemistry

A detailed essay on the chemistry of glass formation is beyond the scope of the present thesis and further information regarding the theory of glass networks can be found in the books by Vogel [24] or Varshneya [23]. However, the concepts detailed by the *Zachariasen-Warren network theory* will be briefly introduced. This theory does not cover all the possibilities of glass formation, especially omitting some unconventional glass melts that could be obtained with particularly stringent cooling rates. Some other criteria were proposed and are only mentioned herein. One was suggested by Sun who considered that the process of glass-forming should be related to the ability (or, better, the inability) of molecular bonds to rearrange in the liquid state, during crystallisation. He proposed that a higher bond strength would correspond to a better glass-forming ability [25]. While this theory is well suited for most of the glass systems, it does not explain the glass formation for covalently bonded solids, such as chalcogenides, for which the so-called Phillips topological constraint hypothesis holds. For a better comprehension of this concept, the reader may refer to [26]. The most comprehensive theory of glass formation is the so-called *kinetic theory*. According to this theory the glass formation can occur, under special conditions, for materials of any composition, bonding, or structural type [23], [24]. However, its description goes beyond the scope of the present work.

The *Zachariasen-Warren network theory* relies on some basic principles [24]:

- A compound tends to form a glass if it easily forms polyhedral groups as the smallest building units.
- Polyhedra should not share more than one corner.
- Anions should not bind more than two central atoms of a polyhedron. Thus, in simple glasses anions form bridges between two polyhedra.
- The number of corners of polyhedra must be less than 6.
- At least three corners of a polyhedron must connect with neighbour polyhedra.

These rules apply to different types of glasses, where the anions are usually O^{2-}, S^{2-}, or F^{-}. The dimensions and coordination numbers of the related cations define the role of the compound in glass formation. The cations used in glass manufacturing can be divided into three main groups: *(i)* glass network formers, such as Si, B, P, Ge, As, Be, etc., with coordination number generally 3 or 4; *(ii)* glass network modifiers, such as Na, K, Ca, Ba, etc., with coordination numbers generally ~ 6; and *(iii)* intermediates, like Ti, Zn, Al, Pb, etc., which may either reinforce the network (coordination number 4) of further loosen the network (coordination numbers 6-8), but cannot form a glass *per se*.

To better highlight the different families of glasses formed by cooling a melt, some information, derived from Doremus [8] and described also by Varshneya [23], are adapted in Table 2.1. This list represents only a partial catalogue of the possible glass systems, but it is useful to clarify the contest of the present work.

When dealing only with oxide systems, it is possible to reformulate the rules for glass formation listed above into four compact and simple rules [23]. In fact, besides being the subject of the present work, those systems are the most common kinds of glass. Considering a compound formed by an anion A and the oxygen O with the stoichiometry A_mO_n, it will form a glass if:

- An oxygen atom is linked to no more than two atoms of A.
- The oxygen coordination around A is small, say 3 or 4.
- The cation polyhedra share corners, not edges or faces.
- At least three corners are shared.

There are some exceptions to these rules, represented by compounds like MoO_3, P_2O_3, As_2O_3, V_2O_5, Sb_2O_5, or Nb_2O_5 that do not fully satisfy the rules by themselves but can form glasses in combination with other oxides that act as stabilising agents.

Table 2.1. A partial list of glass systems

FAMILY	**ELEMENTS OR COMPOUNDS**
ELEMENTAL GLASSES	S, Se, Te, P
OXIDES	B_2O_3, SiO_2, GeO_2, P_2O_5, As_2O_3, Sb_2O_3, In_2O_3, Tl_2O_3, SnO_2, PbO_2, SeO_2 not alone but in binary or multicomponent mixtures: TeO_2, MoO_3, WO_3, Bi_2O_3, Al_2O_3, Ba_2O_3, V_2O_5, SO_3
SULFIDES	As_2S_3, Sb_2S_3, CS_2
SULFIDES	various compounds of B, Li, Ga, In, Te, Ge, Sn, N, P, Bi
SELENIDES	various compounds of Tl, Sn, Pb, As, Sb, Bi, Si, P
TELLURIDES	various compounds of Tl, Sn, Pb, As, Sb, Bi, Ge
HALIDES	BeF_2, AIF_3, $ZNCI_3$, Ag(CI, Br, I), Pb(CI_2, Br_2, I_2), and multi-component mixtures
NITRATES	KNO_3-$Ca(No_3)_2$ and many other binary mixtures containing alkali and alkaline-earth nitrates
SULFATES	$KHSO_4$ and other binary and ternary mixtures
CARBONATES	K_2CO_3-$MgCO_3$
SIMPLE ORGANIC COMPOUNDS	*O*-Terphenyl, toluene, 3-methyl hexane, 2,3-dimethyl ketone, diethyl ether, isobutyl bromide, ethylene glycol, methyl alcohol, ethyl alcohol, glycerol, glucose As droplets only: *m*-xylene, cyclopentane, *n*-heptane, methylene chloride
POLYMERS	polyethylene, polycarbonate, poly(methyl methacrylate), and many others
AQUEOUS SOLUTIONS	acids, bases, chlorides, nitrates, and others
METALLIC ALLOYS	(high cooling rates) Au_4Si, Pd_4Si, Te_x-Cu_{25}-Au_5, and others

Glass industry

Among all the glass systems, oxide glasses are by far the most important in terms of the amount of global production. In the present paragraph, a few data about glass production in Europe are reported to underline the global importance of glass manufacturing as one of the most widespread and commercially fundamental sectors of material processing.

Handcraft and artistic glasses are still diffused in some contexts, see for example the glass district of Murano (Venice, Italy), but the transition towards a scalable production is something that occurred in the 20th century and the actual technologies employed for glass manufacturing are adopting advanced control to reach high productivity with precise repeatability.

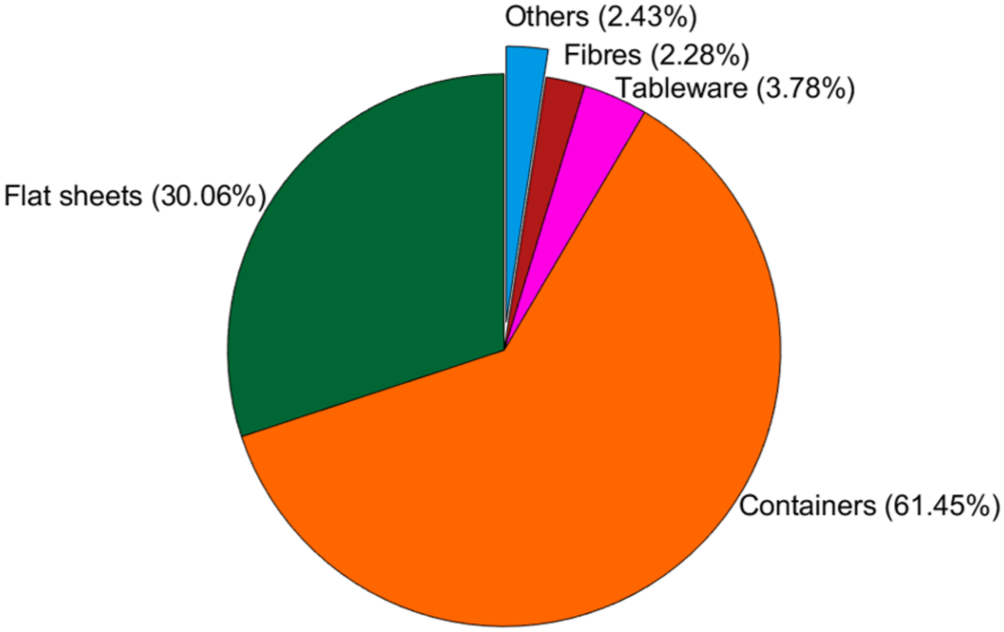

Fig. 2.4. Pie chart reporting the different sectors of glass production in 2018 in the EU-28 countries (data are taken from the latest statistical report of Glass Alliance Europe[5]).

According to the latest statistical report of Glass Alliance Europe[5], the glass production in 2018 in the EU-28 countries has reached a volume of 36.5 million tonnes, with the leading sector of glass containers production responsible for more than 60% of the total glass production (i.e. around 21 million tonnes of bottles and jars produced only in 2018), followed by basic flat sheets (~30% or ~10 million tonnes); the remaining products are glass tableware (<4% i.e. slightly above 1 million tonnes), continuous filament glass fibres with less than 2.3% (~800 thousand tonnes), and almost the same for other glasses including special glasses. All these data are reported in the pie chart of Fig. 2.4. This huge amount of glass, which is produced, consumed, and partially recycled every year, is essentially composed of the so-called soda-lime silicate glass. It features silica as the glass-network former. The main network modifiers are soda and lime that react at high temperature to form Na_2O and CaO. Some other oxides are added to the melt, among which it is possible to cite Al_2O_3, K_2O, MgO, Fe_2O_3, TiO_2, and SO_3. Each one of these network modifiers and intermediates has a specific function in the glass preparation, and the actual recipe is

---

[5] i.e. the European Alliance of Glass Industries (https://www.wko.at/branchen/industrie/glasindustrie/statistical-data-global-glass-sector.pdf)

a trade secret of every glass producer. Eventual variations depend on the final application and the composition of the available raw materials. As the data about glass manufacturing highlight, special glasses, i.e. non-silicate oxide or non-oxide glasses are a small portion of the total amount of industrial production. Nevertheless, they represent an interesting field of research. As will be clearer in the following paragraphs, many intriguing properties of glasses are being discovered in recent years and there are still a lot of compositions as well as processing techniques to be explored.

Phosphate glasses

During this thesis' work, the attention has been focused on the oxide glass system containing phosphorus pentoxide (P_2O_5) as the main glass former. When cooled from the molten state, this compound can quite easily form a glass: P_2O_5 is an excellent glass former per se. Moreover, the addition of other oxides to the composition can vary the properties of the obtained glass within a wide range. In this way, different types of compounds may form [27] and some of those will be described in the following lines.

The first important difference that may be noted when comparing phosphorus pentoxide with the widely employed silicon dioxide is that if the latter has a high melting point that requires the addition of other components to reduce its processing temperatures, with P_2O_5 the opposite is true: since this compound is very reactive, the inclusion of other oxides in the glass melt can increase its durability [28]. As an example, phosphate glasses show the unique properties of being completely soluble in aqueous media, thus favouring their usage in biomedical applications [29]–[32]. However, their solubility may be altered using different modifier oxides, to the point that lead-iron-phosphate glasses have been proposed and employed as stable nuclear waste containers [33].

The main unit of phosphate glasses is the P-tetrahedron PO_4 [27], [28], [34], [35] that is sketched in Fig. 2.5. The presence and the number of bridging-oxygen atoms in the glass network is one of the main responsible for the different properties that phosphate glasses may show. The O/P ratio is determined by the amount and kind of oxides that are added to the melt (forming with P_2O_5 either binary, ternary, quaternary, quintenary, or even more complex systems). By varying the O/P ratio, it is possible to take into consideration the different types of phosphate glasses. Adopting the compact Q^i notation described in Fig. 2.5, where i denotes the number of bridging-oxygen atoms per tetrahedron, the main structural differences that arise by changing the O/P ratio can be highlighted.

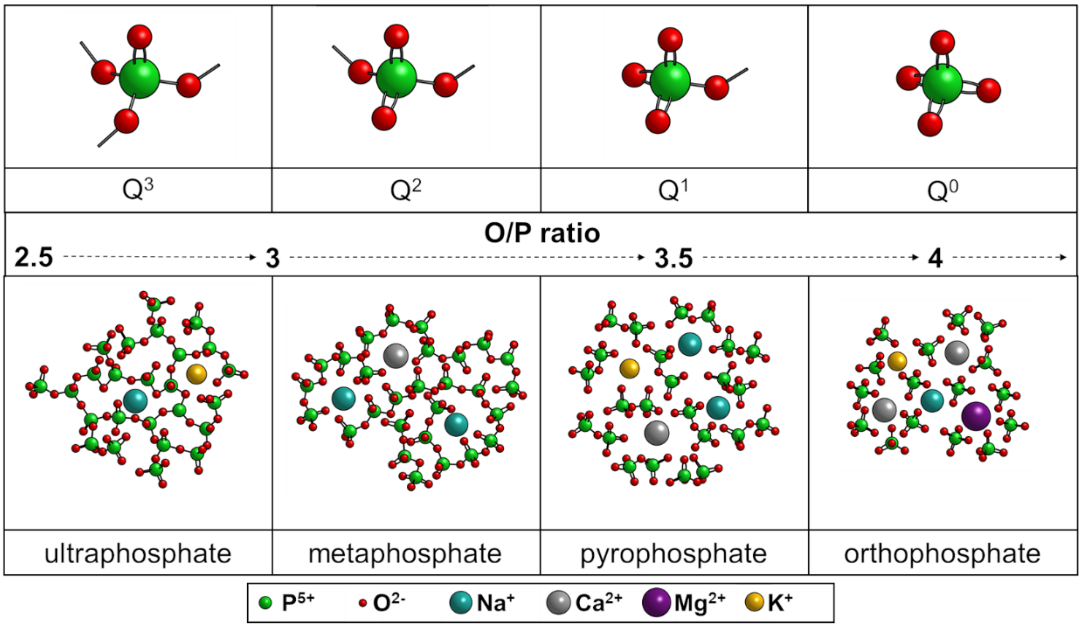

Fig. 2.5. Representation of the basic Q^i units of the phosphate tetrahedron and related matrix network corresponding to different O/P ratios. The coordination numbers (CN) of the ions in the lower part of the figure do not correspond to actual CN values.

Pure P_2O_5 can be obtained in glass form, but it is highly hygroscopic and has poor mechanical properties compared to silica, which limited its diffusion [36]. By focusing on the basic binary composition (xM_2O-$(1-x)P_2O_5$), where M is an alkali metal ion, other structures can be formed (note that almost the same concepts can be detailed with a divalent cation like Ca^{2+} or Mg^{2+}). In this condition, in which $0 \leq x \leq 0.5$ and the ratio O/P is in the range $2.5 \leq O/P \leq 3$, the network is formed of Q^3 units with three oxygen atoms shared between adjacent tetrahedra; these compounds are named ultraphosphate glasses and show the structure of a complex 3D network (see the left part of Fig. 2.5). Starting from the ultraphosphate compositions, by increasing the amount of M_2O some Q^2 units, i.e. *middle* units able to share only two oxygen atoms, start to show. Until $x = 0.5$ and no Q^3 units are present anymore; this is the case of metaphosphate glasses that show a chain-like structure with $O/P = 3$, and the stoichiometry of the tetrahedron is PO_3^-.

When some of the chains end with a Q^1 tetrahedron (which is the *terminal* or *end* unit), the value of x exceeds 0.5 and the ratio O/P becomes $3 \leq O/P \leq 3.5$; in this condition, we are dealing with a polyphosphate chain structure. By further boost the number of cations until $x = 0.67$, the chains reduce to dimers structures, composed of only Q^1 tetrahedron. In these conditions, glass formation is still possible but there is not the standard random network described also by Zachariasen; the structure takes the name of *invert glass* and contains almost isolated or small molecular fragments of tetrahedra linked through non-bridging oxygens by cations; these glasses are called pyrophosphate and show $O/P = 3.5$, with $P_2O_7^{4-}$ being the chemical formula of the tetrahedron. A final increment of the amount of M_2O (or MO) is possible, but the connected Q^1 tetrahedra almost disappear, leaving only *isolated* Q^0. This is the case of an orthophosphate structure, with O/P= 4 due to a set of detached PO_4^{3-} tetrahedra [34], [36]–[38].

The above considerations can be extended to more complex systems composed of more than two oxides. In fact, as general rules, alkali metal oxides (M_2O with $M=Li^+$, Na^+, K^+, Rb^+, and Cs^+) can be added to the glass in order to increase the stability during melting while alkali-earth oxides (MO with $M=Mg^{2+}$, Ca^{2+}, Sr^{2+} and Ba^{2+}) allow to prevent devitrification and to improve the chemical durability; also network intermediates (M_2O_3 with $R=B^{3+}$ and Al^{3+}) can enhance the chemical durability and decrease the solubility in water [39].

In this framework, the composition-related properties of phosphate glasses make them suitable for diverse applications: in terms of chemical stability it is possible to range from degradable [40] to stable [33], [41] materials; the relatively high thermal expansion coefficient allows their usage for glass-to-metal seals [42]; the good electrical conductivity, i.e. fast ionic conduction [43], [44], is important for solid electrolytes and fuel cells materials; above all, the low characteristic temperatures, if compared to silica, aid the whole material processing.

Only one substantial aspect of phosphate glasses has been neglected so far, i.e. their withstanding optical properties that are described in detail in the next paragraph.

2.1.2 Applications of phosphate glasses in photonics

Concerning the optical properties of phosphate glasses, they can show high refractive index [45], moderately low dispersion [46], superior UV transparency due to the high energy of excitation of the bridging and non-bridging oxygen orbitals [47]. An example of the possible compositional variations of phosphate glasses may be seen in Fig. 2.6. In recent years, phosphate glasses have attracted increasing attention as laser glasses. Their very high solubility for rare-earth ions and high photodarkening resistance are of great importance for laser applications. Also, the high cross-sections for stimulated emission, high gain, low concentration quenching, low up-conversion losses, and the absence of clustering effect make phosphate glasses useful as host materials for active laser ions [48], [49].

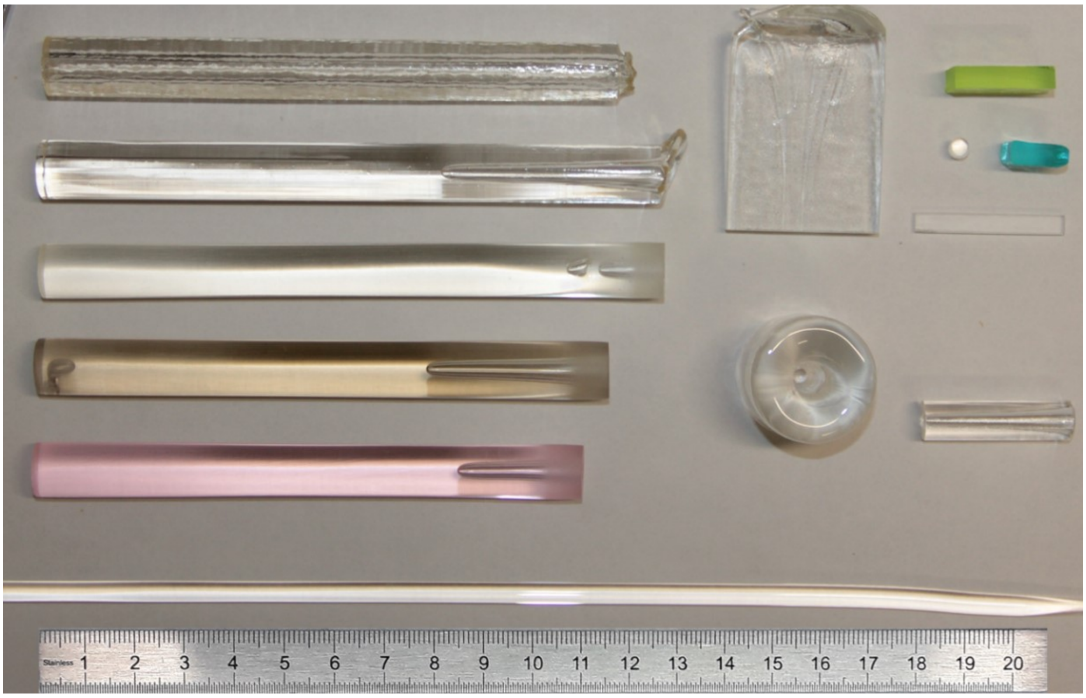

Fig. 2.6. Examples of phosphate glass products obtained with different compositions and in different shapes.

This capability of hosting active ions, i.e. various rare-earth ions (like Er^{3+}, Yb^{3+}, Nd^{3+}, Tm^{3+}, etc), together with the high transparency of phosphate glasses and the possibility of drawing into fibre-form, allows using phosphate glasses as materials to produce fibre lasers. This is a fast-growing photonic technology, that can be applied to different industrial sectors, from material processing to semiconductor device manufacturing, as well as biomedical devices and remote sensing. One of the key advantages of fibre lasers is that a whole resonator can be realised using all-fibre components, such as fibre Bragg gratings and fibre couplers, thus avoiding the need for optical-to-electrical converters and free-space optics. Such a configuration, combined with the high solubility of active ions shown by phosphate glasses, allows reducing the dimensions of the device, preserving the emitted power. To gain a better idea of the potential reduction in weight and dimension of these devices, further details will be given in Chapter 4, which is focused on active fibres and deals also with sensing applications of phosphate fibre lasers designed to be mounted on unmanned aerial vehicles (UAV). While being attractive for many reasons, the fibre laser also shows some drawbacks, related to the shape of the fibre itself, that is responsible for the occurrence of some non-linear effects, such as stimulated Raman scattering (SRS), stimulated Brillouin scattering (SBS), and self-phase modulation (SPM). Those effects are mainly due to the confinement of the laser radiation in a small area (a few μm within the core of the fibre) and represent the main restriction of RE-doped fibre laser systems, to date [50], [51].

Another important sector in which phosphate glasses have been widely used and are recently showing interesting photonics properties is the biomedical field. Here, the possibility of guiding light for example to a target inner tissue of a patient, and to sense or stimulate the reaction of a drug, or of the tissue itself, is opening several routes. On the one hand, phosphate glasses are already employed as scaffolds for bone and tissue engineering and phosphate glass fibres without optical properties are used for dental, maxillofacial, and orthopaedic implants [34]. On the other hand, optical phosphate glass fibres could be used to connect and drive the growth of muscle-precursor cells ex vivo and then implanted to replace the injured tissue. Furthermore, optics can allow orientating the cells along the axis of the fibres to grow myotubes ex vivo [52]. Also, some studies show the possibility of using such fibres to drive a nerve conduit [53] and regeneration [54], and others suggest useful wound-healing applications [55].

In recent times, new photonics technologies are being developed every year and phosphate glass optical fibres offer great chances for advanced biomaterial research. In this framework, a new glass composition that is not only transparent on a wide spectral range, i.e. from ultraviolet (UV) to near-infrared (NIR), but is also biodegradable into the body without releasing any harmful component has been developed by our research group [56]. In the present thesis, this special glass composition is used to produce microstructured fibres with the preform extrusion method. This topic will be treated in Chapter 5.

Furthermore, a bioresorbable phosphate glass composition with the addition to the glass melt of a small percentage (1 mol%) of some well-known antibacterial oxides like CuO, CeO_2, ZnO, etc., can avoid bacterial growth on the glass surface. These glass compositions are also explored in the present work to study the behaviour of antibacterial bioresorbable phosphate glasses for photonics applications. This aspect will be examined with more details in Chapter 6.

The next paragraphs will introduce the glass preparation method employed in the present thesis along with the thermophysical and optical characterisations techniques of glass samples.

2.2 Bulk glass preparation

The present section is focused on glass preparation, characterisation, and post-processing techniques. Even though some aspects are introduced herein, to be discussed in detail in the dedicated chapters, the purpose of the present section is to analyse the glass forming technologies and the possibilities that glass designers, researchers, and manufacturers have to prepare, reshape, and analyse a high-quality glass product.

2.2.1 Glass formulation

The properties of phosphate glasses depend upon several aspects related to their composition and fabrication technique. Choosing the right composition involves multiple optimisation steps. Several studies have been published in the recent past, dealing with the composition-properties relationship of glass products. Yet, in glass science, the reproducibility of the glass composition in different environmental conditions, starting with different precursors, or changing some of the processing steps, can be quite difficult. Nevertheless, the present work is carried out within a research group that has been working on the optimisation of phosphate glass compositions for more than 10 years, and deep knowledge of all the details of the best process for a reproducible glass formation has been achieved. Thanks to this, we had the chance to work on the thorough characterisation and processing optimisation of some glass compositions that were designed before the beginning of the present thesis as well as to develop some new promising glass formulations.

The main component of each glass employed in the present work is P_2O_5, with an amount that is typically around 50 mol%. In this way, we are confident that a metaphosphate or, in some case, a polyphosphate structure develops giving stability to the glass. This high P_2O_5 content guarantees glass formation, avoiding crystallisation, without requiring excessive cooling rates. Furthermore, aiming at advanced functionalities, the produced glasses are formed by even six, seven, eight, or nine compounds, and the high P_2O_5 content is mandatory to ensure compositional homogeneity, mechanical stability, and high glass-forming ability. More information about the chosen compounds are given in the following paragraph and will be further examined in the dedicated sections of Chapters 4, 5, and 6.

Three main target applications are considered for the formulated phosphate glasses in the present thesis: active optical fibres, bioresorbable optical fibres, and antibacterial optical glass. For active fibre production, a core and a cladding are needed to obtain the light guiding and optical amplification properties. The core must be doped with one or more active ions: in our case, we use either Er^{3+} or a combination of Er^{3+} and Yb^{3+}. The quantity of active ions introduced is between 1.0 mol% and 5.25 mol% depending on the specific glass. On the other side, the cladding must be free of active ions, so they are replaced by other lanthanides, like Gd^{3+}. All the other components of the core and the cladding glasses for the active fibre are added to both compositions, to give the required properties to the mixture and minimise the compositional difference for better compatibility in fibre drawing. Regarding the different glass components, a high percentage of P_2O_5 ensures good glass formation; K_2O and SiO_2 favour stable melting conditions; BaO prevents devitrification; Al_2O_3, B_2O_3, and PbO guarantee the chemical durability of the product; lanthanides, like Gd_2O_3 and La_2O_3, balance the refractive index variation, which is needed between core and cladding for proper light-guiding properties, but they show no optical activity in the spectral regions of our applications.

The bioresorbable glasses for optical fibres are synthesised with fewer components, i.e. P_2O_5, CaO, MgO, Na_2O, B_2O_3, and SiO_2. A detailed study on the composition-related properties of these glasses can be found in [56], where the effect of the substitution of CaO with MgO is investigated. For most of the bioresorbable glasses employed in the present work, the chosen amount of MgO is 23 mol%. In these conditions, several properties of the glass (temperature working-window, refractive index, dissolution time in physiological conditions) are more stringent, thus representing a worst-case condition. The successful handling of this glass directly implies the ability to manage less-demanding compositions.

Finally, for the antibacterial compositions, the same compounds are employed but a different bioresorbable glass is selected as a base material, i.e. the *BPh2* glass presented in [56]. This is a more robust glass, in comparison with the non-antibacterial bioresorbable composition previously mentioned. It contains a lower amount of MgO (8 mol%) which corresponds to a higher amount of CaO (25 mol%). Starting with this composition, we decided to add 1 mol% of different oxides, to prove their antibacterial effect and cytocompatibility, along with the resulting glass properties. The chosen antibacterial ions are CeO_2, CuO, Ga_2O_3, SnO, and ZnO.

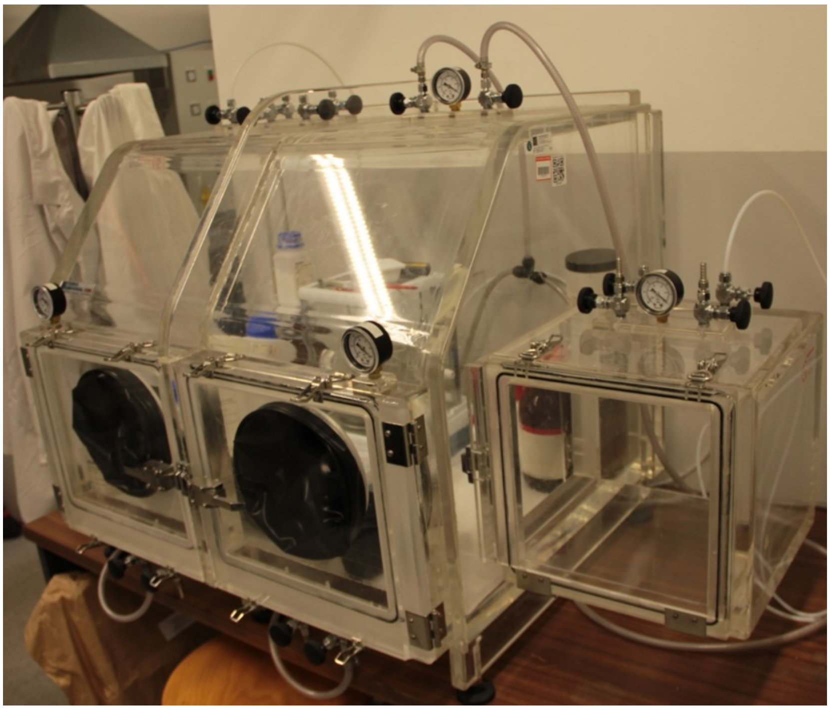

Fig. 2.7. The dry box employed for the weighting of the powder reagents.

Due to its physicochemical properties, handling phosphorus pentoxide is a delicate task. The reagent in powder form is highly hygroscopic and corrosive. All the weighting of the components needed for each glass batch must be carried out in a controlled-atmosphere environment with low relative humidity and low oxygen content. This controlled environment is achieved inside a dry box (shown in Fig. 2.7). Furthermore, special care must be taken on the cleaning of the employed tools and vessels.

The dry powders are mixed together and then heated up to melting temperature. If the powders incorporate some OH^- groups, the final quality of the glass is negatively affected. Indeed, besides a physical issue, i.e. the powders tend to agglomerate and it becomes very difficult to obtain a good mechanical mixing of the different reagents, there is also another very important aspect, especially in active fibres applications: the presence of hydroxyl groups (OH^-) is the main cause of unwanted radiation absorption in the IR spectrum at wavenumbers of around 3000 cm^{-1} [48]. Since this absorption is responsible for an increased attenuation loss in the infrared band, the content of OH^- ions must be minimised.

2.2.2 Melting, casting, annealing

Melting and casting is a well-consolidated technique for glass manufacturing. The prepared powders are mixed and heated up to the melting temperature inside crucibles, which can be made of high-density alumina, pure quartz, or platinum/rhodium alloy, depending on the quantity of the reagents, the heating process, and the required purity. A couple of examples are given about the crucible selection: alumina crucibles are not used for biomedical glasses to avoid any possible contamination of the glass batch with alumina, which is not biocompatible; on the other side, our platinum crucibles cannot hold more than a volume of 40 cm^3, so the selection of the right crucible also depends on the amount of glass powder that has to be melted.

The casting and melting temperatures vary between 1200 and 1400 °C mainly depending on the glass composition and the amount of glass to be processed, i.e. the dimension and number of crucibles. These temperatures have to guarantee the complete fusion and a fully-developed reaction of all the compounds, as well as a thorough homogenisation of the formed glass mixture. The glass melt is cast on a cold plate (melt-quenching) or into a preheated mould (made either of brass or stainless steel). The mould must be preheated to a precise temperature (which depends on casting temperature, thermal properties of the casted glass, and dimensions of the mould itself) in order to avoid cracking of the glass or sticking to the mould surface. Furthermore, except for melt-quenching products, the cast samples must be annealed, i.e. re-heated to a temperature close to the glass transition temperature T_g of the cast material, left at that temperature for a time long enough to relieve any internal stress due to thermal contraction, and then slowly cooled down to room temperature to avoid thermal shock. This procedure must be quickly carried out after the casting. If the glass samples are not properly annealed, no further processing can be carried out without the risk of breakage of the samples and/or personal injuries.

Although other glass preparation routes could have been followed, like sol-gel techniques that reduce the high-temperature procedures, the attempt to focus the attention on subsequent glass processing approaches as well as on advanced glass characterisation techniques has led to the choice of the most simple and stable method for basic glass production.

2.2.3 Glass characterisation

Among the several techniques used to characterise glasses for different properties, some are employed to analyse the thermal and thermomechanical behaviour of the produced glasses, like Differential Thermal Analysis (DTA) and dilatometry or thermal expansion coefficient (CTE) measurement. Furthermore, the latter may also be extended to derive an indirect measurement of the viscosity in a range of great interest for the proposed applications. Other techniques are more focused on the optical behaviour of glass, like Ultraviolet-visible-Near Infrared (UV-vis-NIR) or Fourier-Transform Infrared (FTIR) spectroscopies, and refractive index measurement. Finally, surface properties are also measured, like surface roughness, to assess the quality of the produced glasses as well as of the polishing procedures. In the following paragraphs, it is possible to find a description of all these techniques.

DTA

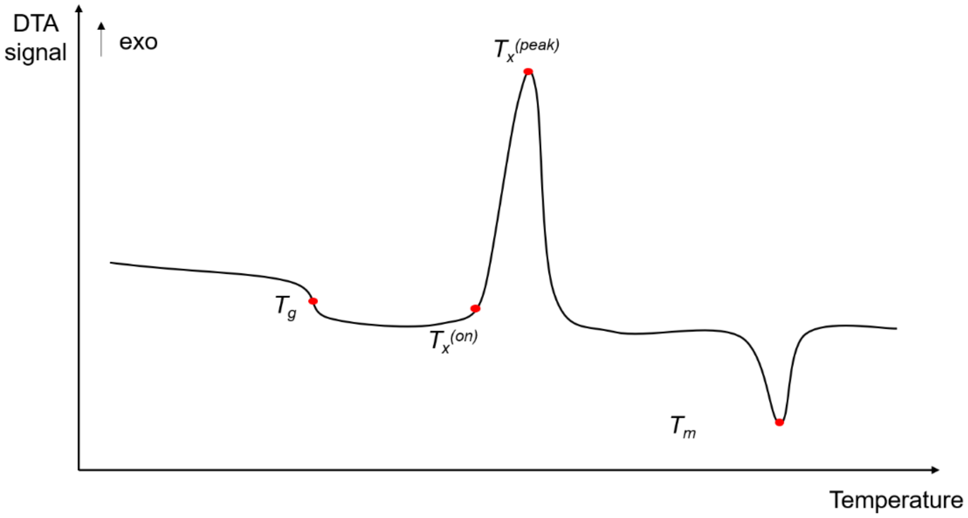

Fig. 2.8. Typical DTA curve showing the characteristic temperatures: the glass transition temperature T_g at the inflexion point, the onset and the peak of the exothermic crystallisation ($T_x^{(on)}$ and $T_x^{(peak)}$) and the endothermic melting temperature T_m.

The thermal behaviour of glasses is of great importance for the manufacturing and post-processing steps, but also for their employment in practical applications. For this reason, a Differential Thermal Analysis is carried out, to determine the temperature *working window* i.e. the difference between the temperature $T_x^{(on)}$ at which the onset of crystallisation occurs and the glass transition temperature T_g. The characteristic temperatures that can be extracted from a DTA curve are reported in Fig. 2.8. The tested samples are annealed before the measurement and around 50 mg of bulk glass is loaded into a platinum crucible of a NETZSCH DTA/TG STA 2500 Regulus equipment. The sample is heated with a heating rate of 5 K/min under constant nitrogen flux. The obtained data show the difference of temperature between the glass sample and a reference crucible which is left empty. The typical DTA curve shows a point of inflexion at the glass transition temperature of the material, an exothermic peak at the crystallisation temperature, and eventually, an endothermic peak when melting occurs. Sometimes, if the crystallisation is not fully developed, it is possible to see a continuous rise in the exothermic signal with no definite peak. Yet, during the processing of our glasses, we want to prevent the formation of the very first nucleus of crystals, thus the onset of the crystallisation is more important than the temperature at which the full development of the phenomenon occurs. For this reason, we assume this onset value as our reference for the crystallisation temperature.

Dilatometry

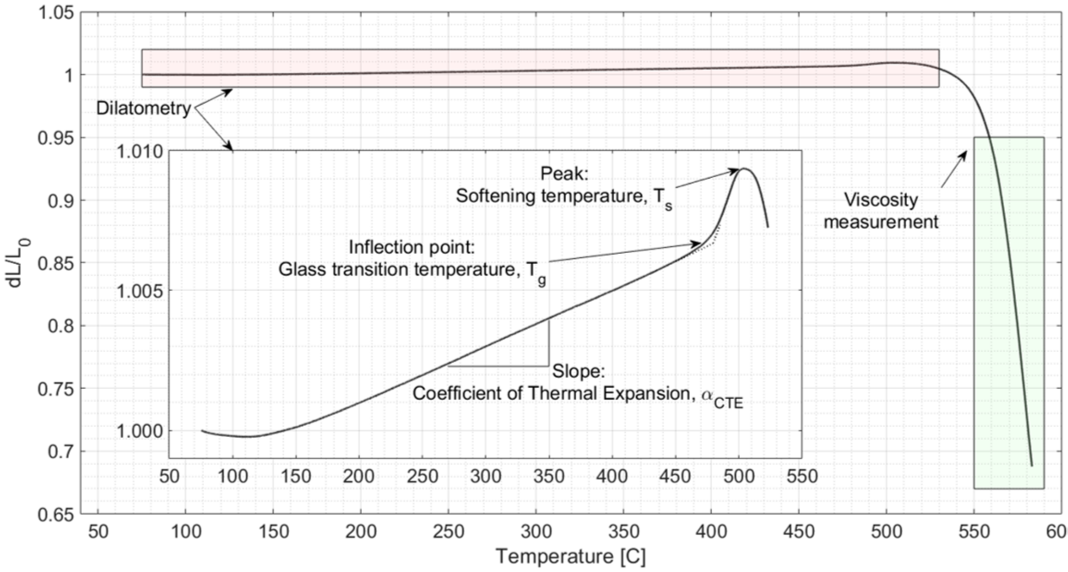

Fig. 2.9. Example of a dilatometric curve extended above the softening temperature to measure the temperature-viscosity relationship for viscosities in the range 10^8 – 10^4 Pa·s. In the inset, the parameters obtainable from the standard dilatometry are highlighted.

Dilatometric measurement is of great interest when dealing with every class of material. The linear expansion of the material during heating (and consequent contraction during cooling) is responsible for thermal stresses and it is a frequent cause of failure of glasses in common applications. Especially during some processes like the drawing of a preform into a fibre, the matching of the CTEs of the involved glasses (in the basic case a core and a cladding, but sometimes there could be more than two materials involved) is a crucial aspect to avoid breakage. In our laboratory, we employed a NETZSCH 402 DIL Expedis with horizontal set-up for some of the measurements and a SETARAM—SETSYS Evolution with a vertical set-up for some others. In both cases, the instrument is uploaded with a cylinder of glass (nominally 4 mm diameter and 6 mm height) and heated at 5 K/min. The system records the micrometric movement of the loading piston which is due to the thermal expansion of the sample.

The slope of the curve is constant and represents the CTE of the glass. At the glass transition temperature, the slope of the curve increases (the sample expands much faster when the mobility of the constituent molecules is higher, i.e. at temperatures above the T_g). Then, when the temperature reaches the softening of the glass T_s, the piston starts to compress the glass, which is no longer capable of bearing the load. At that time, the usual dilatometry is interrupted but the measurement can be extended, with the instrument featuring the vertical set-up, to measure the viscosity/temperature dependence in the range 10^8 – 10^4 Pa·s, as will be described in the next paragraph. The distinction between these two separate measurements is depicted in Fig. 2.9, along with the information acquired from a standard dilatometry curve.

Derived viscosity measurement

As detailed in the ASTM Standard C1351M-96 *Standard Test Method for Measurement of Viscosity of Glass Between 10^4 Pa·s and 10^8 Pa·s by Viscous Compression of a Solid Right Cylinder*, the viscous compression of the sample can be measured. We carried out this measurement by employing the Thermo-mechanical analyser (TMA, model SETARAM—SETSYS Evolution) with a vertical set-up shown in Fig. 2.10, and extending the recording to a temperature above the T_s. The viscosity of the glass can be derived by measuring the variation of the height of the sample during heating, and then applying the following formula:

$$\eta = 2\pi \frac{Mgh^5}{30V(dh/dt)(2\pi h^3 + V)}$$

where M is the applied load, g is the acceleration due to gravity, V is the specimen volume, and h is the specimen thickness at time t.

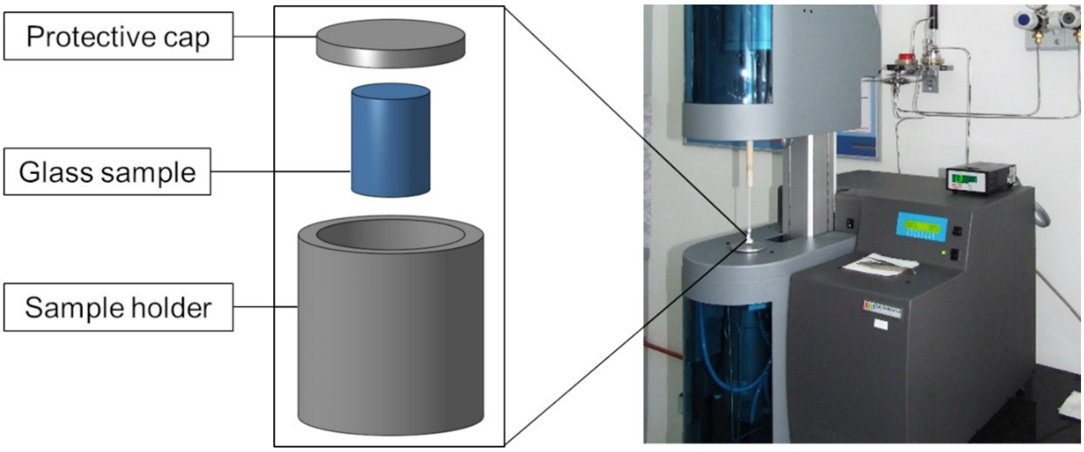

Fig. 2.10. A schematic representation of the sample holder (left) and a picture of the instrument employed for viscosity measurement (right).

This is an indirect measurement of viscosity which still is quite simple and useful. It covers a range of high viscosities which is often neglected in usual laboratory tests, (considering that viscosity of gases, liquids and most common polymers of industrial or research interest are usually well below these values, which in turn are near the lower limit of solid elastic behaviour [57], [58]). In our case, the sample employed for the dilatometric measurement is heated well above the softening temperature, measuring the decrease in the height of the sample. The glass cylinder (with nominally 4 mm diameter and 6 mm height) is placed inside a small steel container and covered with a protective cap (see Fig. 2.10). The piston exerts its load on the cap and it moves down until it reaches its maximum distance (i.e. 2 mm). During this time, the sample starts to deform filling the available space in the container, but do not get into contact with the container's wall. The resulting curve may be compared with calculated viscosity data.

UV-vis/NIR spectroscopy

The glasses that are studied in the present thesis are substantially transparent in the visible region. Yet, to get a deep knowledge of the optical behaviour of the produced glasses, which is of great importance when dealing with materials for optical applications, we carried out UV-visible-Near infrared spectroscopy on the glass samples. This measurement allows quantifying the absorbance of the glass at different wavelengths in the ultraviolet, visible, and in the first portion of the infrared spectrum regions. We cut and polished a thin piece of bulk glass (with a thickness of around 1 mm) on both sides to reach optical quality polishing. Then, we inserted the sample into a Shimadzu UV-visible-NIR spectrophotometer 2600-2700 and scanned in wavelength in single-beam configuration to measure the transmittance spectrum. The schematic set-up of the instrument is reported in Fig. 2.11.

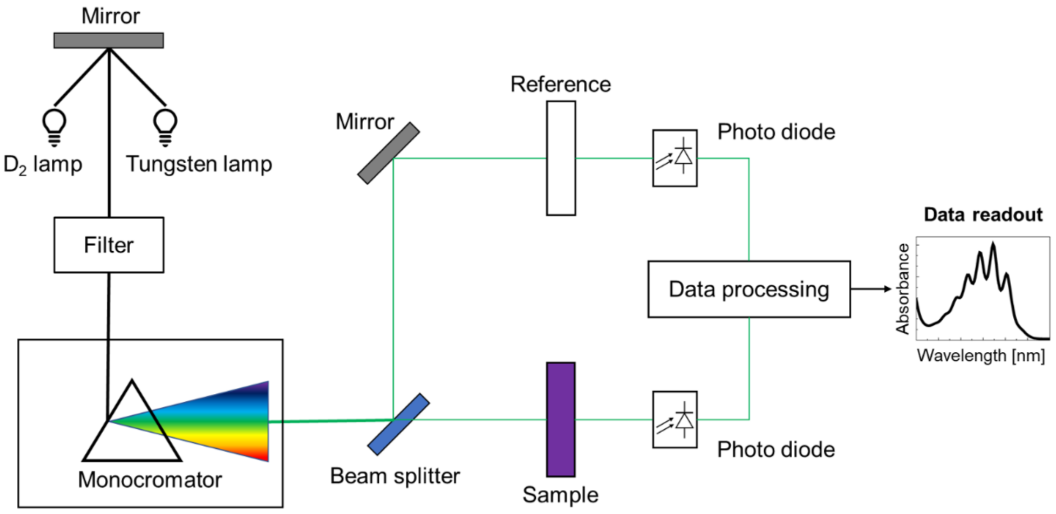

Fig. 2.11. Schematic of the UV-vis-NIR spectrophotometer.

FTIR spectroscopy

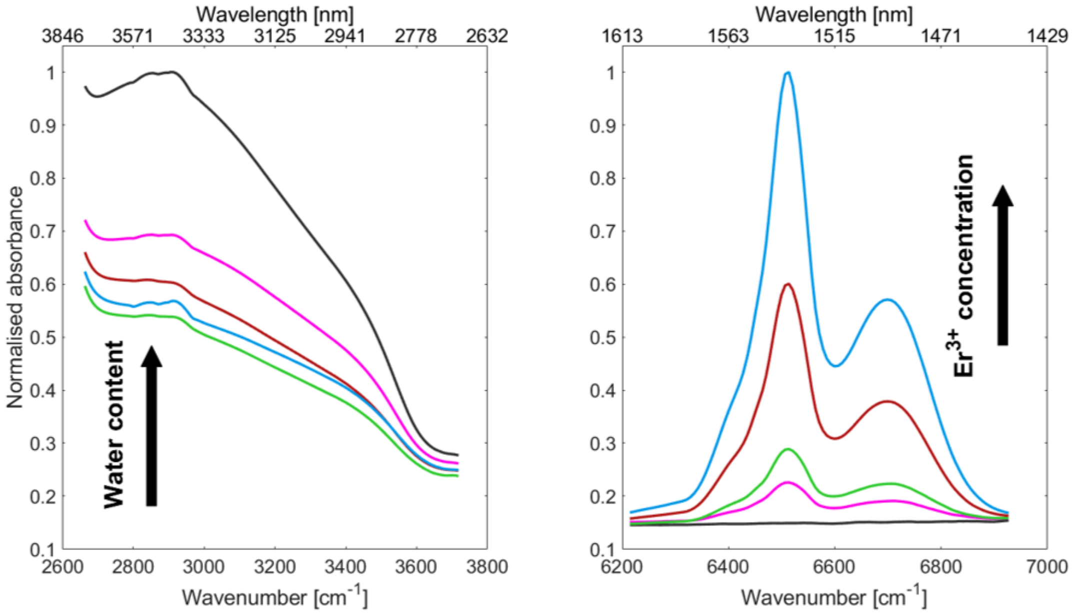

Fig. 2.12. Example of FTIR spectra. (a) The peak attributed to the stretching of the OH^- groups can give an estimation of the quantity of water in the sample. (b) The characteristic peak of Er^{3+} is centred around 6350 cm^{-1} (i.e. at a wavelength of 1535 nm).

The Fourier Transformed Infrared (FTIR) spectroscopy has been used to characterise glass samples for optical applications. In our case, the presence of hydroxyl groups, which is of great importance for some optical applications, can be quantified by measuring the absorption peak at a wavelength of around 3300 nm, i.e. for wavenumbers of around 3000 cm^{-1} [59]. To get a quantitative value, the measurement has to be carried out in transmittance mode. This technique can be also useful to determine the characteristic absorptions of different ions like the rare-earths. Typical portions of FTIR spectra for samples with different concentrations of specific ions are reported in Fig. 2.12. Furthermore, Attenuated Total Reflection (ATR) FTIR can be a valid method to perform structural analysis. It could be used to identify the nature of P-O-P bonds in a phosphate glass since it allows distinguishing the different transitions related to the Q^0, Q^1, Q^2, or Q^3 bonds [60].

Refractive index measurement

The precise measurement of the refractive index is carried out using a Metricon 2010 prism-coupled system, equipped with five lasers at different wavelengths (633, 825, 1061, 1312, and 1533 nm). The mechanism of signal detection is depicted in the sketch of Fig. 2.13a, while the typical signal measured with the detector is reported in Fig. 2.13b. The laser beams are launched through a prism on the polished surface of a glass sample. The sample is cut from the manufactured glass and is polished only on one side, i.e. the one which is brought into contact with the prism.

The scanning of the angle of incidence of the light onto the sample allows determining the total-internal-reflection angle with the formula $\theta_c = \arcsin(n/n_p)$, where n is the refractive index of the sample, n_p is the refractive index of the prism, and θ_c is the critical angle. By measuring θ_c, the system calculates and returns the value of the refractive index of the glass.

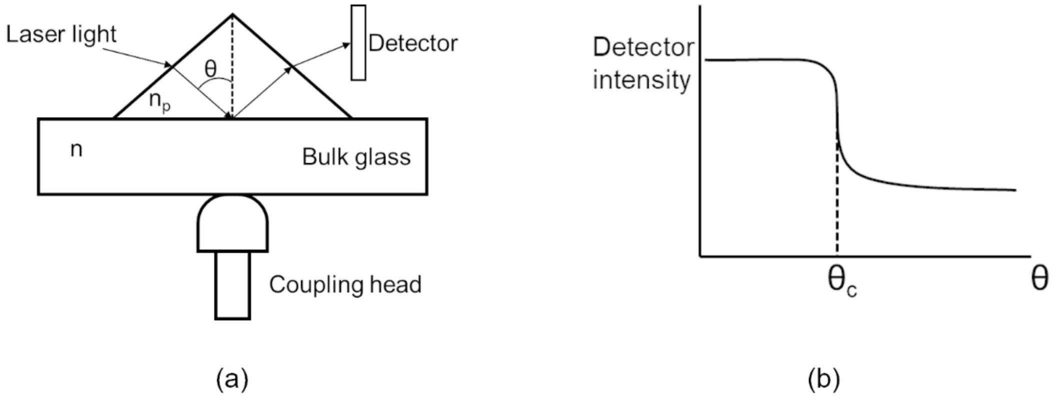

Fig. 2.13. The prism-coupling technique employed to measure the refractive index of glasses. (a) Schematic of the measurement and (b) typical signal detected, that allows measuring the critical angle θ_c.

Surface roughness determination

Surface roughness is an important parameter for several applications, especially in the optical field. We adopted different techniques to measure the surface properties of the produced glasses. We employed a contact profilometer (model Taylor Hobson Intra Touch 3D) to estimate the surface roughness and a BRUKER Innova Atomic Force

Microscopy (AFM) to go into details in the characterisation of the surface. The main limitation of the contact profilometers, related to the inaccuracy of the measurement in the situations described in Fig. 2.14, may be overcome with the AFM. Both measurements were conducted either on flat or on concave/convex samples. In the latter cases, post-processing was needed to subtract a curved profile from the measured data, allowing for the evaluation of conventional roughness parameters like the R_a. The determination of the R_a has been done according to the international standard UNI EN ISO 4288:2000 *Geometrical Product Specifications (GPS) – Surface texture: Profile method – Rules and procedures for the assessment of surface texture*.

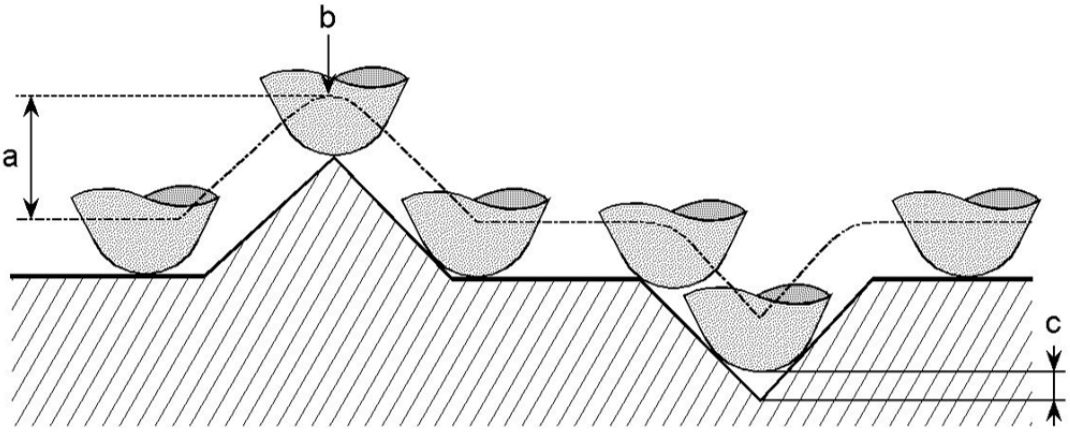

Fig. 2.14. The contact profilometer may have low accuracy. The dimension of the contact probe can influence the quality of the measurement.

2.2.4 Cold reshaping

Glass is commonly treated as such a fragile material that the possibility of cold-working is considered to be limited if not completely absent. However, with some careful attention, it is possible to reshape a bulk glass piece with almost the same conventional methods employed for metals. The following paragraphs present the most common techniques, employed also during the current work.

Drilling

Some of the analyses described above are carried out on a cylindrical glass sample, which is obtained by drilling a bore with an Optimum BF20 Vario vertical drill. The bore is carried out using core diamond-coated drills with an internal diameter of 6 mm, under a constant water flux on the drilling surface. In this way, both the heat and the debris are removed from the working area and a cylindrical sample with a diameter of 4 mm is obtained. The speed of the drill must be selected depending on the dimension of the bore, with a small hole, like in our case, corresponding to higher speed whereas a bigger hole requires lower speed.

Polishing

The polishing of a glass sample is a crucial aspect of glass manufacturing for optical applications. The cast glass shows a rough surface that must be polished – often by hand – to obtain the desired surface finish. This is carried out using standard SiC polishing papers with different textures, starting from the rougher. Furthermore, as explained above for some of the optical measurements, the requirement of the surface optical quality is mandatory. To achieve this on flat samples, with lateral dimension in the order of a 10 – 20 mm maximum and thickness of around 1 mm, a semi-automatic polishing machine (model Logitech PM 5) is employed. The samples are mounted on a sample holder using molten wax and the sample holder is inserted into a system that has an analogic indicator of the worn material. In this way, it is possible to limit the wearing to the prescribed amount. Different polishing materials are used on the polishing machine, made of powder of alumina diluted into water (with powder fineness ranging from 9 μm to 1 μm) or of diamond paste, the latter assuring the best quality of the results.

Cutting

The necessity of cutting glass samples arise for different reasons. The most common one is the removal of an unwanted part from the final product, e.g. the suction cone formed during cooling from the melt, at the end of the conventional process of fusion, casting into a mould, and annealing. This effect is due to standard shrinkage of the material upon cooling and, in glass manufacturing, unlike metals, it is not avoidable using special mould design, such as sprues. In the case of the casting of a glass cylinder, the suction cone must be removed to obtain an even bulk object. Furthermore, several samples employed in the standard analyses described above, or in other techniques like the ones described in Chapter 6, are obtained by cutting thin discs from the cast glasses. The cut is performed with a Bruehler IsoMet cutting machine, using a diamond-coated saw with oil as a lubricant. The speed of the cut is kept slow at both the beginning and the end of the cut, to avoid unwanted cracks.

2.2.5 Hot reshaping

Processing at high temperature is the most common technique for reshaping glass products. In the case of the present thesis, the employment of phosphate glasses allows reducing the working temperature in comparison with standard silica glass. Both the T_g and the T_s of these glasses are always below 600 °C. However, to have a homogeneous product, the casting of the glasses must be carried out at higher temperature (i.e. 1000-1400 °C, still well below the standard melting temperature of pure silica, but comparable with the processing temperature of soda-lime silicate glasses [1]).

Hot forming

The melting, casting, and annealing are among the most important aspects of glass manufacturing. A picture of the glass casting with a Pt/Rh crucible is reported in Fig. 2.15. The weighted reagents in powder-form and/or the pieces of the already cast glass are heated to the melting temperature, which is selected on the base of the glass composition. The facilities of our lab comprise a Nabertherm (max. temperature 1600 °C) and two vertical furnaces (maximum temperature 1400 °C) for glass melting. The molten glass can undergo two different treatment: if no definite shape of the product is needed the glass is melt-quenched on a cold flat plate. However, if there is the need for casting into a mould, the mould is pre-heated at a temperature that depends on the casting temperature, the shape of the mould, and the glass composition.

Fig. 2.15. Casting from a Pt/Rh crucible.

The casting operation must be carefully performed to avoid the formation of bubbles. Right after the casting, the mould with molten glass inside is placed into a furnace which is heated at a temperature around the T_g of the glass, left at that temperature for a few hours (usually between 2 and 5 hours depending on the size of the cast product), and then slowly cooled down to room temperature, so that any thermal stress is relieved. This process, called annealing, can be carried out in our lab in one of the following furnaces: Carbolite-Gero CWF 1200, Manfredi Warmy 9 muffle furnace, or Carbolite-Gero LHT 6-60. According to the formal definition, the *annealing point* is positioned at the temperature at which 95% of the internal stresses are relieved in 15 min [23]. The glass viscosity at that temperature is 10^{12} Pa·s, which is sometimes defined as the viscosity at the T_g. Besides, at the *strain point* the stress release occurs within around 6 h and the glass viscosity is $10^{13.5}$ Pa·s. Since we carry out the annealing at a temperature near the T_g, we prefer to extend the duration of this thermal treatment, to be sure that all the internal stresses have been relieved.

Extruding

The extrusion process will be explained in detail in Chapter 3 and its application to glasses is one of the main subjects of the whole thesis. Here it is introduced as one of the hot forming techniques that may be employed for glass reshaping. In general, extrusion consists of forcing a softened material to pass through a matrix, called *die*, and then hardening the obtained product to fix its shape. In the case of interest within the present work, extrusion is carried out by heating a bulk glass piece, squeeze it into the die, and then cool it down to harden the obtained extrudate. In comparison with glass melting and casting, the extrusion is carried out at a lower temperature since the glass must not flow under its own weight. However, the glass must also be soft enough to be forced to pass through a die. The actual extrusion temperature is determined, according to the shape of the die, by knowing the thermal behaviour of the glass – i.e. its characteristic temperatures (T_g, T_s, and $T_x^{(on)}$) and the viscosity-temperature relationship. About these temperatures, some details must be specified: the softening point is defined as the temperature at which a fibre, 0.55 – 0.75 mm diameter and 23.5 cm long of which the top 10 cm is heated at a rate of 5 K/min when suspended vertically in a furnace of specified characteristics, elongates under its own weight at a rate of 1 mm/min. This definition was formulated by Littleton [61] and is employed also by ASTM *C338 - 93(2019) Standard Test Method for Softening Point of Glass*. Furthermore, in our case, we measure the so-called *Dilatometric Softening Point* (*DSP*), which is the temperature at which a glass specimen starts to deform under a specific weight, i.e. a lower temperature compared to Littleton's softening point. For this reason, the extrusion trials are carried out at a temperature slightly higher than the measured DSP.

Drawing

The drawing of a preform is the final step in the realisation of a fibre. In optical applications, the preform must be designed and manufactured with specific attention to avoid contamination. Furthermore, the preform is often obtained as an assembly of different materials. The most common situation involves two glasses: a core and a cladding, i.e. glasses with respectively higher and lower refractive index, and with several dimensional, thermal, and optical requirements. However, also a combination of three or even more materials with diverse shapes can be adopted, thus obtaining multi-material fibres. During the work for the present thesis, several fibres have been made, using the drawing tower facility present inside the LINKS Foundation laboratories. In this brief introduction, we can describe a drawing tower as an apparatus consisting of a preform holder, whose movement is controlled via a micrometric screw, a heating element, and a winding drum. The preform is fed into the heated portion of the system, and the heating temperature must be above the T_s of the glass but still at a lower temperature than the one required during casting. In this way, the glass starts falling under its own weight, and the filament that is formed is quickly cooled and woven on the winding drum. The special characteristic of a drawn fibre is that it retains the geometrical proportions of the preform, scaled down by a factor of $10^2 – 10^4$. This is a great option to miniaturise the product and achieve optical, electrical, and mechanical properties that are all related to its micrometric features.

2.3 Conclusions

In the present chapter, phosphate glasses have been introduced in terms of their peculiar properties, applications, and characterisation techniques. The main processing technologies employed during the current work have also been considered and will be further analysed in the next chapters. The potential impacts and applications of the designed, produced, and studied glasses are quite broad and will be discussed in detail within the dedicated paragraphs of the next sections. However, as a result of an applied research thesis, the three main glass compositions introduced in the current chapter, and the acquired knowledge that was necessary to manufacture, handle, and characterise them, represent a milestone in the educational path of a material scientist. Working with oxide glasses, as emerged in the current chapter but will be even clearer in the following, does not only mean learning how to handle the glass itself, but requires a complex awareness of the interaction of this material with other substances, which can be another glass, a different solid (metal, ceramic, or polymer), an organic/inorganic liquid, or a gas. Furthermore, post-treatment techniques were required, either at ambient temperature or with heating involved, and proficiency in the phenomena of wear, corrosion, fracture mechanics, and general mechanical behaviour has been necessary and well addressed during the course of the present research. Among the aims of the present thesis, there is not only to develop new materials but also to learn how to forge them, and post-process them, as well as study their behaviour through advanced modelling, in order to match the requirement of the final applications, which must be kept in mind at all time. For this reason, the next chapter deals with the main glass processing techniques adopted in the present work to transform a material with interesting properties into a usable device.

References

[1] G. W. Morey, *The Properties of Glass*, 2nd ed. New York, NY: Reinhold Publishing, 1954.

[2] Pliny The Elder, H. T. Riley, e J. Bostock, *The Natural History of Pliny*, 6 voll. London, UK: H. G. Bohn, 1855.

[3] W. M. F. Petrie, *The Making of Egypt*. London, UK: Sheldon Press, 1939.

[4] D. L. Morse e J. W. Evenson, «Welcome to the Glass Age», *International Journal of Applied Glass Science*, vol. 7, n. 4, pagg. 409–412, 2016, doi: 10.1111/ijag.12242.

[5] S. Johnson, *How We Got to Now - Six Innovations That Made the Modern World*. New York: Riverhead Books - Penguin Group, 2014.

[6] W. H. Zachariasen, «The atomic arrangement in glass», *Journal of the American Chemical Society*, vol. 54, n. 10, pagg. 3841–3851, 1932, doi: 10.1021/ja01349a006.

[7] G. H. J. A. Tammann, *Der Glaszustand*. Leipzig, Germany: Leopold Voss Verlag, 1933.

[8] Doremus, R.H., *Glass Science*. New York, NY: Wiley-Interscience, 1973.

[9] A. R. Cooper e P. K. Gupta, «An Operational Definition of the Glassy State», *Journal of the American Ceramic Society*, vol. 58, n. 7–8, pagg. 350–351, 1975, doi: 10.1111/j.1151-2916.1975.tb11507.x.

[10] J. Wong e C. A. Angell, *Glass: Structure by Spectroscopy*. New York, NY: Marcel Dekker, 1976.

[11] E. A. Mari, *Los vidrios : propiedades, tecnologías de fabricación y aplicaciones*. Buenos Aires, Argentina: Editorial Américalee, 1982.

[12] J. Zarzycki, *Les verres et l'état vitreux*. Paris, France: Masson, 1982.

[13] P. K. Gupta, «Non-crystalline solids: Glasses and amorphous solids», *Journal of Non-Crystalline Solids*, vol. 195, n. 1–2, pagg. 158–164, 1996, doi: 10.1016/0022-3093(95)00502-1.

[14] K. J. Rao, *Structural Chemistry of Glasses*. Oxford, UK: Elsevier, 2002.

[15] J. E. Shelby, *Introduction to Glass Science and Technology*, 2nd ed. London, UK: Royal Society of Chemistry, 2015.

[16] I. S. Gutzow e J. Schmelzer, *The Vitreous State: Thermodynamics, Structure, Rheology, and Crystallization*, 2nd ed. Heidelberg, Germany: Springer International Publishing, 2013.

[17] A. Varshneya e J. C. Mauro, «Comment on misconceived ASTM definition of 'glass'», *Glass Technology. European Journal of Glass Science and Technology. Part A*, vol. 51, n. 1, pagg. 28–30, 2010.

[18] A. Varshneya, *Fundamentals of Inorganic Glasses*, 2nd ed. San Diego, CA: Academic Press, 2013.

[19] E. D. Zanotto e J. C. Mauro, «The glassy state of matter: Its definition and ultimate fate», *Journal of Non-Crystalline Solids*, vol. 471, n. March, pagg. 490–495, 2017, doi: 10.1016/j.jnoncrysol.2017.05.019.

[20] A. I. Popov, «What is glass?», *Journal of Non-Crystalline Solids*, vol. 502, n. January, pagg. 249–250, 2018, doi: 10.1016/j.jnoncrysol.2018.01.039.

[21] E. D. Zanotto e J. C. Mauro, «Response to comment on "The glassy state of matter: Its definition and ultimate fate"», *Journal of Non-Crystalline Solids*, vol. 502, n. January, pagg. 251–252, 2018, doi: 10.1016/j.jnoncrysol.2018.01.040.

[22] R. Rajaramakrishna e J. Kaewkhao, «Glass material and their advanced applications», *UNNES International Conference on Research Innovation and Commercialization 2018, KnE Social Sciences*, pagg. 796–807, 2019, doi: 10.18502/kss.v3i18.4769.

[23] A. Varshneya e J. C. Mauro, *Fundamentals of Inorganic Glasses*, 3rd ed. Cambridge, MA: Elsevier, 2019.

[24] W. Vogel, *Glass Chemistry*, 2nd ed. Heidelberg, Germany: Springer International Publishing, 1994.

[25] K. Sun, «Fundamental Condition of Glass Formation», *Journal of the American Ceramic Society*, vol. 30, n. 9, pagg. 277–281, 1947, doi: 10.1111/j.1151-2916.1947.tb19654.x.

[26] J. C. Phillips, «Topology of covalent non-crystalline solids: Short-range order in chalcogenide alloys», *Journal of Non-Crystalline Solids*, vol. 34, pagg. 153–181, 1979, doi: 10.1016/0921-4526(95)00390-U.

[27] J. R. van Wazer, *Phosphorus and Its Compounds*. New York, NY: Interscience Publishers, 1974.

[28] J. C. Knowles, «Phosphate based glasses for biomedical applications», *Journal of Materials Chemistry*, vol. 13, n. 10, pagg. 2395–2401, 2003, doi: 10.1039/b307119g.

[29] D. S. Brauer, «Degradable Phosphate Glasses and Composite Materials for Biomedical Applications», PhD Thesis, Friedrich-Schiller-Universität, Jena, Germany, 2005.

[30] E. A. Abou Neel e J. C. Knowles, «Biocompatibility and other properties of phosphate-based glasses for medical applications», in *Cellular Response to Biomaterials*, Woodhead Publishing, 2009, pagg. 156–182.

[31] E. A. Abou Neel *et al.*, «Bioactive functional materials: a perspective on phosphate-based glasses», *Journal of Materials Chemistry*, vol. 19, pagg. 690–701, 2009, doi: 10.1039/b810675d.

[32] E. Ceci Ginistrelli, «Advanced applications of phosphate glass optical fibres in photonics and biophotonics», PhD Thesis, Politecnico di Torino, Turin, Italy, 2018.

[33] P. Y. Shih, «Properties and FTIR spectra of lead phosphate glasses for nuclear waste immobilization», *Materials Chemistry and Physics*, vol. 80, n. 1, pagg. 299–304, 2003, doi: 10.1016/S0254-0584(02)00516-3.

[34] N. Sharmin e C. D. Rudd, «Structure, thermal properties, dissolution behaviour and biomedical applications of phosphate glasses and fibres: a review», *Journal of Materials Science*, vol. 52, n. 15, pagg. 8733–8760, 2017, doi: 10.1007/s10853-017-0784-4.

[35] C. K. Loong, K. Suzuya, D. L. Price, B. C. Sales, e L. A. Boatner, «Structure and dynamics of phosphate glasses: From ultra- to orthophosphate composition», *Physica B: Condensed Matter*, vol. 241–243, pagg. 890–896, 1998, doi: 10.1016/S0921-4526(97)00747-3.

[36] R. K. Brow, «Review: the structure of simple phosphate glasses», *Journal of Non-Crystalline Solids*, vol. 263–264, pagg. 1–28, mar. 2000, doi: 10.1016/S0022-3093(99)00620-1.

[37] R. K. Brow, R. J. Kirkpatrick, e G. L. Turner, «The short range structure of sodium phosphate glasses», *Journal of Non-Crystalline Solids*, vol. 116, n. 1, pagg. 39–45, 1990, doi: 10.1016/0022-3093(90)91043-Q.

[38] R. K. Brow, C. A. Click, e T. M. Alam, «Modifier coordination and phosphate glass networks», *Journal of Non-Crystalline Solids*, vol. 274, pagg. 9–16, 2000.

[39] E. Mura, J. Lousteau, D. Milanese, S. Abrate, e V. M. Sglavo, «Phosphate glasses for optical fibers: Synthesis, characterization and mechanical properties», *Journal of Non-Crystalline Solids*, vol. 362, n. 1, pagg. 147–151, 2013, doi: 10.1016/j.jnoncrysol.2012.11.029.

[40] B. C. Bunker, G. W. Arnold, e J. A. Wilder, «Phosphate glass dissolution in aqueous solutions», *Journal of Non-Crystalline Solids*, vol. 64, n. 3, pagg. 291–316, 1984, doi: 10.1016/0022-3093(84)90184-4.

[41] B. C. Sales e L. A. Boatner, «Physical and chemical characteristics of lead-iron phosphate nuclear waste glasses», *Journal of Non-Crystalline Solids*, vol. 79, n. 1–2, pagg. 83–116, 1986, doi: 10.1016/0022-3093(86)90040-2.

[42] J. A. Wilder, «Glasses and glass ceramics for sealing to aluminum alloys», *Journal of Non-Crystalline Solids*, vol. 38–39, pagg. 879–884, 1980, doi: 10.1016/0022-3093(80)90548-7.

[43] T. Minami, Y. Takuma, e M. Tanaka, «Superionic Conducting Glasses: Glass Formation and Conductivity in the AgI-Ag2O-P2O5 System», *Journal of Electrochemical Society*, vol. 124, pagg. 1659–1662, 1977, doi: 10.1111/j.1151-2916.1981.tb10277.x.

[44] S. W. Martin, «Ionic Conduction in Phosphate Glasses», *Journal of the American Ceramic Society*, vol. 74, n. 8, pagg. 1767–1784, 1991, doi: 10.1111/j.1151-2916.1991.tb07788.x.

[45] M. J. Weber, L. A. Boatner, e B. C. Sales, «Optical properties of Nd3+ in lead phosphate glasses», *Journal of Non-Crystalline Solids*, vol. 74, n. 1, pagg. 167–170, 1985, doi: 10.1016/0022-3093(85)90410-7.

[46] B. C. Sales, L. A. Boatner, e S. W. Allison, «Lead-Indium Phosphate Glasses for Optical Applications», in *SPIE's 1994 International Symposium on Optics, Imaging, and Instrumentation*, 1994, vol. 2287, pagg. 0–6.

[47] J. A. Duffy e M. D. Ingram, «An interpretation of glass chemistry in terms of the optical basicity concept», *Journal of Non-Crystalline Solids*, vol. 21, n. 3, pagg. 373–410, 1976, doi: 10.1016/0022-3093(76)90027-2.

[48] D. Pugliese *et al.*, «Concentration quenching in an Er-doped phosphate glass for compact optical lasers and amplifiers», *Journal of Alloys and Compounds*, vol. 657, pagg. 678–683, 2016, doi: 10.1016/j.jallcom.2015.10.126.

[49] R. Stepien, M. Franczyk, D. Pysz, I. Kujawa, M. Klimczak, e R. Buczynski, «Ytterbium-phosphate glass for microstructured fiber laser», *Materials*, vol. 7, n. 6, pagg. 4723–4738, 2014, doi: 10.3390/ma7064723.

[50] N. Boetti, D. Pugliese, E. Ceci-Ginistrelli, J. Lousteau, D. Janner, e D. Milanese, «Highly Doped Phosphate Glass Fibers for Compact Lasers and Amplifiers: A Review», *Applied Sciences*, vol. 7, n. 12, pag. 1295, 2017, doi: 10.3390/app7121295.

[51] D. J. Richardson, J. Nilsson, e W. A. Clarkson, «High power fiber lasers: current status and future perspectives [Invited]», *Journal of the Optical Society of America B*, vol. 27, n. 11, pag. B63, 2010, doi: 10.1364/josab.27.000b63.

[52] I. Ahmed, C. A. Collins, M. P. Lewis, I. Olsen, e J. C. Knowles, «Processing, characterisation and biocompatibility of iron-phosphate glass fibres for tissue engineering», *Biomaterials*, vol. 25, n. 16, pagg. 3223–3232, 2004, doi: 10.1016/j.biomaterials.2003.10.013.

[53] Y.-P. Kim *et al.*, «Phosphate glass fibres promote neurite outgrowth and early regeneration in a peripheral nerve injury model», *Journal of Tissue Engineering and Regenerative Medicine*, vol. 9, n. 3, pagg. 236–246, 2015, doi: 10.1002/term.

[54] C. Vitale-Brovarone, G. Novajra, J. Lousteau, D. Milanese, S. Raimondo, e M. Fornaro, «Phosphate glass fibres and their role in neuronal polarization and axonal growth direction», *Acta Biomaterialia*, vol. 8, n. 3, pagg. 1125–1136, 2012, doi: 10.1016/j.actbio.2011.11.018.

[55] E. A. Abou Neel, I. Ahmed, J. Pratten, S. N. Nazhat, e J. C. Knowles, «Characterisation of antibacterial copper releasing degradable phosphate glass fibres», *Biomaterials*, vol. 26, n. 15, pagg. 2247–2254, 2005, doi: 10.1016/j.biomaterials.2004.07.024.

[56] E. Ceci-Ginistrelli *et al.*, «Novel Biocompatible and Resorbable UV-Transparent Phosphate Glass Based Optical Fiber», *Optical Materials Express*, vol. 6, n. 6, pagg. 2040–2051, 2016, doi: 10.1364/OME.6.002040.

[57] D. S. Viswanath, T. K. Ghosh, D. H. L. Prasad, N. V. K. Dutt, e K. Y. Rani, *Viscosity of liquids - Theory, Estimation, Experiment, and Data*. Dordrecht, The Netherlands: Springer International Publishing, 2007.

[58] T. G. Mezger, *The Rheology Handbook*, 4th ed. Hanover, Germany: Vincentz Network, 2014.

[59] A. M. Efimov e V. G. Pogareva, «Water-related IR absorption spectra for some phosphate and silicate glasses», *Journal of Non-Crystalline Solids*, vol. 275, n. 3, pagg. 189–198, ott. 2000, doi: 10.1016/S0022-3093(00)00250-7.

[60] P. Stoch, A. Stoch, M. Ciecinska, I. Krakowiak, e M. Sitarz, «Structure of phosphate and iron-phosphate glasses by DFT calculations and FTIR/Raman spectroscopy», *Journal of Non-Crystalline Solids*, vol. 450, pagg. 48–60, ott. 2016, doi: 10.1016/j.jnoncrysol.2016.07.027.

[61] J. T. Littleton, «The Softening Point of Glass», *Transaction of the Society of Glass Technology*, vol. 24, pagg. 176–185, 1940.

Chapter 3.

Glass extrusion and fibre drawing

3.1. Introduction

In the current chapter, we will focus on the two main glass processing technologies adopted in the framework of the present thesis: extrusion and fibre drawing. These techniques were already introduced in Chapter 2.

The next paragraphs will deal with an introduction about some common techniques adopted in glass manufacturing together with their evolution; afterwards, some fundamentals of process control and data recording will be introduced. Finally, the two main topics will be explained in detail in two dedicated sections, specifying all the steps that can lead to the optimisation of the extrusion process and the subsequent drawing of the extruded preform into an optical fibre.

3.1.1. Glass processing technologies

Glass production is currently a worldwide fundamental field of manufacturing, involving several industrial processes and requiring profound expertise. The greatest part of glass production has shifted, in the last century, towards the industry. Molten glass is usually reshaped by standard blowing, pressed in a mould (hot-pressing), directly cast from the melt into the desired final shape, with eventual final steps of hot “fire” polishing or cold mechanical finishing, etc. One great example of the recent (r)evolution of the glass sector is the manufacturing of flat glass, which has passed from a complex and heavy handcrafted job that yielded low-quality products to an automated, scalable, and exceptionally productive industrial process. In fact, for several centuries, the flat glass used for windows has been produced by two main routes: the *Crown* process and the *cylinder* processes [1], [2].

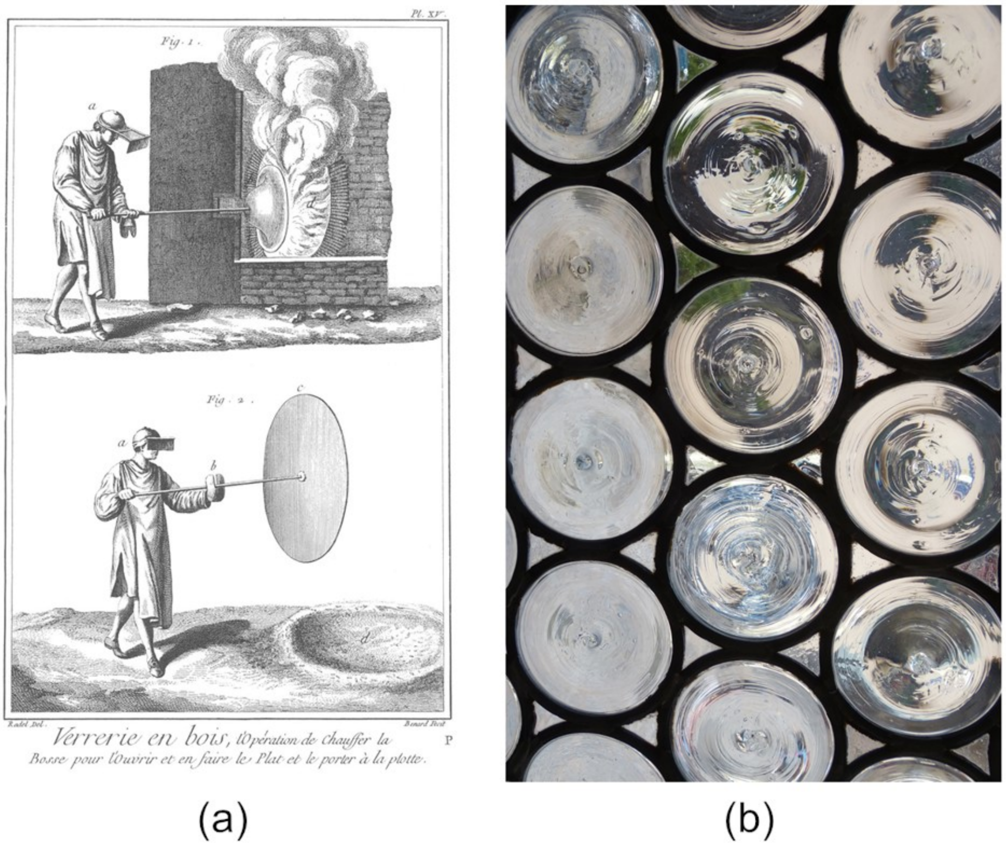

Fig. 3.1. Illustration showing the process of Crown flat glass production, taken from *Encyclopédie ou Dictionnaire raisonné des sciences, des arts et des métiers. XVIII sec (France)*. Image available in the public domain. (b) Bull's-eye windowpane window from Albrecht Dürer's house in Nuremberg (Bavaria, Germany) [Author: Wolfgang Sauber]. Image adapted under Creative Commons Attribution-Share Alike 4.0 International license.

The first one is illustrated in Fig. 3.1a and consists of blowing an almost spherical glass globe and putting it under rotation, so to produce a flat glass disc thanks to the centrifugal effect. In this way, several rounded glass discs were produced and mounted together on a metal grid to obtain a semi-transparent window (the so-called stained glass), shown in Fig. 3.1b; while it seems easy to explain the principle of this process, it requires great skills and know-how, and the result has poor quality. The *cylinder* process is even more complex because it involves the blowing of a huge cylinder (Fig. 3.2a) which is then split open and flattened by reheating; besides a deep and unconventional mastery, this latter technique is also labour-intensive and requires great physical strength; furthermore, the obtained piece is uneven (see Fig. 3.2b), and its flatness only relies upon the artisan skills.

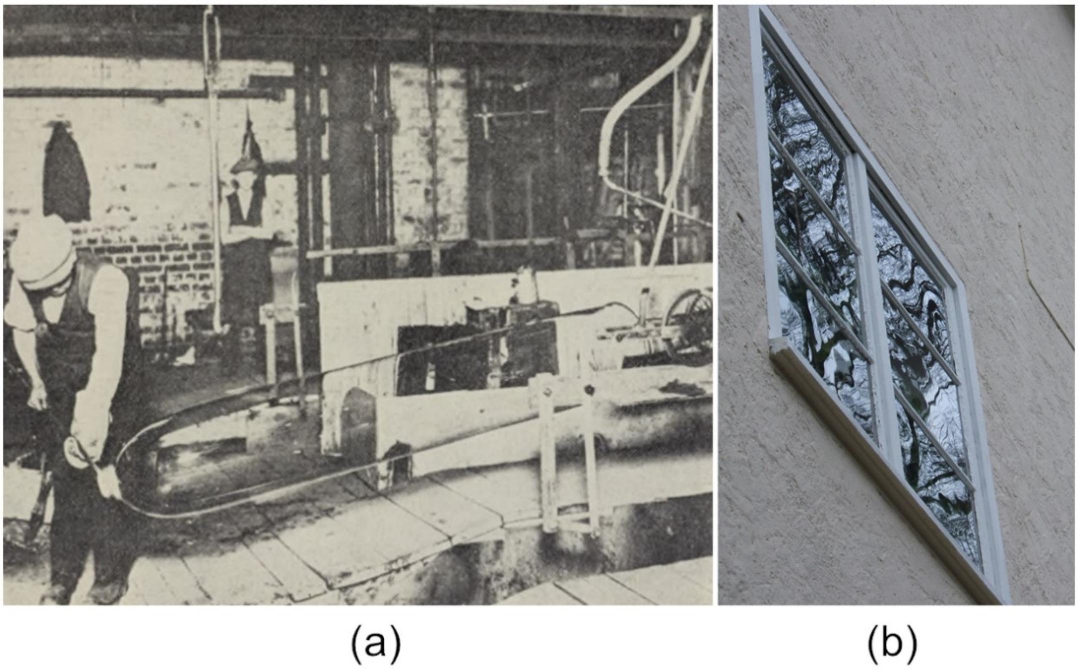

Fig. 3.2. (a) Glass made by the cylinder process had to be split and flattened for windows, adapted from [3]. (b) An old window made from soda-lime flat glass; the distorted reflections of a tree indicate the uneven surface of the glass. Image available in the public domain.

Several other processes have been developed during the 20th century to produce flat glass: the Fourcault flat glass drawing process, the Colburn-Libbey-Owens flat drawn process, the Corning fusion draw, and the Boudin continuous double-roll process, to give some examples [2]. Going into details of these processes is outside the scope of the present thesis, although it is worth underlining the progress that allowed to reach the best-quality glass products.

The decisive solution had come from a simple and brilliant idea finally developed in the '50s and explained in detail a few years later in a paper by Sir Alastair Pilkington [3]. A schematic representation of the so-called *Pilkington* or *float glass* process was included in that paper and is shown in Fig. 3.3. This is an automatic process that allows producing high-quality and low-distortion glass sheet with virtually no limitations in dimensions. This process takes advantage of the buoyancy of the molten glass over a tin bath; the glass floats on the tin bath and two highly uniform surfaces are obtained, one in contact with the metal and the other with a reducing atmosphere. The introduction and the subsequent refinements of the float glass process have revolutionised the glass industry [4]. Almost all the flat glass produced nowadays is obtained with the Pilkington process [5].

The previous example shows how the glass industry has changed during the current technological revolution. Yet, especially in the research field and in the art-glass manufacturing, the basic processes involved are not so different from the most ancient

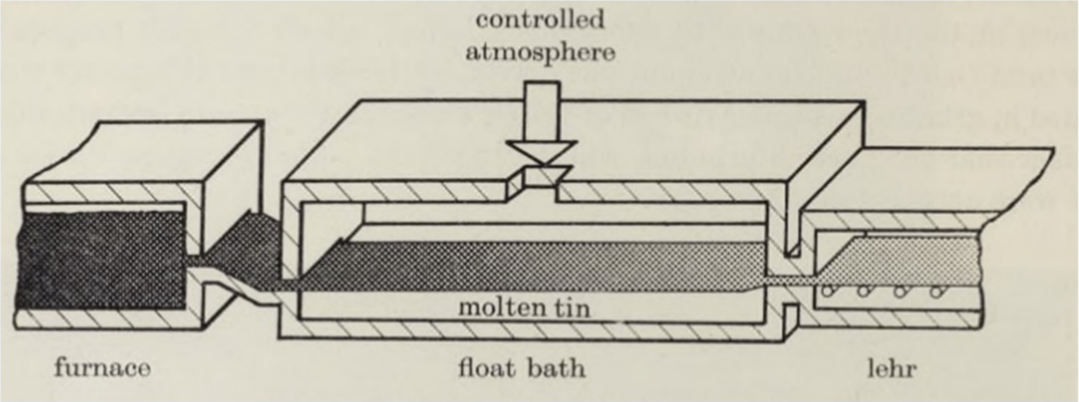

Fig. 3.3. Diagram of the float process, reproduced from [3].

ones: melting and casting from a crucible, blowing, drawing, or moulding, cold reshaping with hard diamond tools, to cite a few. Still, during the last fifty years, a tremendous improvement in the understanding of the physics and chemistry underneath the glass production has been experienced, due to the constant work of glass manufacturers and researchers. This growing knowledge is modifying how we perceive the glassy state and its applications. As it is clear from the debate on the formal definition of the word *glass* in the scientific community, illustrated in Chapter 2, the progress in glass science and technology is still ongoing, despite the *art* of making glass is something that humankind has learned since its civilisation.

After the Industrial Revolution, and especially along the 20th century, the increasing demand for glass product manufacturing – and related process control and automation – has pushed the scientific sector to question the nature of glass and its behaviour. Moreover, some of the modern discoveries, such as, in the technological field, electron microscopies or molecular spectroscopies, but also extensive measurement devices and related data analyses, or advanced simulation tools provided by the constantly increasing computing power of PCs, allowed to unveil aspects of the glass science that were unexpected beforehand. In glass science, like in the whole material science, there is still a lot to be discovered, starting from the material compositions and processing, but also moving further and investigating the interaction of different materials for the production of multi-material multifunctional devices [6]. Focusing on glass science, as suggested by Morse & Evenson [7] there is the need to reveal the great capabilities, versatility, and potential impacts of new discoveries to the widest public. The same authors also suggest that bridges are needed in the global glass community to create deep collaborations between corporations, universities, and professional associations so to obtain a supply of funding from government agencies and the private sector, ensuring both the greatest benefits to society and career opportunities for glass scientists and engineers. Finally, Morse & Evenson argue that "we need to invest in the science of glass processing as well as glass composition because that is how we turn innovative compositions into useful objects" [7].

In the optics field, Bach & Neuroth, affirm that “Glass has been and will continue to be the material of choice for imaging optics” [8]. And they also think that new applications of glass in optics and optoelectronics are numerous and among those, it is possible to mention substrate glass, micro-lenses, gradient index optics, precision moulding of optical glass, integrated optics, glasses for light modulation, etc [8].

A process like the drawing of glass fibre can have (and already had in the recent past) great importance in the development of modern devices. In fact, as a vision for the near future, some also suggest the possibility of having smart fabrics and textile, that “hear, sense and communicate” [9]. The power of this idea is disruptive. Furthermore, if we focus on optical fibres for telecommunication it is worth noting that their employment had a terrific growth: the theoretical background for light guiding was established in the 1850s by Tyndall, or, as recently demonstrated, even a few years before by Daniel Colladon [10]. Then, Bell’s Photophone had shown the feasibility of optical communication, back in 1880 [11]. Yet, the first modern optical fibres for telecommunication were started to be laid in the late 1970s, and since then, with the worldwide spreading of the internet, the rate of growth is exponential [12]. Some information is here reported to give an idea of the global optical fibres demand: the estimated length of submarine optical cables (composed of a huge bundle of multiple glass fibres) in service at the moment is 1.2 million km[6], i.e. enough to wind up the equator 30 times. Furthermore, the International Cablemakers Federation in 2016 has estimated the global consumption of optical fibres[7] beyond 400 million km: more than five trips to Mars! This tremendous increase in the global need for glass fibres for optical telecommunications was allowed also by the high scalability of the drawing process: the drawing of telecom fibres from preform allows to produce more than one km of ready-to-use product each minute[8], and for 1 kg of preform material, nearly 32 km of fibre are obtained[7].

The present thesis is focused on two strictly related glass manufacturing processes, i.e. preform making and fibre drawing. In particular, we will deal with novel optical fibres made of *soft glasses* and intended to be used for applications in biomedicine or environmental sensing. Some introductory aspects were described herein, but our glasses are neither similar to the common containers and windows glasses nor to the standard telecom optical fibres glass; and our process of fibre drawing is comparable, for some aspects, to the industrial drawing of silica fibres but also shows remarkable differences.

---

[6] TeleGeography: https://www.submarinecablemap.com/

[7] Intl. Cablemakers Federation: https://www.icf.at/news/icf-news-78-2017-apr/raw-materials-update/

[8] The Fiber Optics Association Inc.: https://www.thefoa.org/tech/fibr-mfg.htm

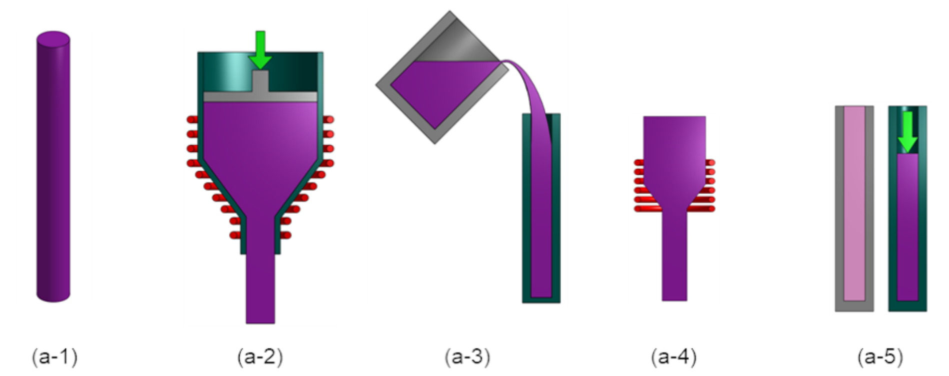

(a) core

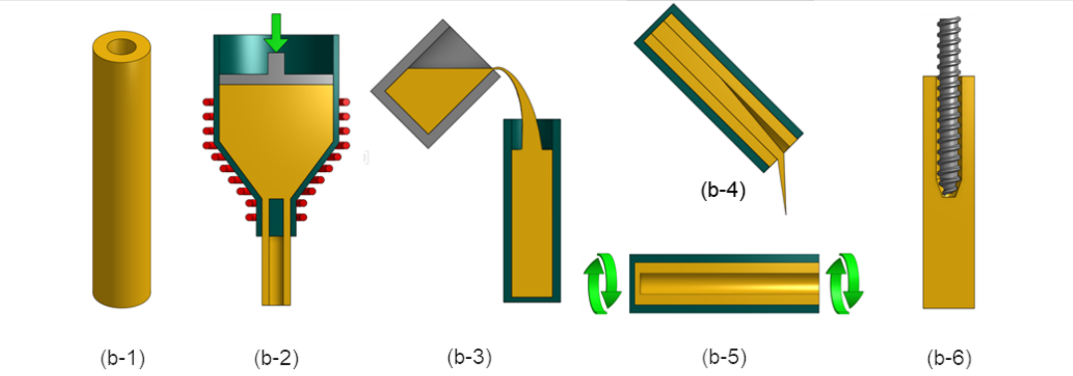

(b) cladding

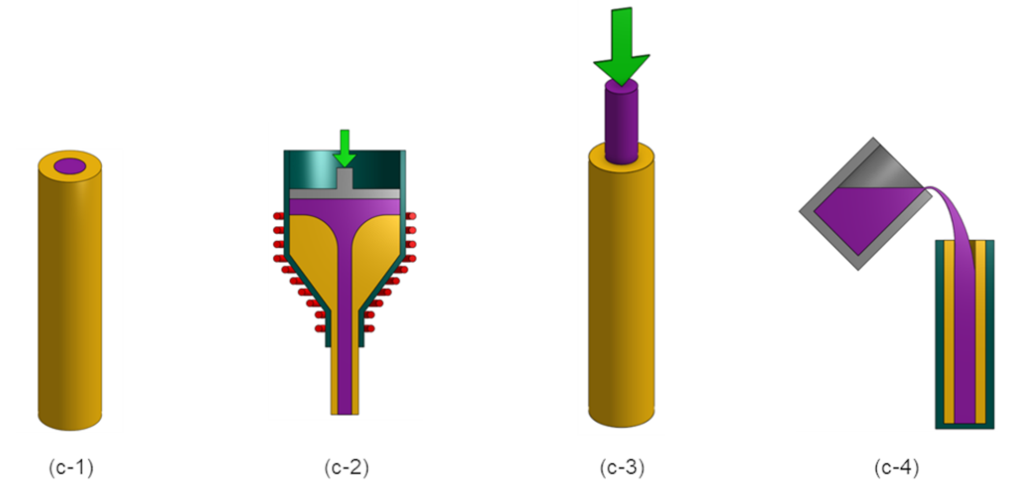

(c) core/cladding

continued

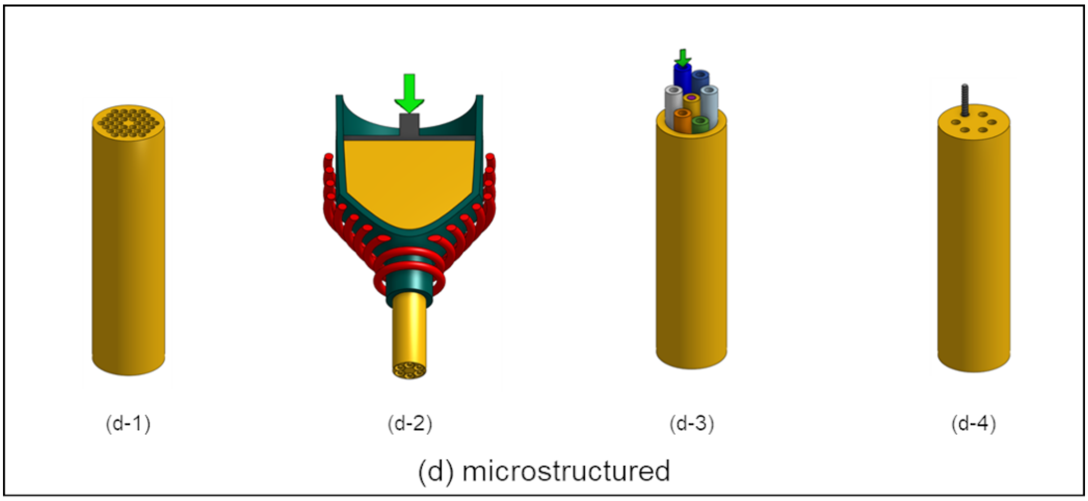

(d) microstructured

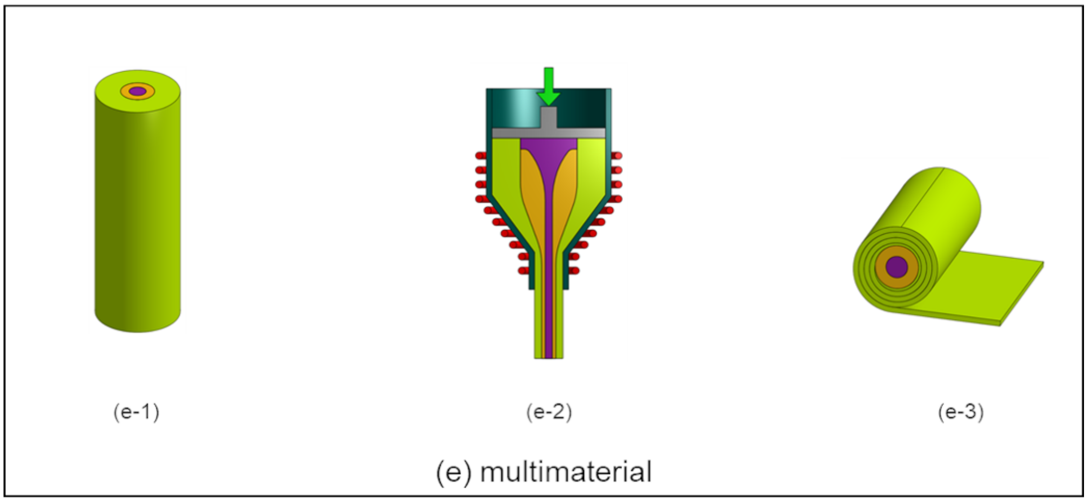

(e) multimaterial

Fig. 3.4. The main techniques employed in preform making: (a) core production, (b) cladding production, (c) core/clad preform, (d) microstructured preform, (e) multi-material preform. In detail: a core rod (a-1) can be obtained either through (a-2) extrusion, (a-3) casting, (a-4) thermal drawing, or (a-5) hot pressing. A cladding tube (b-1) can be formed by (b-2) extrusion, (b-3)-(b-4) direct casting or (b-3)-(b-5) rotational casting, as well as (b-6) hole drilling. A core/cladding preform (c-1) can be produced by (c-2) direct core/cladding co-extrusion, (c-3) rod-in-tube assembly, or (c-4) rod-in-tube casting. A microstructured preform (d-1) can be obtained via (d-2) direct microstructured extrusion, (d-3) stack-and-draw, or (d-4) hole drilling. Finally, a multi-material preform (e-1), composed of core/cladding glasses and polymer jacket, can be formed either with (e-2) direct multi-material co-extrusion or (e-3) polymer film rolling.[13].

The glass-preform making, at a laboratory level, usually always start with mould casting, a simple yet effective and widely adopted system. For the basic preform, i.e. a rod, this method can be self-sufficient. However, to obtain more complex structures, several routes can be followed: the cast rod can be reshaped by drilling, coring, and polishing, but it can also be fused with different materials with a rolling technique [13], [14] or combined with other rods or tubes, thus obtaining multi-material fibres [6], [15], [16]. A pictorial overview of the most important methodologies employed for preform production is presented in Fig. 3.4.

The simplest structure for optical confinement of light is the core/cladding structure of a standard optical fibre, which can be obtained by drawing from crucible [17], co-extrusion [18], [19], as well as a straightforward method like the rod-in-tube technique [20]–[22]. This latter process consists of directly inserting the casted rod into a tube, to obtain a preform. Despite its simplicity, it can allow forming structures with a high level of complexity [23], [24], by combining several rods, which can be made of different materials, with a tube that can be produced with several holes.

Mechanical or ultrasonic drilling of a tube was demonstrated for polymer materials [25], as well as for glasses [26]. This technique can lead to interesting results, but the cleaning of the preform to obtain a polished surface can be rather difficult [27], [28].

In general, the main advantage of glass in comparison with other crystalline materials is the possibility of the transition from the liquid-like to the highly viscous behaviour, and finally to the solid-state without degradation. This explains why the methods that involve reshaping at high temperature are substantially more powerful when dealing with glass, even if sometimes low-temperature mechanical processing is unavoidable (one important example of this latter aspect is the production of high-quality lenses, where cold polishing is mandatory [8]). In the field of industrial tube production, the power of glass reshaping from the molten state is demonstrated with the continuous casting for the fabrication of long tubes, which are used in many common applications, from pipes to neon lights [2]. On a lab-scale, a technique often employed is rotational casting, which consists of casting the molten glass into a high-speed rotating mould, so to produce a hollow structure due to the centrifugal effect. This method has been widely employed in our research group with interesting results [29]–[35] but it has limited flexibility in terms of dimensional ratio, which indeed hinders both the design flexibility and the option to scale up the process.

In the framework of the present thesis, the chosen method to produce complex and hollow structures is extrusion. This is a highly flexible, scalable, and powerful technique [36]–[41]. It allows producing preforms with arbitrary shapes, by purposely designing the extrusion die. The disadvantages are related to the unwanted preform distortions, which may be overcome with some expedients that will be discussed in the next paragraphs and chapters. The combination of preform extrusion and fibre drawing is a great option to investigate: two adaptable techniques that, together, offer potential interests either for a research project or in an applied manufacturing field.

In the following sections, the two techniques are presented along with the methods employed for their control and analysis. After a brief introduction about the fundamentals of process control, and the importance of significant data collection during experiments, the extrusion system developed during the present thesis is analysed, detailing all the aspects of the extrusion process. The choices that have been made during the design of the current extruder are explained, also with the support of systems analysis and modelling tools employed to achieve optimal control of the process. Then, the soft glass drawing tower is described and some of the results are presented.

3.1.2. Automatic process control

Every industrial or laboratory process that involves two or more variables like the ones described herein, could be the subject of a standalone work focused on process control. Both the techniques of preform extrusion and fibre drawing involve simultaneous heating and the application of a force, either by pushing or pulling the glass material. The design of a system to continuously track and even control these two variables together is fundamental. In the present paragraph, these two processes will be considered separately for the sake of clarity and without loss of generality.

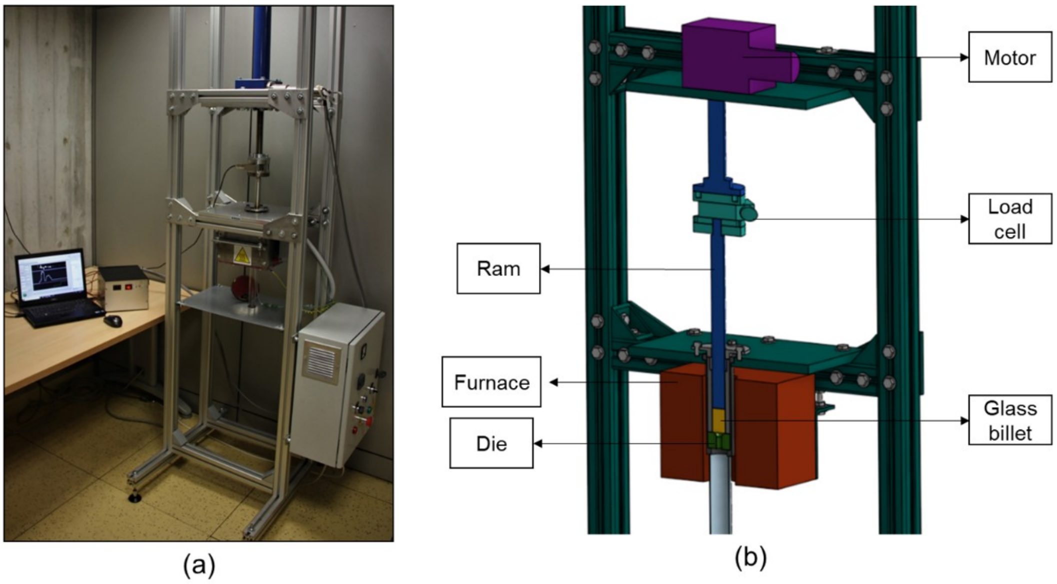

Fig. 3.5. The extrusion system. (a) Picture of the extruder together with the controlling unit, situated within the LINKS Foundation laboratories; (b) cutaway 3D drawing highlighting the main extruder components.

The vertical extrusion systems, like the one described herein, need a partially viscous material. In our case, the optimal glass viscosity result to be in the range between 10^7 – 10^9 Pa·s. With these viscosity values, the glass is sufficiently soft to be pushed inside the extrusion die but not too fluid to lose the imposed shape because of elongation due to gravity. The heat necessary to soften the material is supplied through an electrical heating system. The control of the heating is provided with a thermocouple, which must be near the glass itself but cannot get into contact with it, to avoid contamination of the product and sticking of the glass to the thermocouple. In the case of the extruder built during this thesis, the controlling thermocouple is positioned at the base of the extrusion die, and the heating elements surround the whole glass-holding metal supports. A picture of the extruder is reported in Fig. 3.5, while more detailed representations are provided in the next sections. The electrical heating resistances are controlled through a Eurotherm 3216 PID (Proportional-Integral-Derivative) controller, which has been calibrated on purpose. In this way, a stable temperature value can be reached and maintained, with minimum overshooting. Furthermore, the temperature can be changed rapidly during the extrusion process, according to the specific need. The other controlled element of the extruder is the ram, which is connected to a Maxon motor (model. DCX35L GB KL 24V equipped with planetary gearhead and speed sensor controlled by an ESCON 70/10 servo controller) with a calibrated digital-to-analogue conversion. The moving ram is also connected to a load cell that measures the load exerted on the heated glass piece. The load cell allows having a feedback control on both the speed of the motor and the temperature of the furnace. As will be further explained in the next paragraphs, the shape of the load curve when the piston encounters the glass gives an indication about the tendency of this latter to flow (i.e. about the viscosity of the glass) thus the eventual need of modifying the temperature or the motor speed.

The extruder employed in the present work is currently situated in the LINKS Foundation laboratories. Some of its components were built before the beginning of the present PhD, but its current shape is the result of several substantial interventions, carried out as part of the current project, that allowed for a thorough optimisation of the system. Also, to obtain a more functional and reliable extrusion system, we improved the control of the system, starting with the replacement of the simple on/off furnace controller with a more accurate device. Furthermore, no solution was developed to simultaneously control and monitor the temperature of the glass, the speed of the piston, and the applied load. On the contrary, the current set-up features an integrated system that allows to track, control, and log data about each of the mentioned variables.

One of the aims of the present thesis was to achieve better control of this system. We implemented a LabVIEW-based code to handle the motor speed and the temperature, recording at the same time the measured load and logging all the data. This latter aspect is crucial and will be discussed in the next paragraph. As for the controlling system, an attempt has been made to automate the whole process, either by speed control or load control.

The load control is based on a simple idea: it should be possible to carry out the extrusion at a given load by adjusting both the speed and the temperature accordingly. If we fix the temperature (i.e. the glass viscosity) then, by moving the ram, the load will increase. With automatic control, the system could be programmed to keep the ram movement until a certain load is reached and then control the pushing speed to avoid load variations. However, the full automation of the system has demonstrated to be very difficult to achieve, mainly because of some small changes – e.g. in the position of the thermocouple, in the alignment of the piston, in the die shape, or even in the thermal behaviour of the glass – that can lead to large differences in the measured load, thus affecting in several aspects the final product quality, like its shape retention, surface quality, tendency to crystallise, etc.

However, while load control has demonstrated to be quite difficult to reach, the automatic speed control was easier to achieve. The motor speed can be set to reach the desired value by small speed increments and to further increase only if the system reacts in the desired way– i.e. if the load smoothly increases when the glass is squeezed into the die. This level of automation has been partially achieved, even though the presence of a human operator is still essential at the moment, to double-check the system behaviour.

Furthermore, the implementation of a web-based platform to keep control of the extruder even if not in physical presence is also mandatory. This option has also been studied during the present thesis, employing a Python-based code that should guarantee a more robust way of handling this complex system. At present, the first tests are ongoing to finalise its development.

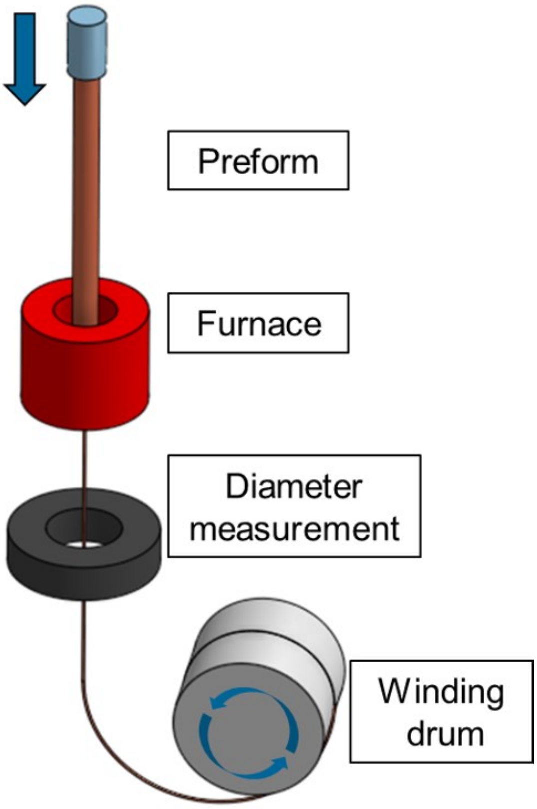

Fig. 3.6. The preform drawing: scheme of the main components of a drawing tower.

The drawing tower is even a more complex system. A scheme of the tower is visible in Fig. 3.6. To achieve a good drawing, the preform, which is mounted on a proper device on the top of the tower, must be moved into the heated region. A finely controlled screw moves the preform holder to insert the preform into the heated region. The formed fibre is wound up on a drum that is positioned at the bottom of the drawing tower, i.e. nearly three meters below the heated region. Both the feeding rate and the winding speed are crucial aspects. Overall, in this system, we have to deal with two moving elements (the feeding mechanism of the preform from above and the winding drum that pulls the fibre from below) and a heated furnace. All these three variables contribute to the realisation of the fibre. The heating needs to be properly chosen so that the preform can be soft enough to form a fibre and the fibre must be thin enough to be able to coil up on the winding drum without breaking. Once reached this step, the feeding speed must provide a continuous flow of material to the pulled fibre which has to be correctly wound. An automatic controlling mechanism is provided in our drawing tower through an optical diameter measurement, positioned below the heated region. This system can measure the diameter of the fibre and, by using a feedback loop provided by a LabVIEW code, the system can adjust both the feeding of the preform and the winding speed of the fibre accordingly.

3.1.3. Recording experimental data

An effective controlling mechanism must be coupled with a continuous system for data monitoring and recording. While the global social debate on the importance of data (see for example [42], where *datafication* is defined as “the process whereby life-processes must be converted into streams of data inputs for computer-based processing”) is moving towards unpredicted directions, there is no doubt that, especially in the scientific and research fields, the possibility of registering information and data about a process or an event is the basis of the experimental method. Data recording gives the chance to think about all the aspect of the evolution of a system and often leads to a better understanding of the investigated phenomenon. It is with this idea that data collection during all the extrusion experiments is here considered crucial and the optimisation of the system has passed through several observations all derived from the analysis of the collected data. For this reason, the LabVIEW designed software that enables to control the extruder also allows to constantly record the information about the measured load, the applied motor speed, and the temperature, as well as all the details about both dimensions and shape of the extruded product.

3.2. Soft glass extrusion

The main method chosen during the present work to produce soft glass preform is extrusion. As mentioned, there are several other techniques to produce glass preforms: rod-in-tube or stack-and-draw techniques both require the production of rods and tubes which can be achieved for example, by direct, continuous, or rotational casting, as well as drilling; furthermore, the preforms for telecom optical fibres need such level of purity that only Chemical Vapour Deposition (CVD) techniques can be employed.

The glass extrusion method is particularly interesting since it allows great flexibility in terms of the product dimensions also supporting the design of preforms with complex features. Although some distortions, which represent the main issues encountered today in the production of preforms by extrusion, this method is here proposed for phosphate soft glass preforms both with simple shapes, i.e. rods and tubes with a wide range of diameters, and for more complex non-symmetric structures. Several solutions are proposed in the next sections and chapters to overcome the present limitations of the technique.

3.2.1. Bulk extrusion vs. powder extrusion

The extrusion facility employed in the present work is partially inspired by the design presented by Roeder [43]. In 1971, Roeder proposed a method for the extrusion of glass starting from powders. The first powder extrusion results had several defects like inclusions and crystallites [43]. Indeed, besides the interesting and ground-breaking idea at that time, powder extrusion shows several issues related to inhomogeneities. Thus, in our extrusions, as well as in most of the extrusion experiments carried out by other research groups, bulk glass is preferred as the starting material [37], [44]–[46]. The glass homogeneity can be controlled by choosing high-purity powder reagents and performing the casting with special care, to avoid the presence of bubbles and inclusions in the glass billet. Furthermore, crystallisation can be shifted to higher temperatures by avoiding the interaction among grain powders during the extrusion process. This behaviour was reported by several works [47], [48], which studied the influence on the crystallisation kinetics for glasses with different particle sizes. These studies were conducted with glass powders with micrometric size and had demonstrated that the crystallisation peak can be increased by more than 20 °C by varying the average particle sizes by a factor of 10. Thus, when moving from powders to bulk billets, this shift might be further enhanced.

We were particularly interested in studying the behaviour of single material extrusion. In fact, phosphate glass extrusion has been seldom studied [49]–[55]. We wanted to assess the performances of our custom glasses employed either in active laser fibre production or in biomedical applications. Especially in this latter field, we will study the possibility of producing a single-material solid-core microstructured bioresorbable fibre, which offers intriguing perspectives for sensing applications in biomedicine. Some techniques like simultaneous core/clad extrusions have been proposed starting from stacking of glasses with different properties [19], [56]–[59]. For chalcogenide glasses, several stacking techniques have been studied, like multilayer preform production for either all-solid [60] or hollow-core [61] photonic bandgap fibres, disc-to-fibre approach [62], or the recently emerged Isolated Stacked Extrusion (ISE) [63]–[66] and the peeled-off ISE technique [67]–[69]. These techniques are summarised in Fig. 3.7. On the contrary, only a few works can be found on core/cladding co-extrusion of phosphate glasses [38], [70]. Yet, in these studies, the control of the dimensions of the preform have demonstrated to be rather difficult and preforms for highly multimode fibres were often obtained. Instead, for reasons that will be clearer in the next chapters, we were interested in exploring the possibility of direct extrusion either of preforms for single-mode fibre or of microstructured preforms. Both these kinds of preforms cannot be achieved by core/cladding extrusion.

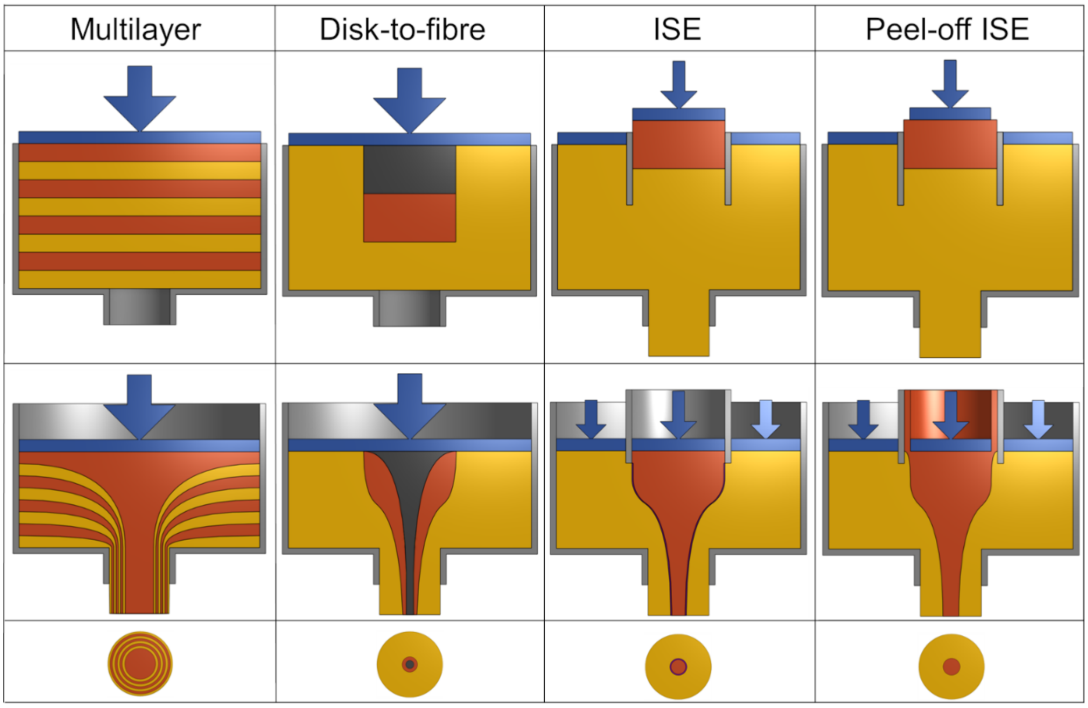

Fig. 3.7. Schematic illustration of some co-extrusion methods. From top to bottom, the initial stacking, the extrusion-in-progress, and the related preform cross-section are shown for each method. From left to right, the multilayer extrusion used for photonic bandgap fibres [60], [61], the disk-to-fibre approach [62], the Isolated-Stacked-Extrusion (ISE) with traces of debris at the core/cladding interface [63]–[66] and the peel-off ISE [67]–[69].

Due to all the above-mentioned reasons, the extrusion experiments carried out in the present work are all performed starting from single-material bulk glass billets, obtained via the melting and mould casting technique illustrated in the previous chapter.

3.2.2. Extruder set-up

The extruder set-up can be seen in Fig. 3.8. The system is composed of an aluminium frame that holds in place a furnace and a moving part, i.e. the ram. A motor is placed on the top of the system and is driven by a dedicated controller: Through a designed mechanism of gearwheels, the motor's circular movement is converted into a linear shift of the piston. A load cell (OMEGA model LCM411-1K-USBH) is placed between the two parts of the ram, one connected to the motor mechanism, and the other in contact with the glass billet. In this way, it is possible to measure the force that the ram exerts on the glass.

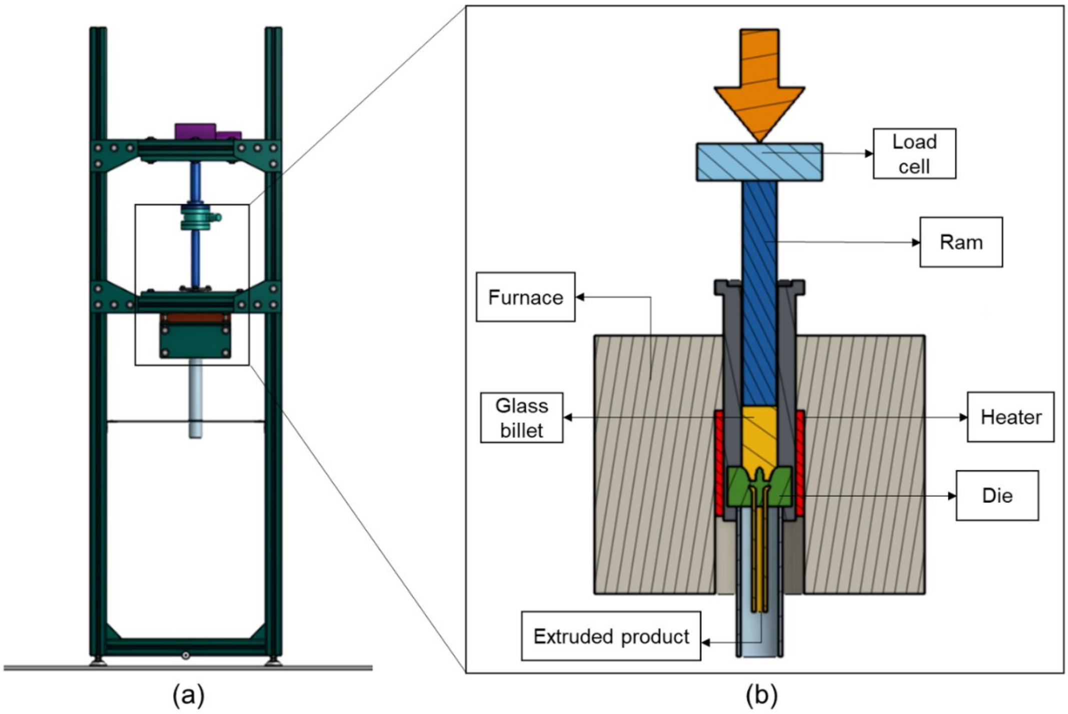

Fig. 3.8. Detailed 3D drawing of the extruder set-up. (a) Lateral view of the whole system and (b) cross-section of the core of the extruder with highlighted the main components.

The glass itself is held in place inside the furnace within an Inconel holding element, able to deliver the heat with minimum distortion and reduced oxidation. Below the glass billet, a specific die is inserted, according to the desired shape of the extrudate. The furnace controlling temperature is measured at the bottom of the die, using an external thermocouple. However, during each extrusion experiments, other thermocouples are placed in different positions to monitor the temperature distribution all over the system, near the hot region but also on the load cell, which must not be heated above 80 °C. Below the die, a hollow quartz cylinder is positioned to protect the emerging extrudate from thermal shocks. All the components, i.e. the furnace and the motor controller, as well as the load cell and the external monitoring thermocouples, are connected to a PC positioned nearby and able to control and check the system evolution (see Fig. 3.5). Furthermore, close to the extrusion apparatus, another furnace (Carbolite-Gero model LHT 6-60) is employed at the end of the process to anneal the extrudate.

3.2.3. Process control: fundamental parameters

During the extrusion process, the controlled variables are the speed of the ram and the temperature of the glass. Alongside, an important parameter that is measured during the extrusion is the force that the ram exerts onto the glass. Fig. 3.9 shows an ideal load curve during extrusion together with a real one. In these curves it is possible to see the three-regions behaviour: an initial increase called *start up*, with some fluctuations due to the settlement of the whole system, a nearly constant intermediate region (defined as the *steady state*), and a final sharp increase due to the contact between the ram and the die, when the softened glass has all flowed into the die and the temperature is raised to allow for the *neck-down*.

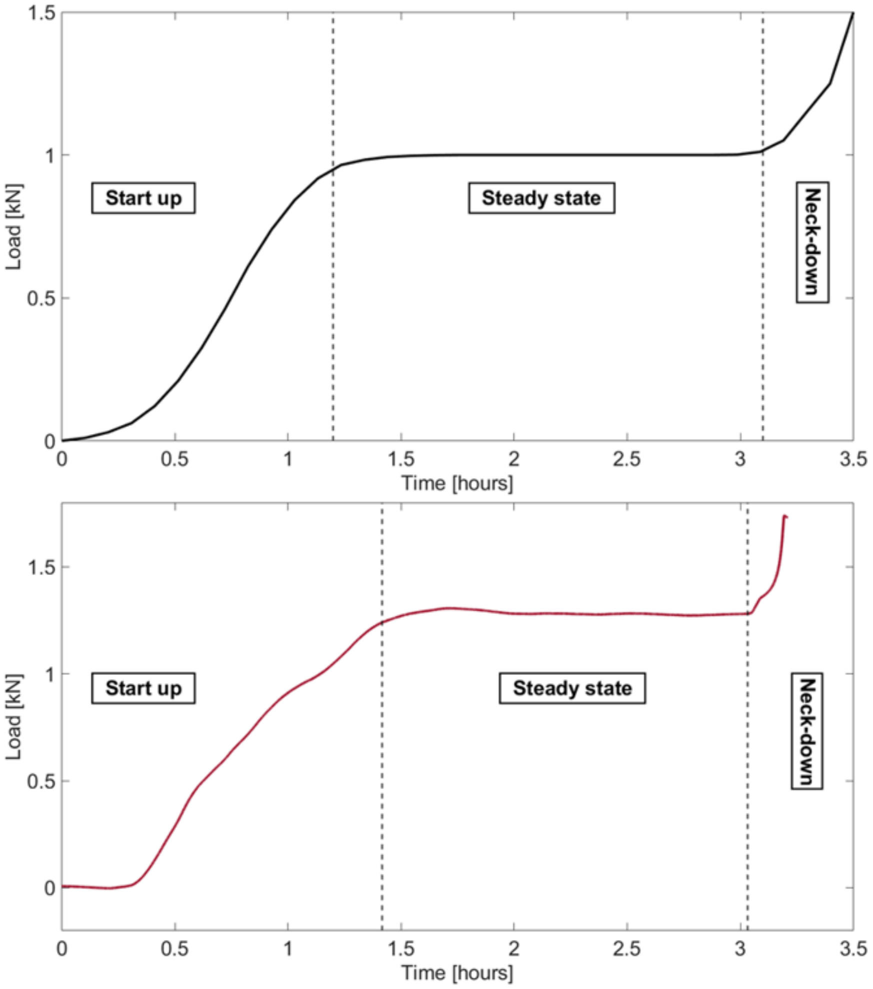

Fig. 3.9. Load measurement during an extrusion trial, in the ideal case (upper part, black curve) and real case (lower part, red curve). The curves show three distinct regions: the start up, the steady state and the neck-down region.

When the ram starts to force the glass to pass through the die, the response of the system, i.e. the measured load, is correlated to the viscosity of the glass and the speed of the ram. The extrusion should be carried out when the glass has a viscosity of around $10^7 - 10^9$ Pa·s [71]–[73].

However, the desired speed of the ram cannot be predicted a priori for all the systems, because it depends on the dimensions of the die as well as on other aspects, such as the glass tendency to crystallise and the glass/metal interaction within the die. With a viscosity in the above-mentioned range, the glass behaves like a viscous fluid, while at a lower temperature, i.e. for higher viscosity, it is more similar to a rigid elastic body.

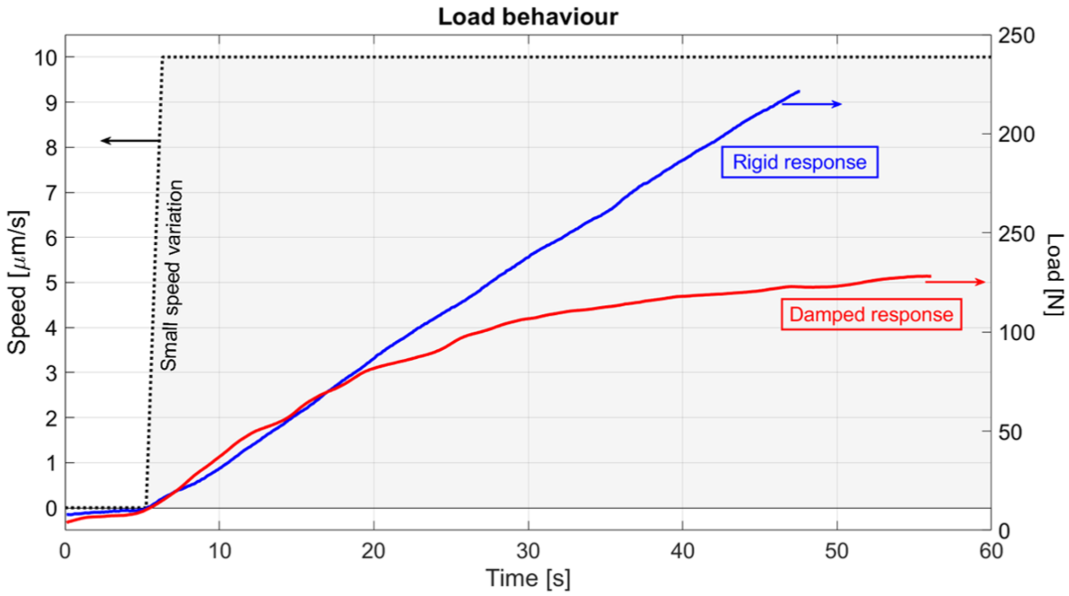

Fig. 3.10. Load response to a small speed variation (0 – 10 μm/s) at different temperatures: in blue a rigid response, obtained at a low temperature (high viscosity) and in red a damped response, due to the sufficiently high temperature (low viscosity).

The glass composition, the rate of deformation, and the shape of the die can also influence the response of the system to the pushing of the ram: the response can vary between an elastic behaviour, i.e. a sharp and linear increase of the load, to the perfect flow of a viscous fluid, in which the load may even show a reduction with the increasing ram speed. The optimal extrusion condition is usually in-between these two extreme situations and is represented by the damped response illustrated in Fig. 3.10. By looking at the shape of the measured load, the temperature can be adjusted according to the need.

In other words, if we apply a fixed movement to the ram, at a certain temperature and for a defined glass composition, the load measure provides an estimation of the viscous behaviour of the glass: if the curve is too steep, the temperature (viscosity) is too low (high); if, on the contrary, the curve shows a small increase or even a decrease, the temperature may be too high or the glass viscosity too low; in this latter condition, the material is flowing under its own weight and will not retain the shape imposed by the die.

The speed of the moving ram and the load could be both employed in principle as the main controlled variable. An attempt has been made, at the beginning of the present work, to implement a load control. The idea is to decide at which load the extrusion must be performed and set it up. Then, through an automatic controller (PID or other), the speed of the ram should be adjusted to reach and maintain that load. Yet, two main issues arise: the first one is related to the process controlling system, and the second is connected to the physical phenomena occurring during the extrusion.

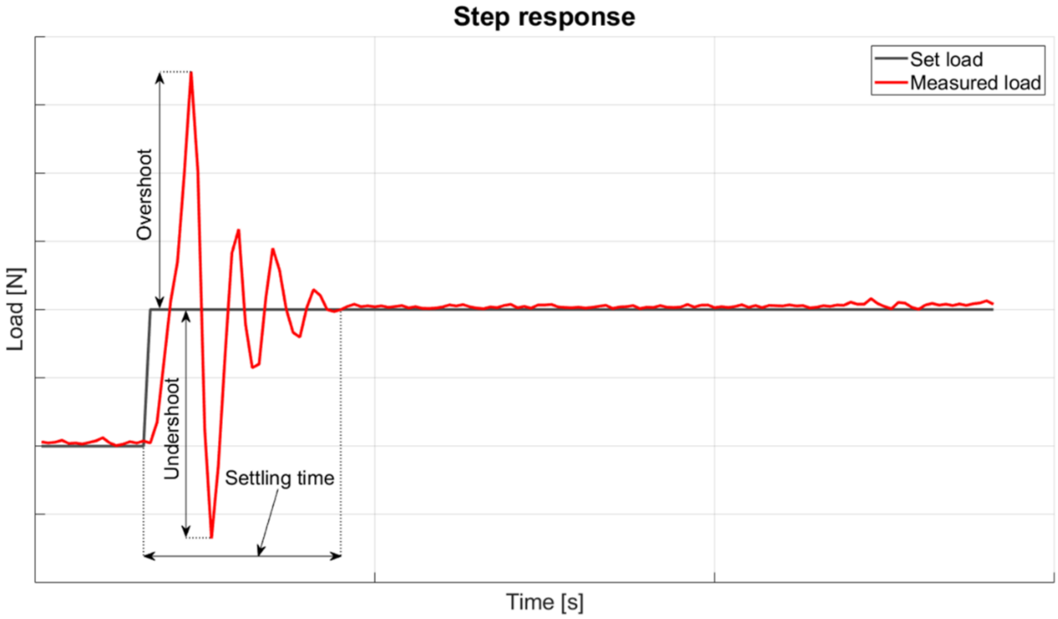

Fig. 3.11. Step response: when the set load (black curve) is varied, the measured load (red curve) varies accordingly, showing some oscillations (*overshoot* and *undershoot*) that are damped within a *settling time*.

To properly set-up an automatic control system, there is the need to adjust the parameters of the controlling unit to find their optimum combination. In other words, we needed to verify and refine the system reaction in the case of a variation of the controlled variable, described by the so-called step response, illustrated in Fig. 3.11. In our case, this means that we may set up a load, let’s say 1 kN, and the extruder’s ram starts to move and push the glass until the set load is reached. According to the slope of the load curve, the speed of the ram should be adjusted to reach that load in a reasonable time, slightly exceed that value (see the *overshoot* in Fig. 3.11) and then, within a few small oscillations that last for the *settling time*, finally maintain the desired load. However, to react accordingly, the system should be calibrated for every different glass composition and each die. And even in the presence of such calibrations, the eventual misalignment of some portions, or a small temperature variation could have dramatic effects since the automatic controller would not be able to react properly, which may cause system breakage.

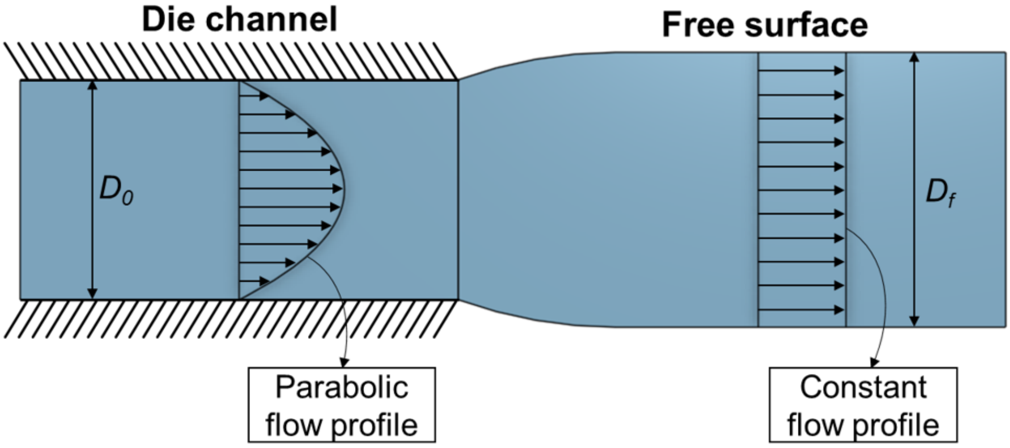

Fig. 3.12. The phenomenon of *die swelling*. On the left of the figure, the die channel, where, in the presence of friction between the glass and the die walls, the velocity profile is parabolic. On the right, the glass flow, out of the die, shows a constant velocity profile but an increased cross-section compared to the dimension of the die.

The second aspect that can compromise the load control is the relation between the extrusion speed and the phenomenon of *die swelling*. In polymer science, but also in general fluid dynamics, the die swelling (sometimes known as the *Barus effect*) is a well-known issue: when a fluid passes through an orifice, its cross-section after the exit of the hole is distorted (usually is bigger than the hole itself). A representation of this effect is reported in Fig. 3.12, where it can be seen that the velocity profile of a fluid that flows inside a channel is almost parabolic (left part of Fig. 3.12) having a null velocity near the wall of the channel and a maximum at its centre. This is caused by the friction between the fluid and the channel walls, i.e. the molten glass and the die: the so-called *no-slip condition*. This latter concept is derived from Computational Fluid Dynamics (CFD) and will be explicitly considered in Chapter 5. At a microscopic level, the phenomenon of friction arises from both physical and chemical interactions at the interface, depending on the materials involved. Indeed, it is known that some die materials, like e.g. stainless-steel, cause sticking of the glass while others, like graphite or boron nitride, let the glass slip over the die surface [43], [74]. By choosing the right die material and/or treating the die surface with specific processes we can partially control this phenomenon. Once the fluid has passed through the exit of the channel, the velocity profile becomes constant all over the section (right part of Fig. 3.12) and the final shape of the extrudate is consolidated. If we look at the transition region at the die exit, near the channel walls, the balances of mass and momentum must consider the velocity of the fluid v, which is zero before the die exit and equal to the constant speed of the whole fluid afterwards. With some calculations, it is possible to derive that the ratio of the fluid diameter downstream D_f and upstream D_0 from the die exit is related to the Reynolds number ($Re = \rho v D/\mu$, where ρ is the density, v is the fluid speed, D is the channel diameter, and μ is the viscosity) [75].

In the case of Newtonian fluids, Middleman & Gavis have demonstrated both experimentally and analytically that for small Re the maximum ratio $D_f/D_0 = 1.12$, while for high Re the minimum ratio is $D_f/D_0 = 0.87$ [75], [76]. For non-Newtonian fluids, the relations are way more complex involving also the elastic strain recovery, and the effective section increase can have a ratio $D_f/D_0 \gg 2$ [77]–[79]. If we fix the material and the die shape, the amount of the swelling is related to the fluid speed, i.e. in our case to the applied ram speed. The oscillations of the ram speed introduced by the attempted load control resulted to have a negative influence on the die swelling phenomenon.

Finally, considering the concepts detailed in Section 2.1 about the glass network, with phosphate glasses it is possible to have a polymer-like response related to the percentage of Q^i-chain structures. This phenomenon depends on the glass composition and is particularly evident when dealing with polyphosphate glasses. For this reason, the die swelling cannot be neglected when working with complex die shapes and especially with some phosphate glass compositions (showing O/P ratio $3 \leq$ O/P ≤ 3.5) since their behaviour may be non-Newtonian. Thus, we decided to handle this issue by avoiding the load control and preferring a gradual increase in the speed to reach a specific value and then try to avoid further variation of the speed. Once again, the target speed value depends on the glass composition and the die shape. In this way, during the steady-state portion of the extrusion, we can allow some load variations that usually are reduced to ± 10% of the average load value during the steady state. To achieve and maintain the steady-state load is not always easy and small adjustments of the speed and the temperature may be done during the experiments to obtain the best results.

3.2.4. Thermo-mechanical modelling

Besides load and speed, the temperature distribution inside the extruder is a crucial aspect to properly control the system behaviour. Indeed, the temperature is not constant all over the glass billet and there is a temperature gradient between the upper punch and the lower die. To investigate this aspect, a temperature measurement campaign was set up. The first temperature measurements were carried out with a single thermocouple (Fig. 3.13) moved along the extruder. This led to an inaccurate measurement of temperature because the huge portion of air volume surrounding the thermocouple leads to measurements always below the furnace controller value.

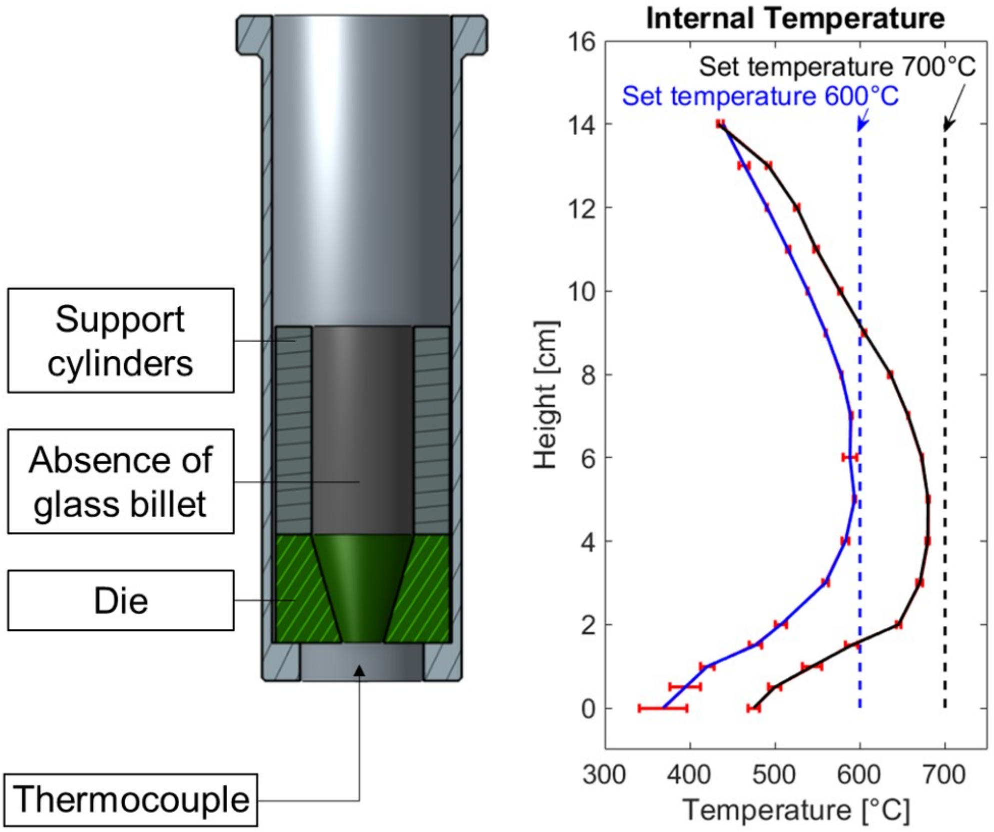

Fig. 3.13. The temperature measurement inside the extruder with a single thermocouple inserted from below. On the left a sketch of the extruder's lateral cross-section; on the right the temperature measured at corresponding heights for furnace temperatures of 600 °C and 700 °C. The measurements are carried out without any glass piece.

An improved measurement setup was implemented by inserting a set of five thermocouples into a reshaped glass billet (as depicted in Fig. 3.14a and Fig. 3.14b) that allowed measuring the temperature distribution along its section. In this way, the temperature values resulted to be more reliable since they experimentally include the thermal inertia of the glass. Furthermore, by measuring five values across the billet section and computing the average, it was possible to reduce the influence of the measurement error. As shown in Fig. 3.14c, the controlling temperature measured with the furnace thermocouple is comprised between the temperature on the top and on the bottom of the glass piece (these latter are average values).

These experiments were carried out at a low temperature, i.e. during heating from ambient temperature to 100 °C. Thus, the actual temperature differences during extrusion that typically occurs at above 500 °C are probably smaller, due to the higher thermal conductivity of the softened glass.

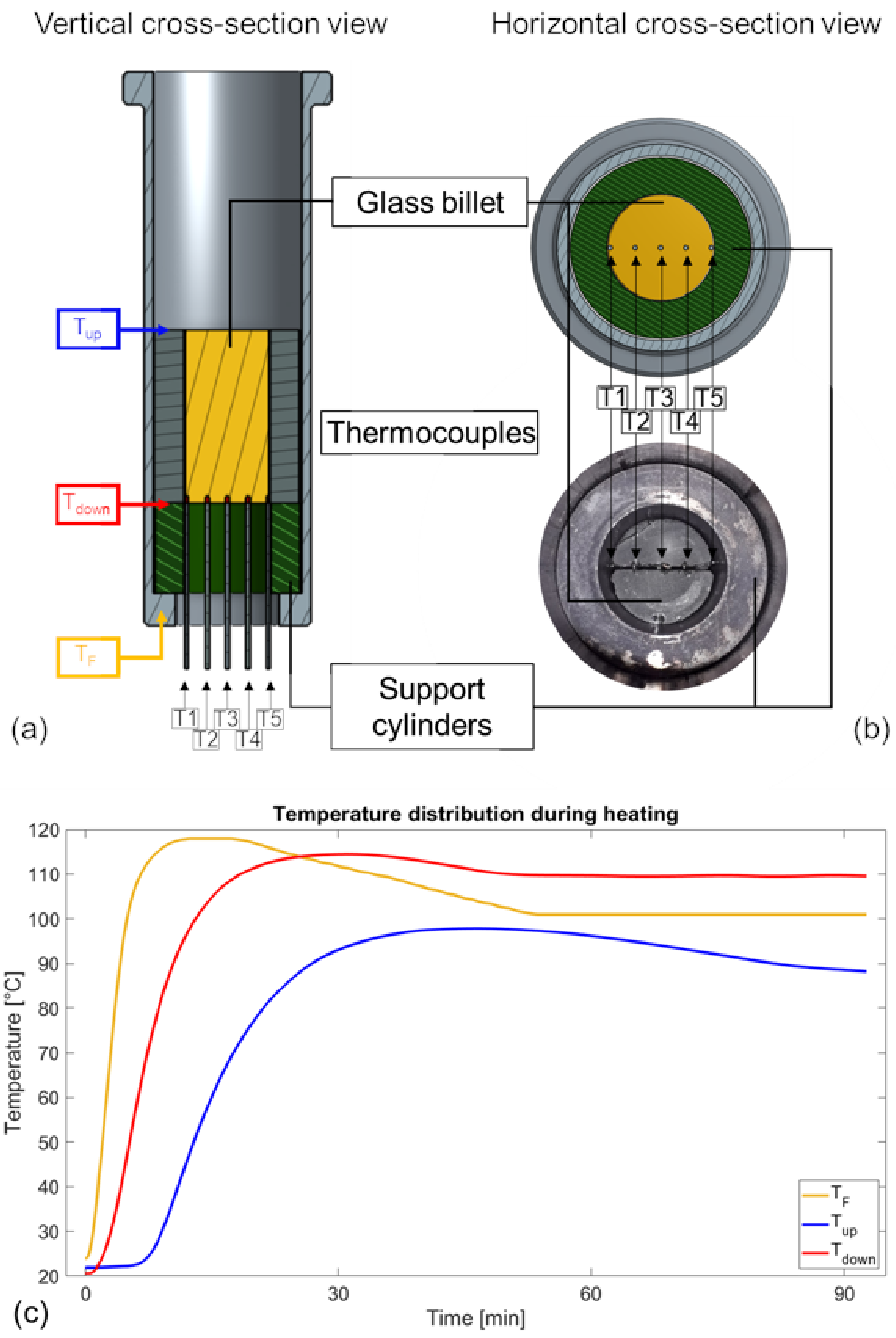

Fig. 3.14. The temperature measurement inside the extruder with a set of five thermocouples inserted from below. (a) Sketch of the extruder's vertical cross-section; (b) a sketch of the extruder's horizontal cross-section (top) and a picture of the glass billet prepared for the measurements (bottom), with the indication of the position of each thermocouple; (c) a plot of the average temperature measured on the upper (T_{up}) and lower (T_{down}) part of the glass billet in comparison with the furnace controller temperature at the base of the die (T_F); the measurement is carried out during heating from ambient temperature to 100 °C, until full stabilisation.

These results allowed us to determine the importance of the dwell time, highlighted in several works [80], [81], and gave an indication of the time required for temperature stabilisation in the die as detailed hereafter.

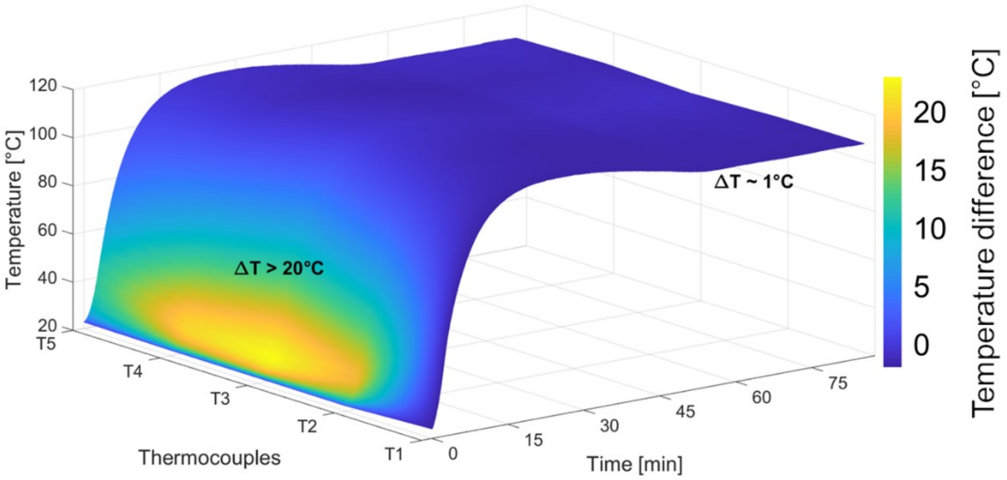

Fig. 3.15. The temperature evolution inside the glass billet is plotted against time for the different thermocouples depicted in Fig. 3.14. The colour variation shows the cooler region in yellow and the hotter region in blue. After a dwell time of more than one hour, the temperature difference is stabilised within ±1 °C.

During extrusion, the temperature controller receives feedback from a thermocouple placed in contact with the lower part of the die. The controller is programmed to reach and maintain that temperature. However, when the furnace thermocouple has reached the target temperature, this is not homogeneous over the whole system, and a dwell time is required to uniform the temperature. This can be noted in Fig. 3.15, where the temperature evolution inside the glass billet (i.e. for the five different thermocouples of Fig. 3.14) is plotted vs. time. Concerning the temporal evolution, we can identify a start-up period in which the temperature difference between the surface and the centre of the billet (12-mm distance) is higher than 20 °C.

As the temperature stabilises, i.e. after nearly 70 minutes, the temperature difference becomes lower than ±1 °C. This aspect evidences how it is crucial to wait enough time to let the glass temperature homogenise before starting to exert a load with the punch. Regardless of the temperature, the glass has a low thermal conductivity (compared to metal, for example) and since a small temperature variation can cause a huge difference in the glass viscosity, the achievement of a uniform temperature is of great importance. Since the die has generally a complex three-dimensional shape, we performed the temperature measurement over the whole extruder, and we carried out a thermo-mechanical simulation to determine the overall temperature 3D distribution also in regions where the direct measurement is not possible.

By performing such calculations, it has been also possible to have an estimation of the eventual deformations that can occur on the system. The thermo-mechanical model has been implemented using the SimScale® open-source web platform and is shown, together with some of the results, in Fig. 3.16 and Fig. 3.17. This simulation is a partial result since it accounts only for the conductive heat transfer and no convection or irradiation are computed. Furthermore, the resistance filaments are approximated to small cylinders and the coefficients of heat conduction of the different materials are taken from the literature and not directly measured. Nevertheless, this tool can provide a qualitative and to a certain extent quantitative insight into the die configuration, highlighting the critical aspects such as unwanted heat wells, load concentrations, or excessive deformations that could compromise the performances of the extrusion.

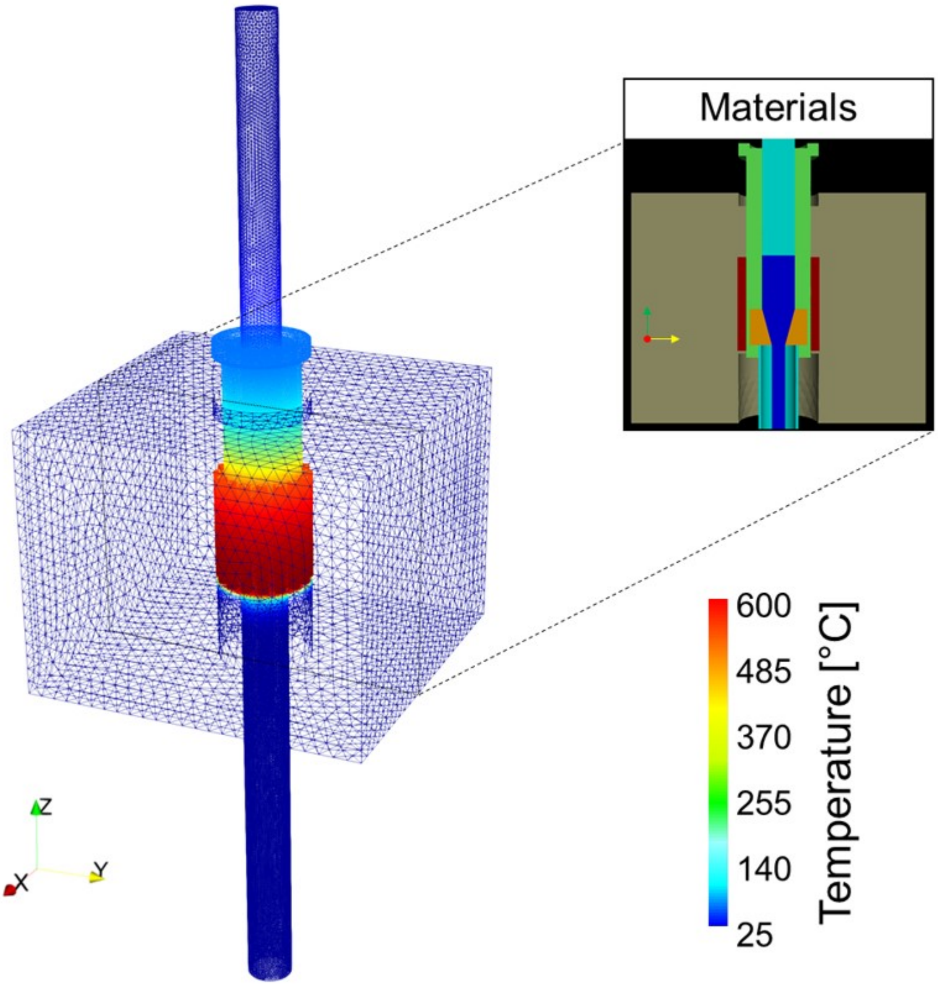

Fig. 3.16. The set-up of the thermomechanical simulation of the extruder. 3D view of the whole simulated system, with temperature distribution after 10 minutes of heating. In the inset, the different materials employed are shown (i.e. glass, different metals, and the thermal insulator of the furnace).

The tool employed has the advantage of being compatible with OnShape®, i.e. the Computer-Aided Design (CAD) software employed for most of the 3D drawings required for the present work. Furthermore, with a free academic account, the SimScale® platform provides the user with some free hours of calculation on their servers. Thanks to this tool, several simulations have been run and could be easily reproduced with the aim of building a new extrusion facility with improved performances, to check the system behaviour before finalising the design.

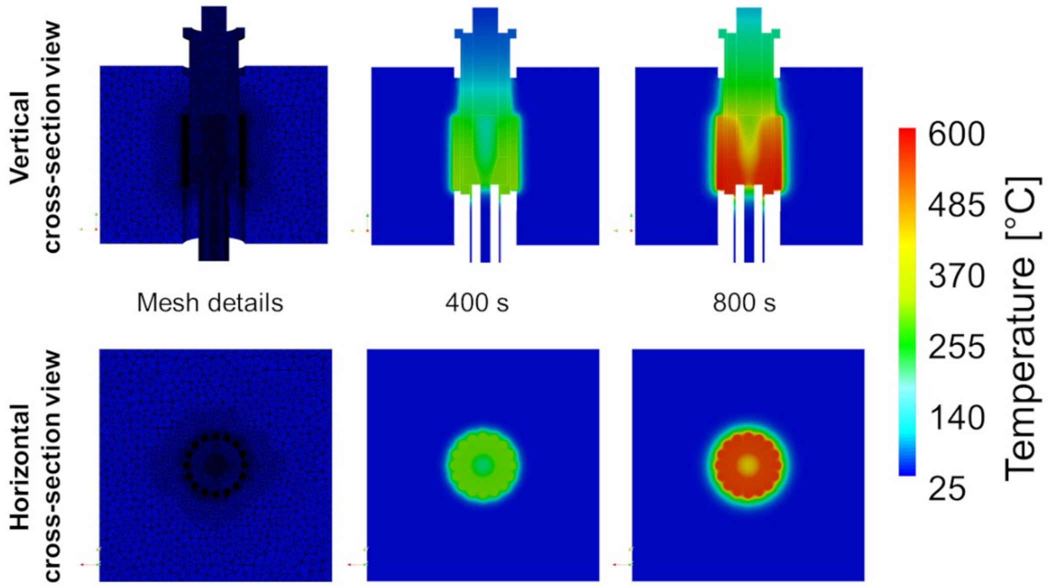

Fig. 3.17. Vertical and horizontal cross-sections of the simulated extruder showing: from left to right, the detail of the employed mesh, the temperature distribution after 400 s, and after 800 s.

3.2.5. Extruder optimisation

Taking advantage of all the steps described in the previous paragraph, the extrusion system has been thoroughly optimised. In particular, the controlling unit was the first optimisation step to be carried out, by adopting a precise speed control and by continuously monitoring the load variation, to track any misbehaviour. To implement a more automatic process, we developed a LabVIEW code that allowed us to control all the fundamental parameters (motor speed, temperature, etc.), monitor the load, and continuously log the acquired data.

Furthermore, the temperature measurement, along with the thermo-mechanical simulation of the whole system are other steps towards the optimum management of the extrusion facility. With these tools, we achieved knowledge of the temperature distribution inside the extruder, which allowed us to redesign the position and the dimensions of the so-called *spider-die* [82], [83]. In this way, an enhanced length of the welding chamber, i.e. the portion of the die below the arms of the *spider*, is suggested, as a way to reduce the influence of the arms on the glass flow [73], [84]. The evolution of a few models of the designed dies is presented in Fig. 3.18. The improvements in the quality of the extrudates, in terms of prediction of distortions, reduction of surface and bulk defects, control of the swelling and the bending of the preform, are all results of the described optimisation steps.

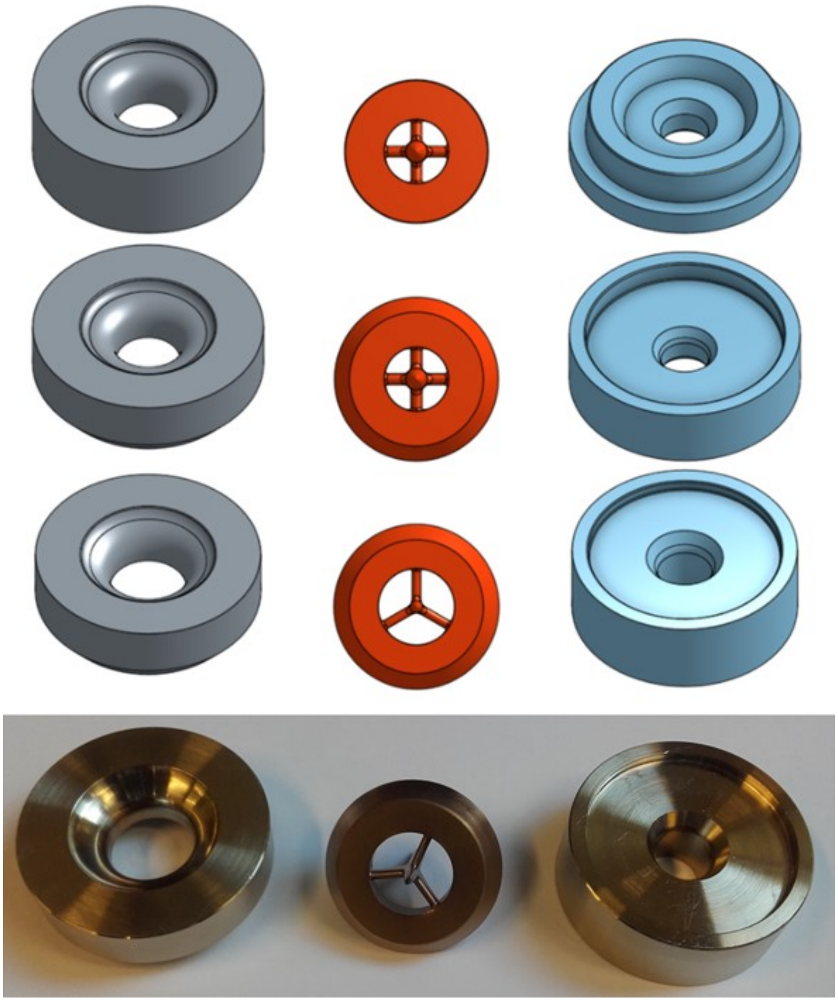

Fig. 3.18. Examples of extrusion dies for the production of tubes. On the upper part, a few 3D sketches of the extrusion dies are presented to highlight the evolution in the design from the oldest (on the top of the figure) to one of the newest. A real picture of this latter die is shown on the lower part of the figure.

3.3. Fibre drawing

The process of fibre drawing is of fundamental importance for optical telecommunication, a fast-growing sector. Optical fibres have also a great application potential in many other fields like sensing in biomedical, automotive, aerospace, or environmental applications to cite a few. Although there is not a precise definition of the minimum dimension with which a thin rod can be called *fibre*, usually, fibres made of several glass systems are not easy to bend with diameters higher than 200 – 300 μm. During the present work, we obtained several fibres, with diameters usually ranging from 100 to 200 μm, and starting from preforms with diverse shapes and a maximum external diameter of 12 mm. A general overview of the system employed for fibre drawing is presented in the next paragraphs.

3.3.1. Preform drawing

In optical glass manufacturing, there are two main methods employed for fibre production: drawing from crucible (or the *double crucible method*) and preform drawing. The former has been used for the first core/cladding fibre production but has several limitations [2], [85]. In fact, only certain dimensions are achievable, and nothing but fibres with cylindrical symmetry can be obtained. On the other hand, the drawing from a preform is a highly flexible technique, which converts into micrometric or sub-micrometric features all the details of the produced preform. Improved results can be obtained by combining the extrusion facility that allows producing different kinds of preforms, with the drawing tower that can convert them into flexible fibres.

3.3.2. Soft glass drawing tower

When dealing with soft glasses, the drawing tower can be a simpler structure than the ones designed for pure silica drawing. In our case, within the facilities of LINKS Foundation, there is a soft glass drawing tower, through which the drawing of several kinds of phosphate and tellurite glasses have been successfully performed. A picture of the drawing tower is visible in Fig. 3.19a.

The tower is composed of an induction system designed to deliver power ranging from 150 W to 250 W. In this way, the temperature of the heated region can be varied. A graphite ring is placed in the centre of the inductor and this allows the delivery of localised heating to the preform. After the first step, called neck-down, in which the glass is softened until a drop of material is formed and starts to fall from the lower part of the preform, the fibre is collected on a rotating drum placed at the bottom of the tower. The overall tower height, from the top of the feeding system to the winding drum, is around 4 m. By controlling the winding speed of the drum and the feeding of the preform into the heated region, it is possible to set the desired fibre diameter. A conservation law can be applied to the system with the equation $D_p \cdot v_p = D_f \cdot v_f$, where D_p and D_f are the preform and fibre diameters, and v_p and v_f are their velocities, respectively. By rearranging this equation, the fibre diameter can be calculated: $D_f = D_p \cdot v_p / v_f$. This latter equation is used to control the diameter of the drawn fibre with a tolerance of ±3 μm, using an automatic controlling system designed with a LabVIEW code (a screenshot of the control window is visible in Fig. 3.19b).

Furthermore, the system is equipped to work under N_2 flux and some improvement can allow also to draw fibres under pressurisation. Between the heated region of the preform and the winding drum, an optical diameter control device is installed, and a UV-curing system for the polymer coating can be mounted according to the needs.

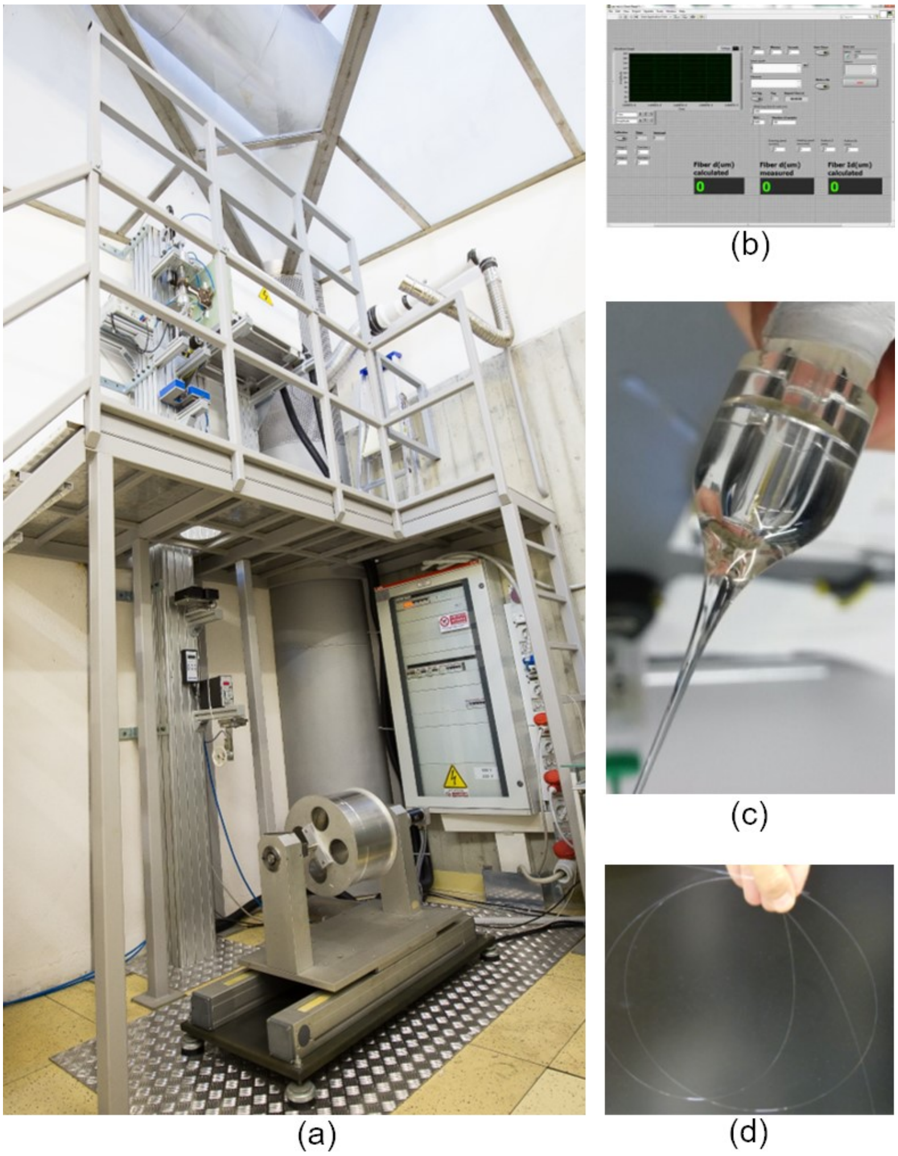

Fiber d(um) calculated 0
Fiber d(um) measured 0
Fiber Id(um) calculated 0

Fig. 3.19. The fibre drawing: (a) picture of the drawing tower facility situated within LINSK Foundation laboratories, (b) a screenshot of the LabVIEW code used to control the drawing process, (c) a core/cladding preform after the neck-down, and (d) a picture of a fibre that can be easily bent.

3.3.3. Experimental results

Several fibres have been obtained during the three years of the current work. A picture of a core/cladding preform after the drawing process is visible in Fig. 3.19c, while Fig. 3.19d shows a portion of a fibre that can be easily bent. We carried out several drawings for active fibre production to be used as laser fibres for environmental sensing. In this case, a tube is extruded with precise dimensions and, through the rod-in-tube technique, is combined with an active core obtained through the stretching of a cast rod. Further information about this topic can be found in Chapter 4. We also demonstrated the feasibility of the drawing of bioresorbable phosphate glass preforms made by extrusion. Two or more extruded preforms are usually combined using rod-in-tube or stack-and-draw techniques. Then, the preforms are mounted onto the holder of the drawing tower. Employing the feeding-mechanism controller, the preform is inserted into the furnace and heated to the drawing temperature. As soon as the fibre is formed, it is spun on the winding drum and several meters of fibre are collected, adjusting the diameter according to the needs. Details about these bioresorbable phosphate glasses and the obtained fibres are presented in Chapter 5. Finally, we hypothesise the possibility of coating the bioresorbable glass with a bioresorbable antibacterial phosphate glass. This latter experiment is at a proof-of-concept stage and, even though preliminary studies of the glass composition and its properties are ongoing, the fibres have not been obtained during the present work. Nevertheless, details about the design of this system are given in Chapter 6.

References

[1] G. W. Morey, *The Properties of Glass*, 2nd ed. New York, NY: Reinhold Publishing, 1954.

[2] A. Varshneya e J. C. Mauro, *Fundamentals of Inorganic Glasses*, 3rd ed. Cambridge, MA: Elsevier, 2019.

[3] L. A. B. Pilkington, «The Float Glass Process», *Proceedings of the Royal Society London*, vol. 314, n. 1516, pagg. 1–25, 1969, doi: 10.1088/0031-9112/21/4/018.

[4] O. Uusitalo, *Float Glass Innovation in the Flat Glass Industry*. Cham, Switzerland: Springer International Publishing, 2014.

[5] M. L. F. Nascimento, «Brief history of the flat glass patent – Sixty years of the float process», *World Patent Information*, vol. 38, pagg. 50–56, set. 2014, doi: 10.1016/j.wpi.2014.04.006.

[6] G. Tao, A. M. Stolyarov, e A. F. Abouraddy, «Multimaterial Fibers», *International Journal of Applied Glass Science*, vol. 3, n. 4, pagg. 349–368, 2012, doi: 10.1111/ijag.12007.

[7] D. L. Morse e J. W. Evenson, «Welcome to the Glass Age», *International Journal of Applied Glass Science*, vol. 7, n. 4, pagg. 409–412, 2016, doi: 10.1111/ijag.12242.

[8] N. Bach, Hans; Neuroth, *The Properties of Optical Glass*, Springer. 1998.

[9] A. F. Abouraddy *et al.*, «Towards Multimaterial Multifunctional Fibres That See, Hear, Sense and Communicate», *Nature Materials*, vol. 6, n. 5, pagg. 336–347, 2007, doi: 10.1038/nmat1889.

[10] J. Hecht, «Illuminating the Origin of Light Guiding», *Optics & Photonics News*, vol. 10, n. 10, pagg. 26–30, 1999, doi: 10.1364/OPN.10.10.000026.

[11] S. Thompson, «The photophone», *Nature*, vol. 22, pag. 481, 1880, doi: 10.1038/023058a0.

[12] R. Noé, *Essentials of Modern Optical Fiber*, 2nd ed. Heidelberg, Germany: Springer International Publishing, 2016.

[13] G. Tao *et al.*, «Infrared fibers», *Advances in Optics and Photonics*, vol. 7, pagg. 379–458, 2015, doi: 10.1364/AOP.

[14] W. Yan *et al.*, «Thermally drawn advanced functional fibers: New frontier of flexible electronics», *Materials Today*, vol. 35, pagg. 168–194, 2020, doi: 10.1016/j.mattod.2019.11.006.

[15] C. Dong, A. G. Page, W. Yan, T. Nguyen-Dang, e F. Sorin, «Microstructured Multimaterial Fibers for Microfluidic Sensing», *Advanced Materials Technologies*, vol. 4, n. 10, pagg. 1–6, 2019, doi: 10.1002/admt.201900417.

[16] F. Sorin *et al.*, «Multimaterial photodetecting fibers: A geometric and structural study», *Advanced Materials*, vol. 19, n. 22, pagg. 3872–3877, 2007, doi: 10.1002/adma.200700177.

[17] J. Kobelke, J. Kirchhof, M. Scheffler, e A. Schwuchow, «Chalcogenide glass single mode fibres - preparation and properties», *Journal of Non-Crystalline Solids*, vol. 256, pagg. 226–231, 1999, doi: 10.1016/S0022-3093(99)00461-5.

[18] S. D. Savage, C. A. Miller, D. Furniss, e A. B. Seddon, «Extrusion of chalcogenide glass preforms and drawing to multimode optical fibers», *Journal of Non-Crystalline Solids*, vol. 354, n. 29, pagg. 3418–3427, 2008, doi: 10.1016/j.jnoncrysol.2008.01.032.

[19] G. Tao, S. Shabahang, E.-H. Banaei, J. J. Kaufman, e A. F. Abouraddy, «Multimaterial preform coextrusion for robust chalcogenide optical fibers and tapers», *Optics Letters*, vol. 37, n. 13, pag. 2751, 2012, doi: 10.1364/OL.37.002751.

[20] E. Mura, J. Lousteau, D. Milanese, S. Abrate, e V. M. Sglavo, «Phosphate glasses for optical fibers: Synthesis, characterization and mechanical properties», *Journal of Non-Crystalline Solids*, vol. 362, n. 1, pagg. 147–151, 2013, doi: 10.1016/j.jnoncrysol.2012.11.029.

[21] N. Boetti, D. Pugliese, E. Ceci-Ginistrelli, J. Lousteau, D. Janner, e D. Milanese, «Highly Doped Phosphate Glass Fibers for Compact Lasers and Amplifiers: A Review», *Applied Sciences*, vol. 7, n. 12, pag. 1295, 2017, doi: 10.3390/app7121295.

[22] E. Ceci-Ginistrelli *et al.*, «Novel Biocompatible and Resorbable UV-Transparent Phosphate Glass Based Optical Fiber», *Optical Materials Express*, vol. 6, n. 6, pagg. 2040–2051, 2016, doi: 10.1364/OME.6.002040.

[23] X. Feng, T. Monro, P. Petropoulos, V. Finazzi, e D. Hewak, «Solid microstructured optical fiber», *Optics Express*, vol. 11, n. 18, pag. 2225, 2003, doi: 10.1364/oe.11.002225.

[24] Z. G. Lian, Q. Q. Li, D. Furniss, T. M. Benson, e A. B. Seddon, «Solid microstructured chalcogenide glass optical fibers for the near- and mid-infrared spectral regions», *IEEE Photonics Technology Letters*, vol. 21, n. 24, pagg. 1804–1806, 2009, doi: 10.1109/LPT.2009.2033208.

[25] H. Bao, K. Nielsen, H. K. Rasmussen, P. U. Jepsen, e O. Bang, «Fabrication and characterization of porous-core honeycomb bandgap THz fibers», *Optics Express*, vol. 20, n. 28, pag. 29507, 2012, doi: 10.1364/oe.20.029507.

[26] J. C. Knight, «Photonic crystal fibres», *Nature*, vol. 424, n. August, pagg. 847–851, 2003, doi: 10.1038/nature01940.

[27] X. Feng, A. K. Mairaj, D. W. Hewak, e T. M. Monro, «Nonsilica glasses for holey fibers», *Journal of Lightwave Technology*, vol. 23, n. 6, pagg. 2046–2054, 2005, doi: 10.1109/JLT.2005.849945.

[28] R. Kostecki, H. Ebendorff-Heidepriem, S. C. Warren-Smith, e T. M. Monro, «Predicting the drawing conditions for Microstructured Optical Fiber fabrication», *Optical Materials Express*, vol. 4, n. 1, pag. 29, 2014, doi: 10.1364/OME.4.000029.

[29] J. Lousteau *et al.*, «Er 3+ and Ce 3+ codoped tellurite optical fiber for lasers and amplifiers in the near-infrared wavelength region: Fabrication, optical characterization, and prospects», *IEEE Photonics Journal*, vol. 4, n. 1, pagg. 194–204, 2012, doi: 10.1109/JPHOT.2011.2181974.

[30] N. G. Boetti *et al.*, «Multiple visible emissions by means of up-conversion process in a microstructured tellurite glass optical fiber», *Optics Express*, vol. 20, n. 5, pag. 5409, 2012, doi: 10.1364/oe.20.005409.

[31] V. M. Sglavo, E. Mura, D. Milanese, e J. Lousteau, «Mechanical Properties of Phosphate Glass Optical Fibers», *International Journal of Applied Glass Science*, vol. 5, n. 1, pagg. 57–64, 2014, doi: 10.1111/ijag.12040.

[32] E. Ceci-Ginistrelli *et al.*, «Nd-doped phosphate glass cane laser: from materials fabrication to power scaling tests», *Journal of Alloys and Compounds*, vol. 722, pagg. 599–605, 2017, doi: 10.1016/j.jallcom.2017.06.159.

[33] E. Ceci-Ginistrelli *et al.*, «Drug release kinetics from biodegradable UV-transparent hollow calcium-phosphate glass fibers», *Materials Letters*, vol. 191, pagg. 116–118, 2017, doi: 10.1016/j.matlet.2016.12.103.

[34] L. Di Sieno *et al.*, «Towards the use of bioresorbable fibers in time-domain diffuse optics», *Journal of Biophotonics*, vol. 11, n. 1, pagg. 1–11, 2018, doi: 10.1002/jbio.201600275.

[35] P. L. Iscoa *et al.*, «Design , processing , and characterization of an optical core - bioactive clad phosphate fiber for biomedical applications», *Journal of the American Ceramic Society*, n. April, pagg. 6882–6892, 2019, doi: 10.1111/jace.16553.

[36] D. Furniss e A. B. Seddon, «Towards monomode proportioned fibreoptic preforms by extrusion», *Journal of Non-Crystalline Solids*, vol. 256, pagg. 232–236, 1999, doi: 10.1016/S0022-3093(99)00463-9.

[37] K. M. Kiang *et al.*, «Extruded singlemode non-silica glass holey optical fibres», *Electronics Letters*, vol. 38, n. 12, pagg. 546–547, 2002, doi: 10.1049/el:20020421.

[38] E. T. Y. Lee e E. R. M. Taylor, «Two-die assembly for the extrusion of glasses with dissimilar thermal properties for fibre optic preforms», *Journal of Materials Processing Technology*, vol. 184, n. 1–3, pagg. 325–329, 2007, doi: 10.1016/j.jmatprotec.2006.11.115.

[39] H. Ebendorff-Heidepriem e T. M. Monro, «Extrusion of complex preforms for microstructured optical fibers», *Optics Express*, vol. 15, n. 23, pag. 15086, 2007, doi: 10.1364/OE.15.015086.

[40] J. Lousteau, G. Jose, D. Furniss, A. B. Seddon, T. M. Benson, e A. Jha, «A novel approach for the fabrication of planar waveguides from heavy metal oxide glasses», *Journal of Non-Crystalline Solids*, vol. 355, n. 37–42, pagg. 1973–1979, 2009, doi: 10.1016/j.jnoncrysol.2009.01.058.

[41] C. A. G. Kalnins, K. J. Bachus, A. Gooley, e H. Ebendorff-Heidepriem, «High precision extrusion of glass tubes», *International Journal of Applied Glass Science*, vol. 10, n. 2, pagg. 172–180, apr. 2019, doi: 10.1111/ijag.13092.

[42] N. Couldry e J. Yu, «Deconstructing datafication's brave new world», *New Media and Society*, vol. 20, n. 12, pagg. 4473–4491, 2018, doi: 10.1177/1461444818775968.

[43] E. Roeder, «Extrusion of glass», *Journal of Non-Crystalline Solids*, vol. 5, n. 5, pagg. 377–388, 1971, doi: 10.1016/0022-3093(71)90039-1.

[44] D. Furniss e A. B. Seddon, «Extrusion of gallium lanthanum sulfide glasses for fiber-optic preforms», *Journal of Materials Science Letters*, vol. 17, n. 18, pagg. 1541–1542, 1998, doi: 10.1023/A:1006502029189.

[45] H. Ebendorff-Heidepriem, P. Petropoulos, R. Moore, K. Frampton, D. J. Richardson, e T. M. Monro, «Fabrication and optical properties of lead silicate glass holey fibers», *Journal of Non-Crystalline Solids*, vol. 345–346, pagg. 293–296, 2004, doi: 10.1016/j.jnoncrysol.2004.08.098.

[46] H. Ren *et al.*, «Chalcogenide glass fibers with a rectangular core for polarized mid-infrared supercontinuum generation», *Journal of Non-Crystalline Solids*, vol. 517, n. March, pagg. 57–60, 2019, doi: 10.1016/j.jnoncrysol.2019.05.010.

[47] V. C. S. Reynoso, K. Yukimitu, T. Nagami, C. L. Carvalho, J. C. S. Moraes, e E. B. ArauÂjo, «Crystallization kinetics in phosphate sodium-based glass studied by DSC technique», *Journal of Physics and Chemistry of Solids*, pag. 4, 2003, doi: 10.1016/S0022-3697(02)00204-4.

[48] J. Massera, M. Mayran, J. Rocherulle, e L. Hupa, «Crystallization behavior of phosphate glasses and its impact on the glasses ' bioactivity», *Journal of Materials Science*, pagg. 3091–3102, 2015, doi: 10.1007/s10853-015-8869-4.

[49] M. Braun, Y. Yue, C. Rüssel, e C. Jäger, «Two-dimensional nuclear magnetic resonance evidence for structural order in extruded phosphate glasses», *Journal of Non-Crystalline Solids*, vol. 241, n. 2–3, pagg. 204–207, 1998, doi: 10.1016/S0022-3093(98)00802-3.

[50] Y. Yue, G. Carl, e C. Rüssel, «Rheological properties of calcium metaphosphate melts during extrusion», *Glass Science and Technology: Glastechnische Berichte*, vol. 72, n. 3, 1999.

[51] Y. Yue, C. Carl, G. Rüssel, M. Braun, e C. Jäger, «Structural order of extruded calcium metaphosphate glasses», *Physics and Chemistry of Glasses*, vol. 41, n. 1, pagg. 12–16, 2000.

[52] A. Paleari, V. N. Sigaev, N. V. Golubev, R. Lorenzi, e P. D. Sarkisov, «The role of networking in the optical anisotropy of hot-extruded calcium phosphate glass», *Materials Chemistry and Physics*, vol. 128, n. 1–2, pagg. 12–15, 2011, doi: 10.1016/j.matchemphys.2011.02.066.

[53] C. A. G. Kalnins, H. Ebendorff-Heidepriem, N. A. Spooner, e T. M. Monro, «Radiation dosimetry using optically stimulated luminescence in fluoride phosphate optical fibres», *Optical Materials Express*, vol. 2, n. 1, pag. 62, 2012, doi: 10.1364/ome.2.000062.

[54] C. A. G. Kalnins, H. Ebendorff-Heidepriem, N. A. Spooner, e T. M. Monro, «Enhanced radiation dosimetry of fluoride phosphate glass optical fibres by terbium (III) doping», *Optical Materials Express*, vol. 6, n. 12, pag. 3692, 2016, doi: 10.1364/ome.6.003692.

[55] E. Ceci Ginistrelli, «Advanced applications of phosphate glass optical fibres in photonics and biophotonics», PhD Thesis, Politecnico di Torino, Turin, Italy, 2018.

[56] G. Maze, V. Cardin, e M. Poulain, «Fluoride Glass Fibres For Telecommunications», *New Optical Materials*, vol. 0400, n. September 1983, pagg. 60–65, 1983, doi: 10.1117/12.935478.

[57] K. Itoh, K. Miura, I. Masuda, M. Iwakura, e T. Yamashita, «Low-loss fluorozirco-aluminate glass fiber», *Journal of Non-Crystalline Solids*, vol. 167, n. 1–2, pagg. 112–116, 1994, doi: 10.1016/0022-3093(94)90374-3.

[58] G. Tao *et al.*, «Robust multimaterial tellurium-based chalcogenide glass fibers for mid-wave and long-wave infrared transmission», *Optics Letters*, vol. 39, n. 13, pag. 4009, 2014, doi: 10.1364/OL.39.004009.

[59] G. Tsiminis, K. J. Rowland, H. Ebendorff-Heidepriem, N. A. Spooner, e T. M. Monro, «Extruded single ring hollow core optical fibers for Raman sensing», *23rd International Conference on Optical Fibre Sensors*, vol. 9157, pag. 915782, 2014, doi: 10.1117/12.2059407.

[60] D. J. Gibson e J. A. Harrington, «Extrusion of hollow waveguide preforms with a one-dimensional photonic bandgap structure», *Journal of Applied Physics*, vol. 95, n. 8, pagg. 3895–3900, 2004, doi: 10.1063/1.1667277.

[61] M. Zhu *et al.*, «Fabrication of an IR hollow-core Bragg fiber based on chalcogenide glass extrusion», *Applied Physics A: Materials Science and Processing*, vol. 119, n. 2, pagg. 455–460, 2015, doi: 10.1007/s00339-015-9017-3.

[62] G. Tao, S. Shabahang, S. Dai, e A. F. Abouraddy, «Multimaterial disc-to-fiber approach to efficiently produce robust infrared fibers», *Optical Materials Express*, vol. 4, n. 10, pag. 2143, 2014, doi: 10.1364/OME.4.002143.

[63] Y. Sun *et al.*, «Fabrication and characterization of multimaterial chalcogenide glass fiber tapers with high numerical apertures», *Optics Express*, vol. 23, n. 18, pag. 23472, 2015, doi: 10.1364/oe.23.023472.

[64] C. Jiang *et al.*, «Preparation of chalcogenide glass fiber using an improved extrusion method», *Optical Engineering*, vol. 55, n. 5, pag. 056114, 2016, doi: 10.1117/1.oe.55.5.056114.

[65] L. Jiang *et al.*, «Fabrication and characterization of chalcogenide polarization-maintaining fibers based on extrusion», *Optical Fiber Technology*, vol. 39, n. July, pagg. 26–31, 2017, doi: 10.1016/j.yofte.2017.09.020.

[66] J. Xiao *et al.*, «Investigation of tellurium-based chalcogenide double-clad fiber for coherent mid-infrared supercontinuum generation», *Optical Fiber Technology*, vol. 55, n. August 2019, pag. 102144, 2020, doi: 10.1016/j.yofte.2020.102144.

[67] Z. Xue *et al.*, «Mid-infrared supercontinuum in well-structured As–Se fibers based on peeled-extrusion», *Optical Materials*, vol. 89, n. January, pagg. 402–407, 2019, doi: 10.1016/j.optmat.2019.01.036.

[68] Z. Zhao *et al.*, «A novel chalcohalide fiber with high nonlinearity and low material zero-dispersion via extrusion», *Journal of the American Ceramic Society*, vol. 102, n. 9, pagg. 5172–5179, 2019, doi: 10.1111/jace.16439.

[69] X. Liang *et al.*, «Ultra-high germanium-contained Se-chalcogenide glass fiber for mid-infrared», *Infrared Physics and Technology*, vol. 104, n. November 2019, pag. 103112, 2020, doi: 10.1016/j.infrared.2019.103112.

[70] I. Ahmed, S. S. Shaharuddin, N. Sharmin, D. Furniss, e C. Rudd, «Core / Clad Phosphate Glass Fibres Containing Iron and / or Titanium», *Biomedical Glasses*, pagg. 20–30, 2015, doi: 10.1515/bglass-2015-0004.

[71] E. Roeder, «Flow Behaviour of Glass During Extrusion», *Journal of Non-Crystalline Solids*, vol. 7, pagg. 203–220, 1972, doi: 10.1016/0022-3093(72)90290-6.

[72] H. Ebendorff-Heidepriem e T. M. Monro, «Analysis of glass flow during extrusion of optical fiber preforms», *Optical Materials Express*, vol. 2, n. 3, pag. 304, 2012, doi: 10.1364/ome.2.000304.

[73] M. Trabelssi e P. F. Joseph, «Hole distortion and drift in extruded microstructured optical fiber glass preforms: Part I – Sensitivity analysis», *Journal of Non-Crystalline Solids*, vol. 481, n. July 2017, pagg. 208–224, 2018, doi: 10.1016/j.jnoncrysol.2017.10.045.

[74] H. Ebendorff-Heidepriem, J. Schuppich, A. Dowler, L. Lima-Marques, e T. M. Monro, «3D-printed extrusion dies: a versatile approach to optical material processing», *Optical Materials Express*, vol. 4, n. 8, pag. 1494, 2014, doi: 10.1364/ome.4.001494.

[75] S. Middleman, *Fundamentals of Polymer Processing*. New York, NY: McGraw-Hill, 1977.

[76] S. Middleman e J. Gavis, «Expansion and Contraction of Capillary Jets of Newtonian Liquids», *The Physics of Fluids*, vol. 4, n. 3, pag. 355, 1961, doi: 10.1063/1.1706332.

[77] R. I. Tanner, «A theory of die-swell», *Journal of Polymer Science Part A-2: Polymer Physics*, vol. 8, n. 12, pagg. 2067–2078, 1970, doi: https://doi.org/10.1002/pol.1970.160081203.

[78] R. I. Tanner, «A theory of die-swell revisited», *Journal of Non-Newtonian Fluid Mechanics*, vol. 129, n. 2, pagg. 85–87, 2005, doi: 10.1016/j.jnnfm.2005.05.010.

[79] J. Vlachopoulos e N. D. Polychronopoulos, *Understanding Rheology and Technology of Polymer Extrusion*. Dundas, ON, Canada: Polydynamics, 2019.

[80] M. Trabelssi, H. Ebendorff-Heidepriem, K. A. Richardson, T. M. Monro, e P. F. Joseph, «Computational modeling of hole distortion in extruded microstructured optical fiber glass preforms», *Journal of Lightwave Technology*, vol. 33, n. 2, pagg. 424–431, 2015, doi: 10.1109/JLT.2015.2388733.

[81] K. Bhowmick, D. Furniss, H. P. Morvan, A. B. Seddon, e T. M. Benson, «Predictive, Miniature Co-Extrusion of Multilayered Glass Fiber-Optic Preforms», *Journal of the American Ceramic Society*, vol. 99, n. 1, pagg. 106–114, 2016, doi: 10.1111/jace.13937.

[82] A. Belwalkar, H. Xiao, W. Z. Misiolek, e J. Toulouse, «Extruded tellurite glass optical fiber preforms», *Journal of Materials Processing Technology*, vol. 210, n. 14, pagg. 2016–2022, 2010, doi: 10.1016/j.jmatprotec.2010.07.018.

[83] S. Kainth, Die Design for Extrusion of Plastic Tubes and Pipes - A practical guide. Munich, Germany: Carl Hanser Publishing, 2017.

[84] M. Trabelssi e P. F. Joseph, «Hole distortion and drift in extruded microstructured optical fiber glass preforms: Part II – Optimization», *Journal of Non-Crystalline Solids*, vol. 481, n. July 2017, pagg. 412–423, 2018, doi: 10.1016/j.jnoncrysol.2017.11.021.

[85] J. E. Shelby, *Introduction to Glass Science and Technology*, 2nd ed. London, UK: Royal Society of Chemistry, 2015.

Chapter 4.

Active fibres for optical applications

Active fibres are one of the main subjects of the present work. Production and characterisation of these fibres were supported by the collaboration with LINKS Foundation. There is a long-lasting interaction between GLANCE (Glasses, Ceramics and Composites) group belonging to the Institute of Material Physics in the Department of Applied Science and Technology of Politecnico di Torino and LINKS Foundation. In recent years, fruitful teamwork involved our research group, which is focused on glasses for photonics, and the LINKS' PhotonLab. Some of the experiments described in the present chapter have been conducted inside the LINKS Foundation laboratories. These latter are equipped with the facilities to produce, characterise and post-process different kinds of active fibres, especially the ones made of soft glasses. On the other hand, in the labs at Politecnico di Torino, there is the equipment to design, produce, and process different kinds of glasses. Among these, chalcogenide and phosphate glasses are the best candidates for the design of optical amplifiers and lasers since they show a high solubility for rare-earth (RE) ions. For laser applications, the capability of highly doping the glass with RE ions allows increasing the concentration of active elements per unit volume. This, in turn, has fostered the design of compact devices even for high-power applications overcoming the main limitations of RE doped silica-based glasses. The possibility of designing miniaturised devices such as optical amplifiers may be useful in several applications. Thus, in the present thesis, phosphate glasses have been chosen and successfully employed to manufacture optical amplifiers with different characteristics and performances targeted at different optical design requirements coming from projects developed by the LINKS Foundation. Indeed, LINKS Foundation collaborates with Politecnico di Torino in several research projects involving international partners, like the Laser Zentrum of Hannover e.V. (LZH), the Tampere University of Technology (TUT), the Ben-Gurion University of the Negev (BGU), the United States Army Research Laboratory (U.S.ARL). Some of these projects are also supported by external funding such as the NATO – *Science for Peace and Security Programme*.

The present chapter is focused on the work realised in the framework of these projects in which glass extrusion has been used as one of the steps in the production of active fibres.

The main goal concerning this part of the thesis work was to realise novel and custom active fibres for optical amplifiers. The requirements of these amplifiers were the compactness and the capability of working in high-power applications. Such target devices have driven the choice of the material towards phosphate glass fibres doped either with ions of Er^{3+} or with a combination of Er^{3+} and Yb^{3}.

4.1 The design of active fibres for optical applications

Both the design and the production of glass fibres for optical applications are complex tasks, involving multidisciplinary knowledge, indeed:

(i) some aspects are related to **material science and chemistry**, like the selection, synthesis, and characterisation of the employed materials (glasses for the fibre, polymer for the coating, metals or ceramics for the processing equipment);

(ii) some aspects are more focused on the **physics** of light propagation and **optical** measurements and simulations;

(iii) the **electronic system** must be considered as well, either for the material processing or for the fibre characterisation;

(iv) **technological and software design** skills are also needed, in particular for the design of the extrusion and the control of the process during all the fabrication steps.

During the current chapter, we will also present the results that we achieved with an active phosphate glass fibre (made with a partially extruded preform) co-doped with Er^{3+} and Yb^{3+} and tested in a Master Oscillator Power Amplifier (MOPA) configuration [1]. This is a standard configuration for optical amplification. The system is composed of two stages: a laser seed stage, where a laser pulse is generated and may be modulated according to the needs, and a proper amplification stage. A simplified sketch of the system is reported in Fig. 4.1. The main advantage of this system is the ability to decouple the high-power section from all the other components; this allows increasing the system flexibility. In our case, the amplification stage has been designed with a custom fibre, obtained by drawing a preform obtained using extrusion. The active fibre lengths were in the order of a few centimetres.

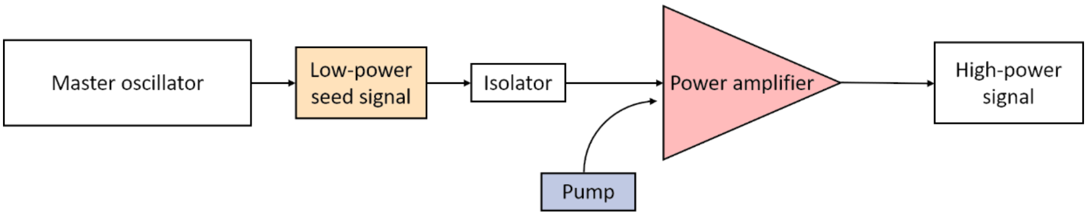

Fig. 4.1. Simplified scheme of a MOPA system. The power amplifier is the component specifically developed during the present work.

The high doping level (3.86×10^{20} ions/cm^3 of Yb^{3+} and 1.93×10^{20} ions/cm^3 of Er^{3+}) allowed reaching high gain (10.9 dB) within only 14 cm of fibre. This is a great advantage compared to usual silica fibres that typically achieve a gain in the order of 2-3 dB/m [1]. The high amplification obtained with our phosphate fibre allows using a weak power seed signal and designing a device featuring high performances with reduced dimension. This can be useful for a portable laser system, that can be mounted on a flying drone, like the one required in the *CompAct eye-safe LIdar source for airBorne lasER scanning* (CALIBER) project, to which both LINKS Foundation and Politecnico di Torino are participating. This international project is aimed at the analysis of the integration of a phosphate glass-based LIDAR system into a small to medium unmanned aerial vehicle (UAV). Such a system finds wide applications and is intended to be employed for monitoring strategic sites. As mentioned, Politecnico di Torino has contributed to the project in the design and fabrication of the fibre for the amplification stage.

In this framework, the employment of the extrusion technique for the realisation of part of the preforms offered several advantages, the main one being related to the preforms' dimension. In particular, the ratio between the internal and external diameters is a special feature of our extruded preforms. Especially the preforms produced for single-mode active fibres show a very small core diameter. Except for vapour deposition techniques, preforms for these kinds of fibres are usually obtained with a double cladding assembly, to allow for the required core dimensions [2]–[4]. One of the main methods to produce lab-scale glass tubes is the rotational casting technique. This technique has substantial limitations in terms of the allowed core/cladding ratio. In fact, during casting the molten glass adheres to the mould surface due to the centrifugal effect, and a hole is formed in the middle. The hole dimensions are related to glass viscosity and speed of rotation and, despite the efforts to vary these parameters, the core/cladding ratio of a rotational cast preform in the case of phosphate glasses cannot exceed the values of 0.4 – 0.6 [5]. Thus, a double-cladding technique was often employed: the core/1st cladding assembly is stretched to fit into the hole of a 2nd cladding. This allows for a more flexible core/external cladding ratio, but it is a time-consuming technique since both the tubes and the core rod have to be polished by hand. On the contrary, the extrusion process allows removing all these steps and directly obtaining the final shaped tube, with more flexibility in terms of hole dimension. The minimum core/cladding ratio obtained during the present work with the preform extrusion technique is around 0.1.

In this scenario, to achieve the desired efficiency for the fibre amplifier, the main steps can be summarised as follow:

(i) define a suitable glass composition and production techniques;
(ii) characterise the glass and calculate the related NA, based on the refractive index difference between the core and cladding glasses;
(iii) use the NA to calculate the required fibre core diameter that leads to single-mode light propagation;
(iv) calculate the desired die dimensions based on the required core/cladding ratio, also taking into account the flexibilities of both the extrusion and drawing process;
(v) design and produce the extrusion die;
(vi) produce the core by casting, polishing, and stretching the active glass
(vii) produce the cladding by casting and extruding the passive glass;
(viii) assembly core and cladding with the rod-in-tube-technique, thus obtaining the final preform;
(ix) draw the preform into a fibre;
(x) characterise the fibre and test it into the final configuration of the device.

During this thesis's work, a contribution was given in all the mentioned fields, except for fibre characterisation, conducted by Dr Nadia G. Boetti and her collaborators in the PhotonLab at LINKS Foundation as well as in BGU laboratories.

In the next paragraphs, the target applications will be described first. Then, details about the theoretical background are provided together with the practical results of glass synthesis, processing, as well as the design, production, and characterisation of active fibres.

4.1.2 Laser Imaging Detection And Ranging (LIDAR)

Also called LIght Detection And Ranging in analogy with its ancestor, i.e. the radar (RAdio Detection And Ranging), in recent times the LIDAR technology represented a great advance especially for topographic investigation and physical detection. The idea has been developed in the early days of the laser, at the beginning of the 1960s, with the name *Colidar*, where the prefix *co-* was used to highlight the coherence of the emitted light.

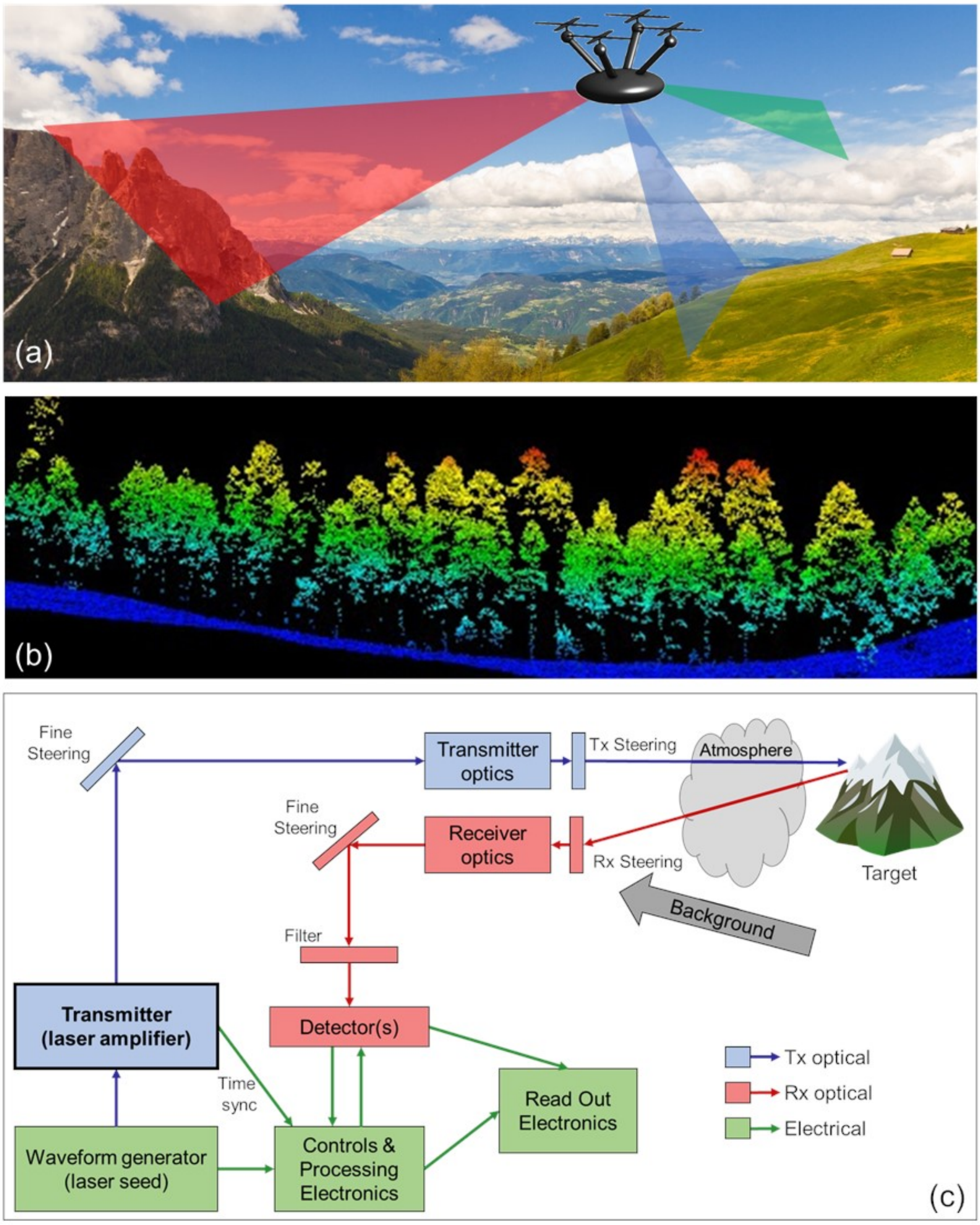

Fig. 4.2. Working principles of LIDAR. (a) Rendering of the mechanism of a LIDAR system mounted on a UAV. (b) Example of a LIDAR image of a forest (image in the public domain, taken from the United States Department of Agriculture). (c) Sketch of the main components of a LIDAR system; the laser amplifier, subject of the present work, is highlighted with a bold font (image adapted from [6]).

The basic mechanism of the LIDAR is intuitive: a laser signal, usually pulsed, is emitted through the environment under study and the reflected signal is collected by a photodetector. Depending on the wavelength of the emitted signal and on the type of scattering that is detected, the processing of the reflected signal can provide lots of information. The rendering of Fig. 4.2a illustrates the behaviour of a LIDAR system mounted on a UAV, while Fig. 4.2b is an example of a LIDAR image and Fig. 4.2c shows a scheme of the main components of a typical LIDAR. By now, the system is employed in a wide variety of fields. It is worth showing a list of the main applications to have an idea of their diversity: geology, topology, astronomy, archaeology, atmospheric measurements (clouds, aerosols, gases, wind, temperature, pollution), agriculture, biology and forest conservation, automotive (obstacle and road environment recognition for autonomous vehicles but also speed detection for traffic enforcement), military, forensic, mining and rock mechanics, etc. A research on the database of *Web of Science* for the word “LIDAR” gave more than 40k results. Fig. 4.3 shows the trend in publications for this search key. The first scientific paper appeared in 1965 [7] and, since then, the growth in the number of publications per year fit an exponential curve. Furthermore, as the inset in Fig. 4.3 shows, the list of *Web of Science Categories*, i.e. the main topics of the publications, is also quite long: 178 different topics can be connected to the word “LIDAR”. Among these topics, the most important are Remote Sensing, Optics, and Meteorology, followed by Electrical & Electronical Engineering, Geoscience, and Imaging Science. Yet, only 14 topics show more than one-thousand publications each, 93 topics have between one-thousand and ten publications each and 71 topics have less than ten publications each. From this broad distribution, it is possible to see the diversity of applications that involve LIDAR as the main subject.

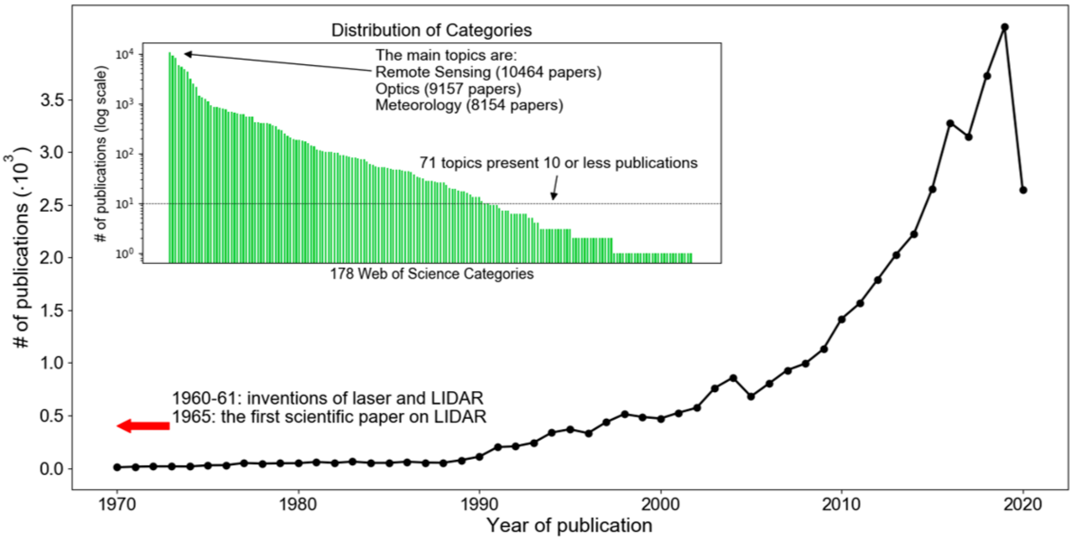

Fig. 4.3. A plot of the number of publications during the last fifty years regarding “LIDAR”. The inset shows a semilogarithmic plot of the distribution of categories associated with each publication. The most recurrent topics are Remote Sensing, Optics and Meteorology, but the tail of the distribution comprises also 71 topics with 10 or fewer publications each.

Within the CALIBER project, a LIDAR system was designed to be mounted on a UAV for environmental monitoring of specific areas. Thus, the target application required to work in normal conditions (ambient temperature and pressure). To reach the desired laser power, an optical amplifier is needed, which must work at specific wavelengths (all in the eye-safe range, around 1.5 µm) and is required to sustain a nearly single-mode propagation. The proposed solution satisfied the requirement of the project and is now further investigated to finalise the device.

4.1.3 Optical amplifier

An optical amplifier is a device in which the gain medium may be an active glass fibre and the signal to be amplified is coupled with a pump signal into the core of the fibre.

The contribution of the present work to this subject has been related to the development of a phosphate glass doped with Er_2O_3 or a combination of Yb_2O_3 and Er_2O_3, to produce the active core of optical fibres. The extrusion process was then employed to realise hollow structures required for the cladding of the fibre preforms. Indeed, the cladding of the fibre must be made of a passive glass in which the active ions have been replaced by other lanthanides oxides (such as La_2O_3 or Gd_2O_3). Several billets of such passive glasses have been produced and characterised in terms of their refractive index and thermal behaviour. The billets were then extruded with a die specifically designed for each application. The extruded tube was assembled with a stretched rod made of the active glass, and the preform, obtained with this *rod-in-tube* technique, is drawn to a 125 – 250 µm fibre.

Active fibre principles

In active fibres, the core, i.e. the region in which the light is confined, is typically made of a glass doped with active ions. When the light travels inside the fibre, if the incoming radiation has the proper wavelength, the active ions may absorb and release some energy (not all, due to non-radiative decays) by emitting a photon at a slightly higher wavelength. This process is called *stimulated emission* and is the fundamental phenomenon involved in the generation of laser light and optical amplification. The wavelength of the incoming light is of crucial importance, since each ion shows a different absorption spectrum, with characteristic peaks at specific wavelengths. In Fig. 4.4 the absorption spectrum of Er^{3+} is plotted for wavelengths ranging from 300 to 1700 nm. The most interesting absorption peaks for laser applications are highlighted with red arrows. The inset of Fig. 4.4 shows the model of a 2- or 3-level laser system, with the indication of the associated transitions. The peaks around 1500 nm are particularly relevant for environmental LIDAR applications since these wavelengths belong to the so-called *eye-safe range*. The interaction of the human retina with light at wavelengths of 1.4 – 1.8 µm is negligible, thus allowing for laser shine in an open environment without the risk of personal injuries.

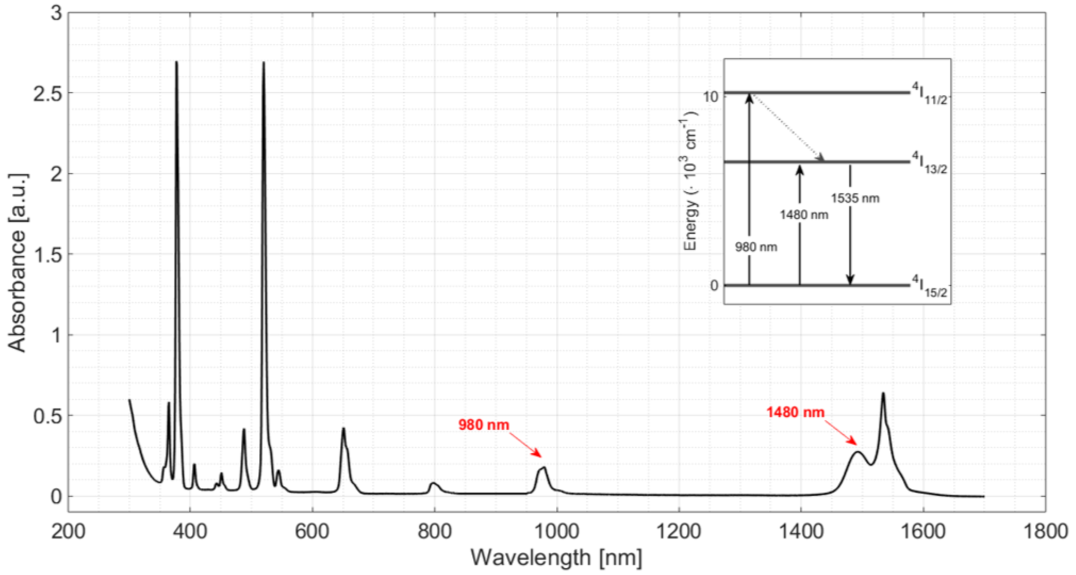

Fig. 4.4. Absorbance spectrum of Er^{3+} ions acquired with a UV-vis-NIR spectrophotometer. The red arrows highlight the most important absorption peaks employed for laser emission (adapted from [8]). In the inset, the 2- or 3-levels laser schemes are reproduced, showing the main transitions of Er^{3+}: the absorptions at 980 nm or 1480 nm are represented with arrows pointing up, the emission at 1535 nm with a downwards arrow and the non-radiative transfer between the levels $^4I_{11/2}$ and $^4I_{13/2}$ with a dashed arrow. (Energy levels are taken from [9])

Indeed, to generate laser light, the stimulated emission is not sufficient by itself but there is the need for some amplification (the word *laser* is the acronym of Light Amplification by Stimulated Emission of Radiation). To get amplification, we need a cavity, i.e. a confined structure that allows multiple reflections of the incoming light. To build a laser, which is a confined optical amplifier, an active medium has to be shined with two optical signals: the pump signal is used to create the so-called *population inversion*, i.e. to have enough ions in the excited energy state; then, the ions illuminated by another optical signal can decay to the lower energy state by emitting a photon, which is in phase with the incoming signal. This description represents the working mechanism of an optical amplifier. The second signal is the one that is amplified, and the pump signal is the one providing the energy for the amplification. If the radiation travels many times in the active region, because of confinement at the ends of the fibre provided by mirrors (or, better, by fibre Bragg gratings), the amplification is increased, and we are finally able to generate coherent laser light.

In the near-infrared region (0.7 – 3 μm) most of the lanthanides, or rare-earths ions, exhibit several transitions. These ions can be added in the form of oxides to the core glass composition. During the glass fabrication for the core, they are dissolved into the glass matrix and become part of the glass network.

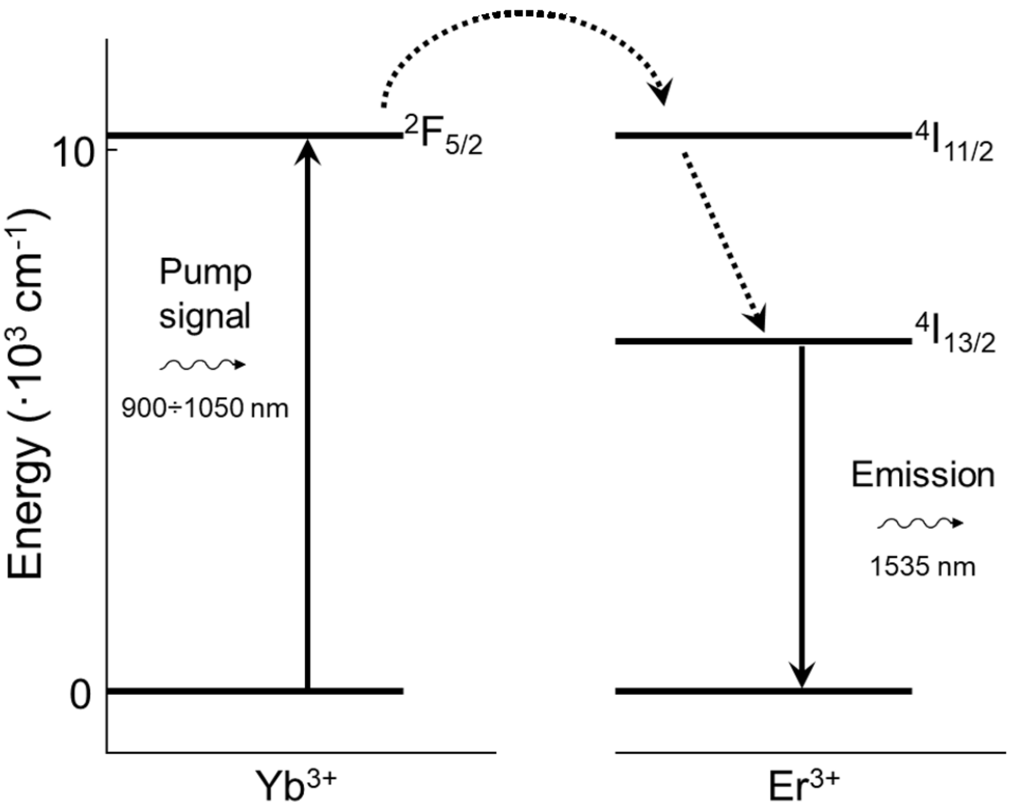

Fig. 4.5. Laser scheme of a Yb-Er co-doped system. The pump signal excites the Yb^{3+} ions to the high-energy level, the $^2F_{5/2}$ level. The energy is transferred with non-radiative processes to the $^4I_{11/2}$ level and then to the $^4I_{13/2}$ level of Er^{3+} ions, from which laser emission finally occurs, with a wavelength of 1535 nm.

In this way, in a system doped with a single active ion, i.e. Er^{3+}, the pump radiation excites the ions to the lasing level (i.e. the $^4I_{13/2}$ level of Fig. 4.4) and the signal induces the transition with the emission of the amplified radiation. Er^{3+} ions can be excited either at 1480 nm or at 980 nm. In both cases, the emission peak is centred at 1535 nm. In an Er^{3+}/Yb^{3+} co-doped glass, each different active ion has its role. Fig. 4.5 shows the energy level diagram of such systems. The $^2F_{5/2}$ level of Yb^{3+} ions is populated due to the absorption of pump radiation. Usually, the pump wavelength is 980 nm due to the high availability of light sources operating at that wavelength, such as semiconductor laser diodes. Yet, the absorption spectrum of Yb^{3+} is quite wide and extends down to 900 nm and up above 1000 nm. The ions in the populated high-energy state of Yb^{3+} may transfer their energy to the $^4I_{11/2}$ level of Er^{3+}, from which the $^4I_{13/2}$, i.e. the usual lasing level of Er^{3+}, is filled through nonradiative decay. For this mechanism to be efficient, the transfer of energy should proceed only from Yb^{3+} to Er^{3+} and not in the opposite direction. This can be controlled by minimising the lifetime of ions that populates the $^4I_{11/2}$ state of Er^{3+}. In this way they directly tend to transition to the $^4I_{13/2}$ level by nonradiative decay, thus the back-transfer from Er^{3+} to Yb^{3+} ions is minimised. Furthermore, the lifetime of the $^2F_{5/2}$ level of Yb^{3+} should be long enough to allow the transfer to Er^{3+} and avoid spontaneous Yb^{3+} emission. The interaction of the Er^{3+} and Yb^{3+} ions has been extensively studied in both alkali silicate glasses and phosphorus-doped silica but it was demonstrated to be more effective in phosphate glasses [10].

If the proper quantity of active ions is added to the core glass composition, a uniform *cloud* of active elements is formed inside the core. When the light is forced to propagate inside the core, the higher the active ions content, the higher is the probability of light/ion interactions. This explains the research interest in using phosphate glasses since they offer the possibility to increase the doping level above the values usually employed with silica.

4.1.4 Active glasses

Bulk active glasses have appeared in the early 1960s [11] and, within a few years, also active glass fibres were demonstrated [12]. In the following decades, several studies on the optical properties of different lanthanides ions dissolved into various glass matrixes have been conducted [10]. The importance of active fibres has further increased when Erbium Doped Fibre Amplifiers (EDFAs) have been developed. Those are optical amplifier made with an Er^{3+}-doped silica fibre (the glass composition may contain also GeO_2, Al_2O_3, P_2O_5, B_2O_3) [13]. In optical communications, the possibility of the employment of an all-optical amplifier has been a fundamental upgrade, that allowed avoiding the double conversion of optical signals to electrical and vice versa.

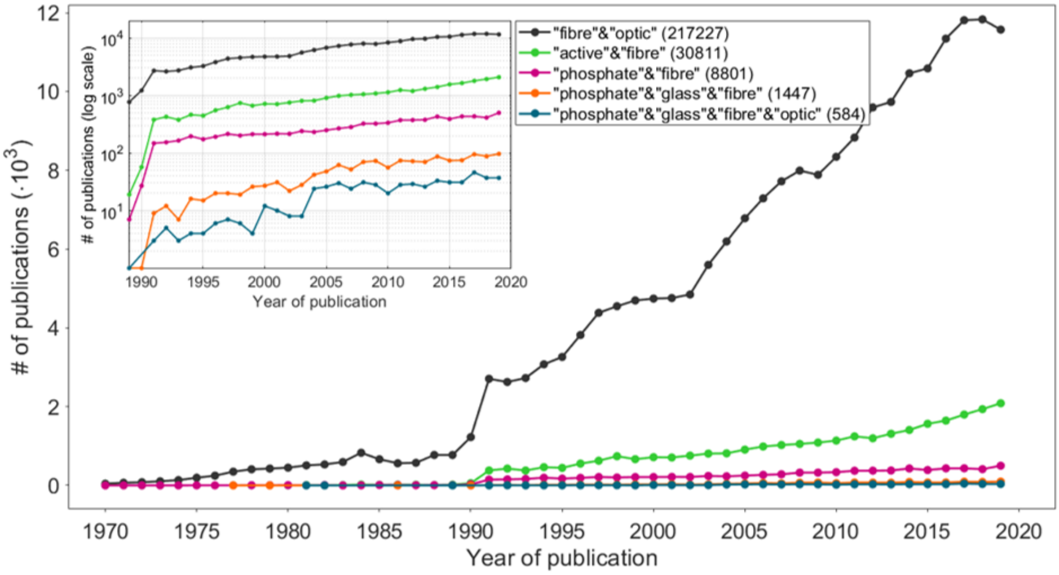

Fig. 4.6. A plot of the number of publications during the last fifty years for a combination of different search keys. The search keys for each curve are detailed in the legend, with the number of results shown in parentheses. To better highlight the trend of publications over time also for the less common results, a semilogarithmic plot of the same quantities is shown in the inset. Data are taken from the *Web of Science* online database.

Fig. 4.6 shows a trend of the number of publications for different search keys. The data are derived from the *Web of Science* online database [9]. The increasing interest in the research about “fibre optic” is demonstrated by more than 217k papers on the subject with more than 10k publications each year in the last five years.

Furthermore, from the inset of Fig. 4.6, it is possible to note how also the topics of “active fibre”, “phosphate fibre”, “phosphate glass fibre”, and “phosphate glass optical fibre” show a trend similar to “fibre optic”, whereas for a lower total number of papers. Also, the topics of “phosphate fibre”, “phosphate glass fibre”, and “phosphate glass fibre optic” are quite recent, since only a few publications were available before 1990. The inventions of optical amplifiers and EDFA, together with other discoveries and studies in the field of optical communication, are the main ones responsible for the sharp increase in the published works in all the fields that occurred in the last decade of the 20th century. The other interesting information in this graph is evidenced by the gap between “phosphate glass fibres”/“phosphate glass fibre optic” and general “phosphate fibre”, accounting for the research of *fibres*-related topics concerning biomedical or mechanical applications of fibrous non-optical material. In recent times, this gap is narrowing due to the growing interest in optical applications.

Phosphate glasses are excellent candidates for active glass fibres applications. One of the main reasons is the high solubility of RE ions that may reach levels of 10^{21} ions/cm^3, typically 50 times higher than standard silica glass [2]. Furthermore, phosphate glasses show the largest cross-section for stimulated emission among the oxide glasses, with values up to 4.8 10^{-20} cm^2 [14]. A high cross-section means that high optical gain can be achieved. Unfortunately, the counter effect is usually a reduction of the fluorescence lifetime value, which is typically one-half of silicate glasses [14]. The optical properties of Er^{3+}-doped or Er^{3+}/Yb^{3+} co-doped phosphate glasses are the subject of several studies [2], [8] [15]. In some of these works [8], the attention is focused on the occurrence of concentration quenching. This phenomenon takes place at high concentrations of RE elements. In fact, at sufficiently low concentrations (the specific value varies with the host glass composition), the RE ions immersed in the glass matrix can be thought of as *isolated* or not influenced by the environment. Yet, above a certain concentration of active RE, that is specifically related to the host material, these ions are not fully coordinated by the bridging and non-bridging oxygens present in the glass network: they also interact with one another and tend to cluster together. This proximity causes the RE ions at the ground level and at the excited state to exchange some energy, causing non-radiative cooperative relaxation phenomena [10]. Phosphate glasses can host a higher amount of Er^{3+} ions

---

[9] https://www.webofknowledge.com

than silicate glasses, due to the specific electronic environment that is locally created. However, it is reported how a maximum amount of Er^{3+} of 10.5 mol% showed a reduced lifetime for the $^4I_{13/2}$ transition of nearly 2 ms, compared with the value of 7 ms obtained for the glass with 1.0 mol% of Er^{3+} ions [8]. Diminished emission performances, or as in this case, a reduction of the lifetime, can be related to different absorption phenomena. In the case of the cited work, the influence of the OH^- groups absorption may also be significant.

In pure silica, Er^{3+} ions tend to cluster even at a concentration below 1 mol% [16]. The co-doping of silica with aluminium helps to reduce the concentration quenching phenomenon [13]. Many other glasses have been tested as hosts for RE ions. Among them, fluoride (fluorozirconate) and chalcogenide glasses show another important property which is low phonon-energy. This feature helps in controlling the rate of multiphonon nonradiative relaxations. Those events may reduce the population of the excited state, thus hindering the emission performances. Another well-known issue is the presence of OH^- ions in the glass composition [10], [14]. The coupling of the rare-earth states with the high-energy vibrations (around 3000 cm^{-1}) of OH^- can induce nonradiative decay. The contribution of this latter phenomenon to the overall nonradiative decay is considered to be larger than that of the multiphonon relaxation process [10]. Furthermore, the stretching vibration of OH^- groups is responsible for the absorption around 3.0 μm that limits the applications at that wavelength [14]. The excited-state absorption (ESA) is also an unwanted phenomenon that affects laser behaviour. ESA happens when an ion in a metastable state is excited to a higher energy level, usually followed by nonradiative decay back to the starting level. As an example, in tellurite glasses, co-doping with Ce^{3+} reduced the excited state absorption from the $^4I_{11/2}$ level of Er^{3+} and allowed improving the gain of the laser [17].

These and other phenomena contribute to the decrease of efficiency of lasing performance and are mainly related to the host glass composition. The efficiency of amplification is not the only aspect to consider when designing an amplifier. The competition between gain and fluorescence lifetime sometimes promotes intermediate candidates [8].

One of the most critical aspects in the fabrication of phosphate glasses for active fibres is the presence of OH^- groups that are not easy to remove during the glass synthesis. The negative effect of the OH^- groups is not only limited to radiation absorption, but they may also interact with the RE ions inducing nonradiative emissions. The presence of the OH^- groups can be detected by FTIR spectroscopy and is visible in the FTIR spectra reported in Fig. 4.7. In that figure, FTIR measurements are compared for glasses with different concentration of Er^{3+} ions. The peak around 6500 cm^{-1}, i.e. centred at a wavelength of 1535 nm, is associated with Er^{3+} emission and, as expected, becomes more intense by increasing the amount of Er_2O_3 in the glass composition.

The broad peak at around 3000 cm^{-1} gives evidence of the presence of OH$^-$ groups. In the case of the curves shown in Fig. 4.7, the OH$^-$ absorption peaks show a reduced intensity, related to the reduced water content in the glass. Yet, some small differences between the samples doped with a different amount of Er^{3+} are present and are ascribable to tiny variations in the process conditions. In detail, the sample with the lowest Er^{3+} concentration resulted to have slightly higher water content.

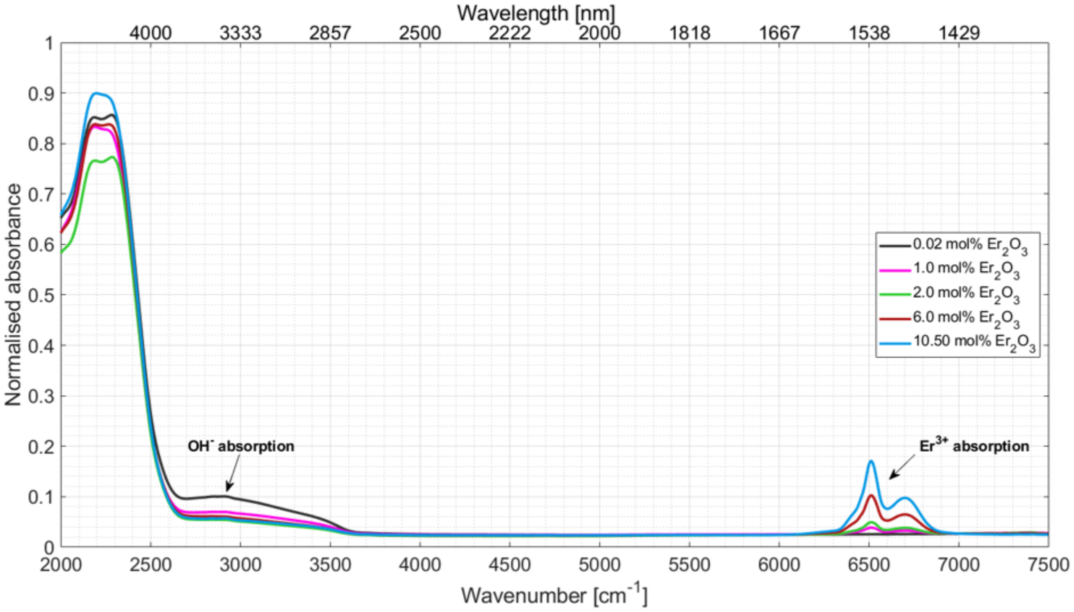

Fig. 4.7. A plot of FTIR spectra of different phosphate glasses with different Er_2O_3 mol%. The absorption peaks related to Er^{3+} ions and OH$^-$ groups are highlighted (data are adapted from [8]).

Due to this high sensitivity to external conditions, during glass fabrication, constant attention is dedicated to the minimisation of humidity inside the working environment. The weighting of the reagents is carried out in a controlled N_2 atmosphere environment, with relative humidity lower than 0.1%. During each step of the process, the powders are preserved from any contact with humid air. The melting process is also designed to remove any residual moisture: a controlled atmosphere is kept inside the furnace for the whole fusion process, thus forcing the residual H_2O to evaporate.

To satisfy the requirements of the different projects, we synthesised several custom-made phosphate glass compositions. The specific choice of each component of the glass matrix, and its quantity, influences the thermal, mechanical, chemical, and optical properties of the glass. This is the reason why we modified an already known composition, adapting it to the specific needs of each application. During the current work on active fibres, we prepared, characterised, extruded, drawn, and tested several slightly different glass systems all based on P_2O_5 as the main network former. The prepared glasses also contained different portions of K_2O, Li_2O, BaO, B_2O_3, PbO, SiO_2, La_2O_3, Gd_2O_3. The selection of phosphate glasses is also supported by technical considerations: our available facilities, like the extruder and the drawing tower, are designed to work with soft glasses and could not operate at higher temperatures, like the ones used in the processing of silica. Tellurite or chalcogenide glasses could be also good alternatives in terms of processing temperatures, but they are less performant in terms of RE solubility, chemical stability in environmental conditions, and processability (tellurite glasses have a *steep* viscosity-temperature curve often accompanied by a high tendency to devitrification [18], [19])

4.2 Active glass and passive billet fabrication

The preparation of an active fibre by rod-in-tube technique requires at least two glasses: an active core and a passive cladding. In the present work, the core is made by stretching a rod of phosphate glass doped with active RE ions. At the same time, the cladding is made by billet extrusion of passive phosphate glass. The cladding hole and core rod dimensions are calculated to meet the project specifications. The extrusion process allowed obtaining tubes with a sufficiently small central hole, to match the project needs that are related to light-guiding properties, as further detailed in the following paragraphs.

4.2.1 Glasses preparation and characterisation

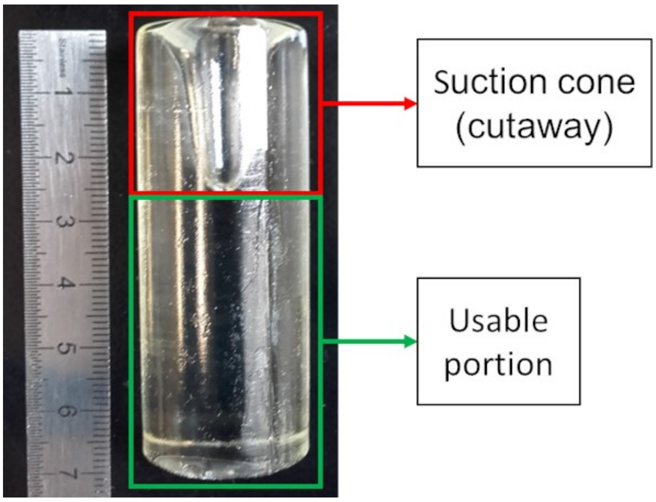

Fig. 4.8. Example of a glass billet with highlighted the usable portion and the suction cone, which has to be removed before the extrusion.

Syntheses of the glasses are realised as described in Chapter 2. The powder reagents are mixed in a controlled atmosphere environment, to avoid contamination with external agents, especially environmental humidity. During the core glass preparation, also some compounds of active elements such as Er_2O_3 and Yb_2O_3 are added to the mixture. The amount of RE ions that is introduced is calculated for the specific application, according to the desired performances. In the present research projects, the amount of Er_2O_3 is varied between 0.75 mol% and 1 mol%, and eventually, Yb_2O_3 is added with a ratio Er:Yb ranging between 1:2 and 1:4. The glass batch is melted in a furnace at 1200 °C. The melting is carried out in alumina or Pt/Rh crucibles. Part of the cast glass is melt-quenched on a cold metal surface for laboratory analysis and quality control, e.g. to detect any compositional inhomogeneities and to carry out some preliminary measurements such as DTA. Instead, the rod for the core is obtained by casting the molten glass into a preheated cylindrical mould with a diameter of 12 mm and 150-mm height. The cast rod is then annealed to release internal stresses.

After casting and annealing the rod must be polished by hand, with polishing papers of different grades. In this way, it is possible to smooth all the signs of the mould and then gradually refine the surface to remove any scratch visible to the naked eye and reach an R_a lower than 100 nm. The polished core rod is then mounted onto the drawing tower and heated until it stretches to a diameter between 1 and 2 mm, according to the size required by the specific preform that varies for each application.

The glass synthesis for the cladding preparation differs from the core one only concerning the absence of active elements since all the weighting, mixing, melting, and casting are carried out in the same way. Besides, the employed mould for cladding has the shape of a billet, i.e. a 25-mm diameter, 50-mm height cylindrical mould in our case. After casting and annealing, the obtained billet is cut to remove the suction cone (see Fig. 4.8) and then is inserted into the furnace of the extruder. By employing the proper die, the cladding tube is then formed via billet extrusion.

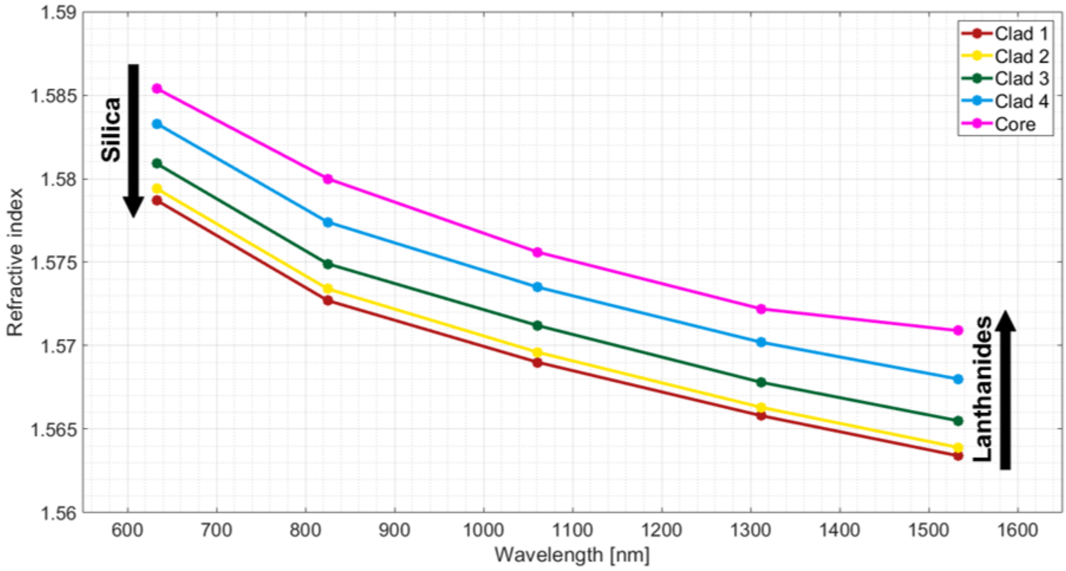

Fig. 4.9. Dependence of the refractive index on the wavelength, for different glass compositions. Different cladding glasses have been prepared by varying the glass compositions. The high refractive index of the core glass is obtained by adding rare-earth oxides (both passive and active ions).

The optical characterisation of the cast glass is carried out with UV-vis-NIR spectroscopy (see Fig. 4.4) and refractive index measurement. The influence of the glass composition on the refractive index of the glass is visible in Fig. 4.9. By varying the relative amount of SiO_2 and lanthanides (either passive La_2O_3 and Gd_2O_3 for the cladding or active Er_2O_3 and Yb_2O_3 for the core), the refractive index of the cladding may be varied to match the required parameters. The value of the refractive index is of great importance for the guidance and mode characteristics of the fibre and it is fundamental for the fibre design, thus the measurement is usually repeated several times in different positions of the sample, to verify the homogeneity of the glass and to reduce the sources of systematic error.

The thermal characterisation is also important, and DTA or DSC curves are acquired for each glass. Furthermore, by using dilatometry, the coefficient of thermal expansion during heating is also registered, together with the dilatometric softening temperature, and the viscosity-temperature relationship of the glass.

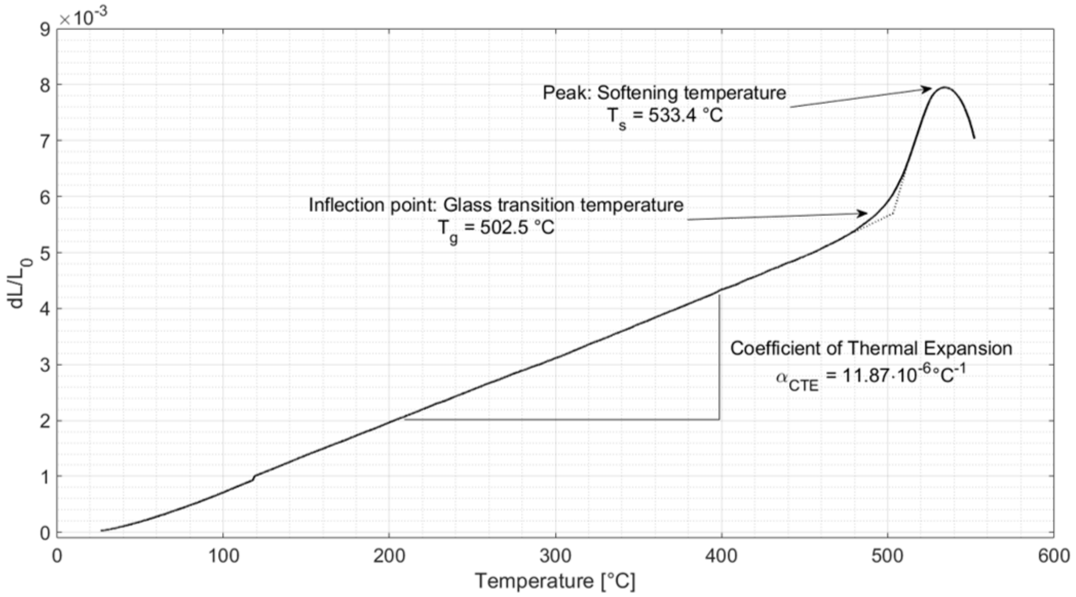

Fig. 4.10. Dilatometry of an active phosphate glass doped with Er^{3+} and Yb^{3+}. The slope of the curve in the linear range (up to 460 °C) represent the Coefficient of Thermal Expansion α_{CTE}. The inflexion point of the curve represents the T_g and the peak evidences the dilatometric softening temperature T_s. The measurement is conducted with a heating rate of 5 °C/min.

The dilatometric curve of an active phosphate glass co-doped with Er^{3+} and Yb^{3+} is shown in Fig. 4.10, while DSC associated with viscosity measurement is plotted in Fig. 4.11.

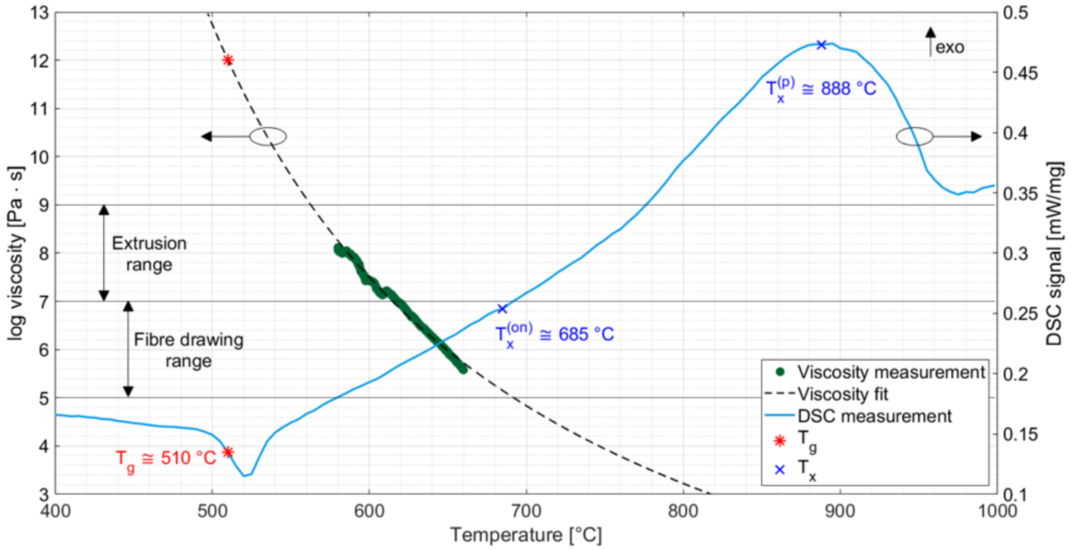

Fig. 4.11. Thermal behaviour of the Er:Yb co-doped active glass. The viscosity is measured with the cylinder compression test over the temperature ranges of extrusion and fibre-drawing (dark-green dots). The measured values fit a Vogel-Fulcher-Tamman exponential curve (dashed black line) intercepting the T_g (red star) for a viscosity of 10^{12} Pa·s. The results of a DSC measurement are also reported (light-blue line), with the indication of glass transition temperature T_g at the inflexion point (red star) and both the onset and the peak of crystallisation temperature T_x (blue crosses).

The investigation of optical and thermal properties of the glass has also the goal of enlarging the spectrum of knowledge on the behaviour of different glasses as well as on the influence of both the composition and the processing on glass properties.

4.2.2 Preform design for single-mode active fibre

Light propagation properties in the fibre are of paramount importance and are determined by the geometric characteristic of the core/cladding and the refractive index of the materials employed. Optical properties can be designed by considering these factors and studying the propagation of modes inside the fibre. Indeed, when the electromagnetic field is calculated by applying Maxwell's equations to a confined space, like the core of an optical fibre, the solutions can be considered in terms of transverse modes, travelling with specific propagation constant [20]. As represented in Fig. 4.12a, the fibre is considered as an infinite medium in the *z*-direction, or the direction of propagation, while the symmetry of the system is circular on the *x*-*y* plane.

When applying Maxwell's equations to this geometry, the solutions take the form of the so-called Helmholtz's wave equation. Only the light waves that satisfy Helmholtz's equation can propagate inside the fibre. These propagating waves are described as a superposition of transverse modes. The fundamental mode, represented by a Gaussian beam with its maximum in the centre of the fibre core, is present even for very small core diameters (the minimum allowed dimension for the core also depends on the wavelength of the radiation, as explained next). By increasing the core

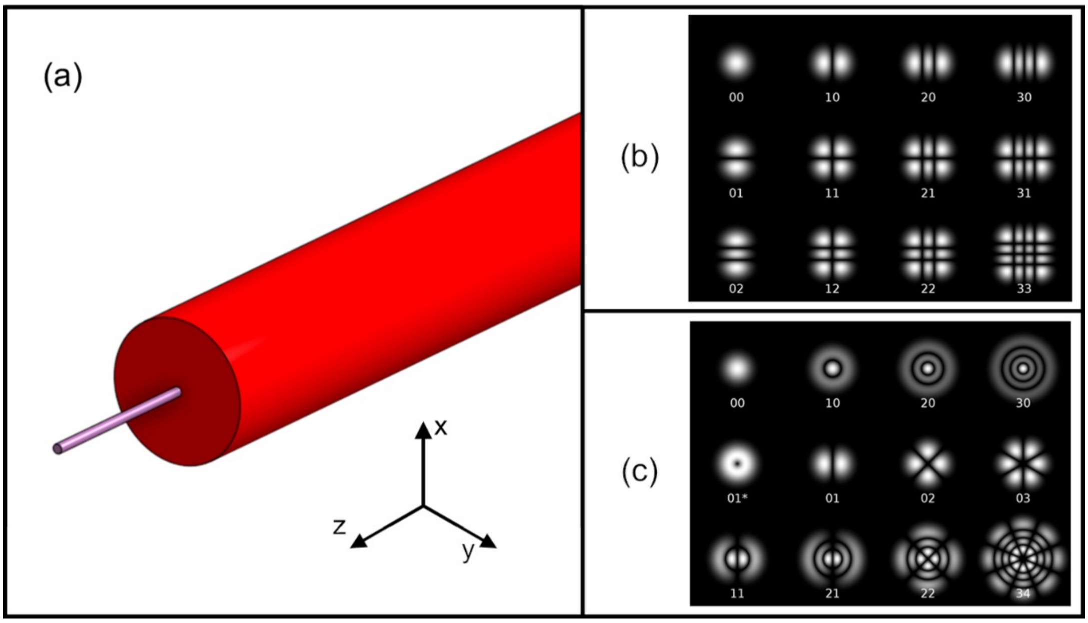

Fig. 4.12. Fibre propagation properties: (a) sketch of the fibre; (b) Hermite-Gauss and (c) Laguerre-Gauss transverse mode patterns assumed by the propagating light in the core of the fibre [author of (b) and (c): Bob Mellish]. Images available under the Creative Commons Attribution-Share Alike 3.0 Unported license.

radius or the refractive-index difference between core and cladding, high-order modes are allowed to propagate. The shape of these higher-order modes can be measured, and analytically derived, for each specific system. From a mathematical point of view, the shape of the mode can be calculated as a combination of the Gaussian beam solution with higher-order polynomial functions (such as Bessel's, Laguerre's, or Hermite's polynomials). All the higher-order modes have more than one off-centred maximum [20]. The shape of Hermite-Gauss and Laguerre-Gauss modes is depicted in Fig. 4.12b and Fig. 4.12c respectively.

To avoid mode dispersion and other detrimental effects due to multimode propagation, the single-mode regime is preferred when working with optical amplifiers. Indeed, it is demonstrated that the gain of the amplifier can be increased in single-mode devices [1].

The mode propagation properties inside the fibre can be predicted by computing the *V number*. This quantity is also called the *normalised frequency* and is expressed by the equation:

$$V = \frac{2\pi a}{\lambda} NA$$

where a is the core radius, λ is the wavelength of the propagated light and NA is the numerical aperture, which is related to the refractive index difference between the core and the cladding ($NA = \sqrt{n_{core}{}^2 - n_{cladding}{}^2}$).

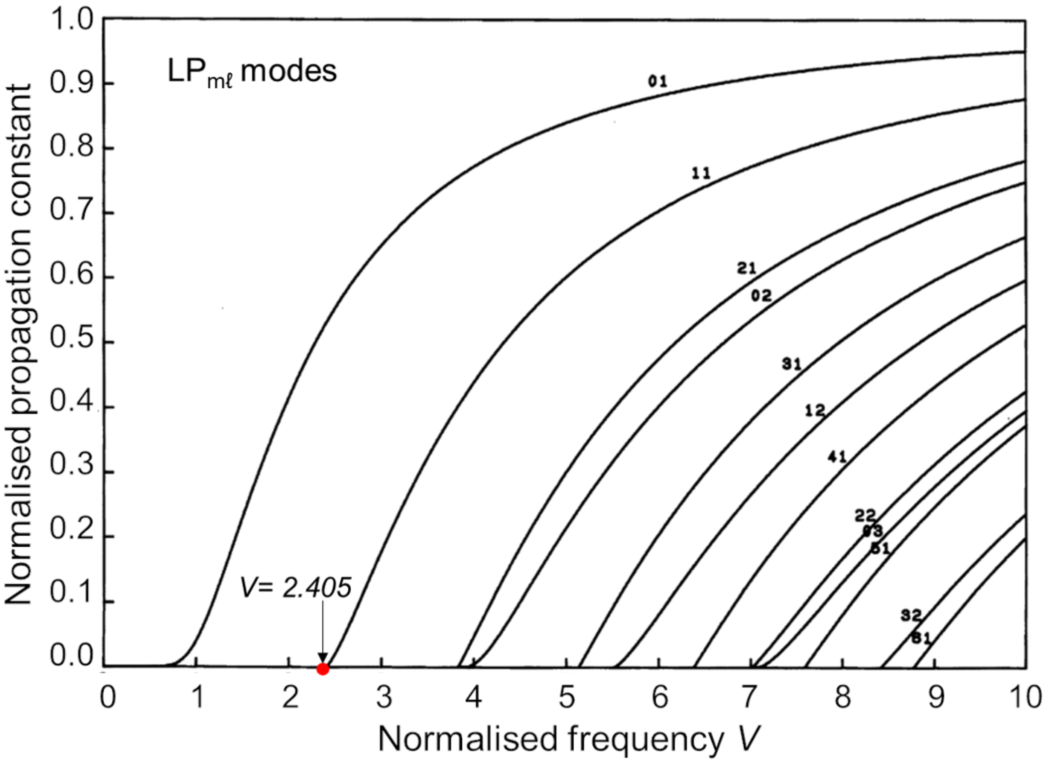

Fig. 4.13. Dispersion curves of the Linearly Polarised (LP) modes in step-index fibres (adapted from [21]).

The propagation modes in a step-index fibre can be observed through the dispersion curves, reported in Fig. 4.13. Without going too much into details, these curves represent the dependence of the propagation constant from the normalised frequency and are obtained by solving the dispersion equation applied to a step-index fibre [21]. The curves highlight an important property of the V number: if V<2.405, the only mode available is the linearly polarised LP_{01} mode, i.e. the fundamental mode. In this condition, the fibre is single-mode. If, on the contrary, V>2.405, the fibre is multimodal since several high-order modes may also propagate (LP_{11}, LP_{21}, etc.). During the glass characterisation and the design of fibre dimensions, the V number helps in predicting the behaviour of the fibre. After the refractive index measurements of core and cladding glasses, the maximum fibre radius allowing for single-mode propagation can be calculated through the V number. In the case of the produced fibres, the core diameter is ranging between 9 and 100 μm the wavelength is around 1.5 μm and the *NA* is varying between 0.07 and 0.11.

In the designed amplification systems, multimodal propagation is detrimental since it leads to a low level of collimation and high intermodal dispersion. To switch from multimode to single-mode, we can work either on the glass composition or on the radius of the core. The wavelength is determined by the emission spectrum of the active ions (Er^{3+} in our case, with its emission peak centred at 1535 nm). Even small variations in the glass composition can lead to a change in the refractive index of the glasses (see Fig. 4.9). By refining the glass processing procedure, we were able to limit the variations of the refractive index below $\pm 1 \cdot 10^{-4}$ between different batches of glasses with the same compositions.

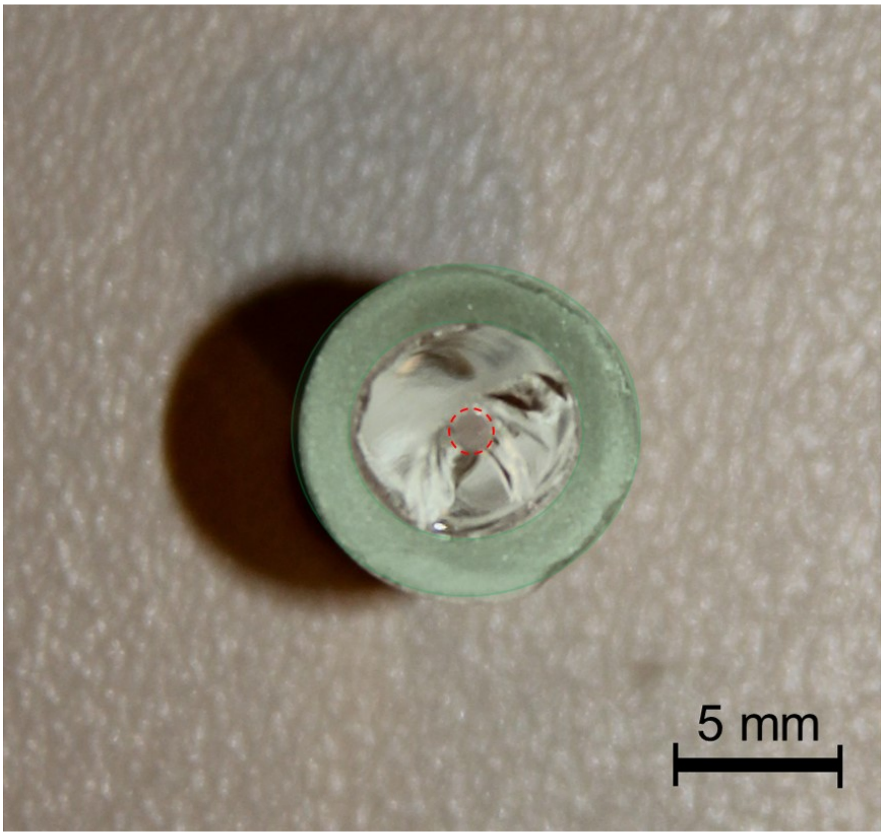

Fig. 4.14. Cross-section of an extruded preform. The green-shaded area represents the portion of the preform that has been cut. The red dashed line highlights the central hole for the core which is preserved from contact with the lubrication oil.

To measure the refractive index of the glasses, a small sample (~10x10x2 mm) is obtained by cutting a portion of both glasses: the rod for the core and the billet for the cladding. The difference of refractive indexes between the core and the cladding allows calculating the NA and, with that, the maximum fibre core diameter to get a single-mode fibre can be obtained by fixing the value of the V number. In this way, also the required dimensions for the cladding preform are derived. The cladding glass is cast into a billet and the billet is extruded through a dedicated die. The die must show proper dimensions, that account also for the distortions due to the die swelling phenomenon described in Chapter 3. Our effort, during the present research, was aimed at reducing the possible sources of error through the employment of automatic calculations for the dimensions of the extruder dies. Furthermore, the adoption of some strategies to control the side effects (before, during, and after the extrusion) allowed us to obtain interesting results.

The main employed techniques are:

- *(i)* pre-treat the extrusion dies by polishing, cleaning, and thermally pre-oxidise the stainless-steel pieces before extrusion;
- *(ii)* set the temperature and speed control during extrusion to fulfil the dimensional requirement and limit the presence of extrudate distortions as well as of flow lines inside the bulk of the product;
- *(iii)* replace the standard cutting procedure of the extruded tube (which used to cause the contamination of the preform with lubrication oil and the subsequent requirement of complex cleaning procedures) with a direct indentation-cut that allows preserving especially the internal surface from unwanted contaminations (Fig. 4.14). This procedure consists of producing an indentation on the surface of the tube and then forcing the crack to propagate by applying flexural stress.

These design and control strategies are further detailed in the next paragraphs.

4.2.3 Active core production

To match the needs of different applications, and to study the effect of the addition of RE elements to the phosphate glass composition, we prepared core glasses with different dopants and different doping levels.

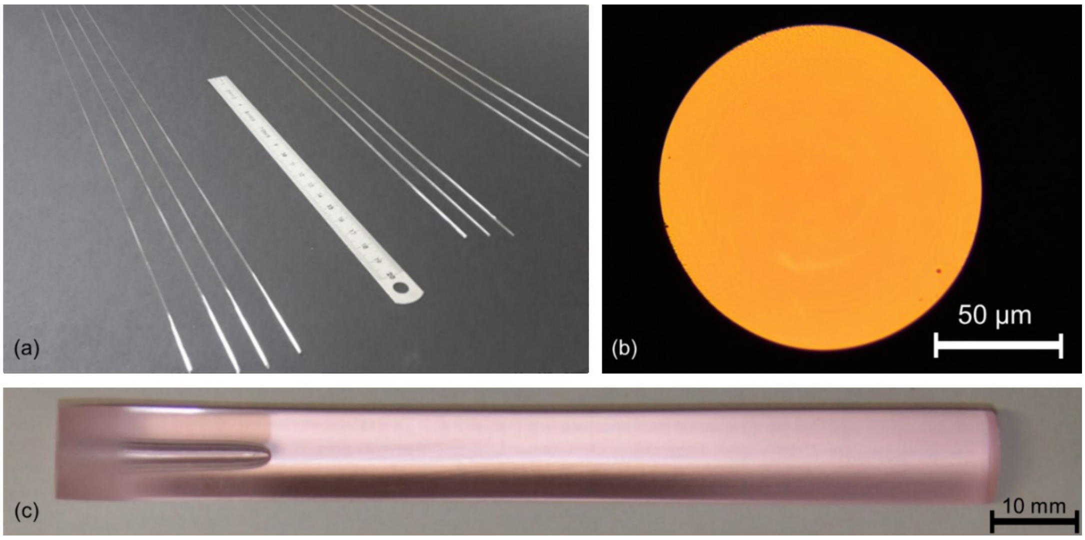

Fig. 4.15. Different steps of the projects. (a) The stretched single material thin rods can be employed as single-material waveguides; their average diameter is 1 mm. (b) The transmission optical microscope image of the bare single-material fibre. (c) A RE-doped active core rod after casting and polishing.

Some studies have been conducted on Er^{3+}-doped glass containing 1 mol% of Er_2O_3. These works are part of international projects involving several academic and technical institutions (LZH, U.S.ARL). To test the glass for drawing, a single-material 125-µm diameter fibre is drawn from a 12-mm polished core rod. The obtained bare fibre has shown to be homogeneous and no sign of crystallisation during drawing is present (see Fig. 4.15).

Table 4.1. Details of the produced fibres with an Er:Yb ratio of 1:2 (data adapted from [1]). The production techniques for the cladding are reported for each fibre as R.C. (rotational casting) or Extr. (extrusion); n_{core} and n_{clad} are the refractive indexes of the core and cladding glasses; NA is the numerical aperture of the fibre.

Fibre		**1**	**2**	**3**	**4**	**5**
Production technique (cladding)		R.C.	R.C.	R.C.	Extr.	Extr.
Diameters [µm]	**Core**	100	78	50	20	12
	Clad	230	178	125	125	125
n_{core}		1.5661	1.5661	1.5661	1.5681	1.5661
n_{clad}		1.5620	1.5620	1.5620	1.5636	1.5639
NA		0.11	0.11	0.11	0.12	0.08
Attenuation Losses [dB/cm]		0.036	0.036	0.036	0.022	0.020
V number		23.13	18.04	11.57	4.85	2.03
Optimum length [cm]		4	4	4	14	16
Average output power [mW]		24.5	31.5	48	246	147
Peak power [kW]		-	-	1.6	8.25	4.93
Energy per pulse [µJ]		-	-	1.2	6.15	3.67
Amplification [dB]		-	-	3.8	10.9	8.67

Another study, developed in collaboration with BGU and TUT, was related to the interaction between Er^{3+} and Yb^{3+} within a co-doped system. In this case, the composition of the core glass was fixed with an Er:Yb ratio of 1:2, and the diameter of the fibre was varied to investigate the influence of the fibre dimension on the light propagation. Table 4.1 shows a summary of the produced and tested fibres with the cited ratio of active elements. The calculation of the V number shows that only the fibre with the smallest-core can be considered a pure single-mode fibre. As expected, in practical conditions, this fibre showed the lowest attenuation loss. The amplification results obtained with these fibres are also reported in the table and will be discussed in the final section of this chapter.

In all the above-mentioned cases, the core is obtained by casting an active glass into a cylindrical rod mould (with a diameter of 12 mm and 150-mm height). After annealing and polishing, the core rod is stretched, to match the desired dimensions for fibre drawing. This is done within the drawing tower facility by setting a temperature lower than the one used during the proper drawing process. The heat is forcing the glass to slowly flow under its own weight, thus forming a thin rod, i.e. the stretched core which may be employed for preform production via the rod-in tube technique. After the stretching process, long portions of the active core rod are obtained, with diameters ranging between 0.8 and 2 mm. The obtained thin rod is inspected, and a region showing a useful and homogeneous diameter is cut and inserted into the tube for the final drawing.

4.3 From glass extrusion to fibre drawing

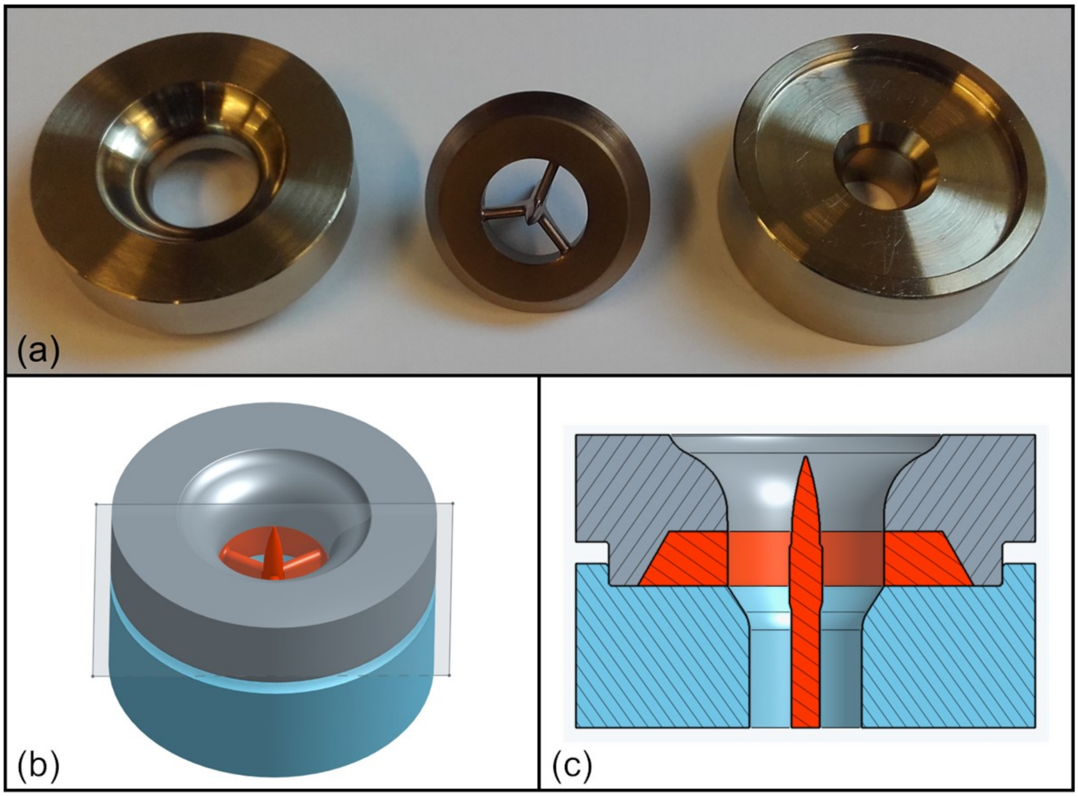

Fig. 4.16. The components of the die. (a) A picture of the three main elements that form one of the dies employed in the production of cladding preforms for active fibres, i.e. from left to right: the top part, the spider-die, and the bottom part; (b) a 3D rendering of the designed die and (c) a section view along the shaded plane in (b).

The core rod production is a straightforward and well-consolidated process. On the contrary, cylindrical tubes are more complex to obtain. Although rotational cast tubes are also employed for some tests (for example fibre #1 – 3 in Table 4.1), the preform specifically produced for the present work are made by extrusion. These latter tubes are obtained by casting the cladding glass into a billet mould. The billet is then extruded to form the cladding tube.

In our design, three main elements compose the die (see Fig. 4.16): a *top part*, to direct glass flow, a central part, i.e. the *spider die* (also called *bridge* or *porthole* die) [22], [23], that gives the proper shape to the hole, and a *bottom part*, the welding chamber, in which the external diameter of the tube is finally shaped. The spider die consists of a 3- or 4-arms suspended pin that allows forming a hole in the extrudate. All the die components are made of machined AISI 310 stainless steel.

Tubes with external diameters ranging from 10.8 to 12 mm have been produced, featuring a central hole with dimensions comprised between 1.2 mm and 2.2 mm. The final dimensions of the tube do not precisely correspond to the designed die dimension, due to the die swelling phenomenon. The swelling causes the external diameter of the preform to increase and the hole in the preform to decrease, compared to the respective die dimensions. The effective variation is in the ratio of core/cladding diameters of the die and the preform. This ratio between core and cladding can be calculated both for the die ($R_{cc}{}^{(Die)} = \frac{\phi_{Pin}}{\phi_{Die}}$), considering the dimensions of the pin (ϕ_{Pin}) and of the die aperture (ϕ_{Die}), as well as for the extrudate ($R_{cc}{}^{(Extr)} = \frac{\phi_{Hole}}{\phi_{Tube}}$), measuring the preform's hole dimension (ϕ_{Hole}) and the average external preform diameter (ϕ_{Tube}). These ratios are $R_{cc}{}^{(Die)} > R_{cc}{}^{(Extr)}$. The core/cladding ratio is lower in the extrudate compared to the die since the numerator and the denominator are diverging, due to the swelling phenomenon.

In the die design phase, compensation for the swelling to obtain extrudates with satisfactory tolerances must be adopted and the proposed strategies are described in the following section. After extruding and annealing, the tube is cut, to remove the terminal parts; in fact, only the central straight and homogeneous portion of the tube can be employed, since the beginning of the tube is usually bent, and the end is elongated (pictures of extruded tubes are reported in Fig. 4.20)

The cladding tube and the core rod are assembled and held in position using Teflon tape. The assembled preform is then mounted onto the drawing tower, to finally form a fibre.

4.3.2 Precision cladding extrusion

A picture of two billets is presented in Fig. 4.17, reporting the difference between the as-cast billet and the ready-to-extrude billet, which has been cut, polished and washed with a mild solvent.

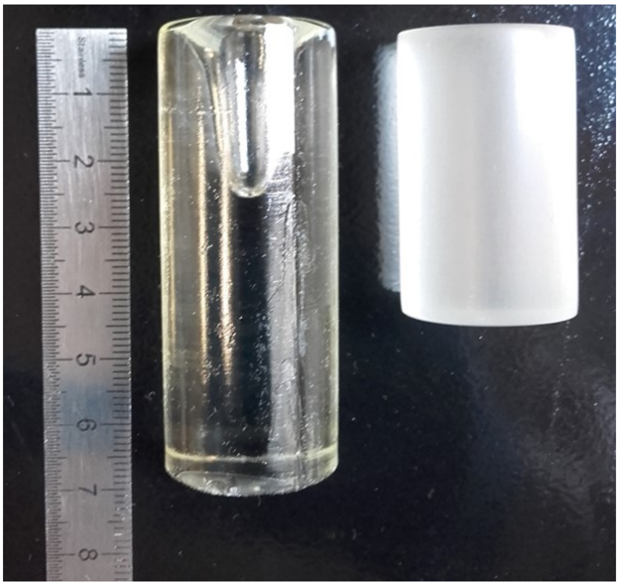

Fig. 4.17. Two glass billets employed for the extrusion of cladding tubes. On the left of the picture, a billet just after casting: the suction cone is visible at the top. Before extrusion, the suction cone is cut. A roughly polished and washed billet is shown on the right of the picture.

Despite the many advantages of the extrusion of preforms, one issue of the process is related to the small distortions that can affect the extrudate such as bending [24] and tapering phenomena [25], die swelling [26]–[29], shape distortion for non-symmetrical or multi-holes structures [30]–[33], and striae in the bulk of the glass, also called *shear bands* or *mandrel lines*, related to the glass flow perturbation exerted by the spider-die arms [23].

In the present paragraph, we demonstrate how some of these distortions can be avoided, while others can be partially controlled and minimised. All these phenomena, and the adopted strategies to cope with them, are summarised in Table 4.2.

The bending phenomenon is always present during glass extrusion since it is related to unavoidable pressure or temperature inhomogeneities during the process [34]. In particular, this phenomenon is evident in the first part of the extrudate which typically emerges from the die with a high bending, or equivalently a small curvature radius. However, as soon as the extrusion proceeds, the bending is reduced and, during the steady part of the process, the extrudate recovers an almost rectilinear shape. Since the first portion is sacrificial and is cut and discarded, our attention has been focused on reducing bending during the steady-state.

Table 4.2. Distortions during extrusion

Type of distortion	Description	Solution
Bending	Macroscopic curvature of the extrudate	Add a weight to the extrudate’s tip or precisely control temperature and load
Tapering	Elongation and thickening of the extrudate	Constantly increase speed and slightly reduce the temperature
Die swelling	Enlargement of the section of the extrudate (and related reduction of the section of the holes)	Account for swelling during the design of the die components
Holes distortion	Non-circularity of the holes	Negligible in a symmetrical structure
Mandrel lines	Striae in the bulk of the extrudate	Increase temperature and reduce speed

One solution to the distortions due to bending has been proposed by Stokes [24], who suggests applying a small weight to the end of the preform to force the extrudate on a straight path. Although effective, this approach can have also a detrimental effect, i.e. the tapering of the preform. A simpler way of reducing the bending is avoiding load distribution inhomogeneities and controlling the temperature during the whole process with a tolerance of less than ± 1 °C. Simulations performed with polymers melt demonstrate the effectiveness of this approach [34].

Distortions due to bending are inversely related to the ones associated with tapering. This latter is a phenomenon that starts to be relevant when the extrudate is already partially formed and begins to exert weight on the softened glass. The glass may then flow under its own weight and the tube’s external and internal dimensions are reduced, causing the extrudate to taper. The phenomenon has been studied in detail [35] and we adopted some expedients to control it. Two solutions have been found to mitigate this effect: increasing the speed of the extrusion and lowering the extrusion temperature. In general, we prefer to avoid temperature variation during extrusion, since it may show a delayed response due to the thermal inertia of the glass. However, the speed increase has also some drawbacks, since it causes an increased die swelling and can also favour extrudate bending and striae formations in the bulk. For these reasons, a combination of the two solutions is adopted: the speed is slightly increased, until the load remains below a specific value, with the maximum being 5 kN, the safety limit of the system; at the same time, when the extrudate has exceeded its half, the temperature is gradually reduced of a few degrees, while always looking at the load variation. Fig. 4.18 illustrates these concepts. The tapering is substantially limited with this solution, without causing other major problems.

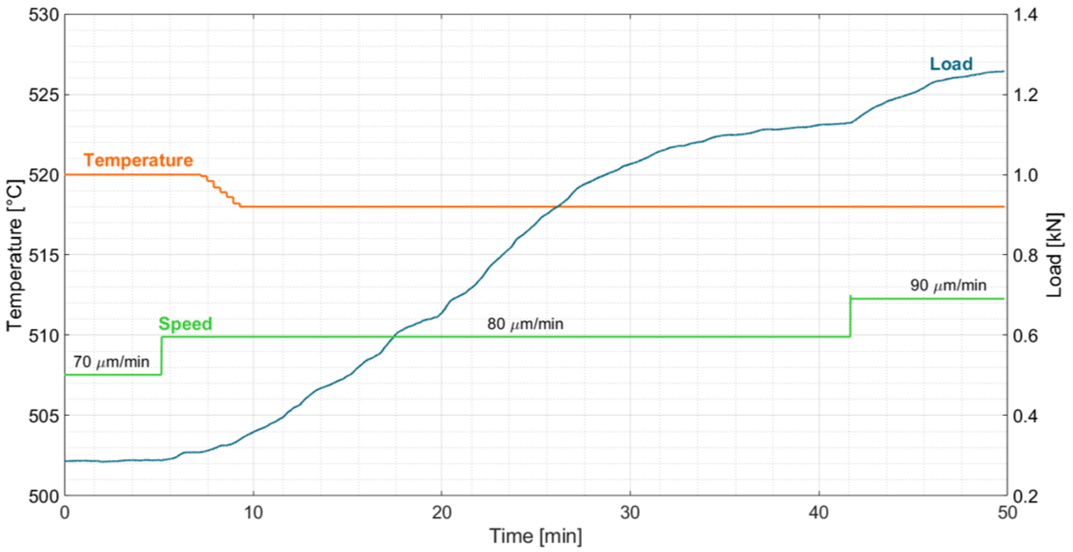

Fig. 4.18. Partial report of an extrusion trial. Each curve represents a different quantity, but all the curves are related to each other: when the temperature is reduced (- 2 °C), the load increases (+ 0.9 kN) without any apparent correlation with the speed; when the temperature stabilises, a further small speed increase (+ 10 μm/min) causes only a small load increment (+ 0.1 kN).

Die swelling is almost unavoidable when working with stainless-steel dies, due to the sticking of the glass to the metal surface, as explained in Chapter 3. Several studies have been made to replace stainless steel with graphite or boron nitride (BN) [36], [37]. These materials introduce other problems in terms of contamination of the preform and/or machinability. Thus, we decided to work with stainless steel dies and try to cope with the effects of the swelling phenomenon.

Fig. 4.19 shows the resulted external extrudate diameters for two tubes, processed at different loads, and associated speed. All the other extrusion variables (i.e. glass composition, die dimensions, and temperature) are kept constant. In Fig. 4.19, the die diameter is compared with the extrudates external dimensions, highlighting the influence of the extrusion load on the final diameter of the product.

The die swelling effect may be described with a single parameter S, obtained as the difference between the extrudate's diameter ϕ_{Tube} and the diameter of the die ϕ_{Die}, normalised with ϕ_{Die}, and usually expressed in per cent values: $S = (\phi_{Tube} - \phi_{Die})/\phi_{Die} \cdot 100$. For lower extrusion loads, the swelling is assessed between 3% and 5%, while with higher loads, the swelling may be around 15 – 16%. In some conditions (i.e. extremely high speed and load during extrusion), the swelling may reach 20%. In Fig. 4.19 there is a difference of more than 1 mm between the external diameters of the two experiments, and this value may have a strong impact on the ratios of the core/cladding preform and, consequently, of the fibre.

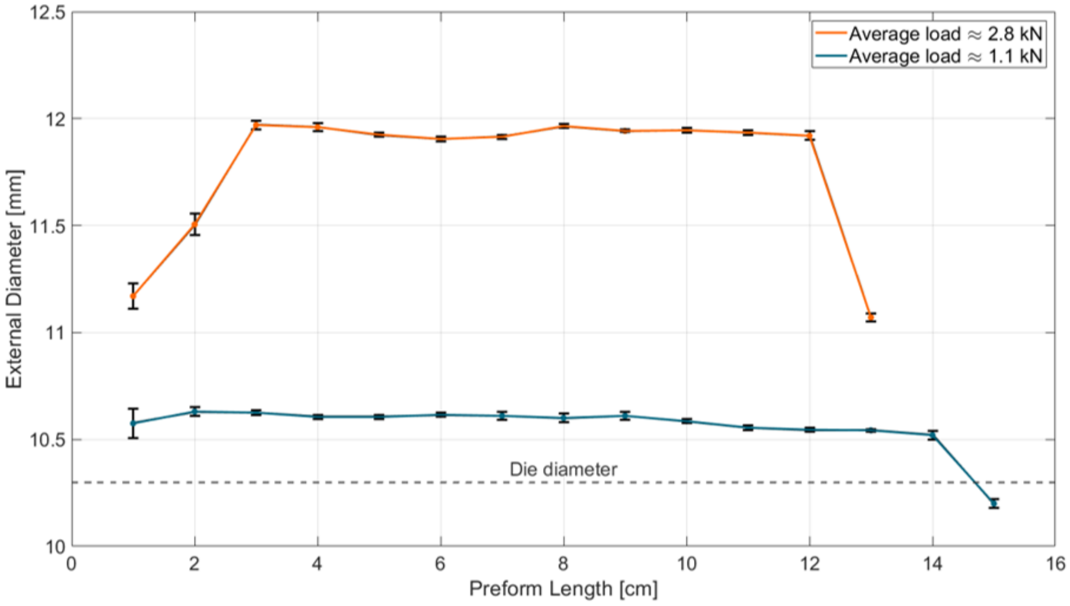

Fig. 4.19. Measured external diameters of extruded tubes. The red line is the result of an extrusion performed at a high average load (≈ 2.8 kN) which leads to a high swelling. On the contrary, the blue line result is obtained by extruding at a lower average load (≈ 1.1 kN). The measurement is performed twice at 90° for each point, and the error bars are reported in the graph. The average error in the measurement is ±0.04 mm for the 2.8 kN curve and ±0.02 mm for the 1.1 kN curve.

For the project described in the present chapter, the die swelling phenomenon is particularly important since the dimensions and the refractive index difference must be tightly adjusted to obtain the desired fibre properties. To reduce the effect of the swelling, we had to find the proper extrusion load and speed for a given glass/die pair and then we replicated the optimised extrusion conditions. In this way, the swelling can be controlled and directly compensated in the design of the die. Thus, when designing the die, the outer die diameter is decreased of a quantity related to the expected swelling, and the pin diameter is increased to compensate for the reduction of the preform hole.

To account for the swelling phenomenon and calculate the required diameter of the spider-die pin (ϕ_{Pin}) to obtain a specific fibre core diameter ($\phi_{Core} = 2a$), an equation has been derived:

$$\phi_{Pin} = 2a\frac{\phi_{Die}(1+\hat{S})}{\phi_{Fibre}(1-\hat{S})}.$$

Here, ϕ_{Fibre} is the diameter of the fibre, $\hat{S} = (\phi_{Tube} - \phi_{Die})/\phi_{Die}$ is the predicted die swelling (expressed in decimal units), and the diameter of the core is written in terms of the core radius a, obtained from the V number equation: $a = \frac{V\cdot\lambda}{2\pi\cdot NA}$.

A simple computational tool has been developed using Microsoft Excel and then has been improved by writing a Python script. With this latter tool, it is possible to select the diameter of the die aperture, the dimensions of the fibre, the expected die swelling, the working wavelength, and the refractive indexes of both the core and the cladding glasses. When all the parameters are provided, the script calculates the diameter of the pin that allows obtaining the biggest core diameter in the single-mode region (i.e. for V=2.405).

Other distortions that occur during extrusion are related to the non-circular shape of the preform holes. This effect is particularly evident in the presence of preforms featuring non-centred holes. As deeply investigate by Trabellsi et al. [30]–[33], the position of the hole in the cross-section of the preform influences its distortion. However, this effect is minimised when dealing with a simple core/cladding structure, featuring a single hole located in the axial centre of the preform. Thus, it is neglected in the present study, but will be considered for the production of multi-holes preform, as described in Chapter 5.

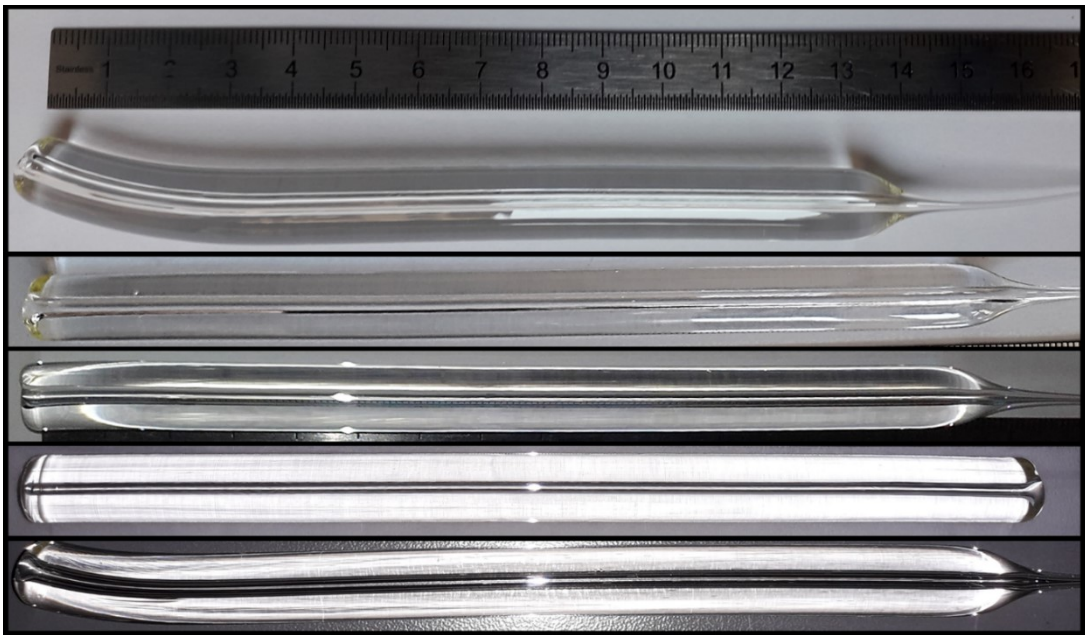

Fig. 4.20. Some of the tubes obtained with the extrusion of phosphate glasses. The ruler shows a cm scale.

The phenomenon of striae formation due to inhomogeneity of glass flow is also evaluated [23]. The presence of these striae, also called mandrel lines, is attributed to the shear rates present within the glass flow during extrusion. This issue is more pronounced for relatively higher load, higher speed, and lower temperature and its impacts may be significant especially on the optical performances of the fibre leading to high scattering losses. The presence of these striae can be limited by reducing the strain rates, which means increasing the extrusion temperature or reducing both the extrusion load and speed.

In conclusion, obtaining an extrudate completely free of distortions can be challenging, and the best performances are obtained with a compromise between conflicting needs. Some of the tubes obtained in this portion of the present work can be seen in Fig. 4.20. The main point to be addressed is the need to find optimal extrusion conditions for each glass/die pair. This allows to compensate for any eventual distortion and finally obtaining a good matching between the design and the results. Thanks to the proposed solutions, we achieved good extrusion results with a semi-automatic control system.

4.3.3 Preform assembly

The assembly of the preform has some aspects to be addressed. The shape of the assembled preform is directly responsible for the final fibre features. The assembly operations must be carried out in a clean environment since any kind of contamination of the interface between the core and the cladding can act as a strong scattering centre. The core rod is obtained via a stretching aided by gravity, thus, it is perfectly straight (±10 μm over 200 mm). The insertion of the core rod into the cladding tube should avoid contact of the core rod with the tube walls, to minimise surface flaws, even if the glass/glass interaction is not dangerous as metal/glass interaction in terms of scratches. One way to reduce the rubbing of the core rod onto the internal cladding wall has been found: the cladding preform is designed to show a slightly bigger hole than the core rod. This tolerance T (usually $T < 0.5$ mm) substantially improved the ability to couple the core and the cladding preforms. Attention must be paid to the gap between core and cladding: during the drawing stage, this gap may not collapse, and an air void can be still present in the fibre. This air gap at the interface between core and cladding may act as a scattering centre inducing high propagation losses. Thus, the presence of this air region must be avoided. An optimal combination of dimensional tolerance and air suction during drawing can lead to the best results.

In the previous paragraph, a computational tool for swelling accounting has been described. This tool is further improved by introducing the tolerance T due to the rod-in-tube technique. The equation for the calculation of the diameter of the pin can be rewritten accordingly:

$$\phi'_{Pin} = 2a\frac{\phi_{Die}\left(1+\hat{S}\right)}{\phi_{Fibre}\left(1-\hat{S}\right)} + T.$$

This tool allows for a straightforward calculation of the required die dimensions to achieve single-mode operation, also considering the tolerances of both the extrusion and of the rod-in-tube technique.

When the core rod has been inserted into the cladding tube, the assembled preform is ready to be mounted into the clamping system of the drawing tower. Teflon tape is employed to fasten together the core and the cladding and to mount the preform onto the drawing tower feeding stage. The Teflon tape also avoids the contact between glass and metal that could cause cracking due to mechanical or thermal stresses.

4.3.4 Single-mode active fibre drawing

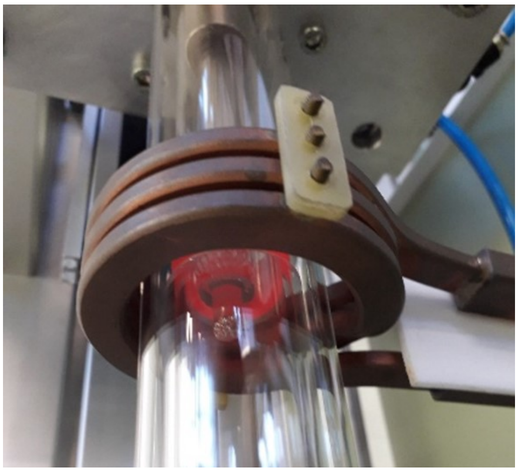

Fig. 4.21. A close picture of the induction coil, with a heated preform visible at its centre. A scheme of the drawing tower may be found in Fig. 3.6, and a full picture in Fig. 3.19a.

At the beginning of the process of fibre drawing, the preform has one end fastened to the clamping support and the other pending in the centre of the induction coil, i.e. in the hot region of the drawing tower. A close view of this part of the drawing tower may be seen in Fig. 4.21, while more general representations are reported in Fig. 3.6 and Fig. 3.19. When heated, the preform starts to neck-down and the fibre is formed and coiled up on the winding drum as described in Chapter 3.

Table 4.3. Details of the produced single-mode Er^{3+}-doped phosphate fibre obtained by cladding extrusion; n_{core} and n_{clad} are the refractive indexes of the core and cladding glasses; NA is the numerical aperture of the fibre.

Fibre diameters [µm]	**Core**	12
	Clad	125
Preform diameters [mm]	**Core**	0.98
	Clad	10.30
n_{core}		1.5709
n_{clad}		1.5684
NA		0.09
V number		2.154
Optimum length [cm]		60

For the different active fibres produced, several parameters were varied during the drawing process. Both single and multimode fibres with different core/clad ratios or different NA were produced. The best results obtained with an Er^{3+}-doped fibre are reported in Table 4.3. This fibre showed a small doped core, suitable for single-mode propagation (see Fig. 4.22).

4.3.5 Fibre properties and laser characterisation

The produced fibres are firstly analysed by visual inspection eventually under a transmission optical microscope. This allows us to detect not only some geometrical aspects, like the dimension and symmetry of the core, but also to have a preliminary guess about light-guiding properties and homogeneity of the fibre (see Fig. 4.22).

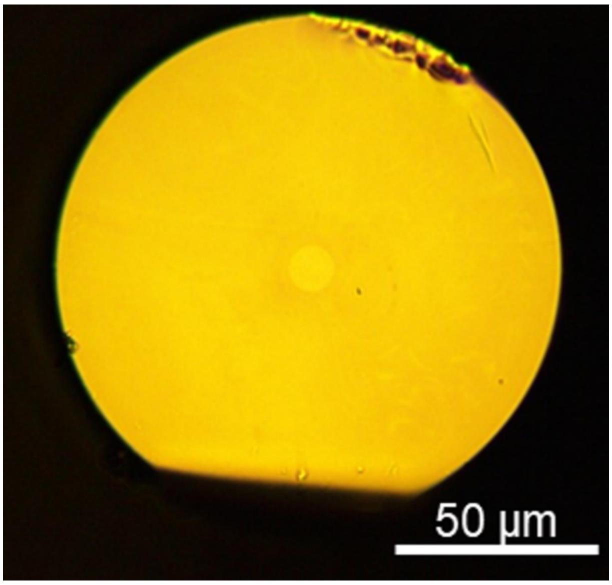

Fig. 4.22. Cross-section of a single-mode Er^{3+}-doped phosphate fibre observed with a transmission optical microscope.

The fibre propagation properties may then be investigated using the cut-back technique. This is a standard laboratory test, in which some light is launched into the core of the fibre and the power is measured at the end of the fibre at different lengths ($P(x_1), P(x_2), ...$). In this way, the attenuation of the fibre can be evaluated as the ratio of the power at the points x_1 and x_2. Results of this kind of measurement are visible in Fig. 4.23.

The detection of the confinement of the light into the fibre core allows us to predict the actual fibre performances. We carried out this test by launching some light on one fibre end and acquiring an image of the opposite end. To do this measurement we used a butt-coupled fibre pigtailed laser diode source emitting at a wavelength of 1300 nm.

To find the best conditions we tested different fibre lengths. For the produced fibres, obtained by drawing preforms made by combining extruded tubes and stretched active

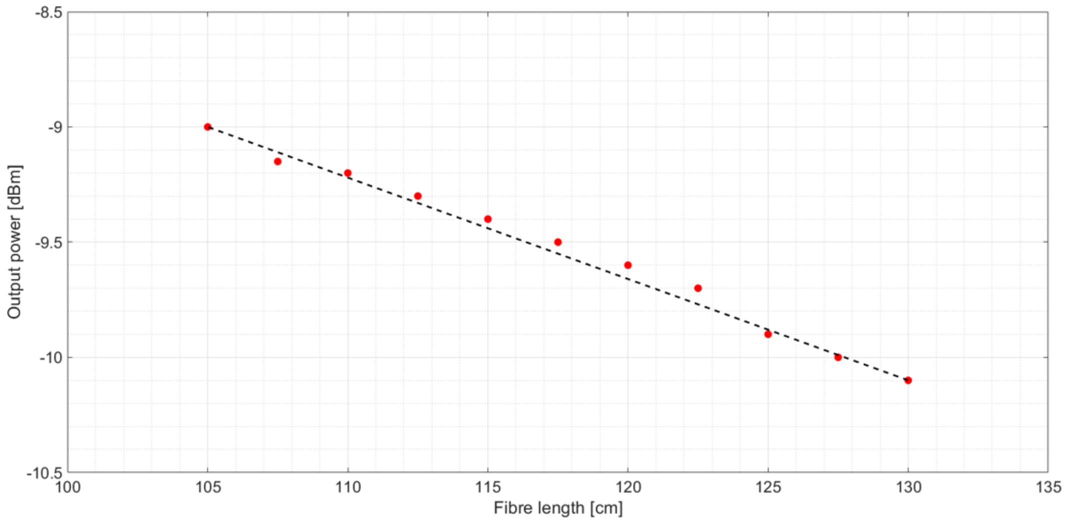

Fig. 4.23. Fibre loss measured with the cut-back technique on Er:Yb co-doped fibre. The measurement is performed on a 20-µm core fibre (i.e. sample #4 of Table 4.1).

rods, the light was found to be partially confined inside the core for a length of 1-2 m. Some light may leak into the cladding and the overall performances of the fibres may then be very poor.

The bad light confinement may be explained either with inhomogeneities inside the core glass, or with defects at the core/cladding interface, or even with the presence of bulk striae inside the cladding glass, which may be effective especially when bending the fibre. This latter hypothesis seems to be valid since the light confinement was very poor in the case of a bent fibre. Yet, by decreasing the fibre length below 60 cm, the light was found to be well confined inside the core of the fibre. Thus, an amplifier produced with this fibre should have an active fibre section in the order of 0.5 m. This length is compatible with the common needs of amplification. Some of the acquired near field images are reported in Fig. 4.24.

Furthermore, some of the fibres produced by extrusion have been tested in operative conditions as described in [1]. These Er:Yb active fibres are used for the amplification stage of a MOPA system. This configuration allows obtaining a high-power laser source by amplifying a laser seed signal. The set-up of the experiment is shown in Fig. 4.25. The seed signal is provided by a CW single-mode semiconductor laser diode. The diode is controlled through an on/off gain switching system that allows emitting short light pulses (with sub-nanosecond length). Two multimode laser diodes were employed for the pump, one at the front and one at the rear facet of the active fibre. The output signal of the amplification stage is filtered (to remove pump signal and Amplified Spontaneous Emission) and is sent to measuring devices (such as power meter, photodiode, or optical spectrum analyser). To maximise the gain, several core diameters and fibre lengths were tested. The dimensions of the tested fibres and

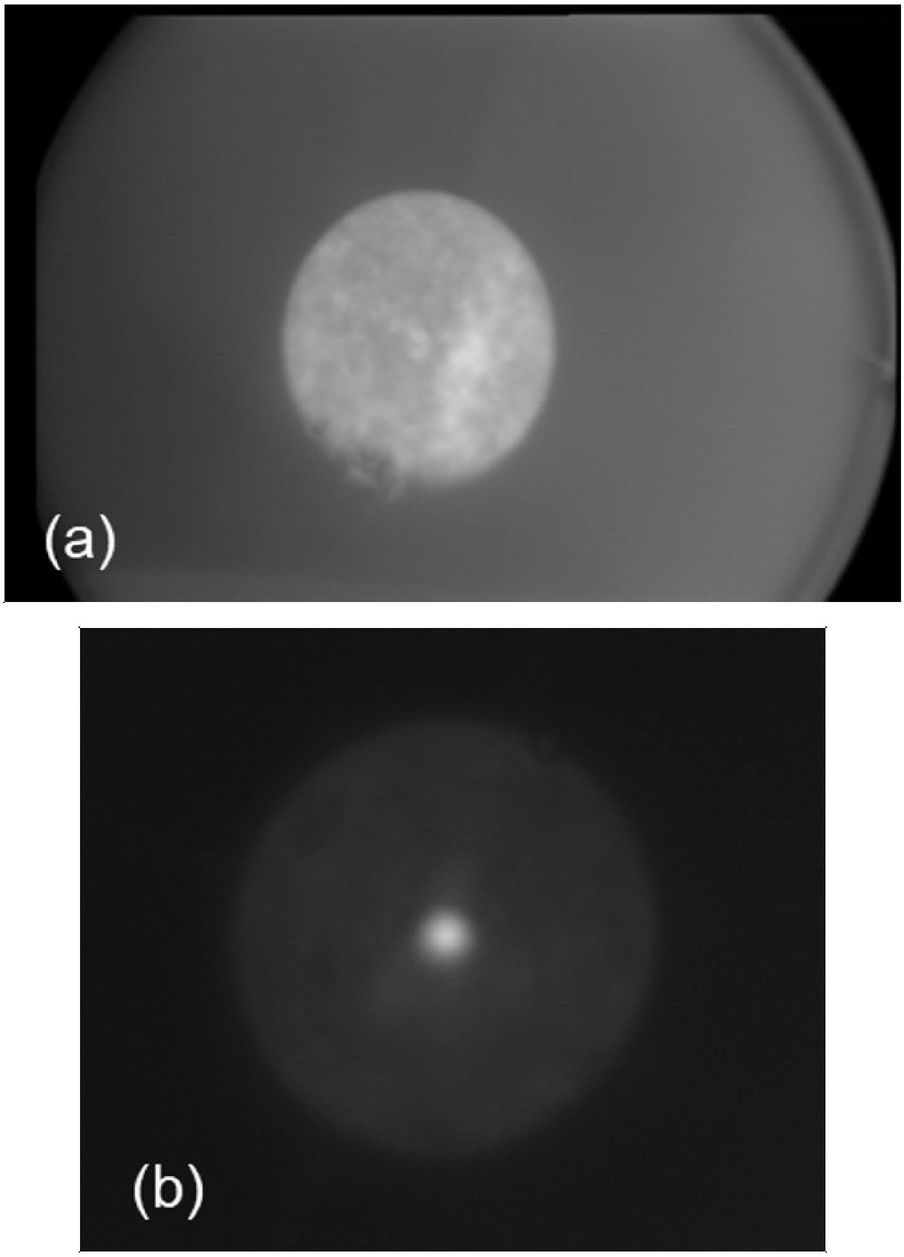

Fig. 4.24. Pictures of the near-field light propagation for the single-mode fibre described in Table 4.3. (a) The light was not properly confined in the core for longer fibres. (b) With a shorter fibre, i.e. below 60 cm, the light was found well confined in the core.

their performances are reported in Table 4.1. For each fibre core/clad ratios, it was possible to find an optimum length showing the higher amplification. In fact, in the small-core, single-mode fibres, absorption is homogeneous all over the fibre and a higher length may be employed, thus increasing the overall amplification. The fibre with 20 µm core and 14 cm length has shown the best performances with a maximum peak power of 8.25 kW, with a pulse duration of 0.7 ns and repetition rate of 40 kHz, corresponding to a net gain of 10.9 dB [1].

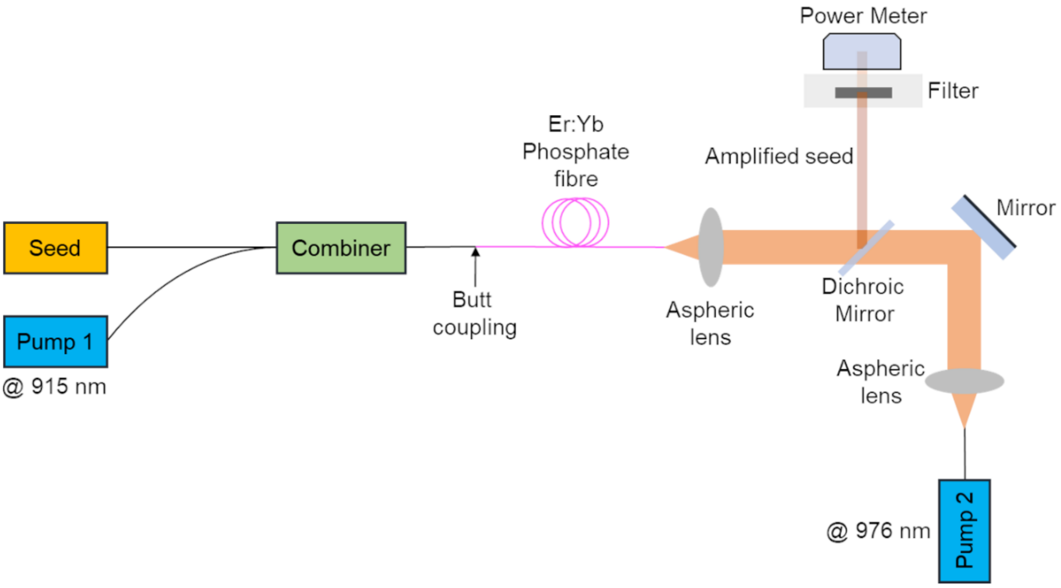

Fig. 4.25. Experimental set-up of the power amplifier with Er:Yb co-doped phosphate fibre (adapted from [1]).

A picture of the cross-section of some of these fibres is shown in Fig. 4.26. All the fibre lengths employed in the case of phosphate glass active fibres are substantially shorter than the ones that are needed for silica-doped fibres without a reduction in the managed power [1].

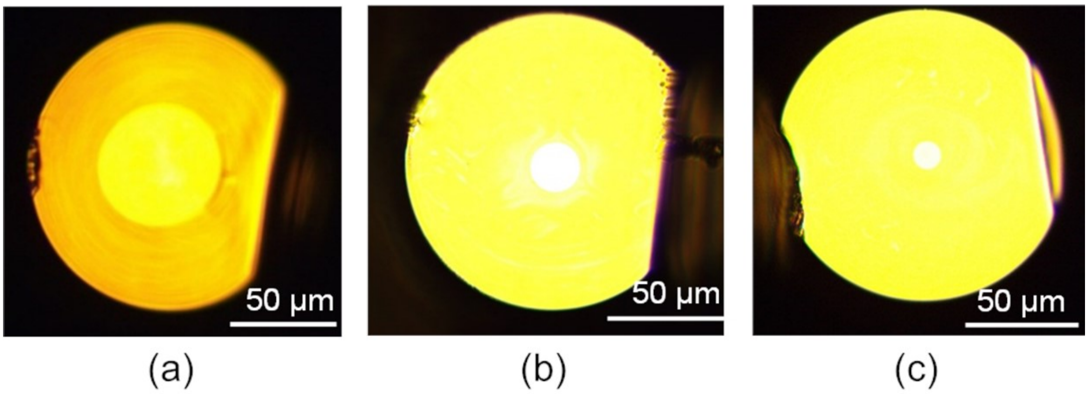

Fig. 4.26. Cross-section of the Er:Yb co-doped phosphate fibres described in Table 4.1. (a) Fibre #2, (b) fibre #4, and (c) fibre #5.

4.4 Conclusions

The present chapter provides an overview of both materials and techniques employed to design, fabricate, and characterise phosphate active fibres. The fibres are obtained by drawing different preforms all realised via the rod-in-tube technique with an active core rod and a passive extruded cladding tube. The glasses are synthesised starting from high purity reagents, that are weighted in a controlled atmosphere environment. The glass powders, either for active or passive glasses, are melted and cast into specific moulds for core and cladding, respectively. After casting, the core is polished with meticulous handwork, while the cladding is extruded to obtain a hollow tube. The extrusion technique has been employed for the first time to produce preforms for phosphate glass active fibres and it has demonstrated to be an effective process. In the production of the preform cladding, i.e. hollow tubes, the main advantage of extrusion compared to other soft glass preform production techniques is the ability to obtain unusual ratios of inner to outer diameters. We were able to produce preforms for single-mode active fibres featuring extremely small cores. The preforms for these fibres were obtained with a single step extrusion, which is a great advantage compared to the laborious double-cladding procedure necessary to achieve similar results with conventional techniques like rotational casting. The main drawbacks of extrusion are also analysed and their effect on the propagation properties of the fibres is considered. Also, some tools have been developed to account for the possible distortions of the extrudate. The effective minimisation of the die swelling, as well as tapering, bending, and shear bands of the preform are important advancements. The quality of the extruded preforms has been substantially improved using the proposed strategies. The extruded preforms allowed to obtain fibres with different dimensions. Several single-mode active fibres were also produced. These fibres have been observed using optical microscopy and near-field propagation images. With these analyses, the optimum length of the fibre has been derived. The obtained dimensions are particularly suitable for the design of compact devices for optical amplifiers. A MOPA configuration was also tested and allowed to achieve amplification of several kW with sub-nanosecond pulse duration and high-optical gain within a short fibre.

References

[1] O. Moschovitz et al., ‘Characterization of sub-nanosecond pulsed laser amplification with Er : Yb co-doped phosphate glass fibers’, *Optics Letters*, vol. 45, no. 18, pp. 5291–5294, 2020, doi: https://doi.org/10.1364/OL.402575.

[2] N. Boetti, D. Pugliese, E. Ceci-Ginistrelli, J. Lousteau, D. Janner, and D. Milanese, ‘Highly Doped Phosphate Glass Fibers for Compact Lasers and Amplifiers: A Review’, *Applied Sciences*, vol. 7, no. 12, p. 1295, 2017, doi: 10.3390/app7121295.

[3] G. C. Scarpignato, D. Milanese, J. Lousteau, N. G. Boetti, and E. Mura, ‘Fabrication and characterization of a high-gain Yb-Er codoped phosphate glass optical amplifier’, *Journal of Engineering (United Kingdom)*, vol. 2013, 2013, doi: 10.1155/2013/858341.

[4] D. J. Richardson, J. Nilsson, and W. A. Clarkson, ‘High power fiber lasers: current status and future perspectives [Invited]’, *Journal of the Optical Society of America B*, vol. 27, no. 11, p. B63, 2010, doi: 10.1364/josab.27.000b63.

[5] D. Gallichi-Nottiani, D. Pugliese, N. Giovanna Boetti, D. Milanese, and D. Janner, ‘Toward the fabrication of extruded microstructured bioresorbable phosphate glass

optical fibers’, *International Journal of Applied Glass Science*, no. June, pp. 1–9, 2019, doi: 10.1111/ijag.14652.

[6] P. McManamon, *Field guide to lidar*. Bellingham, WA: SPIE Press, 2015.

[7] R. T. H. Collis, ‘Lidar observation of cloud’, *Science*, vol. 149, no. 3687, pp. 978–981, 1965, doi: 10.1126/science.149.3687.978.

[8] D. Pugliese *et al.*, ‘Concentration quenching in an Er-doped phosphate glass for compact optical lasers and amplifiers’, *Journal of Alloys and Compounds*, vol. 657, pp. 678–683, 2016, doi: 10.1016/j.jallcom.2015.10.126.

[9] G. H. Dieke and S. Singh, ‘Absorption and fluorescence spectra with magnetic properties of ErCl3’, *The Journal of Chemical Physics*, vol. 35, no. 2, pp. 555–563, 1961, doi: 10.1063/1.1731968.

[10] M. Yamane and Y. Asahara, *Glasses for photonics*. Cambridge, UK: Cambridge University Press, 2004.

[11] E. Snitzer, ‘Optical maser action of Nd+3 in a barium crown glass’, *Physical Review Letters*, vol. 7, no. 12, pp. 444–446, 1961, doi: 10.1103/PhysRevLett.7.444.

[12] C. J. Koester and E. Snitzer, ‘Amplification in a Fiber Laser’, *Applied Optics*, vol. 3, no. 10, p. 1182, 1964, doi: 10.1364/ao.3.001182.

[13] A. Méndez and T. F. Morse, *Optical Specialty Fibers Handbook*. San Diego, CA: Academic Press, 2007.

[14] H. Bach and N. Neuroth, *The Properties of Optical Glass*. Heidelberg, Germany: Springer International Publishing, 1998.

[15] Y. Hu *et al.*, ‘Performance of high-concentration Er 3+-Yb 3+-Codoped phosphate fiber amplifiers’, *IEEE Photonics Technology Letters*, vol. 13, no. 7, pp. 657–659, 2001, doi: 10.1109/68.930405.

[16] E. Snoeks, G. N. van den Hoven, and A. Polman, ‘Optimization of an Er-Doped Silica tical Waveguide Amplifier’, *IEEE Journal of Quantum Electronics*, vol. 32, no. 9, pp. 1680–1684, 1996.

[17] E. A. Anashkina, ‘Laser sources based on rare-earth ion doped tellurite glass fibers and microspheres’, *Fibers*, vol. 8, no. 5, 2020, doi: 10.3390/FIB8050030.

[18] J. S. Wang, E. M. Vogel, and S. E., ‘Tellurite glass: a new candidate for fiber devices’, *Optical Materials*, vol. 3, pp. 187–203, 1994, doi: 10.1016/0022-3093(90)90274-P.

[19] A. Belwalkar, W. Z. Misiolek, and J. Toulouse, ‘Viscosity study of the optical tellurite glass: 75TeO2-20ZnO- 5Na2O’, *Journal of Non-Crystalline Solids*, vol. 356, no. 25–27, pp. 1354–1358, 2010, doi: 10.1016/j.jnoncrysol.2010.03.011.

[20] R. Noé, *Essentials of Modern Optical Fiber*, 2nd ed. Heidelberg, Germany: Springer International Publishing, 2016.

[21] K. Okamoto, *Fundamentals of optical waveguides*, 2nd ed. San Diego, CA: Academic Press, 2006.

[22] S. Kainth, *Die Design for Extrusion of Plastic Tubes and Pipes - A practical guide*. Munich, Germany: Carl Hanser Publishing, 2017.

[23] A. Belwalkar, H. Xiao, W. Z. Misiolek, and J. Toulouse, ‘Extruded tellurite glass optical fiber preforms’, *Journal of Materials Processing Technology*, vol. 210, no. 14, pp. 2016–2022, 2010, doi: 10.1016/j.jmatprotec.2010.07.018.

[24] Y. M. Stokes, ‘Bending in extrusion of optical fibre preforms’, *ANZIAM Journal*, vol. 51, no. December 2009, p. 124, 2016, doi: 10.21914/anziamj.v51i0.2334.

[25] C. A. G. Kalnins, K. J. Bachus, A. Gooley, and H. Ebendorff-Heidepriem, ‘High precision extrusion of glass tubes’, *International Journal of Applied Glass Science*, vol. 10, no. 2, pp. 172–180, Apr. 2019, doi: 10.1111/ijag.13092.

[26] E. Roeder, ‘Flow Behaviour of Glass During Extrusion’, *Journal of Non-Crystalline Solids*, vol. 7, pp. 203–220, 1972, doi: 10.1016/0022-3093(72)90290-6.

[27] T. C. Papanastasiou, D. G. Kiriakidis, and T. G. Nikoleris, ‘Extrudate swelling: Physics, models, and computations’, *Applied Mechanics Review*, vol. 48, no. 10, pp. 689–695, 1995, doi: 10.1115/1.3005050.

[28] A. B. Seddon, D. Furniss, and A. Motesharei, ‘Extrusion method for making fiber optic preforms of special glasses’, in *SPIE*, 1998, no. September 1998, p. 32, doi: 10.1117/12.323398.

[29] E. T. Y. Lee and E. R. M. Taylor, ‘Two-die assembly for the extrusion of glasses with dissimilar thermal properties for fibre optic preforms’, *Journal of Materials Processing Technology*, vol. 184, no. 1–3, pp. 325–329, 2007, doi: 10.1016/j.jmatprotec.2006.11.115.

[30] M. Trabelssi and P. F. Joseph, ‘Hole distortion and drift in extruded microstructured optical fiber glass preforms: Part I – Sensitivity analysis’, *Journal of Non-Crystalline Solids*, vol. 481, no. July 2017, pp. 208–224, 2018, doi: 10.1016/j.jnoncrysol.2017.10.045.

[31] M. Trabelssi and P. F. Joseph, ‘Hole distortion and drift in extruded microstructured optical fiber glass preforms: Part II – Optimization’, *Journal of Non-Crystalline Solids*, vol. 481, no. July 2017, pp. 412–423, 2018, doi: 10.1016/j.jnoncrysol.2017.11.021.

[32] M. Trabelssi, H. Ebendorff-Heidepriem, K. A. Richardson, T. M. Monro, and P. F. Joseph, ‘Computational modeling of hole distortion in extruded microstructured optical fiber glass preforms’, *Journal of Lightwave Technology*, vol. 33, no. 2, pp. 424–431, 2015, doi: 10.1109/JLT.2015.2388733.

[33] M. Trabelssi, ‘Numerical Analysis of the Extrusion of Fiber Optic and Photonic Crystal Fiber Preforms Near the Glass Transition’, PhD Thesis, Clemson University, Clemson, SC, 2014.

[34] G. Barakos and E. Mitsoulis, ‘Non-isothermal viscoelastic simulations of extrusion through dies and prediction of the bending phenomenon’, *Journal of Non-Newtonian Fluid Mechanics*, vol. 62, no. 1, pp. 55–79, 1996, doi: 10.1016/0377-0257(95)01385-7.

[35] H. Tronnolone, Y. M. Stokes, H. T. C. Foo, and H. Ebendorff-Heidepriem, ‘Gravitational extension of a fluid cylinder with internal structure’, *Journal of Fluid Mechanics*, vol. 790, pp. 308–338, 2016, doi: 10.1017/jfm.2016.11.

[36] E. Roeder, ‘Extrusion of glass’, *Journal of Non-Crystalline Solids*, vol. 5, no. 5, pp. 377–388, 1971, doi: 10.1016/0022-3093(71)90039-1.

[37] H. Ebendorff-Heidepriem and T. M. Monro, ‘Analysis of glass flow during extrusion of optical fiber preforms’, *Optical Materials Express*, vol. 2, no. 3, p. 304, 2012, doi: 10.1364/ome.2.000304.

Chapter 5.

Microstructured fibres for biomedicine

Materials for biomedical applications have gained increasing attention over the past two decades, and several related emerging technologies are contributing to reshaping the whole medical sector. The integration of optical fibres in biomedicine represents a fundamental milestone for applications like surgery, diagnostic, and therapy administration, among others. Nowadays, the use of biocompatible optical fibres in the medical field is a consolidated habit. The main application is related to endoscopes that allow for minimally invasive surgical procedures. Furthermore, in the field of diagnostic, the chance to visualise alive human tissues with an increasing image resolution allows collecting data avoiding dangerous and invasive systems [1]. The sensing capabilities of an optical fibre are not limited to imaging, but several kinds of bioresorbable sensors can be implemented for, e.g., temperature, oxygenation, and neural activity monitoring [2] or the detection of several analytes, such as glucose, urea, ammonia, etc. [3]. Also, the simple but powerful possibility of using a thin capillary to deliver a drug directly onto an internal tissue, avoiding systemic drug assumption with associated side effects, has been a great advancement. Furthermore, laser light at different wavelengths is also employed for therapeutics or tissue ablation and can be delivered using glass fibres. Finally, materials with the ability to dissolve inside the body without consequences, are one of the new frontiers of the medical practice [4]. Their employment is widely accepted since it allows reducing surgery and hospitalisation.

The present work is aimed at demonstrating that peculiar features like imaging, sensing, stimulating, and carrying either liquid or gas can be combined into a new idea of optical fibre for biomedicine. A device that is not only a light carrier but can also interact with the environment to sense or deliver drug topically. At the same time, from the material perspective, this device is made by a combination of pure oxides that are readily dissolved inside the body after a tailorable amount of time. This allows merging both therapeutic and diagnostic actions potentially avoiding the removal of the implant. A whole procedure, that would probably require several surgeries and invasive analysis, is collapsed into a thin filament, strong enough to be inserted into the body through a mini-invasive cut but thin enough to be resorbed within reasonable times. The power of this idea has moved our research group during the last years through joint projects, scientific publications, international conferences, and dissemination events. Furthermore, a patent related to the microstructured bioresorbable fibre for the simultaneous delivery of light and drug, developed by our research group, has been recently approved by the Italian Patent Office [5].

We explored the potential of the proposed technology also verifying the interest of the healthcare personnel about it in several group meetings, interviews, and surveys also prepared by a group of students from the Engineering and Management MSc course of Politecnico di Torino. We acquired opinions from urologist, gastroenterologists, and oncologists, as well as from the medical staff of the Candiolo Cancer Institute IRCCS, a specialised centre for oncological therapy. Thanks to these interactions, we reinforced our research interest toward a multifunctional microstructured bioresorbable fibre, which can offer solutions to several medical issues.

Many projects on biomedical materials are supported by private companies, that may sustain the costs for the whole process, from the development of the idea to the production of the device. This process may be summarised in five steps:

(i) the basic material research;
(ii) the design of the device;
(iii) the production of a prototype and the conduction of standard in vitro and in vivo tests on animals;
(iv) the pilot production and the tests on humans;
(v) the scale-up and marketing of the products.

All these steps require diverse skills and the overall process can take more than ten years. The present study aims at investigating the potential fabrication techniques and applications of a new kind of device. We focused on material development as well as on the technical aspects connected to the design of the device and the preliminary tests. The details about marketing, sale, and related topics are carried out through industrial partnerships currently under development.

In this framework, we employed the tube extrusion for producing optical bioresorbable microstructured phosphate glass fibre for several biomedical applications. A new bioresorbable phosphate glass composition has been developed by our research group during the last years. Yet, the possibility of extruding a tube to obtain a preform and then draw it into an optical fibre has not been demonstrated with this bioresorbable glass. This constitutes the subject of this portion of the thesis work: consolidating the control of the extrusion process to be able to extrude a high-quality glass preform, thus producing a multifunctional bioresorbable optical fibre that overcomes the limitations of standard silica optical fibre in biomedicine. Details about the work carried out in these directions will be given in the following sections.

5.1 Bioresorbable glasses in biomedicine

Materials with a wide variety of properties are employed in the medical sector and are generally named biomaterials. A further classification of biomaterials can be given by their behaviour when in contact with human tissues or fluids. Indeed, they can simply be *biocompatible*, i.e. inert materials that do not cause any inflammatory response of the organism, or *bioactive*, which means that they somehow interact with the body [6]. Different materials may produce different effects depending on their shape and on the local conditions (such as temperature, humidity, pressure, pH, etc.). Besides, some of them can also release some therapeutic element when being in contact with body fluids. Bioactive materials can be sensitive to the action of biological agents (enzymes or microbes), in which case they are named *biodegradable*. Especially for bioactive polymers, there is a further distinction between *bioabsorbable* and *bioresorbable* materials. The former are materials that dissolve or disperse in biofluids, but their constituents (such as small polymeric chain fragments) are eliminated and do not interact with the living tissues. On the contrary, bioresorbable materials are completely dissolved into the body and metabolised by the organism [6].

A thorough description of the evolution of biomaterials over the years has been provided by Hench & Polak [7]. They distinguished the first generation of biomaterials, which was discovered in the 1960s and was mainly composed of biocompatible inert materials; then the second generation, formed by bioactive materials capable either of eliciting some reaction from the organism or, in some cases, of dissolving. Finally, the third generation of biomaterials came out at the beginning of the present century and comprises bioactive materials designed to stimulate a specific cellular response [7]. Furthermore, in recent years, bioactivity is not anymore divided from bioresorbability since bioactive materials are also bioresorbable. Nowadays, sensors or flexible electronic components are often developed using bioresorbable materials [2], [8].

It is worth noting the importance of bioresorbable glasses for biomedicine. The main applications of biomedical glasses are the production of scaffolds for bone reconstruction and the reinforcement of bioresorbable polymeric matrixes. A well-known bioactive glass is the 45S5 Bioglass® discovered at the University of Florida in 1969 [9]. This glass has been thoroughly studied, thanks to its complex interaction with biofluids. Due to its positive response to the tests, the 45S5 Bioglass® has been approved by the Food and Drug Administration (FDA) already in 1985. Nowadays is mainly employed in orthopaedic applications [10]. The dissolution kinetic, the apatite-forming ability for bone regeneration, the production of scaffolds for drug delivery [11], and the possibility of including dopants to stimulate the regrowth of specific tissues or to add, e.g., antibacterial properties (see Chapter 6) are only some of the aspects developed during the years [9]. Furthermore, a great number of bioactive glass compositions have been investigated, belonging to the silicate, borate, and phosphate glass families. The possible applications of these materials are diverse. A quick overview of these applications allows understanding the vastness of the field: ocular implant, peripheral nerve repair, wound healing, antibacterial bone/dental cement, lung tissue engineering, skeletal, muscle, and ligament repair, cardiac tissue engineering, spinal cord repair, etc. [12].

Bioresorbable phosphate glasses are employed to produce bare unclad fibres used as a reinforcing agent for polymeric materials [13]–[17]. These fibres, and the related composites, show extremely good mechanical properties [18], and tailorable dissolution [19], [20]. Furthermore, advanced optical fibres made of different materials have been engineered into multifunctional sensors [21]. For various materials, the implementation of a sensor on the fibre tip has been demonstrated as well as the exploitation of its elongated geometry to get linearly distributed sensing [22]. However, except for a few works [1], [23]–[25], the optical behaviour of bioresorbable phosphate glasses has not been investigated in detail. Some of the cited studies have been conducted with the bioresorbable phosphate glasses synthesised in our laboratory [24], [25]. Among the studies conducted at Politecnico di Torino, a hollow core bioresorbable phosphate glass fibre has also been reported, for fluid transfer supported by capillary force [26]. Light transmission was demonstrated through the cladding of the fibre [26]. The same bioresorbable phosphate glass composition has passed preliminary in vivo tests and no inflammatory response has been detected after subcutaneous implantation in mice [27].

To summarise, bioresorbable glass fibre can be either a load-bearing element, a medium to transmit light, a medium to transport fluid, or a sensor. Our idea is to try to combine some of these features in a single device. In this way, a capillary can become an optical sensor, or a fibre intended to be used as a reinforcement in composite materials can transmit optical signals. Also, an optical fibre developed to be inserted into the body and shine a specific area can, at the same time, deliver a drug to that area and monitor the therapy. This may be an improvement in Photodynamic Therapy (PDT), a treatment that involves the usage of a photosensitive drug, locally activated by light. All the described features can be combined into a bioresorbable fibre, that is implanted and does not need to be explanted, since it simply dissolves within a reasonable time, and its constituents are metabolised by the patient's organism. Besides avoiding surgery for the explant, the bioresorbability may be effective also in another scenario: in the unfortunate case of breaking the fibre inside the body, the sharp tips of the broken fibre will quickly become rounded and will dissolve within a short time, in the case of a bioresorbable fibre. On the contrary, conventional silica fibres may introduce a serious risk of injuries due to their prolonged stability.

Indeed, the topic is wide and has numerous potential implications. Some of them are addressed in the following sections that will describe, at first, the processes of design and fabrication of standard core/clad bioresorbable optical fibre preforms. Then, the topic of multifunctional bioresorbable fibres is addressed, and two main concepts of multifunctional optical fibres are presented: a double-channel fibre and a microstructured fibre.

The double-channel preform is an asymmetric structure, featuring two off-centred holes with different sizes. One of the holes is intended to be filled with a core glass and used to propagate light. The other one is meant to remain hollow and can be used as a pipe to transport fluid, i.e. a drug. The production of such a complex preform presented several challenges that are analysed in the current chapter. A great contribution to face these challenges has been given by Computational Fluid Dynamics (CFD) simulations that allowed to improve the design of the extrusion die and get better control on the preform distortions. Although some authors have also tried to simulate the behaviour of softened glass flow using plasticine at ambient temperature [28], [29], this process still presents many unknowns regarding its applicability to glass extrusion. Thus, we preferred to employ a more robust CFD simulation approach that will be described below.

Once the extrusion process was assessed and optimised by CFD and experiments, a microstructured fibre was developed. The preform has been obtained by extrusion of tubes followed by stacking-and-drawing of an assembled preform. This preform features an array of holes that surrounds the core. Light confinement in the core is sustained by the presence of air voids in the cladding. This is an interesting feature. By filling the holes of the cladding with a gas or a liquid, the refractive index around the core will change, and this is going to affect the interaction of the light guided into the core with the evanescent field penetrating the cladding [30]. So, we may obtain a multifunctional device, able to produce a therapeutic action and, at the same time, sensing the local variation of some quantity. Details about microstructured fibre production and characterisation are provided in the final part of the present chapter.

5.2 Bioresorbable phosphate glass optical fibres

Phosphate glass fibres with specific dissolution properties in vivo are the subject of several studies, mainly related to their capability of interacting with damaged tissues (muscles, nerves, etc.), thus stimulating and directing their regrowth [31]. When in fibre form, these glasses are employed for both hard- and soft-tissue engineering [32]. Yet, biomedical glass fibres are seldom developed to exploit their optical properties. These glasses are often opaque both in the visible and in the NIR wavelength regions. Light absorption can be due to the presence of specific compounds in the glass composition (e.g. Fe_2O_3, used to enhance the mechanical properties of the fibres, is known to induce strong absorption [33]) or to the presence of impurities that can act as scattering centres [1]. These impurities are mainly due to the fabrication method. To obtain good glasses for optical applications it is mandatory to use high-purity reagents and to work in a tightly controlled atmosphere. Only a low level of defects allows enhancing the optical properties of the glass. A few ppm of the wrong component may dramatically alter the optical behaviour. For this reason, great care has been taken during all the manufacturing process of the glass, to minimise contamination.

Bioresorbable glass has been produced and characterised in our research laboratories. A proof of principle study of the biocompatibility of the phosphate glass composition, together with its fibre-forming ability, was conducted in 2011 [34]. In this work, phosphate glass compositions containing different amount of TiO_2 are characterised for their physical and dissolution properties. Furthermore, all the tested glasses were easily processed to draw fibres from bare unclad preforms. Subsequently, in 2016, another research was published, regarding the relation of both the thermal and the optical properties, as well as the dissolution of the glass, with the amount of MgO added to the composition [25]. The study investigates the optical properties of the bulk glasses: these glasses show a wide transparency window, ranging from UV wavelengths up to the NIR region. Moreover, a core/cladding optical fibre has been produced with two different bioresorbable glasses and showed values of attenuation similar to the typical loss values of standard optical fibres made of non-bioresorbable phosphate glasses [24], [25]. The same glass composition has been also analysed to show the possibility of inscribing Fibre Bragg Gratings (FBGs) in the core of the fibre, using an excimer laser radiation [35]. These gratings represent a valid and robust solution to obtain sensing capability in an optical fibre. In biomedical applications, they are interesting as temperature sensors and can also be employed for strain measurement. Furthermore, the study shows the selective dissolution properties of the grating in simulated body fluid, thus demonstrating its sensitivity to specific conditions (e.g. the local variation of pH) [35].

5.2.1 Bioresorbable phosphate core/cladding glasses

The glass composition employed for the extrusion experiments described in the present chapter contains 50% P_2O_5 – 23% MgO – 11.5% Na_2O – 10% CaO – 3% SiO_2 – 2.5% B_2O_3. This is a high-MgO bioresorbable composition proposed by Ceci-Ginistrelli et al. [25]. The presence of a high level of MgO, which is added in place of CaO, essentially affects the thermal properties, the dissolution rate and the refractive index (for details, see Table 5.1). The composition of the glass for the core of the fibre can be obtained, starting from the cladding composition, by replacing part of the MgO with CaO. In this way the refractive index of the glass is raised as depicted in Fig. 5.1, thus leading to a light-guiding structure. The core glass is expected to show also a higher dissolution rate, which is beneficial since the core will be exposed to the external environment only after the complete dissolution of the cladding, i.e. when the device has ceased to work properly. The core glass would also show lower processing temperatures and higher temperature working window. This reduces the chance of crystallisation of the core glass during fibre drawing that could dramatically alter the light propagation.

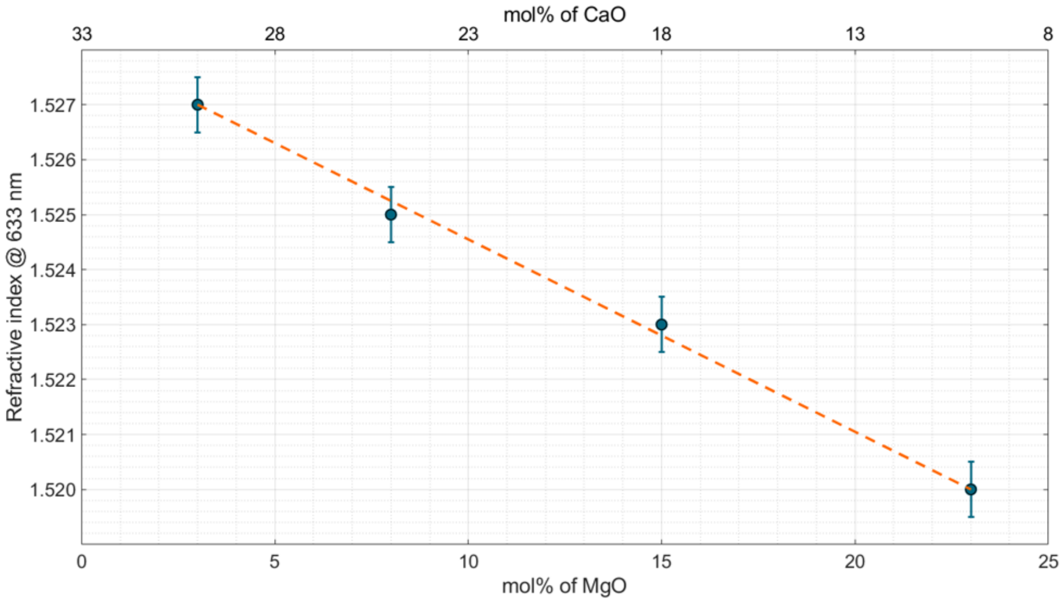

Fig. 5.1. Refractive index (measured @ 633 nm) for different bioresorbable glass compositions with varying amount of CaO and MgO (data are taken from [25]).

The glass preparation is carried out as already explained by weighting powders of high-purity reagents inside a controlled atmosphere environment. The oxide powders are then mixed and melted at 1200 °C in pure silica or Pt/Rh crucibles. The glass is cast into preheated moulds, according to the needs. After the casting, the glass samples are annealed at 440 °C for 5 h.

The core glass mould is a cylindrical rod mould, with 8 or 12 mm in diameter and 150 mm in height. The cladding glass is cast into a billet mould, which has 25 mm in diameter and 50 mm in height. The surface finishing of the core rod is extremely important since any defect at the interface between core and cladding can act as a scattering centre and reduce the light propagation performances of the fibre. For this reason, the polishing is carried out using polishing papers with different grades until an optical-quality is obtained. Then, the core rod is stretched to the desired diameter in the drawing tower facility at LINKS Foundation as detailed in Chapter 3.

The annealed cladding glass billet is mounted on a cutting tool to remove the suction cone. Then, the billet is washed with isopropanol and inserted into the extruder. After extrusion, the preform is annealed again, to remove any thermal stress. Before assembling the preform, the extruded tube must be cleared of the distorted ends. This is done by indentation-cutting, avoiding the contact between the lubricating oil of the cutting tool and the internal surface of the tube, as described in Chapter 4. After a final cleaning procedure using isopropanol with anti-scratch tissues, the cladding tube is ready to be assembled in a preform with the stretched core glass rod.

5.2.2 Glass characterisation

The main properties of the bioresorbable glasses with different magnesium content are reported in Table 5.1.

Table 5.1. Effect of the compositional variation of bioresorbable glasses. The table reports the MgO and CaO mol% variation, and the associated glass transition temperature (T_g), the onset of crystallisation ($T_x^{(on)}$), the temperature working window ($\Delta T = T_x^{(on)} - T_g$), the dilatometric softening temperature (T_s), the coefficient of thermal expansion (CTE), the density (ρ), the refractive index n (measured at a wavelength of 633 nm), and the decrease in the diameter $\Delta\Phi$ of 150 ± 6 μm fibres after immersion in PBS for 21 days. Data are reported from [25]

MgO	CaO	T_g	$T_x^{(on)}$	ΔT	T_s	CTE	ρ	n	$\Delta\Phi$
mol%	mol%	°C	°C	°C	°C	10^{-6} °C^{-1}	g cm^{-3}		μm
3	30	435	658	223	467	12.6	2.606	1.527	89
8	25	435	628	193	471	12.2	2.600	1.525	82
15	18	442	632	190	471	12.0	2.598	1.523	42
23	10	444	625	181	477	12.2	2.589	1.520	31

By observing all these properties, we decided to proceed with the study of the high-MgO content composition. This composition represents the strictest choice in terms of both extruding and fibre-forming ability since it shows the lowest difference between the onset of crystallisation and the glass transition temperature ($\Delta T = T_x^{(on)} - T_g$). The proximity of these temperature implies a higher risk of crystallisation during glass processing. We opted for this composition to demonstrate the processability of the glass: if the working window of temperature is sufficiently wide to process this glass, compositions with lower MgO content are expected to show higher tolerance in terms of working conditions.

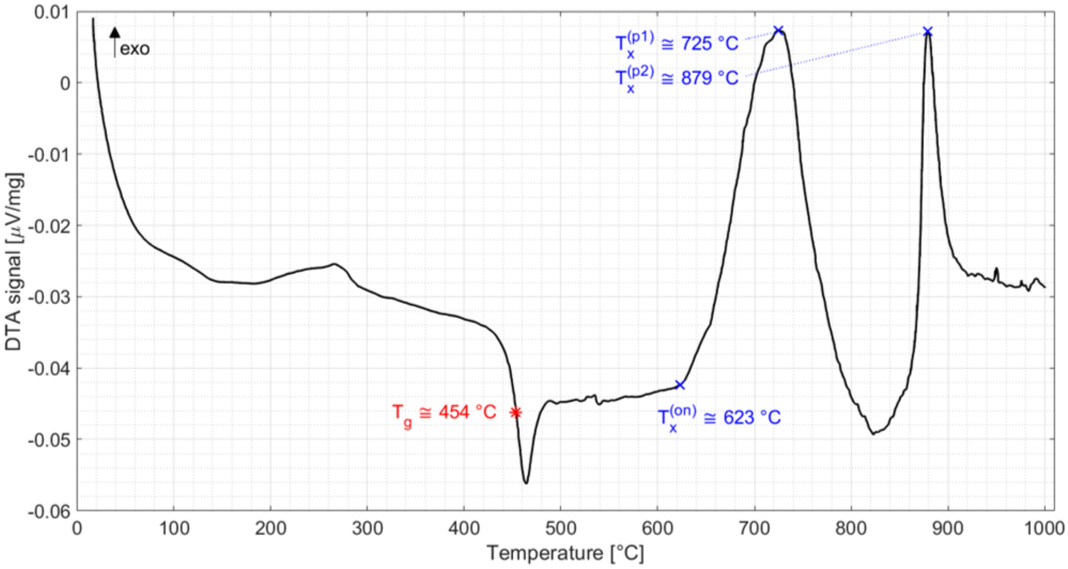

Fig. 5.2. DTA measurement of the bioresorbable phosphate glass employed in the present chapter. The characteristic temperatures (the glass transition temperature T_g, the onset of crystallisation $T_x^{(on)}$, and the two crystallisation peaks, $T_x^{(p1)}$ and $T_x^{(p2)}$) are reported in the graph.

To further investigate the thermal behaviour of the chosen glass, we performed a DTA measurement that is visible in Fig. 5.2. From the curve, it is possible to detect a T_g of 454 °C and two separate crystallisation peaks (related to two crystalline phases) respectively centred at 725 °C and 879 °C. The onset of the lower temperature crystallisation may be located at 623 °C.

The small difference of the glass transition between the tested glass and the one described by Ceci-Ginistrelli et al. [25] may be due to measurement parameters, like the quantity of sample, the presence of a reference, and, most of all, the speed of the temperature increase during the measurement. The value of the T_g is very sensitive to this latter aspect. On the contrary, the measured value of the $T_x^{(on)}$ is consistent with the previous value reported in Table 5.1 for a glass with the same amount of MgO.

As reported in Table 5.1, the dissolution behaviour of bioresorbable phosphate glasses was also investigated by Ceci-Ginistrelli et al. [25]. The glass samples in fibre form have been soaked in Phosphate Buffered Saline solution (PBS), in physiological conditions (37 °C, pH = 7.4). The tested fibres are single-material fibres with a diameter of 150 ± 6 µm. Both the weight and diameter reduction of the fibres were measured at different intervals for 21 days. These tests allowed to demonstrate that, by adding MgO and subtracting CaO, the dissolution time of the glasses can be varied according to the needs. The low-MgO samples can be considered completely dissolved within 30 days, while the high-MgO glasses require a longer dissolution time.

The viscosity-temperature dependence of bioresorbable phosphate glasses is another aspect that was not investigated before. For the extrusion experiments, this information is crucial. To get to know the influence of temperature on the glass viscosity, the usual dilatometric measurement has been extended to higher temperatures, well above the softening temperature T_s of the glass, as described in Chapter 2. By acquiring the rate of deformation of the sample with increasing temperature under a steady load, a derived measurement of the variation of the viscosity during heating is obtained. A plot of the result of the measured viscosity is shown in Fig. 5.3 and fits an exponential model that may be described by the standard Vogel-Fulcher-Tamman (VFT) equation:

$$\mu = \mu_0 \cdot e^{\left(\frac{a}{T-T_0}\right)}. \qquad (1)$$

In this equation $\mu_0 = \mu_{Tg} \cdot e^{\left(\frac{a}{T-T_g}\right)}$, where $\mu_{T_g} = 10^{12}$ Pa·s is the viscosity of the material at the glass transition temperature T_g, while a and T_0 are the VFT parameters.

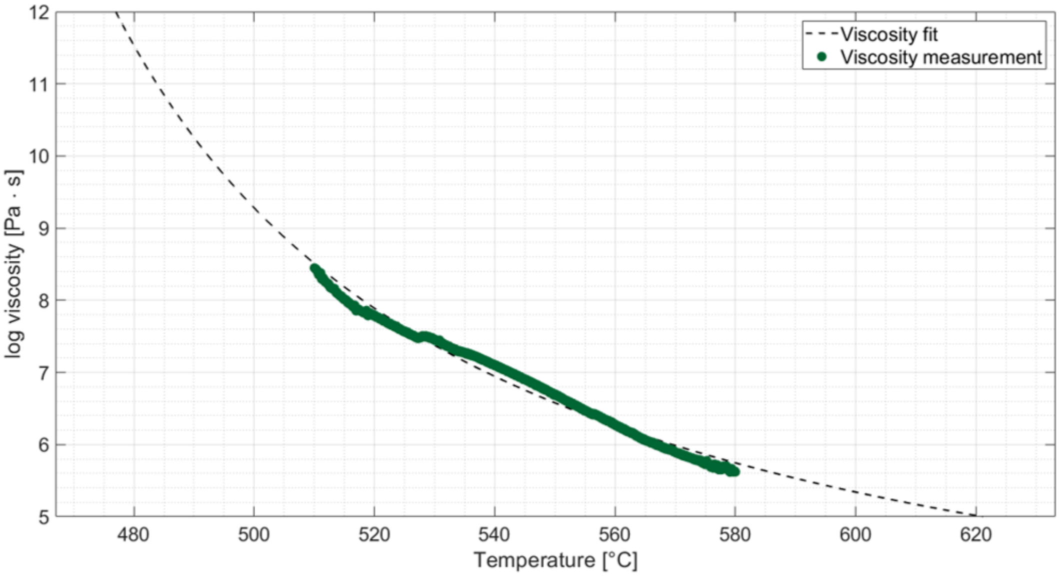

Fig. 5.3. The viscosity of bioresorbable phosphate glass measured with a cylinder compression test and fitted to a VFT exponential model.

The accuracy of the VFT model with a viscosity at T_g equal to μ_{T_g} is assumed to be enough for the present work, although some more accurate viscosity models have been developed, like the Adam-Gibbs equation or the Mauro-Yue-Ellison-Gupta-Allan (MYEGA) equation that take into account also the configurational entropy of the liquid [36]. We used the Greek letter μ to describe the viscosity, in place of the more common η notation, to make a coherent choice adopting the CFD notation for the glass viscosity. In this field, the viscosity is usually considered either in terms of the dynamic viscosity μ or the kinematic viscosity $\nu = \mu/\rho$, where ρ is the fluid density.

To further test the optical properties, flat glass samples are obtained by cutting and polishing a glass rod. The polishing is carried out on a semi-automatic polishing machine using alumina paste with different grain size to obtain an optical quality surface. Both the faces of the samples were free of any visible scratch before the measurement. Light absorbance is measured at different wavelengths with a UV-vis-NIR spectrophotometer.

The result of the UV-vis-NIR measurement of the bioresorbable glass with the highest MgO content is plotted in Fig. 5.4. The broad transparency of the glass is visible from this plot.

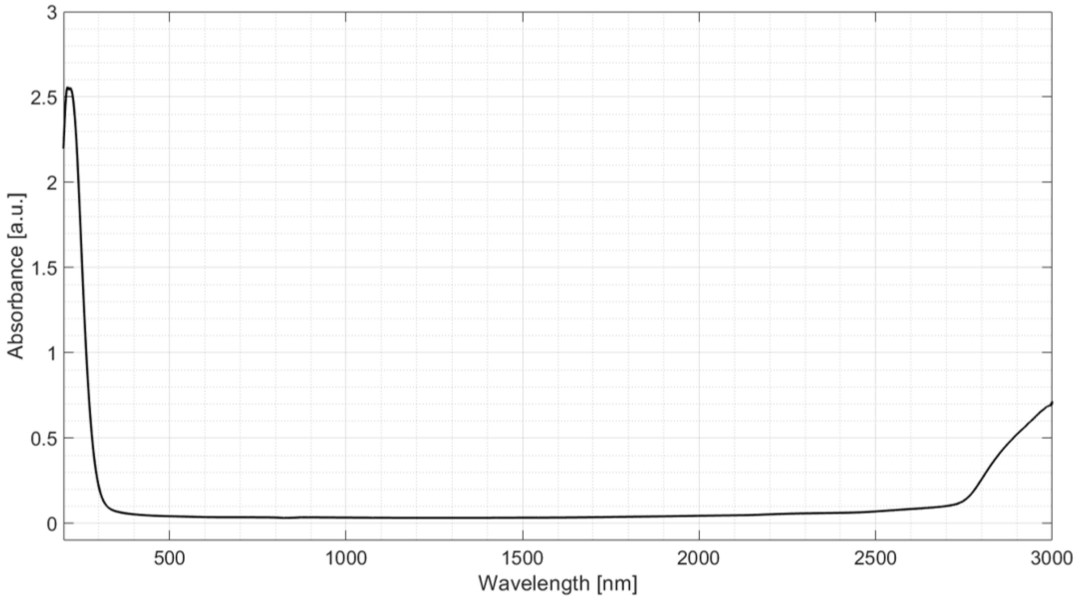

Fig. 5.4. The absorbance of a bioresorbable phosphate glass measured with a UV-vis-NIR spectrophotometer for a wide range of wavelength.

As already mentioned, the same bioresorbable glass compositions have been employed to produce optical fibres, by combining two glasses with different MgO content to get the required refractive index difference [25]. Several lengths of these fibres were tested with the cut-back technique to determine the propagation loss, reported in Fig. 5.5. The fibres were tested using two laser diode sources operating at 633 and 1300 nm and showed attenuation loss coefficients of 4.7 and 1.9 dB/m, respectively. These results are comparable to typical loss values associated with conventional phosphate glass fibres [24], [25].

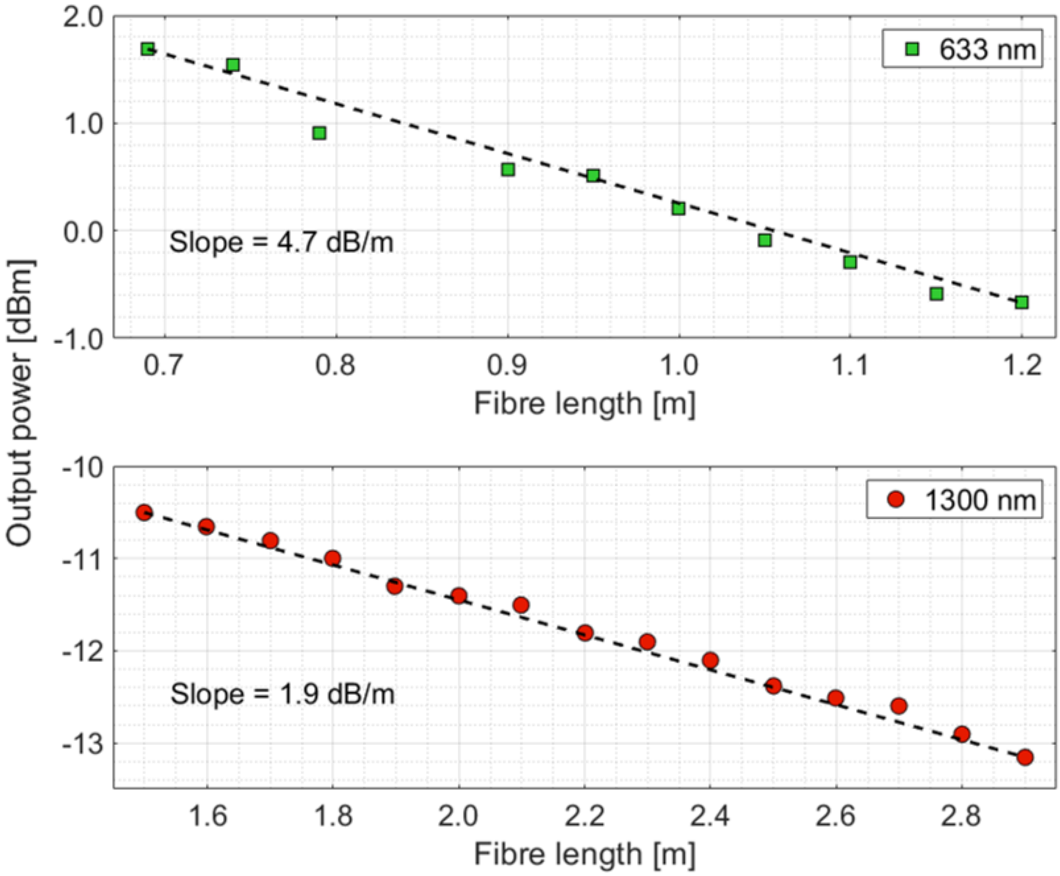

Fig. 5.5. Attenuation loss of a bioresorbable phosphate optical fibre measured with the cut-back technique at 633 nm and 1300 nm (data are taken from [25]).

5.2.3 Preform design and fabrication

The maximum length of the fibre for in-body monitoring or drug delivery is a few tens of cm. Also, the transmitted power is usually lower than the one employed with active fibres described in Chapter 4. These aspects reduce the risk of the occurrence of non-linear side effects. The light confinement in the core can be obtained by selecting the proper couple of core/cladding glasses or by designing advanced microstructured fibres, as will be described in the next paragraphs.

In this scenario, we decided to explore all the possibilities of the extrusion system. Instead of trying to reduce the ratio between internal and external diameters of the extrudate, i.e. the core/cladding ratio ${R_{cc}}^{(Extr)}$, as we did for single-mode active fibre production, we decided to increase it, aiming at a tube with a big central hole. In this condition, the wall of the tube becomes increasingly thinner presenting a technological challenge. After many experimental trials, we reached an important result by reducing the wall thickness of the tube to ≈ 1 mm. Table 5.2 shows a summary of the produced bioresorbable tubes.

By performing these extrusion trials it was possible to tune the extrusion parameters (such as extrusion load, speed, and temperature) until the optimal conditions for the processing of this bioresorbable glass composition were established.

Table 5.2. Summary of extrusion trials for bioresorbable phosphate glass tubes with different dimensions. The parameter $R_{cc}{}^{(Extr)}$ is the ratio between core and cladding, i.e. between internal and external diameters of the extrudate.

Extrusion trial	External diameter [mm]	Internal diameter [mm]	$R_{cc}{}^{(Extr)}$	Wall thickness [mm]
#1	11.90	7.98	0.67	1.960
#2	10.23	5.98	0.58	2.125
#3	11.95	7.90	0.66	2.025
#4	10.42	7.68	0.74	1.370
#5	10.27	5.85	0.57	2.210
#6	10.33	5.75	0.56	2.290
#7	12.08	9.92	0.82	1.080

In particular, once the extrusion temperature has been determined, the maximum load during extrusion can be estimated for each die by observing the $R_{cc}{}^{(Extr)}$. To extrude a tube with a thin wall, i.e. with $R_{cc}{}^{(Extr)} \approx 1$, the process must be carried out at high load (> 1 kN) and low speed (< 100 μm/min). On the contrary, if the wall of the extrudate is thicker, i.e. if the preform hole is small and the glass flow is abundant, the extrusion can be carried out at a lower load and higher speed. It is intuitive to expect that in the presence of a strong obstacle to the flow of the softened glass, i.e. for thin-wall extrudate, the load required to squeeze the glass into the desired shape can be higher.

These results were found heuristically but can also be explained with a basic fluid dynamics approach that considers the reduction in the glass section from the area of the billet $A_B = \frac{\pi \cdot \Phi_B^2}{4}$ to the area of the extrudate $A_e = \frac{\pi}{4}(\varphi_{ext}^2 - \varphi_{int}^2)$. In these formulas the diameter of the billet, Φ_B, is constant ($\Phi_B = 25$ mm) while the external and internal diameters of the extrudate, respectively φ_{ext} and φ_{int}, may vary from case to case. For the most demanding die, i.e. the one that produces the smallest A_e, we have $\varphi_{ext} \approx 12$ mm and $\varphi_{int} \approx 10$ mm (i.e. die #7 of Table 5.2). To satisfy the volume flow conservation law, the product of each section and the average flow velocity over that section must remain constant, or $A_B \cdot v_B = A_e \cdot v_e$, where v_B and v_e are the average velocities of the flows of the billet and the extrudate, respectively. To avoid uncontrolled distortions, v_e is usually kept in the range of 1 – 10 mm/min.

This means that if we reduce A_e but we want a constant v_e, then v_B must be decreased since A_B is constant. In other words, the movement of the billet must decrease if the area of the extrudate is reduced; otherwise, the speed of the extrudate cannot remain constant. The extrusion speed also influences the die swelling phenomenon as well as the overall extrudate distortion. For this reason, the maximum speed of the billet is always kept below 0.2 mm/min. In each extrusion trial, the other parameters will vary accordingly. These considerations are valid for fixed glass composition and extrusion temperature. In fact, by increasing the temperature, the glass viscosity is reduced (see Fig. 5.3) and the velocity of the glass flow may then be increased.

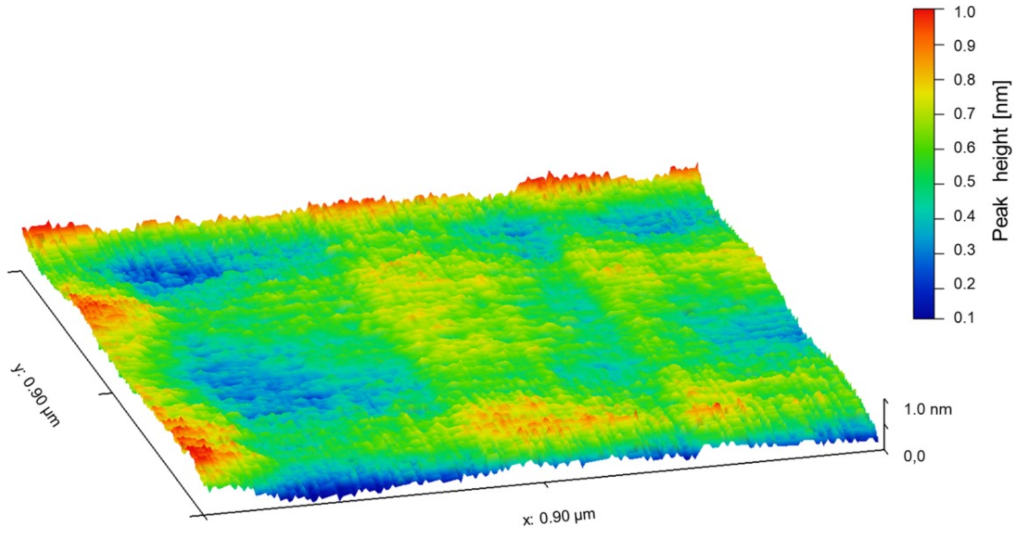

Fig. 5.6. AFM topographic image reconstruction of a portion of the inner surface of an extruded tube.

To assess the quality of the extruded preforms, different kinds of surface roughness measurements are performed especially on the inner surface of the glass cylinder. This measurement can be quite challenging. Since optical profilometry may give unreliable results with transparent glass samples, in the present work, two other characterisation techniques have been employed: Atomic Force Microscopy (AFM) and Contact Profilometry (CP). The AFM technique measures the force of interaction of the tip of a cantilever with the surface atoms of the sample when the probe is put in the proximity of the surface (at least a few nm or, better, Å). The AFM can detect very small features, reaching atomic resolution in particular conditions (i.e. extremely sharp cantilever tips, sensitive instrumentations, etc.). The main limit of the AFM measurement is the small area that can be investigated (a few µm^2 at the most). On the contrary, CP measurements are performed by scanning a probe that is physically put in contact with the surface. As explained in Chapter 2, the resolution of the CP measurement is also affected by the probe dimension. Yet this technique may be employed to scan surfaces up to a few cm^2. We performed both these measurements on a small portion of the surface of an extruded sample investigating with special attention the inner surface of the tube. This is the most challenging area since it is often physically inaccessible. Moreover, the surface quality of this area of the preform is fundamental for optical applications and may affect light propagation. For both AFM and CP techniques, the measurement with the instrument probe on the concave surface of the tubes can be difficult. Furthermore, the concave profile must be subtracted from the measured curves during post-processing, to be able to detect the roughness of the sample. In the performed AFM measurement, the area under investigation was small (0.90 x 0.90 µm), and a very low roughness value of $R_a = 0.37$ nm is obtained. Results of the AFM measurement are shown in Fig. 5.6. Yet, even if the profile of the tube is scanned for more than 2 mm, like in the case of the CP measurement shown in Fig. 5.7, the overall roughness remains low, showing $R_a = 6.4$ nm. By combining the results of these two techniques we investigated both the small-scale features and the average value of the whole sample.

These roughness measurements allowed confirming the capabilities of the extrusion technique in terms of surface quality. These results are not surprising since it has been demonstrated elsewhere that the extrusion process induces a *fire-polishing* on the surface of the extrudate [37]–[40]. Due to the high-temperature, the surface of the glass at the exit of the die is smoothed, and the eventual asperities are flattened.

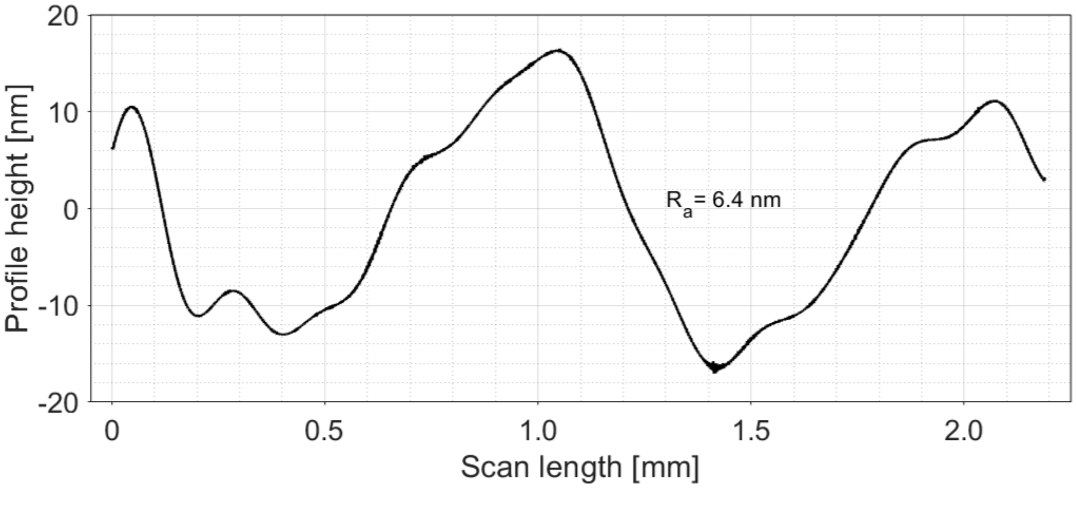

Fig. 5.7. CP scanning acquired along a line on the inner surface of an extruded tube.

A visual comparison between cast and extruded products is presented in Fig. 5.8. Here, a rotational cast tube, a directly cast rod, a polished rod, an extruded tube, and a stretched rod are placed side by side.

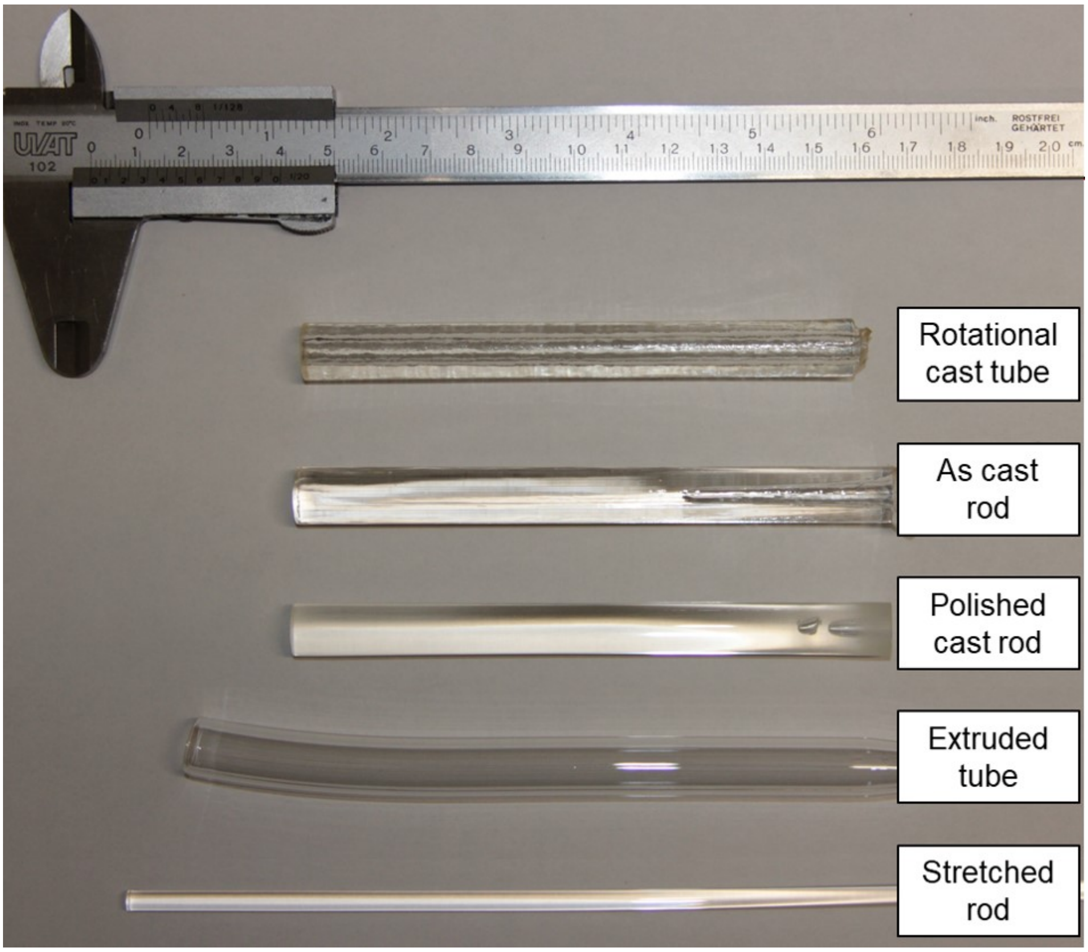

Fig. 5.8. Cast vs. extruded product. The high roughness of the cast products is visible to the naked eye, while the extruded tube and the stretched rod show a fire-polished surface. The surface finishing of the polished cast rod may be enhanced with time-consuming handwork.

The fire-polished surface obtained with the extrusion process is similar to the surface of the stretched rod which has undergone a thermal process in the drawing tower at a temperature well above the T_S. On the contrary, after standard or rotational casting, the surface of the product is highly rough, as is visible in the picture.

Only in some cases, defects have been found on the surface of the extrudate, particularly in the form of bubbles. These bubbles, trapped in the glass billet either during the casting process or during extrusion, are fragmented and aligned according to the glass flow direction (see Fig. 5.9). These bubbles may introduce a disturbance in the flatness of the surface, and their effect is most evident if they do not collapse during the drawing stage. An air bubble at the interface between the core and the cladding of the fibre acts as a strong scattering centre, diffracting the light and causing high propagation losses. Great care has been taken to avoid bubble formation during billet casting.

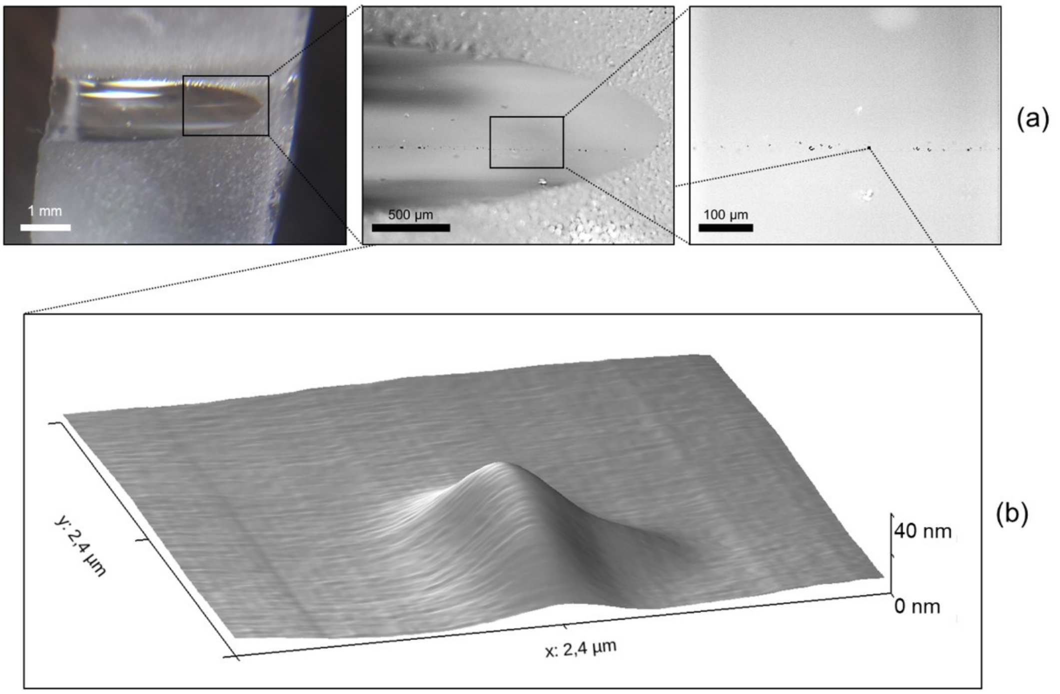

Fig. 5.9. Analysis of the defects on the internal surface of an extruded tube. (a) Pictures of the longitudinally cut tube acquired with an optical microscope at different magnifications; (b) AFM topographic image reconstruction: the presence of a small bubble below the surface was detected.

5.3 Multifunctional bioresorbable fibres

The extrusion process of tubes with different dimensions has shown to be a reliable technique. To exploit the full power of the glass extrusion process, two microstructured bioresorbable phosphate fibres have been designed and fabricated. Details of the obtained preforms, along with the solution proposed to overcome the issues encountered during their realisation, are presented in the next paragraphs.

The first example of a multifunctional fibre is a double-channel fibre. The design of the cladding of such a fibre features two off-centred holes of different sizes. Both the relative position and the size of each hole determine the variation of the glass flow distribution, which affects the distortions of the preform. In the case of a strongly uneven preform cross-section, the distortions might be so high that the desired preform could be difficult to obtain. To deal with complex and challenging geometries of the preform, we developed a CFD model that can predict the distribution of glass flow inside the die. This allowed to test the performance of the designed die and optimise the glass distribution before the actual production of the stainless-steel piece, which is an expensive and time-consuming process.

The other microstructured bioresorbable fibre produced during the present work is a hollow-cladding preform, featuring a solid core surrounded by an array of air holes, all contained into an external cladding. The core and cladding of the fibre are made with the same glass, thus the light confinement is obtained with the presence of a periodic structure in the cladding. To obtain this kind of preform we adopted a multi-step process, which consisted of:

(i) extruding the preform external cylinder;
(ii) extruding the tube that will be used for the internal cylinders;
(iii) stretching the latter tube to obtain thin capillaries with a fixed diameter;
(iv) casting, polishing, and stretching to the desired dimension the solid rod used as the core of the fibre;
(v) assembling the external cladding, with the internal cladding tubes, and the solid core;
(vi) mounting the stacked preform onto the drawing tower and draw it into a fibre with a specific diameter.

5.3.1 Double-channel fibre

The design of a double-channel fibre became of interest when medical practice started to need punctual drug delivery accompanied by localised light irradiation. The idea of using light to stimulate therapeutic action dates back to ancient times. The Nobel Prize in Medicine and Physiology in 1903 has been won by Niels R. Finsen, for the discovery of the beneficial action of the heat-filtered light of a carbon-arc lamp (the *Finsen lamp*) in the treatment of *lupus vulgaris*, a tubercular condition of the skin [41]. This is considered the invention of Photodynamic Therapy (PDT), whereas also ancient Egyptians had discovered the therapeutic action of the ingestion of some plants combined with the exposure to sunlight [42]. Up until recent days, the ongoing discovery of a huge variety of photosensitive molecules, together with the development of different light sources, allowed the PDT to become a robust medical technique. Nevertheless, the most common practice requires the exposure of the body of the patient to a standard (i.e. external) light source, which can have detrimental effects on the exposed tissues. The working mechanism on which PDT is based exploits the destructive potential of singlet oxygen and other radical species that are produced during the photosensitive molecule degradation caused by light exposure. To make an example, photosensitive drug molecules can be accumulated onto some diseased cells like the lung of a patient affected by cancer, and, after light exposure, the localised formation of active radicals can contribute to the destruction of the unhealthy tissue. Furthermore, in the case of the treatment of several localised diseases, the photosensitive drug is usually administered systemically by intravenous perfusion and the selective accumulation onto the diseased tissue may require some time (in the order of a few hours up to a few days). During this time the drug is not harmful to the body since the molecule is not activated, provided that no light source is present. An improper light exposure, e.g. before the completion of the process of accumulation onto the specific tissue, can cause the production of active radicals and singlet oxygen near vital organs that may be accidentally damaged. Of course, this is not a comfortable condition for the patient that needs to be protected from light and, if exposed, might develop reactions all over the body.

One simple way to bypass the waiting time for the drug accumulation onto the target tissue is to employ a topical treatment by directly delivering the drug to the specific site with, e.g., an endoscopic fibre capillary. Furthermore, to avoid the exposure of healthy tissues to the therapeutic radiation, the light can be focused on the target using an optical fibre. These two separate solutions have already begun to be implemented in common medical practice. Interstitial photodynamic therapy (I-PDT) is adopted for several therapies. It has been demonstrated that I-PDT present minimal side effects (compared to surgery and radiation exposure) in the treatment of prostate cancer [43]. On the other hand, a drug delivery system, based on the bioresorbable glass developed by our research group, has been presented some years ago [26]. This system is composed of a bioresorbable capillary with an external diameter of 220 μm. The capillary could be also employed as a hollow waveguide: light propagation in the cladding was successfully demonstrated. These results are encouraging since light propagation within these kinds of devices occurs in a contained length of the fibre (usually below 2 m), thus posing less stringent requirements on the fibre losses. Moreover, also high power laser propagation has been demonstrated in fibre produced with the same glasses [44]. Despite these and other researches on the separate topics of light and drug delivery, the possibility of integrating these two features into a single device has been seldom explored yet [21], [45], [46]. Furthermore, the proposed solutions are not bioresorbable.

In our experiment to produce fibres for simultaneous light and drug delivery, we employed the high-MgO bioresorbable phosphate glass already described. The glass is extruded into a double-channel preform, by using a specially designed die. Other techniques were also available to produce a double core preform, all involving the staking of different pieces together. Several studies have been conducted to produce a double-core optical fibre, in which the two cores can be either on symmetric positions [47], [48] or one in the middle and the other off-centred [49]. All these techniques have intrinsic limitations due to the accuracy of stacking and to the presence of interfaces and inhomogeneities. For this reason, we adopted the extrusion process, which, in principle, should allow us to directly obtain a preform with the designed dimensions.

Direct double-channel preform extrusion

The first step to develop a double-channel preform was to design an extrusion die with an external diameter of 12 mm and internal holes diameter of 1.5 mm and 3 mm. A sketch of the cross-section at the die exit is visible in Fig. 5.10a. The centres of the two holes are equally distanced from the median line of the cross-section. Once preform dimensions and hole positions have been fixed, we tested two different concepts of spider-dies, respectively shown in Fig. 5.10b and Fig. 5.10c. The first type, named *11-arms die*, features a reticulum of supporting structures that hold the die pins in position. The second one, called *multi-holes die*, represents a different solution for sustaining the pins: the die features a planar solid structure with an array of holes distributed over the cross-section. The available area for glass flow represents only ~38% of the cross-section. The design of this latter kind of die is present in several works on glass extrusion [38], [50]–[52]. The 11-arms die shows a more open structure, with around 54% of the area of the cross-section available for glass flow.

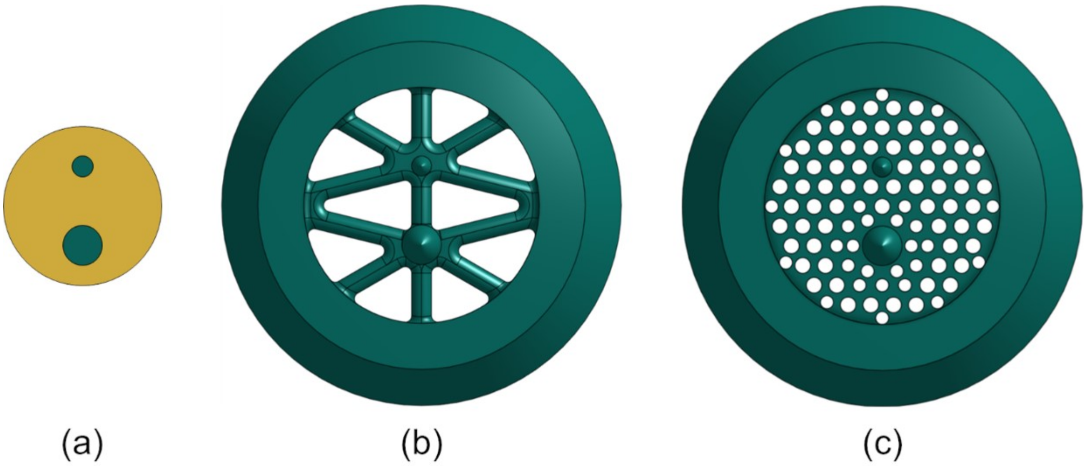

Fig. 5.10. Design of the first types of double-channel extrusion dies. (a) The cross-section at the die exit (the steel parts are represented in dark and the glass in a light colour), (b) the design of the 11-arms and (c) of the multi-holes spider-dies.

The general flow theory says that the multi-holes solution should be interesting since it would favour a more laminar and homogeneously distributed glass flow. If long enough, the array of holes can transform almost any kind of turbulence into a perfect laminar flow [53]. Considering our case, the presence of laminar flow inside the die can be taken for granted in any condition. Indeed, the transition between laminar and turbulent flow can be observed through the value of the *Reynolds number* $Re = \frac{\rho v R}{\mu}$, where $\rho \cong 2600\ \mathrm{kg/m^3}$ is the glass density, $v \cong 100\ \mu\mathrm{m/min}$ is the average speed of the flow, $R = 4 - 6\ \mathrm{mm}$ is the radius of the die hole, and $\mu \cong 10^8\ \mathrm{Pa \cdot s}$ is the dynamic viscosity typically used during extrusion. By simply inserting these numbers in the Reynolds number equation, it is possible to see that in our case we are dealing with $Re \ll 1$. Usually, $Re < 1500$ is associated with laminar flow, while for higher Re, the regime becomes turbulent [53]. Thus, during glass extrusion, the laminar condition is always satisfied.

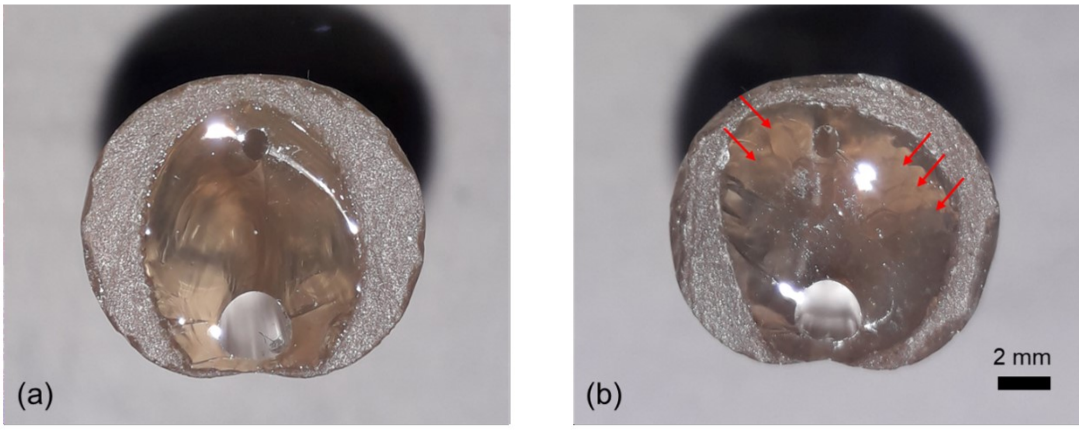

Fig. 5.11. Cross-section of the extruded preforms using the non-optimised double-channel dies. (a) The preform obtained with the 11-arms die and (b) the one with the multi-holes die. The red arrows highlight the defects associated with the glass flow through the multi-holes die.

In Fig. 5.11a and Fig. 5.11b it is possible to see the results of two preform extrusion respectively carried out with the dies of Fig. 5.10b and Fig. 5.10c. The red arrows in Fig. 5.11b highlight the presence of several defects that form a honeycomb structure. These defects are related to the features of the multi-holes die. Furthermore, due to the derived value of Re reported above, the array of holes is not expected to offer any benefit. The laminar condition is already granted by the combination of density, viscosity, speed of flow and radius of the die. On the other hand, Fig. 5.11b demonstrates that the presence of higher shear rates (related to the stronger impediment to the glass flow offered by the multi-holes die compared to the 11-arms die) and the formation of several glass/air interfaces after the transit of the glass inside the multi-holes structure can lead to the appearance of shear bands and inhomogeneities in the preform cross-section.

Apart from the aforementioned defects introduced by the specific features of the die, the overall preform quality appeared to be very poor. In fact, both in the case of 11-arms and of multi-holes die, the distortion of the preform section is pronounced.

The limited space between the bigger hole and the preform external wall creates a substantial glass flow distortion. This affects the cross-section of the preform that has a cuspid shape in place of a circular section. The roundness of the holes is also compromised. Finally, non-homogenous glass flow influenced the longitudinal preform distortions. During these extrusion experiments, the preform bending had to be manually corrected several times since the high distortion was forcing the preform against the extruder’s frame. Fig. 5.12 shows the manufactured dies with the associated distorted preforms in a longitudinal view.

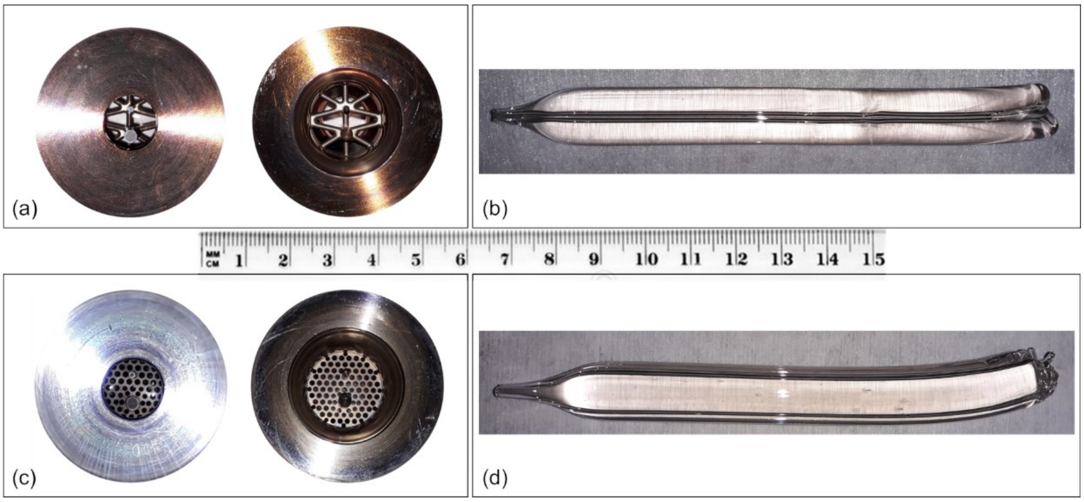

Fig. 5.12. The first versions of the manufactured double-channel dies and the associated preforms obtained. In (a) and (c) pictures of both the bottom and top views of the 11-arms die and the multi-holes die are shown, along with the obtained preforms respectively reported in (b) and (d). The longitudinal pictures of the preforms have a 90° rotational difference: in (b) the two channels are overlapping, while in (d) they are visible on the upper and lower part of the preform.

The results of these first extrusion experiments with a double-channel design are not satisfactory. Moreover, the cost of the whole experiments in terms of both materials processing (the complex spider-dies are obtained by Electrical Discharge Machining of stainless steel) and hours of work are significant.

Moved by these thoughts, we decided that a new route was needed to allow for the prediction of the extrusion results with reduced costs. We needed to develop a model to simulate the glass flow inside the die and somehow forecast the possible distortions. Thus, we decided to employ an open-source CFD analysis tool as OpenFOAM® that allows solving the Navier-Stokes equations for the distributions of different quantities (usually pressure, velocity, and temperature) on a specific die geometry. The mesh creation allows building a map of the whole fluid volume and, by applying specific boundary conditions to the mesh contours, simulate the evolution of the system after an initial stimulus. We are dealing with an incompressible flow of Newtonian fluid, which is computed through the *icoFoam* solver. This is a temperature-independent transient solver, so energy conservation is not considered. Since the source code of the software is editable, we also modified the solver and developed an improved model, that we named *thermoIcoFoam*, intended to be used with incompressible flows of Newtonian fluids in the presence of heat and an exponential viscosity-temperature dependence derived by the VFT equation.

Our model computes the effect of any temperature variation on the distribution of pressure and flow velocity over the whole glass volume. In detail, for each time step, the model calculates the value of pressure and velocity over the whole mesh by solving the so-called momentum predictor and carrying out the PISO-loop[10]. In mathematical form, the momentum equation can be written as:

$$\frac{\partial U}{\partial t} + \nabla \cdot (\varphi U) - \nabla \cdot \nu \nabla U - \nabla U \cdot \nabla \nu = -\nabla p. \tag{2}$$

Here, U is the flow velocity, p is the pressure, $\nu = \mu/\rho$ is the kinematic viscosity, and φ is the volumetric flux of velocity on the cell faces for constant-density flows calculated as

$$\varphi = \oiint_S U \cdot dS. \tag{3}$$

The left term of Equation (2) is the so-called velocity-equation written with implicit derivatives, i.e. in which dependent variables rely on the value of one another from the *current* time step. On the contrary, the pressure gradient on the right is an explicit term (the pressure value is derived either from the *previous* time step or from an initial guess at the first time step).

In our customised model, the viscosity ν is temperature-dependent and is calculated for each time step according to the VFT model with the equation:

$$\nu = \nu_0 e^{\frac{a}{(T-T_0)}}. \tag{4}$$

The values of temperature T are derived from the previous iteration (and ultimately from the boundary conditions) while the values of the constants (ν_0, a, and T_0) are derived by fitting the VFT model (Equation (1) or (4)) to the measured dynamic viscosity, eventually normalising the values with the measured glass density ρ. At each time step, Equation (2) is rewritten in a synthetic matrix form as $MU = -\nabla p$ which allows extrapolating the diagonal coefficients A of matrix M, thus dividing the equation into a diagonal portion multiplied by U and a non-diagonal velocity-dependent portion H: $MU = AU - H(U) = -\nabla p$. The non-diagonal terms are taken into account through specific correctors but the matrix of diagonal coefficients A is invertible and this allows obtaining a new equation for the velocity:

$$U = A^{-1}H - A^{-1}\nabla p \tag{5}$$

This equation leads to the calculation of the continuity equation $\nabla \cdot U = 0$ in a convenient form:

---

[10] https://openfoamwiki.net/index.php/PISO

$$\nabla \cdot (A^{-1} \nabla p) = \nabla \cdot (A^{-1} H). \tag{6}$$

This is the so-called pressure-equation and is initially composed of an implicit term on the left and an explicit term on the right (in the latter, dependent variables rely on the value of one another from the *previous* time step). After several iterations, the pressure values converge, and the velocity is then calculated using only explicit terms. This ends the calculation of the PISO-loop and the obtained values of pressure and velocity are used for the calculation of the subsequent time step.

Furthermore, our model also calculates the temperature-equation (i.e. the Navier-Stokes' energy equation) according to:

$$\frac{\partial T}{\partial t} + \nabla \cdot (\varphi T) = \nabla \cdot \boldsymbol{DT} \nabla T. \tag{7}$$

Here, φ takes into account the dependence of temperature T from flow velocity and the term $\boldsymbol{DT}$ is the thermal diffusivity, which has the units of a diffusion coefficient [m^2/s] and is calculated as $\boldsymbol{DT} = \alpha = \frac{\lambda}{\rho C_p}$, where λ is the thermal conductivity and C_p is the heat capacity at constant pressure. The calculated value of temperature for each time step is updated over the whole mesh to derive the value of dynamic viscosity employed in the velocity-equation.

Finally, regarding the boundary conditions, we usually adopted:

(i) a fixed speed on the inlet of the flow, i.e. we assumed that the glass billet is pushed at a constant speed;

(ii) a *zero-gradient* condition for the pressure at the outlet, which means that there is no pressure drop when the glass exits the die;

(iii) a *no-slip* condition at the die walls, related to the presence of friction between the glass and the die surface, that creates a layer of static fluid near the die walls;

(iv) an optional temperature difference on the outer die wall, that can be linked to the temperature variation imposed by the extruder furnace.

This model can be an interesting tool to detect the influence of the temperature distribution over the whole glass flow. Fig. 5.13 shows some results of these simulations. The modelled volume represents a section of the whole glass volume inside the die. In this case, we wanted to detect the effect of the obstacles on the glass flow at the die exit. The reliability of the model is confirmed by the validation of the results, obtained by deriving the solutions of the standard case of the flow inside a circular pipe and verifying the results with tabulated data.

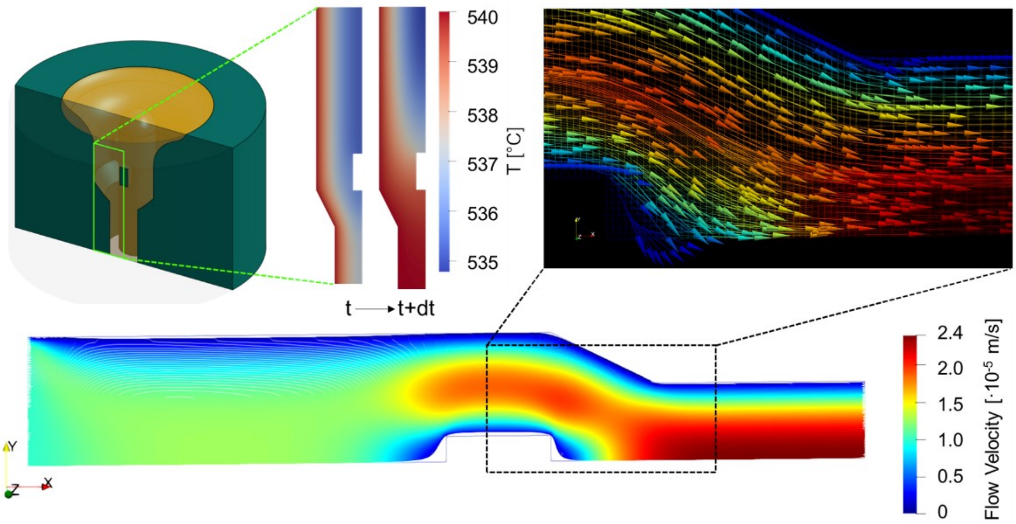

Fig. 5.13. Preliminary results of the simulations conducted with OpenFOAM® custom-designed solver. The 3D design is shown in the top-left part of the image, but the flow of the glass is only computed on a 2D section, evidenced with a green box. The results of the simulations may be observed over the whole meshed region either in terms of the temperature evolution (top) or of the glass flow velocity (bottom). The flow may be analysed also with vectors or flow-lines representation (black box).

Despite the interesting and reliable results of the OpenFOAM® model that we developed, the computational costs of the simulations increase with the mesh complexity, and the application to a 3D geometry can require a huge computational power. The calculations for the results reported in Fig. 5.13 have been performed on an internal server and a full 3D calculation with a high-quality mesh, particularly in the case of a complex die structure, would need a more powerful computational infrastructure. Moreover, in our case, the design of the die is easily accomplished by different CAD software (Onshape®, Solidworks®, Fusion360®) but the conversion into an acceptable *foam* mesh can present different obstacles. For the presented results we employed the OpenFOAM®'s default *BlockMesh* utility. Yet, using this tool to obtain a mesh design of a 3D curvilinear structure like the ones considered herein is very difficult since every single point has to be defined separately. Some external tools like *Gmsh* (an opensource 3D finite-element mesh generator with a built-in CAD engine and post-processor) have been tested.

Our main objective while developing these kinds of tools was to improve and simplify the process of designing the extrusion die. But each of the complex and powerful CFD tools just described requires specific training and their usage may be not straightforward. Furthermore, the need for dedicated intense work for implementing the 3D mesh after each die design is also a contradiction of the purpose of facilitating and speeding up the die design. For this reason, we kept searching for other, simpler solutions. And we finally came up with a web-based computer-aided engineering

(CAE) software named Simscale®, able to perform 3D CFD simulations as well as static and dynamic finite element analysis. One of the main advantages of this platform is its full integration with the Onshape® CAD design software, which we employed for the die design. The Simscale® system exploits the capabilities of dedicated cloud computing, which enables to avoid any local need for computational sources. The platform provides a free academic account with limited performances or the option to buy a one-year subscription. Details about the results of the simulation performed using Simscale® are provided in the next paragraphs.

Computational Fluid Dynamics: preform optimisation

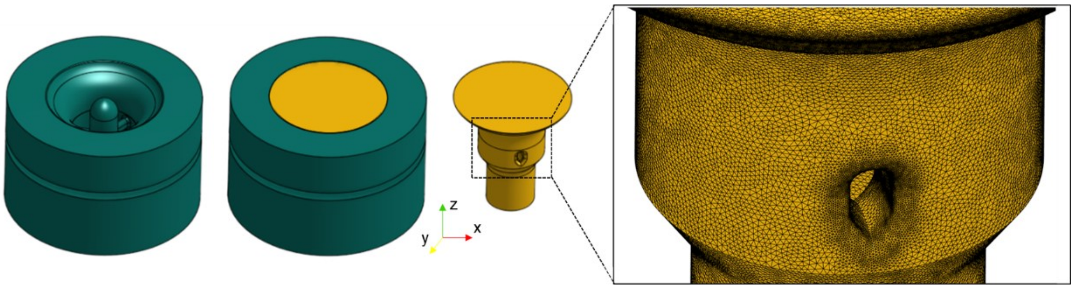

Fig. 5.14. Steps of the 3D flow simulation. From the die design (3D object shown in blue in the left part of the image), the volume of flow is derived (shown in yellow in the middle). A zoomed view of the tetrahedral mesh is visible on the right.

The requirement for a fast and simple tool to predict the extrudate's distortions led us to the exploration of different methods to simulate the glass flow. The most affordable tool in terms of time consumption, reliability of the results, and acceptable complexity of the preform is the on-line platform Simscale®. This software offers a friendly web-based user interface. Once imported the geometry from the Onshape® library, the mesh can be generated. We opted for a *Tet-dominant* meshing algorithm with the best available mesh fineness. This is an automatic meshing algorithm embedded in Simscale® which builds a 3D mesh composed of tetrahedral cells. It is also possible to set a refinement factor to get a higher level of detail, i.e. smaller cells, in particular areas of the mesh, e.g. at the border of the die inlet or near the spider-die arms, as visible in Fig. 5.14. While the mesh is generated, the other parameters can be set, i.e. boundary conditions, material properties, simulation control parameters. The boundary conditions are straightforward: there is a fixed velocity of inlet flow, the absence of a pressure gradient at the outlet, and a *no-slip* condition on all the lateral walls. These boundary conditions are similar to the ones described for the OpenFOAM® simulations, except for the temperature gradient. The only material properties specified are the viscosity and the density, while the thermal dependence is here neglected.

The calculations are performed on dedicated servers and the results can be either post-processed online or downloaded for subsequent independent post-processing using separate software like ParaView®. The amount of work needed for preparing a simulation is substantially reduced compared to the previous model and the results of the calculations are usually available within a few minutes/hours (the effective time consumption depends on the number of employed CPUs as well as the mesh complexity and fineness). This allowed testing several die designs, at first with simple tube structures. The results of the first simulations are visible in Fig. 5.15, where the flow velocity over a vertical cross-sectional plane is visible. Then, with the double-channel configuration, the relative positions and dimensions of the holes have been varied to see the effects on the glass distribution. This process can be effectively integrated into everyday practice, as an improved die design technique.

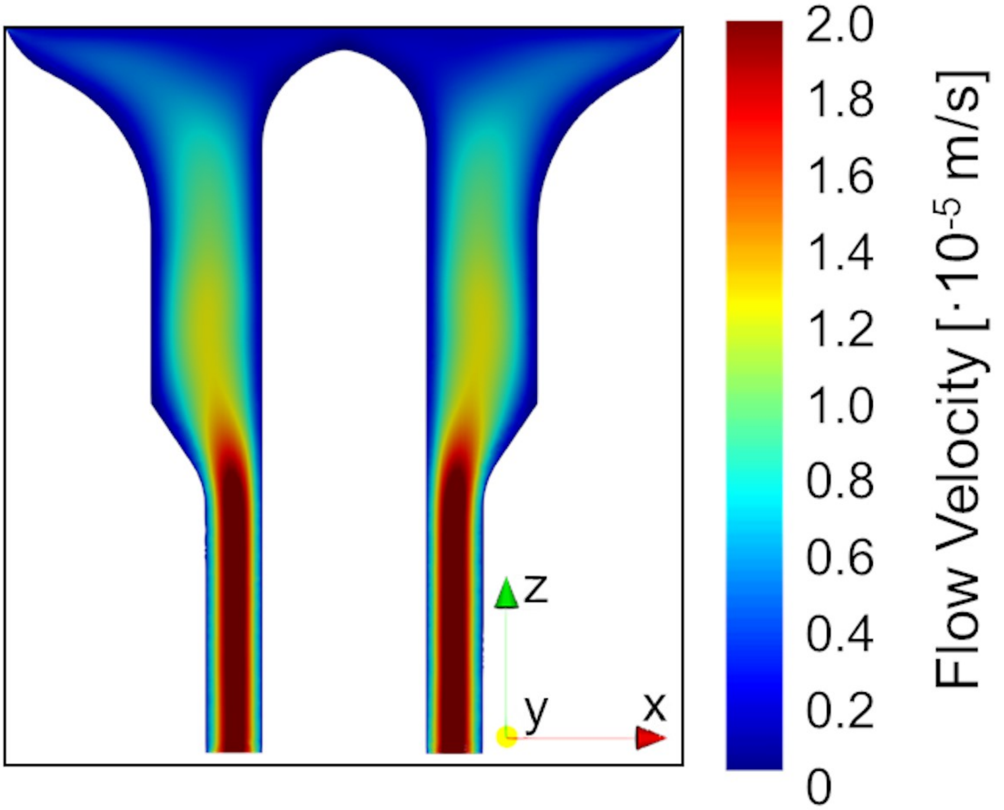

Fig. 5.15. Calculated flow velocity over a vertical cross-sectional plane of the meshed region shown in Fig. 5.14.

The meshed geometry consists of the volume contained inside the die as depicted in Fig. 5.14. The most interesting aspect to analyse is the glass distribution at the die exit. One of the major sources of preform distortions may be connected to an uneven glass distribution over the die section, particularly in the proximity of the generation of the preform interface. As is visible in Fig. 5.16c the glass distribution over the exit section of the first design of double-channel fibre is not uniform, and a strong reduction of the glass flow velocity appears in the same region where a related distortion can be effectively found on the preform. Thus, it is possible to correlate the cuspid-shape of the preform (see Fig. 5.11) to the reduced glass flow in the region between the big hole and the external preform diameter, which is also responsible for a dramatic longitudinal preform bending. By using the described computational tool, we performed different simulations and compared their results, trying to optimise the glass distribution at the die exit. We varied both the position and the dimensions of the holes since both are responsible for the homogeneity of the glass flow.

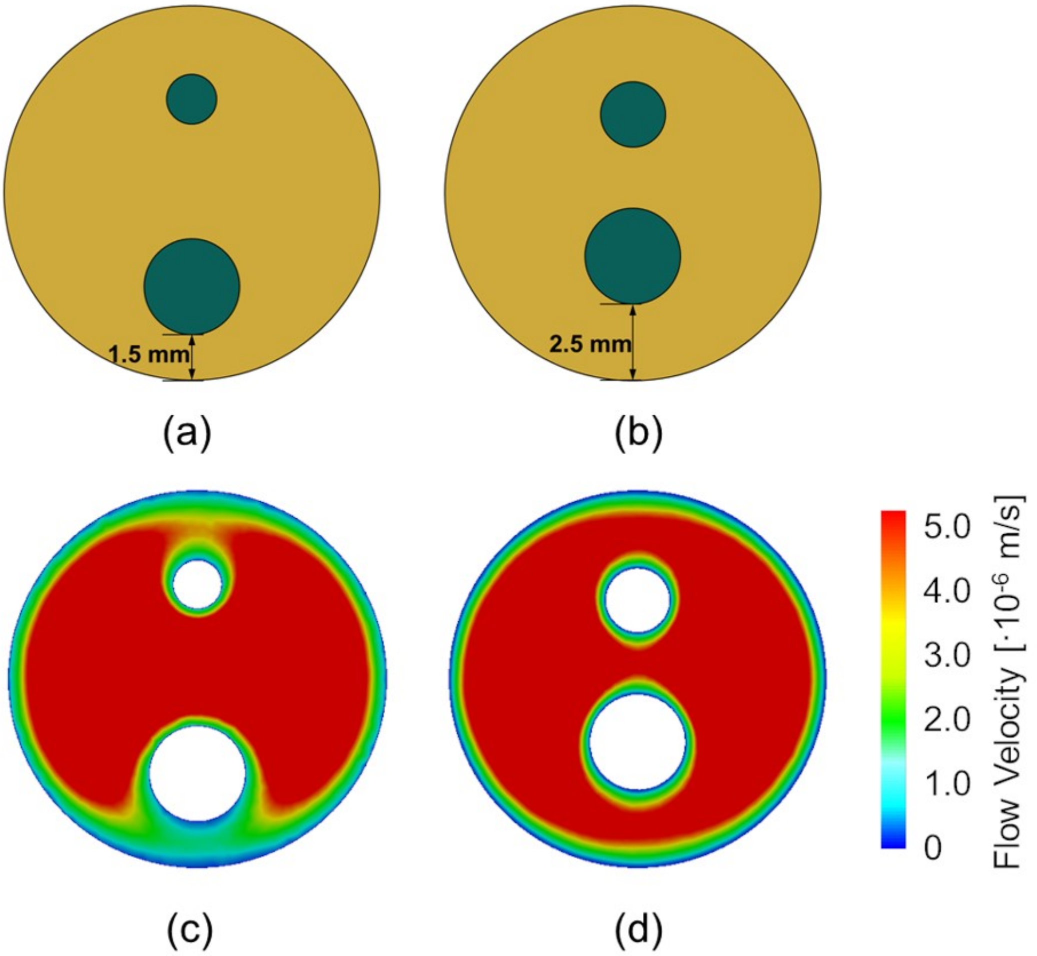

Fig. 5.16. Sketch of the cross-section of the manufactured dies and results of the flow simulations. (a) The first die design, detailed in Fig. 5.10 and (b) the optimised design, with the blocking elements shown in blue and the glass in yellow. The results of the glass flow velocity for the two configurations are respectively shown in (c) and (d).

The optimised die design, shown in Fig. 5.16b features a couple of holes that are not equally distanced from the central axis. The holes are respectively 2 and 3 mm in diameter and their distance from the external wall is kept constant (2.5 mm). This appeared to be the best configuration among the performed tests, and the resulting glass distribution (shown in Fig. 5.16d) demonstrates substantial improvements compared to the previous design (Fig. 5.16a).

Re-designing the extrusion die

Thanks to the results of the simulations of the improved double-channel die, a new die has been fabricated and tested for extrusion with the same glass composition. Apart from the positions of the holes, the new die design also features a lighter structure, with only 5 holding arms and an area of 73% of the cross-section available for the glass flow (Fig. 5.17).

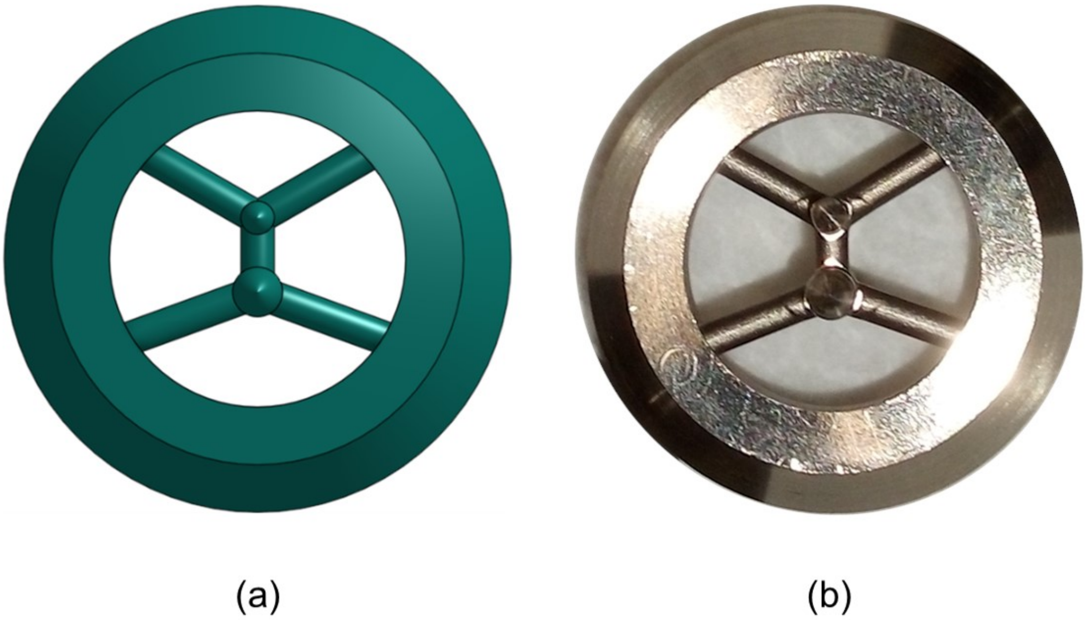

Fig. 5.17. The optimised extrusion die. (a) Sketch of the design and (b) picture of the manufactured stainless-steel die.

The resulted preform features a more circular external section. A comparison of the resulting preforms obtained with the first design and with the optimised design is shown in Fig. 5.18. Small distortions of the shapes of the holes are still visible as also evidenced by the reduction of the speed of the glass flow between the two holes (Fig. 5.16d). Yet, the longitudinal distortions that were present with the first die design resulted to be drastically reduced.

On average, the optimised design allowed a great improvement in the preform quality. The tool has a great potential in helping the work of the designer by suppressing the trial production of the components and consequently shortening the time required to produce a high-quality extrusion die, even with complex shapes.

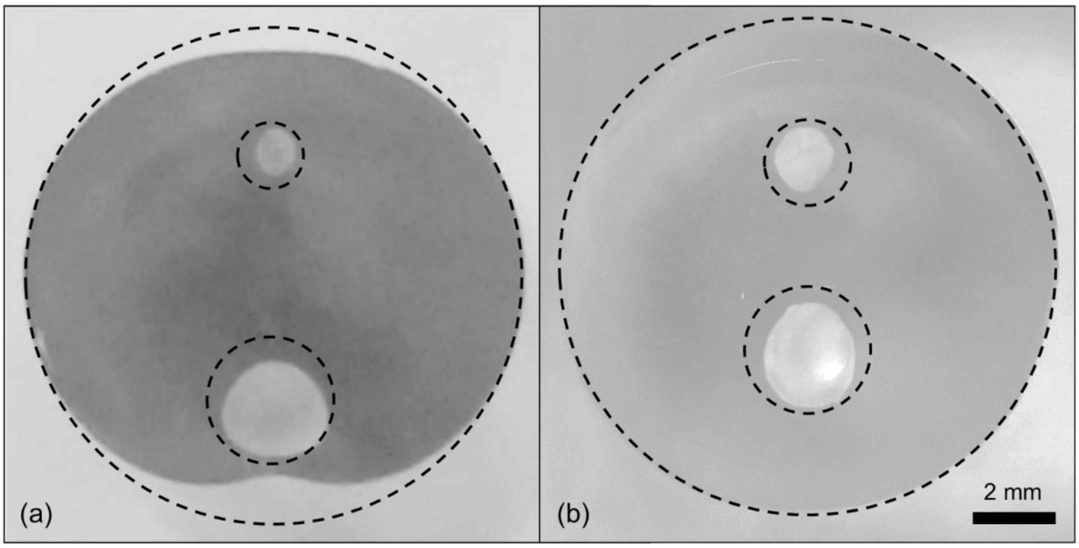

Fig. 5.18. Comparison of the produced double-channel preforms obtained with (a) the first die designs shown in Fig. 5.10 and (b) the optimised die of Fig. 5.17.

5.3.2 Microstructured fibre

One of the limitations of conventional core/cladding structures in sensing applications is that, to achieve distributed sensing capabilities, cumbersome post-processing techniques are needed to expose the core to the external environment. On the contrary, the employment of a hollow-core capillary may allow a continuous overlap between the fluid sample (gas or liquid) and the light. However, in this latter configuration, light propagation is effective only if the refractive-index difference between the glass and the fluid show specific values. In some cases, the multimodal propagation shown by the hollow-core fibres may be detrimental for precise chemical sensing [30].

Another way to achieve light confinement is the use of microstructured fibres. Many complex designs have been proposed but they can be summarised into two main categories: hollow-core photonic-bandgap fibres (HC-PBGs) [54] and solid-core photonic-crystal fibres (SC-PCFs) [55]. We focused our attention on the latter where an array of holes acts as the cladding, with features showing dimensions comparable to the wavelength of light, and provides a guiding structure for the travelling modes in the central core. Small variations in the refractive index of the cladding structure may affect the light propagation. This means that the microstructured fibre may act as a distributed sensor [56]. The holey cladding structure may be filled with a gas or a liquid. Capillary action would force the fluid to flow inside the holes of the cladding and the presence of this fluid will vary the refractive index around the core, thus affecting the evanescent field of the propagating mode.

Often, this kind of microstructured fibre shows a centre-hole omitted triangular lattice (COT) [57]. In other words, the fibre shows a solid core, surrounded by a geometric distribution of holes that can be filled with different fluids. Yet, it is not the refractive index difference between core and cladding, but the presence of an array of holes that determines the light-propagation properties. Thus, the sensing capabilities of this kind of structure are enhanced compared to the hollow-core capillary. Furthermore, single-mode propagation is easier to achieve with these designs [30].

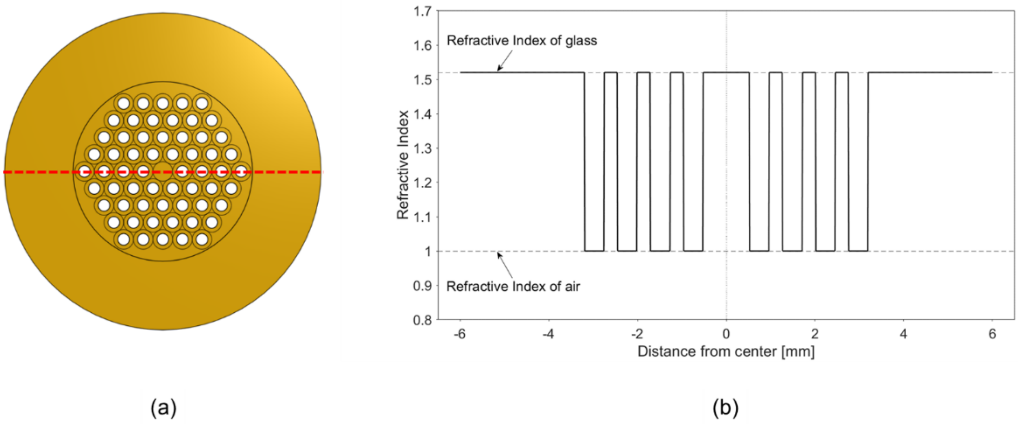

Fig. 5.19. The designed solid-core PCF preform. (a) Sketch of the cross-section of the design and (b) the preform refractive index variation along the red dashed line; in this example, the holes are filled with air ($n_{air} \cong 1$), but light propagation will be sensitive to the variation of the refractive index of the fluid within the holes.

We present here the design, modelling, and realisation of a microstructured fibre, obtained using the extrusion system to produce the preform components. The target design that we wanted to produce is composed of an external cladding that contains 4 rings of holes (i.e. 60 tubes) surrounding the solid core in the middle (see Fig. 5.19a). By looking at the plot in Fig. 5.19b it is possible to see the effective refractive-index variation that surrounds the core. The variation in the refractive index of the cladding material influences the propagation properties of the fibre. This microstructured holey fibre may be then used for biochemical gas or liquid sensing [58]. Sensor with high sensitivity and accuracy may be obtained with this design [59]–[61]. Furthermore, the fibre obtained with this preform should have a large mode area, which is beneficial for the reduction of nonlinearities, also allowing for intense light pulses propagation [62], [63].

Preform extrusion and stretching

The behaviour of the extruder has been optimised to work with the bioresorbable cladding glass composition. The extrusion temperature is set to 520 °C and the maximum applied load varies for each extrusion trials conducted with a different die as already explained. We needed to produce two preforms, one employed for the external cladding and the other for the internal tubes. In the following lines, we will refer to the external cladding with the letter *E* and to the inner tubes with the letter *T*.

The external cladding must show the biggest possible dimensions to contain the whole microstructure. We can vary both the outer diameter $\varphi_{out}^{(E)}$ and inner diameter $\varphi_{int}^{(E)}$ of the external cladding. The aim is to insert all the capillaries that form the cladding together with the solid core into the external cladding, so the bigger $\varphi_{int}^{(E)}$, the easier will be the stacking of all the parts. Furthermore, $\varphi_{out}^{(E)}$ is limited by technological aspects such as the diameter of the preform-clamping system on the top of the drawing tower. For this reason, the need for increasing $\varphi_{int}^{(E)}$ without changing $\varphi_{out}^{(E)}$ may lead to a reduction in the wall thickness. The ratio $R^E = \varphi_{int}^{(E)}/\varphi_{out}^{(E)}$ must be as high as possible, approaching its upper limit of $R^E \approx 1$. On the other hand, the thickness of the walls of the cladding capillaries does not need to be so low. The capillaries that will form the holey portion of the cladding are obtained by stretching an extruded tube. After the stretching, the thin capillaries are cut to the desired length and inserted into the preform stacking.

Fig. 5.20. Examples of some bioresorbable glass extruded tubes.

To proceed with these operations, the tubes are handled in a controlled atmosphere environment to avoid sample contamination, and they must possess enough mechanical strength to avoid cracking during the stacking procedure. Stretched capillaries with thin walls may break at lower stress compared to the thicker ones. On the other hand, in the case of thick walls, i.e. of small-hole tubes, the pressurisation of the holes during drawing may be difficult. With tubes featuring small holes, the surface tension during drawing may force the holes to collapse. For these reasons, an optimum ratio $R^T = \varphi_{int}^{(T)}/\varphi_{out}^{(T)}$ between the cladding tubes inner diameter $\varphi_{int}^{(T)}$ and outer diameter $\varphi_{out}^{(T)}$ is found to be $R^T \approx 0.4$. Finally, to get the solid core, a rod of the same glass is stretched to obtain a diameter close to $\varphi_{out}^{(T)}$.

Table 5.2 reports details about the extrusion trials conducted to optimise the system parameters for the production of the different parts of a microstructured assembled bioresorbable phosphate glass solid-core/holey fibre. Fig. 5.20 also shows some examples of extruded tubes

Preform assembly and fibre drawing

The stack-and-draw method for producing a preform is a multi-step process. Once all the components have been prepared, the stacked preform is manually prepared. The whole assembly operation is conducted in a cleanroom environment, wearing all the required personal protection to avoid preform contamination, especially among the inner parts After stretching the tubes for the holey cladding, the diameter of all the stretched portions is measured with a digital calibre, with a resolution of 0.01 mm. The measurement is taken at regular intervals (of 1 cm) along the whole length of the stretched rod and tubes. The average diameter of the tubes is 0.85 ± 0.02 mm and the portions showing the least diameter variation are selected and cut into pieces with a length of 15 cm. The final preform length is around 10 – 15 cm. The cut is performed with a cleaving tool, and after cutting the glass pieces are cleaned with ethanol using an anti-scratch tissue, to remove any eventual debris. To allow for effective drawing without the risk of hole collapse, the tubes are sealed on both ends by quickly heating their tips with a flame. In this way, the air remains trapped inside the tubes also during the drawing stage. During drawing, to favour a good attachment of all the involved parts, a suction system removes the air and force all the pieces to glue together. To obtain a holey fibre some air must remain inside the cladding tubes until complete solidification of the fibre. One route to get this result is the one that we followed. Another option, currently being implemented on our system, is to handle the pressurisation of the tubes, forcing a controlled flow of air or N_2 inside the fibre during drawing. This could allow us to increase the dimension of the holes and to reduce the thickness of the tube walls, without compromising their mechanical strength during the assembly operations. Furthermore, the control of hole pressurisation allows reducing the distortions in the dimension and shape of the microstructure that may affect the quality of the fibre [38], [51], [52], [64]–[67].

Some steps during the preform assembly are shown in Fig. 5.21. At first, the extruded tubes are cut to remove the distorted ends Fig. 5.21a. Then, the inner tubes and the core rod are stretched to the desired diameters Fig. 5.21b. All the pieces are mounted together to form the final preform Fig. 5.21c. Once completed the assembly, the preform is mounted onto the drawing tower feeding system. The fibre drawing is conducted in the same way as a standard core/clad fibre, by heating the preform at a temperature above 600 °C. The neck-down of the assembled preform during drawing is visible in Fig. 5.21d.

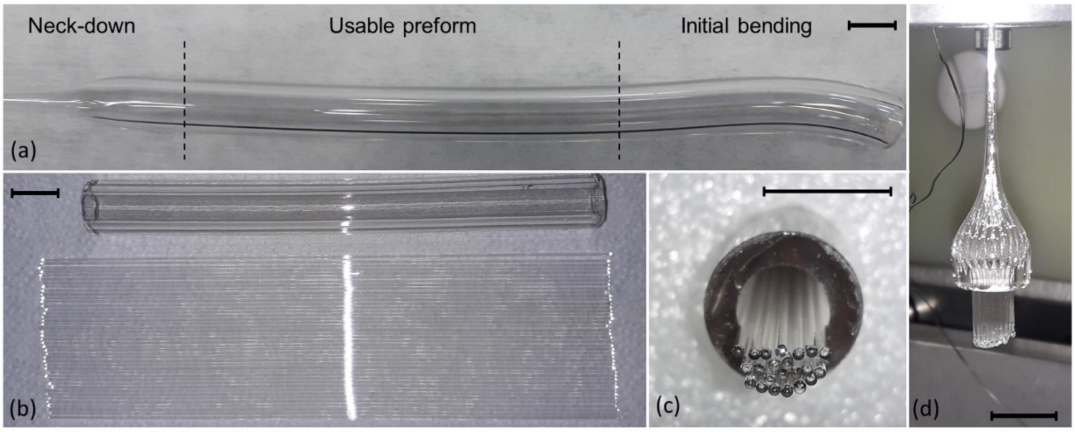

Fig. 5.21. Steps during the preform assembly: (a) the usable portion of the external tube is cut; then all the internal and external tubes shown in (b) are assembled; an intermediate step of the assembly is reported in (c). Finally, the assembled preform is mounted onto the drawing tower and, upon heating, the neck-down occurs (d). All the scale bars are equal to 10 mm.

After the preform neck-down, the fibre is rolled up onto the winding drum. Several tens of meters of fibre have been obtained and the speed of drawing has been varied to get different external diameters. We tuned the optimal drawing conditions to produce a 125 µm fibre, to match the most common standard of fibre diameter. The shape of the fibre cross-section is measured at regular intervals along the fibre length. The geometry of the fibre is conserved all over the fibre length, thus demonstrating the viability of the process.

Fibre characterisation

Fig. 5.22a shows an image obtained with a transmission optical micrograph of the fibre cross-section. Despite some efforts to get a homogeneous capillary diameter, some tiny disturbances may be present in the dimension and straightness of the parts. Compared to the designed structure of Fig. 5.19, the produced external cladding showed a slightly reduced $\varphi_{int}^{(E)}$. This explains why only 42 hollow elements (in the place of 60) plus the solid core are employed to obtain the preform. The symmetry of the structure may be highly affected by these irregularities. The importance of the geometrical homogeneity of the holey tubes, as well as of the accurate prediction and control of the die swelling phenomenon during extrusion may become more evident, in the light of these aspects. The tools that we developed to reduce preform distortions may allow us to get more precise results for the next trials.

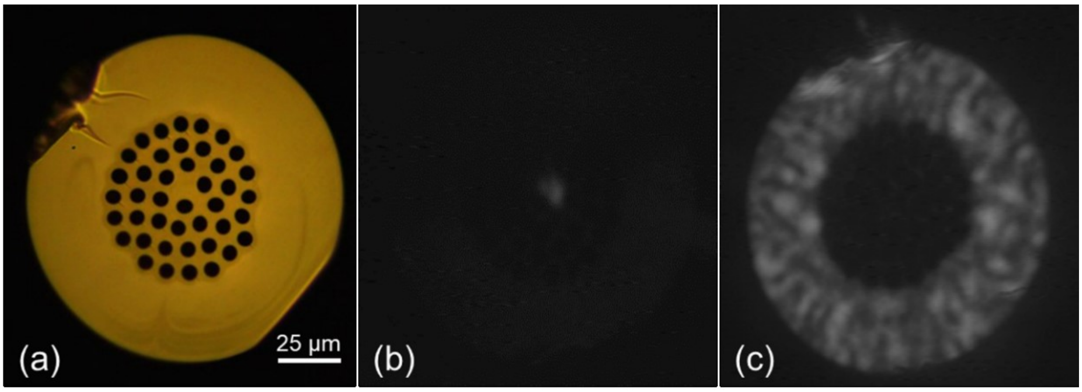

Fig. 5.22. The microstructured bioresorbable fibre. (a) Cross-section of the microstructured fibre (picture acquired with a transmission optical microscope); (b) and (c) are images of the light emerging at one end of the fibre for a core mode and a cladding-guided mode respectively.

A complex stacking has been produced which represent a preliminary but successful result of obtaining a bioresorbable phosphate glass microstructured fibre with the technique of preform extrusion. The performances of the obtained fibre have also been characterised. A near-field light guidance test has been conducted on the produced fibre. The acquired images are shown in Fig. 5.22b and Fig. 5.22c. A laser diode with a wavelength of 1300 nm is coupled on one end of the fibre either in the core or in the cladding. The guided modes are visible both in the core and in the cladding of the fibre. This result further highlights the potential impact of this system, paving the way for the production of a bioresorbable photonic crystal fibre.

Direct microstructured extrusion

To fully exploit the advantages of the extrusion system, the direct production of a preform for microstructured fibre could be carried out. Preform extrusion of glass is particularly suitable in the case of complex structure design. The extrusion die design is more complex than the ones presented, and preliminary tests were necessary.

The analysis of the positions, dimensions, and related distortions of the holes over the cross-section of multi-holes extruded preform has been thoroughly studied [51], [52], [65]. The distortions of the extruded preform can affect the propagation properties; thus, their analysis and prediction are important aspects for the design of a microstructured fibre. A combination of surface tension and viscosity plays a major role in determining the final shape of the holes. Just after leaving the die, the glass is still highly deformable, since its temperature is still above the T_g. The formation of the extrudate occurs when the softened glass appears at the exit of the die. The interface between the softened glass and the stainless steel of the die is replaced by the interface between preform and air, i.e. the free surface of the preform. At that point, both the shape and relative position of the holes rearrange to accommodate for the variation of the flow due to the changed degrees of freedom. Thus, the distortion of both shapes and positions of the holes cannot be avoided but only minimised. One of the ways to minimise these distortions is to redefine the position of the holes to obtain the most uniform glass distribution over the whole cross-section. The uniformity of the glass distribution means that, on average, both the space between the holes and the distance between the blocking elements and the external diameter of the die must be almost constant all over the die cross-section.

Preliminary simulations with an extrusion die for microstructured fibre production showed that the direct extrusion of this kind of preform needs a big die aperture (≥ 20 mm) to be able to force the glass flow into the interstices of the die. In our case, both the extruder and the drawing tower present technological limitations to deal with preform diameters bigger than 14 mm. Thus, considering also the die swelling phenomenon, the maximum allowed diameter of the die aperture is around 12 mm. Hence, direct preform extrusion with the target multi-holes shape seemed to be very difficult with our system. Several simulations have been carried out on different microstructured designs. We tried to reduce the number of holes in the preform to see if the simulation gave better results. Some of these results are presented in Fig. 5.23. The comparison between the two structures presented in Fig. 5.23 allows confirming the need for a design of the die that would favour a homogeneous distribution of both the glass flow and the die features. One simple consideration on the hydrodynamic of the system may be helpful: the glass flow is favoured where less hydraulic resistance is present. If there are regions over the die cross-section showing an ample free space for the glass flow, and other areas presenting only subtle passages fitted between blocking elements, the flow will be more abundant in the first regions, and only a limited (or null) amount of glass would flow in the bottlenecks. In the design of Fig. 5.23a, which is similar to the target design that we wanted to produce (shown in Fig. 5.19), the presence of the blocking elements condensed in the centre of the preform strongly limits the glass flow in that region, as is visible in the flow simulation at the die exit of Fig. 5.23c. On the contrary, the homogeneous distribution of the die features presented in Fig. 5.23b allows for a more homogeneous glass flow distribution, as it is possible to see in Fig. 5.23d. The production of this optimised preform would require a surrounding cladding. However, our target was to produce a 4-rings design featuring a higher number of holes than the one described by these calculations. More simulations or substantial modifications of our extrusion system may be needed to achieve this result by direct extrusion.

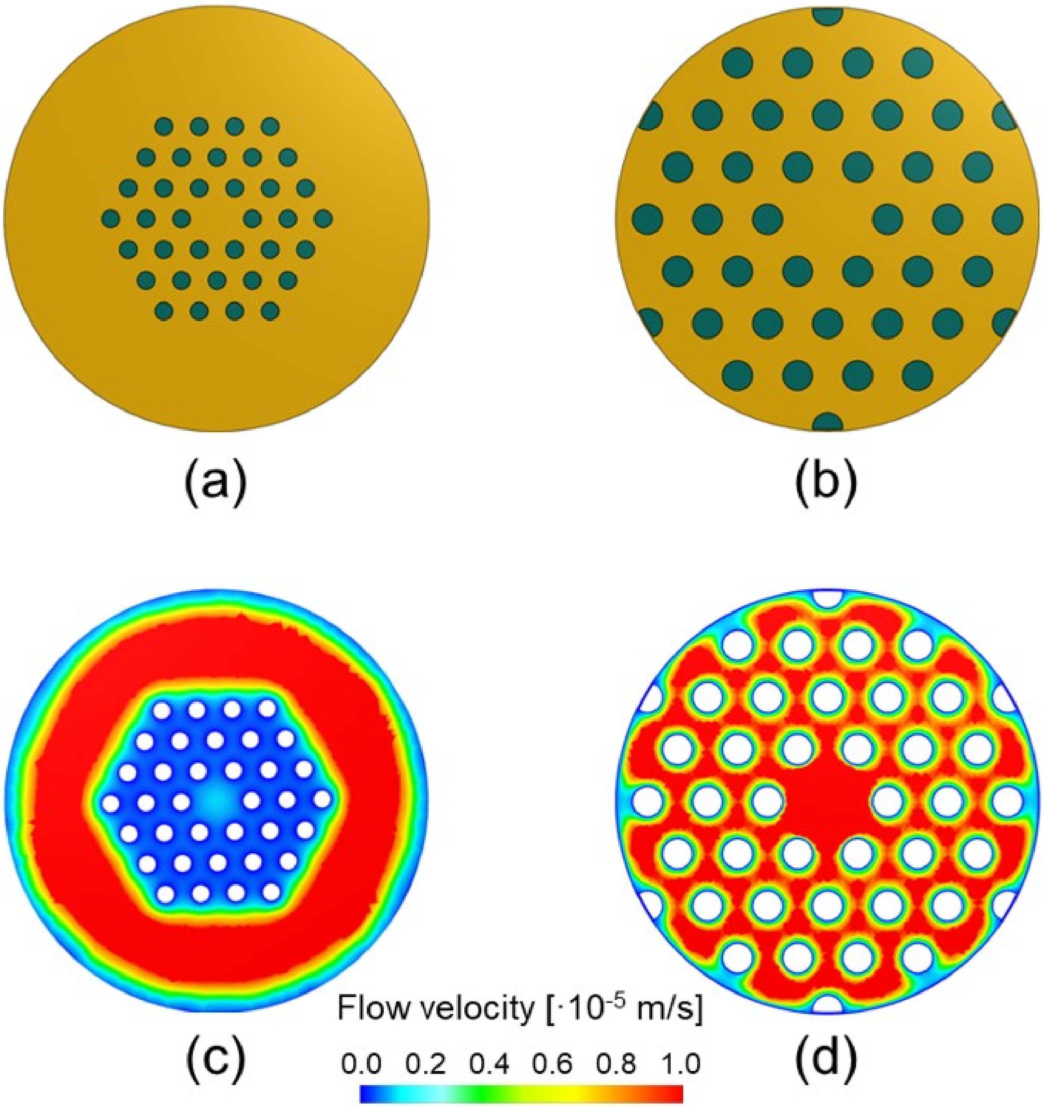

Fig. 5.23. Design of two SC-PCF extrusion dies and results of the glass flow simulations. The cross-sections of the simulation domains at the die exit are represented in (a) for the basic microstructured design and (b) for the optimised microstructured die, with the glass shown in a light colour and the blocking elements shown in a dark colour. The glass flow velocity resulting from the simulations computed on the structures sketched in (a) and (b) are respectively shown in (c) and (d).

In summary, one solution to obtain a complex preform by direct extrusion may be to reduce the external cladding thickness and increase the dimension of each hole of the preform, to have a more open structure, like in the design shown in Fig. 5.23d. This preform can be eventually stretched to fit the required dimension for drawing. Despite the promising results of these simulations, the production of such a die has been postponed. More data about both the extrusion and the drawing conditions of these complex structure are needed. As a first attempt, we preferred to proceed with a more straightforward route. Yet, the quality of the preliminary results achieved by extrusion followed by stack-and-draw demonstrates the potential benefits of this technique in microstructured fibre production.

5.4 Conclusions

Microstructured multifunctional bioresorbable fibres have been designed and successfully fabricated in the framework of the present thesis. The objective was to demonstrate the possibility of realising complex-shaped preforms through the extrusion technique applied to bioresorbable phosphate glasses. These preforms are intended to be used for biomedical optical fibres production. We performed a thorough characterisation of the glass, in terms of both thermal and optical measurement. We also studied the dependence of the viscosity of the glass from the temperature, which is an important parameter for extrusion trials. We also performed several extrusions with bioresorbable phosphate glasses and we characterised the surfaces of the extruded product, demonstrating the extremely low roughness achievable with this system.

We propose a new preform design featuring a couple of non-symmetric unequal holes. The design is intended to be used for the simultaneous delivery of drug and light. The surgical procedures for photodynamic therapy could be substantially simplified by producing this kind of fibre with a bioresorbable glass. Preliminary results demonstrate the interesting perspectives provided by the extrusion process in this context. Furthermore, we developed a method to optimise the production of extrusion dies allowing for a straightforward design that avoids a huge waste of time and energy. This method involves standardised CFD tools and leads to a simple but effective optimisation of the process. The reduction in the distortion of the extruded products after this optimisation step demonstrates the applicability of the method.

We also reported the fabrication of a new microstructured bioresorbable fibre designed to be used as a sensor in biomedicine. A complex preform was obtained by assembly a stacking of extruded tubes. This preform was drawn to a 125 μm fibre and the effective light propagation of this fibre was demonstrated. Such design opens several possibilities for the development of bioresorbable optical sensors.

References

[1] R. Nazempour, Q. Zhang, R. Fu, and X. Sheng, ‘Biocompatible and Implantable Optical Fibers and Waveguides for Biomedicine’, Materials, vol. 11, no. 8, p. 1283, 2018, doi: 10.3390/ma11081283.

[2] W. Bai et al., ‘Bioresorbable photonic devices for the spectroscopic characterization of physiological status and neural activity’, Nature Biomedical Engineering, vol. 3, no. 8, pp. 644–654, 2019, doi: 10.1038/s41551-019-0435-y.

[3] M. Humar, S. J. J. Kwok, M. Choi, A. K. Yetisen, S. Cho, and S. H. Yun, ‘Toward biomaterial-based implantable photonic devices’, Nanophotonics, vol. 6, no. 2, pp. 414–434, 2017, doi: 10.1515/nanoph-2016-0003.

[4] S. Chatterjee, M. Saxena, D. Padmanabhan, M. Jayachandra, and H. J. Pandya, 'Futuristic medical implants using bioresorbable materials and devices', Biosensors and Bioelectronics, vol. 142, no. July, p. 111489, 2019, doi: 10.1016/j.bios.2019.111489.

[5] D. Milanese, D. Janner, D. Pugliese, N. G. Boetti, and E. Ceci Ginistrelli, 'Fibra ottica bioriassorbibile microstrutturata per il rilascio di fluidi, in particolare farmaci, e la trasmissione di luce', 102018000021559, Jul. 01, 2020.

[6] F. Buchanan, Degradation rate of bioresorbable materials Prediction and evaluation. Cambridge, UK: Woodhead Publishing, 2008.

[7] L. L. Hench and J. M. Polak, 'Third-generation biomedical materials', Science, vol. 295, no. 5557, pp. 1014–1017, 2002.

[8] G. D. Cha, D. Kang, J. Lee, and D. H. Kim, 'Bioresorbable Electronic Implants: History, Materials, Fabrication, Devices, and Clinical Applications', Advanced Healthcare Materials, vol. 8, no. 11, pp. 1–20, 2019, doi: 10.1002/adhm.201801660.

[9] L. L. Hench, 'The story of Bioglass®', Journal of Materials Science: Materials in Medicine, vol. 17, no. 11, pp. 967–978, 2006, doi: 10.1007/s10856-006-0432-z.

[10] F. Baino, 'Bioactive glasses – When glass science and technology meet regenerative medicine', Ceramics International, vol. 44, no. 13, pp. 14953–14966, Sep. 2018, doi: 10.1016/j.ceramint.2018.05.180.

[11] E. Boccardi et al., 'Bioactivity and Mechanical Stability of 45S5 Bioactive Glass Scaffolds Based on Natural Marine Sponges', Annals of Biomedical Engineering, vol. 44, no. 6, pp. 1881–1893, 2016, doi: 10.1007/s10439-016-1595-5.

[12] F. Baino, S. Hamzehlou, and S. Kargozar, 'Bioactive Glasses: Where Are We and Where Are We Going?', Journal of Functional Biomaterials, vol. 9, no. 1, p. 25, Mar. 2018, doi: 10.3390/jfb9010025.

[13] C. Zhu et al., 'Novel bioresorbable phosphate glass fiber textile composites for medical applications', Polymer Composites, vol. 39, no. S1, pp. E140–E151, 2018, doi: 10.1002/pc.24499.

[14] N. Sharmin, M. S. Hasan, A. J. Parsons, C. D. Rudd, and I. Ahmed, 'Cytocompatibility, mechanical and dissolution properties of high strength boron and iron oxide phosphate glass fibre reinforced bioresorbable composites', Journal of the Mechanical Behavior of Biomedical Materials, vol. 59, pp. 41–56, 2016, doi: 10.1016/j.jmbbm.2015.12.011.

[15] R. M. Felfel, I. Ahmed, A. J. Parsons, P. Haque, G. S. Walker, and C. D. Rudd, 'Investigation of crystallinity, molecular weight change, and mechanical properties of PLA/PBG bioresorbable composites as bone fracture fixation plates', Journal of Biomaterials Applications, vol. 26, no. 7, pp. 765–789, 2012, doi: 10.1177/0885328210384532.

[16] I. Ahmed, A. J. Parsons, G. Palmer, J. C. Knowles, G. S. Walker, and C. D. Rudd, 'Weight loss, ion release and initial mechanical properties of a binary calcium phosphate glass fibre/PCL composite', Acta Biomaterialia, vol. 4, no. 5, pp. 1307–1314, 2008, doi: 10.1016/j.actbio.2008.03.018.

[17] I. Ahmed et al., ‘Composites for bone repair: Phosphate glass fibre reinforced PLA with varying fibre architecture’, Journal of Materials Science: Materials in Medicine, vol. 22, no. 8, pp. 1825–1834, 2011, doi: 10.1007/s10856-011-4361-0.

[18] R. M. Felfel, I. Ahmed, A. J. Parsons, and C. D. Rudd, ‘Bioresorbable screws reinforced with phosphate glass fibre: Manufacturing and mechanical property characterisation’, Journal of the Mechanical Behavior of Biomedical Materials, vol. 17, pp. 76–88, 2013, doi: 10.1016/j.jmbbm.2012.08.001.

[19] D. S. Brauer, ‘Degradable Phosphate Glasses and Composite Materials for Biomedical Applications’, PhD Thesis, Friedrich-Schiller-Universität, Jena, Germany, 2005.

[20] D. S. Brauer, C. Rüssel, W. Li, and S. Habelitz, ‘Effect of degradation rates of resorbable phosphate invert glasses on in vitro osteoblast proliferation’, Journal of Biomedical Materials Research - Part A, vol. 77, no. 2, pp. 213–219, 2006, doi: 10.1002/jbm.a.30610.

[21] A. Canales et al., ‘Multifunctional fibers for simultaneous optical, electrical and chemical interrogation of neural circuits in vivo - Supporting Information’, Nature Biotechnology, vol. 33, no. 3, pp. 277–284, 2015, doi: 10.1038/nbt.3093.

[22] C. Elosua et al., ‘Micro and nanostructured materials for the development of optical fibre sensors’, Sensors, vol. 17, no. 10, 2017, doi: 10.3390/s17102312.

[23] J. Massera et al., ‘Processing and characterization of novel borophosphate glasses and fibers for medical applications’, Journal of Non-Crystalline Solids, vol. 425, pp. 52–60, 2015, doi: 10.1016/j.jnoncrysol.2015.05.028.

[24] L. Di Sieno et al., ‘Towards the use of bioresorbable fibers in time-domain diffuse optics’, Journal of Biophotonics, vol. 11, no. 1, pp. 1–11, 2018, doi: 10.1002/jbio.201600275.

[25] E. Ceci-Ginistrelli et al., ‘Novel Biocompatible and Resorbable UV-Transparent Phosphate Glass Based Optical Fiber’, Optical Materials Express, vol. 6, no. 6, pp. 2040–2051, 2016, doi: 10.1364/OME.6.002040.

[26] E. Ceci-Ginistrelli et al., ‘Drug release kinetics from biodegradable UV-transparent hollow calcium-phosphate glass fibers’, Materials Letters, vol. 191, pp. 116–118, 2017, doi: 10.1016/j.matlet.2016.12.103.

[27] O. Podrazký et al., ‘In vivo testing of a bioresorbable phosphate-based optical fiber’, Journal of Biophotonics, no. December 2018, pp. 1–6, 2019, doi: 10.1002/jbio.201800397.

[28] Y. M. Stokes, ‘Bending in extrusion of optical fibre preforms’, ANZIAM Journal, vol. 51, no. December 2009, p. 124, 2016, doi: 10.21914/anziamj.v51i0.2334.

[29] H. Sofuoglu and Rasty, ‘Flow behavior of Plasticine used in physical modeling of metal forming processes’, MRS Proceedings, vol. 25, pp. 523–529, 2011, doi: 10.1557/proc-25-633.

[30] A. M. Cubillas et al., ‘Photonic crystal fibres for chemical sensing and photochemistry’, Chemical Society Reviews, vol. 42, no. 22, pp. 8629–8648, 2013, doi: 10.1039/c3cs60128e.

[31] A. \Lapa, M. Cresswell, P. Jackson, and A. R. Boccaccini, ‘Phosphate glass fibres with therapeutic ions release capability–a review’, Advances in Applied Ceramics, vol. 119, no. 1, pp. 1–14, 2020, doi: 10.1080/17436753.2018.1564413.

[32] E. A. Abou Neel et al., ‘Bioactive functional materials: a perspective on phosphate-based glasses’, Journal of Materials Chemistry, vol. 19, pp. 690–701, 2009, doi: 10.1039/b810675d.

[33] S. T. Lin, S. L. Krebs, S. Kadiyala, K. W. Leong, W. C. LaCourse, and B. Kumar, ‘Development of bioabsorbable glass fibres’, Biomaterials, vol. 15, no. 13, pp. 1057–1061, 1994, doi: 10.1016/0142-9612(94)90091-4.

[34] C. Vitale-Brovarone, G. Novajra, D. Milanese, J. Lousteau, and J. C. Knowles, ‘Novel phosphate glasses with different amounts of TiO2 for biomedical applications: Dissolution tests and proof of concept of fibre drawing’, Materials Science and Engineering C, vol. 31, no. 2, pp. 434–442, 2011, doi: 10.1016/j.msec.2010.11.001.

[35] D. Pugliese et al., ‘Bioresorbable optical fiber Bragg gratings’, Optics Letters, vol. 43, no. 4, p. 671, 2018, doi: 10.1364/ol.43.000671.

[36] A. Varshneya and J. C. Mauro, Fundamentals of Inorganic Glasses, 3rd ed. Cambridge, MA: Elsevier, 2019.

[37] H. Ebendorff-Heidepriem, J. Schuppich, A. Dowler, L. Lima-Marques, and T. M. Monro, ‘3D-printed extrusion dies: a versatile approach to optical material processing’, Optical Materials Express, vol. 4, no. 8, p. 1494, 2014, doi: 10.1364/ome.4.001494.

[38] H. Ebendorff-Heidepriem and T. M. Monro, ‘Analysis of glass flow during extrusion of optical fiber preforms’, Optical Materials Express, vol. 2, no. 3, p. 304, 2012, doi: 10.1364/ome.2.000304.

[39] C. A. G. Kalnins, N. A. Spooner, T. M. Monro, and H. Ebendorff-Heidepriem, ‘Surface Analysis and Treatment of Extruded Fluoride Phosphate Glass Preforms for Optical Fiber Fabrication’, Journal of the American Ceramic Society, vol. 99, no. 6, pp. 1874–1877, 2016, doi: 10.1111/jace.14269.

[40] C. A. G. Kalnins, K. J. Bachus, A. Gooley, and H. Ebendorff-Heidepriem, ‘High precision extrusion of glass tubes’, International Journal of Applied Glass Science, vol. 10, no. 2, pp. 172–180, Apr. 2019, doi: 10.1111/ijag.13092.

[41] L. B. Josefsen and R. W. Boyle, ‘Photodynamic therapy and the development of metal-based photosensitisers’, Metal-Based Drugs, vol. 2008, 2008, doi: 10.1155/2008/276109.

[42] M. H. Abdel-kader, ‘The Journey of PDT Throughout History: PDT from Pharos to Present’, in Photodynamic Medicine: From Bench to Clinic, .

[43] G. Shafirstein et al., ‘Interstitial photodynamic therapy—a focused review’, Cancers, vol. 9, no. 2, pp. 1–14, 2017, doi: 10.3390/cancers9020012.

[44] P. Peterka et al., ‘High-power laser tests of phosphate glass-based bioresorbable optical fibers transmission’, in Proc. SPIE 11029, Prague, Czech Republic, 2019, vol. 1102911, p. 40, doi: 10.1117/12.2523188.

[45] M. Jin, D. G. Yu, C. F. G. C. Geraldes, G. R. Williams, and S. W. A. Bligh, ‘Theranostic fibers for simultaneous imaging and drug delivery’, Molecular Pharmaceutics, vol. 13, no. 7, pp. 2457–2465, 2016, doi: 10.1021/acs.molpharmaceut.6b00197.

[46] N. L. Krinick, Y. Sun, D. Joyner, J. D. Spikes, R. C. Straight, and J. Kopeček, ‘A polymeric drug delivery system for the simultaneous delivery of drugs activatable by enzymes and/or light’, Journal of Biomaterials Science, Polymer Edition, vol. 5, no. 4, pp. 303–324, 1994, doi: 10.1163/156856294X00040.

[47] S. R. Vigil, Z. Zhou, B. K. Canfield, J. Tostenrude, and M. G. Kuzyk, ‘Dual-core single-mode polymer fiber coupler’, Journal of the Optical Society of America B, vol. 15, no. 2, p. 895, 1998, doi: 10.1364/josab.15.000895.

[48] G. Schiffner, H. Schneider, and G. Schöner, ‘Double-core single-mode optical fiber as directional coupler’, Applied Physics, vol. 23, no. 1, pp. 41–45, 1980, doi: 10.1007/BF00899569.

[49] P. Peterka, I. Kasik, J. Kanka, P. Honzatko, V. Matejec, and M. Hayer, ‘Twin-core fiber design and preparation for easy splicing’, IEEE Photonics Technology Letters, vol. 12, no. 12, pp. 1656–1658, 2000, doi: 10.1109/68.896339.

[50] H. Ebendorff-Heidepriem and T. M. Monro, ‘Extrusion of complex preforms for microstructured optical fibers’, Optics Express, vol. 15, no. 23, p. 15086, 2007, doi: 10.1364/OE.15.015086.

[51] M. Trabelssi and P. F. Joseph, ‘Hole distortion and drift in extruded microstructured optical fiber glass preforms: Part I – Sensitivity analysis’, Journal of Non-Crystalline Solids, vol. 481, no. July 2017, pp. 208–224, 2018, doi: 10.1016/j.jnoncrysol.2017.10.045.

[52] M. Trabelssi and P. F. Joseph, ‘Hole distortion and drift in extruded microstructured optical fiber glass preforms: Part II – Optimization’, Journal of Non-Crystalline Solids, vol. 481, no. July 2017, pp. 412–423, 2018, doi: 10.1016/j.jnoncrysol.2017.11.021.

[53] R. B. Bird, W. E. Stewart, and E. N. Lightfoot, Transport Phenomena. New York, NY: John Wiley & Sons, 2002.

[54] B. Temelkuran, S. D. Hart, G. Benoit, J. D. Joannopoulos, and Y. Fink, ‘Wavelength-scalable hollow optical fibres with large photonic bandgaps for CO2 laser transmission’, Nature, vol. 420, no. 6916, pp. 650–653, 2002, doi: 10.1038/nature01275.

[55] J. C. Knight, ‘Photonic crystal fibres’, Nature, vol. 424, no. August, pp. 847–851, 2003, doi: 10.1038/nature01940.

[56] S. Asaduzzaman, K. Ahmed, T. Bhuiyan, and T. Farah, ‘Hybrid photonic crystal fiber in chemical sensing’, SpringerPlus, vol. 5, no. 1, p. 748, Dec. 2016, doi: 10.1186/s40064-016-2415-y.

[57] J. M. Fini, ‘Microstructure fibres for optical sensing in gases and liquids’, Measurement Science and Technology, vol. 15, no. 6, pp. 1120–1128, Jun. 2004, doi: 10.1088/0957-0233/15/6/011.

[58] L. Rindorf, J. B. Jensen, M. Dufva, L. H. Pedersen, P. E. Høiby, and O. Bang, ‘Photonic crystal fiber long-period gratings for biochemical sensing’, Optics Express, vol. 14, no. 18, p. 8224, 2006, doi: 10.1364/OE.14.008224.

[59] S.-G. Li et al., ‘Study of the sensitivity of gas sensing by use of index-guiding photonic crystal fibers’, Applied Optics, vol. 46, no. 22, p. 5183, Aug. 2007, doi: 10.1364/AO.46.005183.

[60] R. Jha, J. Villatoro, and G. Badenes, ‘Ultrastable in reflection photonic crystal fiber modal interferometer for accurate refractive index sensing’, Applied Physics Letters, vol. 93, no. 19, p. 191106, Nov. 2008, doi: 10.1063/1.3025576.

[61] V. P. Minkovich, J. Villatoro, D. Monzón-Hernández, S. Calixto, A. B. Sotsky, and L. I. Sotskaya, ‘Holey fiber tapers with resonance transmission for high-resolution refractive index sensing’, Optics Express, vol. 13, no. 19, p. 7609, 2005, doi: 10.1364/OPEX.13.007609.

[62] L. Li et al., ‘Short-length microstructured phosphate glass fiber lasers with large mode areas’, Optics Letters, vol. 30, no. 10, p. 1141, 2005, doi: 10.1364/ol.30.001141.

[63] J. C. Knight, T. A. Birks, R. F. Cregan, P. St. J. Russell, and J.-P. de Sandro, ‘Large mode area photonic crystal fibre’, Electronics Letters, vol. 34, no. 13, p. 1347, 1998, doi: 10.1049/el:19980965.

[64] M. Trabelssi, ‘Numerical Analysis of the Extrusion of Fiber Optic and Photonic Crystal Fiber Preforms Near the Glass Transition’, PhD Thesis, Clemson University, Clemson, SC, 2014.

[65] M. Trabelssi, H. Ebendorff-Heidepriem, K. A. Richardson, T. M. Monro, and P. F. Joseph, ‘Computational modeling of hole distortion in extruded microstructured optical fiber glass preforms’, Journal of Lightwave Technology, vol. 33, no. 2, pp. 424–431, 2015, doi: 10.1109/JLT.2015.2388733.

[66] H. Tronnolone, ‘Extensional and Surface-Tension-Driven Fluid Flows in Microstructured Optical Fibre Fabrication’, PhD Thesis, University of Adelaide, Adelaide, Australia, 2015.

[67] H. Tronnolone, Y. M. Stokes, H. T. C. Foo, and H. Ebendorff-Heidepriem, ‘Gravitational extension of a fluid cylinder with internal structure’, Journal of Fluid Mechanics, vol. 790, pp. 308–338, 2016, doi: 10.1017/jfm.2016.11.

Chapter 6.

Antibacterial glasses

Bacteria are one of the most abundant biological entities on Earth. They have been discovered almost 350 years ago by the Dutch scientist Antony van Leeuwenhoek, who developed a rudimental microscope able to see what he called *animalcules* [1]. Since then, many bacteria have been discovered and their evolution is still a matter of study.

During the centuries, the fundamental role of bacteria in the proper functioning of ecosystems has been confirmed. For example, bacteria naturally present in the soil are responsible for nitrogen fixation; likewise, thousands of bacteria species can be found in the healthy gut flora of human intestines and are responsible for many metabolic processes of our organism. Bacteria have been also employed in different fields of our advanced society: they are key elements in several processes of food production and fermentation as well as in other industrial processes, like the extraction of chemicals (organic acids, ethanol, and acetone are only the most common) or the synthesis of biofuels. Over the centuries, different species of bacteria have also demonstrated to be harmful to the human population. Some examples of the potential impact of dangerous bacteria on human health are: *(i) Yersinia pestis*, the bacterium that carried the Bubonic Plague or "Black Death" that caused nearly 25 million deaths all over Europe in the 14th century [2]; *(ii) Mycobacterium tuberculosis*, responsible for tuberculosis, which still caused 1.2 million deaths worldwide in 2019 [3]; *(iii)* furthermore, post-operative infections due to antibiotic-resistant *Staphylococcus aureus* and *Pseudomonas aeruginosa* are among the most frequent causes of deaths related to after-surgery complications [4]. Fig. 6.1 shows a summary of the most common human pathologies together with the most notable bacteria species involved.

Even though bacteria have been identified only in the past centuries, the antibacterial properties of some materials are known since ancient times. One of these is copper, which was used by ancient Egyptians, Greeks, and Aztecs for wound sterilisation and water disinfection [4]. This is an efficient method of fighting bacteria colonisation,

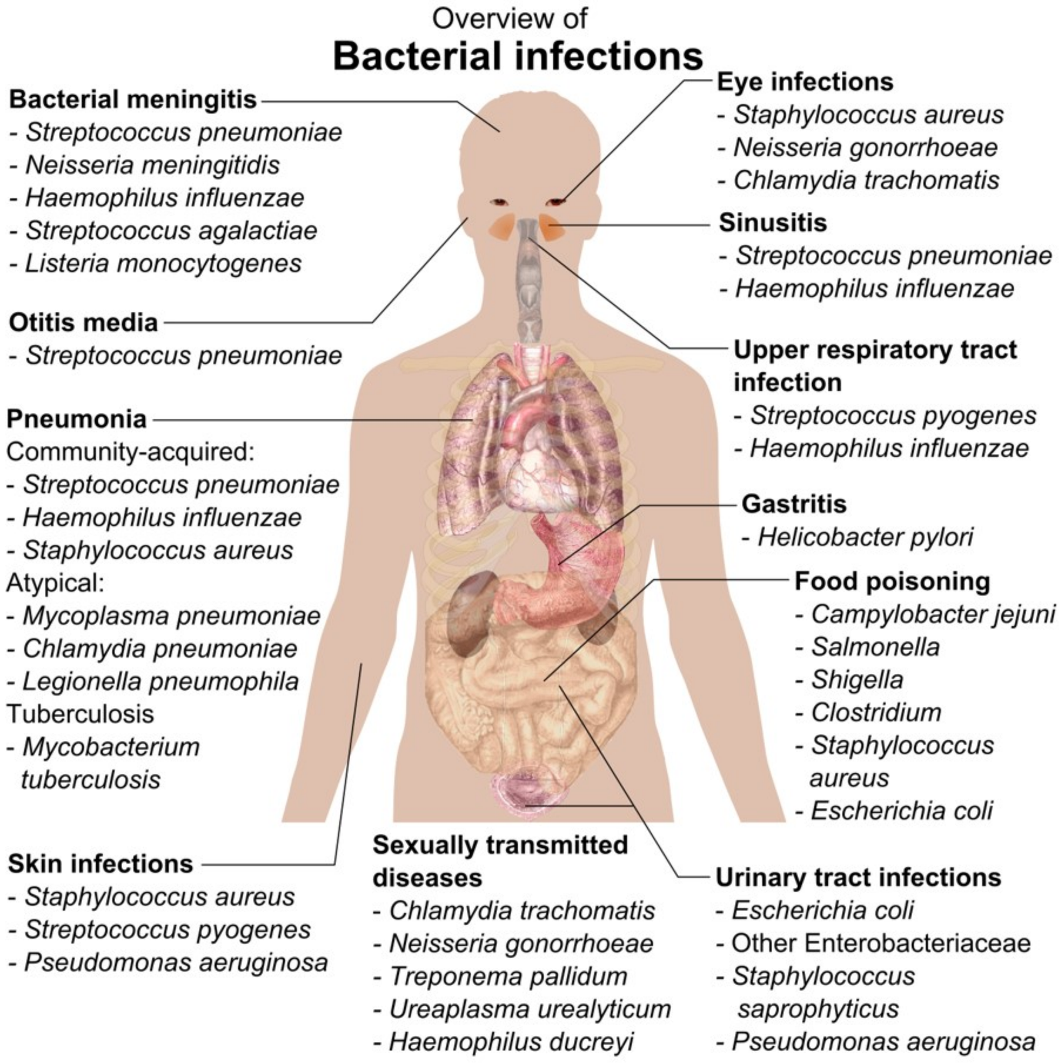

Fig. 6.1. Diagram showing some of the most common human infections associated with specific bacteria [author Mikael Häggström]. Image available in the public domain.

although it may introduce other hazards: it has been demonstrated how chronic exposure to excess copper may be toxic for several metabolic processes [5].

The adaptability of bacteria to specific conditions is one of the most challenging aspects to deal with. Bacteria have a high tendency to acquire new genetic material, and, since they double their population in a short time, they possess a strong capability to develop new mutations and survive even in harsh environments. During the 20th century, several studies led to the discovery of different kinds of antibiotics, i.e. natural and synthetic molecules able to inhibit the growth of bacteria. Sir Alexander Fleming was a Scottish microbiologist, awarded in 1945 with the Nobel Prize in Physiology or Medicine, together with Howard Florey and Ernst Chain, for what is described as the “single greatest victory ever achieved over disease”: the discovery of penicillin [6]. Yet, it was already during his Nobel Lecture that the Scottish scientist himself warned about the possibility of the development of antibiotic-resistant bacteria [7]. Nowadays, this phenomenon has become even stronger, due to the exposure to a constant small dose of therapeutics caused by the massive employment of antibiotics in agriculture, farming, aquaculture, etc. [7].

In the human body, upon administration to the patient of the standard antibiotic therapy, any bacterium that may survive will then flourish in the presence of a lower number of competitors, carrying on the genetic antibiotic resistance and potentially being very dangerous for the patient health.

Bacteria tend to grow and proliferate on the surface of specific materials. In many fields, like e.g. water storage, clothing, paint, and, above all, biomedicine, the colonisation of surfaces by bacteria is often undesired. In the medical field, the presence of bacteria on the surface either of a biomedical device or on gloves, cloths, or tools for medical care may introduce a serious risk of nosocomial infections [8]. Different types of pathogenic microorganisms may be involved, and hospitalised patients may be exposed to a high risk of several kinds of infections, especially in those hospitals where hygienic conditions are not constantly monitored. Pneumonia, lower respiratory tract infection, urinary tract infection, and bloodstream infection are the most common intensive care unit-acquired infections [9]. Comprehensive studies on this field are not so recent and comparative data describe a situation that was already understood in the 1990s. According to different works, it is possible to note that between 5 and 17% of patients admitted to hospitals in Europe and North America have developed some sort of nosocomial infection [9], [10]. This value may rise in the case of patients treated in intensive care units up to more than 20%. Furthermore, more than 40% of patients among all hospitalisations in Asia, Latin America, and sub-Saharan Africa reported bacteria-related infections [11]. Some authors estimated that the annual economic burden of nosocomial infections in the USA corresponded to $4.5 billion in 1992 [10].

Bacteria on the surface of biocompatible materials may form a biofilm. According to IUPAC, a biofilm is “an aggregate of microorganisms in which cells embedded within a self-produced matrix of extracellular polymeric substances (EPSs) adhere to each other and/or to the surface”. This hydrated matrix of polysaccharides and proteins may sustain the formation of a bacteria community [12], in which bacteria proliferation is enhanced. It has been demonstrated that the antibiotic resistance of bacteria within the biofilm may increase compared to planktonic bacteria [13]. The main steps in the formation of a biofilm on the surface of a biocompatible material are sketched in Fig. 6.2. Initially, a few bacteria adhere to the surface. Then, the formation of a biofilm supports bacteria proliferation and separates bacteria from the substrate material and the environment. When the biofilm is fully stable, it may also favour the migration of a few bacteria to another surface.

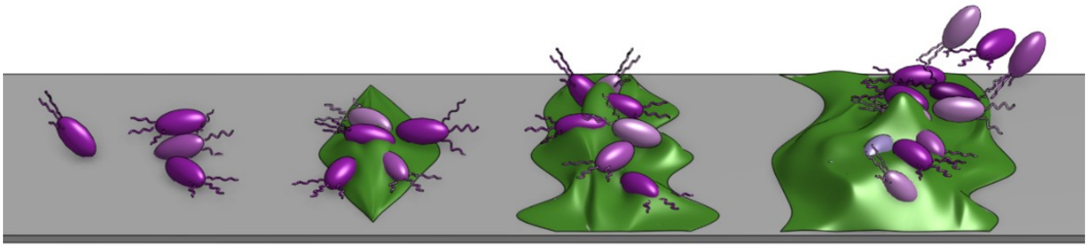

Fig. 6.2. Sequential steps in the formation of a biofilm on the surface of a biocompatible material. From left to right: the adhesion of bacteria, the initial proliferation, the formation of a protective biofilm that enhances bacteria proliferation, the consolidation of the biofilm, and the detachment of a portion of biofilm with living bacteria.

Several strategies have been proposed to minimise the presence of bacteria, the main of which is the sterilisation of the surfaces with specific solvents or with a combination of UV irradiation and heat. However, sterilisation may be difficult in some cases, and it is a time and energy-consuming operation. For this reason, different solutions have been proposed, in the recent past, to design and manufacture materials with antibacterial properties. The surface of these materials may be not suitable for bacteria proliferation (*bacteriostatic*) or not appropriate for the formation of the biofilm (*antibiofouling*). Finally, a material may be effectively harmful to the surrounding bacteria, in which case it is termed *bactericidal* [4]. Depending on specific conditions such as the target bacteria, and the external environment, these properties can also be combined.

Considering the variety of the different fields of applications (biomedicine, agriculture, paints, clothing, etc.) a complete review of all the techniques employed to fight bacteria is beyond the scope of the present work. However, it is important to mention the existence of different approaches and to understand the possibilities of the addition of antibacterial properties to different types of materials.

After studying the behaviour of the bioresorbable phosphate glass for extrusion and fibre drawing, we wanted to experiment with the addition of new characteristics to this glass composition. Thus, we synthesised a set of bioresorbable phosphate glasses doped with different antibacterial ions. These glasses could be able to gradually release therapeutic ions while dissolving. We can think of many possible applications of these glasses either as bulk optical materials, as fibres, or even as coatings. The glasses have been produced in different shapes and characterised in terms of both thermal and optical properties, as well as ion-release kinetics. The effect of the glasses has been tested in vitro on different bacterial cultures and mammalian cells. The microbiological tests have been performed in collaboration with several institutions, all based in Pavia, under the supervision of prof. Livia Visai. Preliminary but promising results of these tests are reported in the last section of the present chapter.

In the following paragraphs, we will concentrate our attention on the biomedical field, briefly mentioning some of the most interesting papers on biomedical antibacterial particles and materials. Then, we will focus on antibacterial glasses with special attention dedicated to antibacterial phosphate glasses.

6.2 Antibacterial glasses and their applications in biomedicine

6.2.1 Biomaterials and biomedical glasses

Biomaterials are widely used as implants exploiting various functions. The implant operation is an immunosuppressive procedure and, usually, preventive antibiotic therapy is administered before and/or after surgery. However, due to antibiotic resistance, the proliferation of bacteria and the consequent development of the infective disease may not be always avoided. This explains the growing interest in scientific and medical research regarding the design of a material capable of exerting an antibacterial action.

Among the most used biomaterials, titanium and its alloys are widely employed for orthopaedic protheses. Different researches have been conducted adopting three main approaches to avoid bacteria proliferation on the surface of Ti implants: *(i)* doping the surface or even the bulk material with antibacterial inorganic elements such as Cu; *(ii)* growing a surface layer of TiO_2 upon the metal surface and doping this oxide layer with antibacterial agents; *(iii)* applying a coating made of TiO_2, hydroxyapatite, or other bioactive material and doping this thin film with antibacterial ions or molecules [14]. Finally, a fourth option was proposed, which consist of engineering a hydrophobic surface with nanostructured pillars through chemical etching or plasma sputtering. These pillars may be sharp enough to physically damage the wall of the cells of the bacteria, thus implementing a so-called mechanobactericidal effect [4]. This latter concept is inspired by nature: cicada wings show a natural antibacterial surface that is made of nanostructured pillars, which can penetrate and disrupt the microbial cells adhered to the surface [15].

In recent times, growing interest is emerging in the usage of nanoparticles to exploit antibacterial functions. In particular, copper and copper oxide nanoparticles have been proposed [16]–[20] as well as several types of nanosilver compounds [21]. Various studies have also been conducted on the effects of Au-based, Mg-based, ZnO, Fe_3O_4, or YF nanoparticles as well as nanodiamond and different organic compounds such as liposomal nanoparticles, and polymer micelles, mainly used as antibiotic nanocarrier [22]. All these nanoparticles are employed for coatings, wound dressing, bone cement, and dental materials [22]. SnO_2 nanoparticles have also been synthesised either with solvothermal or ultra-sonochemical methods and their antimicrobial properties have been demonstrated [23], [24]. A strong antibacterial effect was obtained against the Gram-negative *Escherichia Coli*, but also antifungal properties (against *Candida Albicans*) and cytotoxicity with tumoral cells were reported [24].

Among biomaterials, biocompatible or bioactive glasses and glass-ceramics have a primary role. Biomedical glasses may be classified at a first glance using the main forming oxide, i.e. either SiO_2, B_2O_3, or P_2O_5 [25]; moreover, considering the production method, it is possible to distinguish high-temperature techniques, like melt-quenching and peroxidation [25]–[28] from lower-temperature syntheses like room-temperature precipitation in aqueous solution and sol-gel [25], [29]–[33]; finally, antibacterial glasses may be distinguished concerning the type of antibacterial action exploited: *(i)* the incorporation of antibacterial ions and/or molecules/drugs in the composition of bulk material or on the surface layer, *(ii)* the creation of particular micro-/nanostructured surface features designed to physically harm bacterial cells, or *(iii)* the creation of a bactericidal or antibiofouling layer on the surface of the biomaterial with an ion-exchange technique [34].

One of the most common biomedical glasses is the 45S5 Bioglass®. A lot of studies (2449 papers by the end of 2020 according to the *Web of Science* online database[11]) have been published regarding this silicate glass, and its clinical use either for dental, bone, or soft tissues reconstruction is widespread since 1985 [35]. The antibacterial properties of Bioglass® itself have been reported in vitro and are attributed to the change in pH (acidification) caused by the dissolution of the glass in aqueous media [36]. Furthermore, bacteria adhesion on the glass particles is also considered beneficial, since the cell walls of bacteria are damaged by contact with the glass debris [36]. Besides, the mechanism of action in vivo may be different and this was still a matter of debate in the last years [37]–[39].

The action of antibacterial glasses may be much more direct in the case of glasses specifically designed to avoid biofilm formation or to kill bacteria. These glasses are widely employed either as bulk materials or as bioactive coatings. When dealing with bioactive or bioresorbable oxide glasses, antibacterial ions may be simply added to the glass composition. Also, ion exchange in molten salts as well as in aqueous solution has been demonstrated. The usage of this technique has been reported with a bioactive glass composed of SiO_2-CaO-Na_2O, where Na^+ ions are exchanged with Ag^+ ions. The interesting aspect of this method is that it allows creating an antibacterial non-cytotoxic layer by using a small number of antibacterial ions [34].

---

[11] https://www.webofknowledge.com

Furthermore, bioactive glass nanoparticles are used in combination with Ag^+, Sr^{2+}, Cu^{2+}, Ce^{2+}, Zn^{2+}, and various organic naturally occurring substances [25]. These materials are designed for different soft tissue, orthopaedic, and dental applications, including tissue engineering and regenerative medicine. The cited ions are effective against *Escherichia coli*, *Pseudomonas aeruginosa*, *Saprospira grandis*, *Streptococcus aureus*, and *Streptococcus faecalis* [25]. Despite all the concern on the development of antibiotic resistance of bacteria, some studies also explore the possibility of using drugs in combination with antibacterial ions. Glass scaffolds for xbone regeneration can be loaded with drugs such as antibiotics. The synergistic effect of doping calcium-phosphate-silicate bioactive glass with ZnO and loading a scaffold made of this glass with different antibiotics has been recently reported [40].

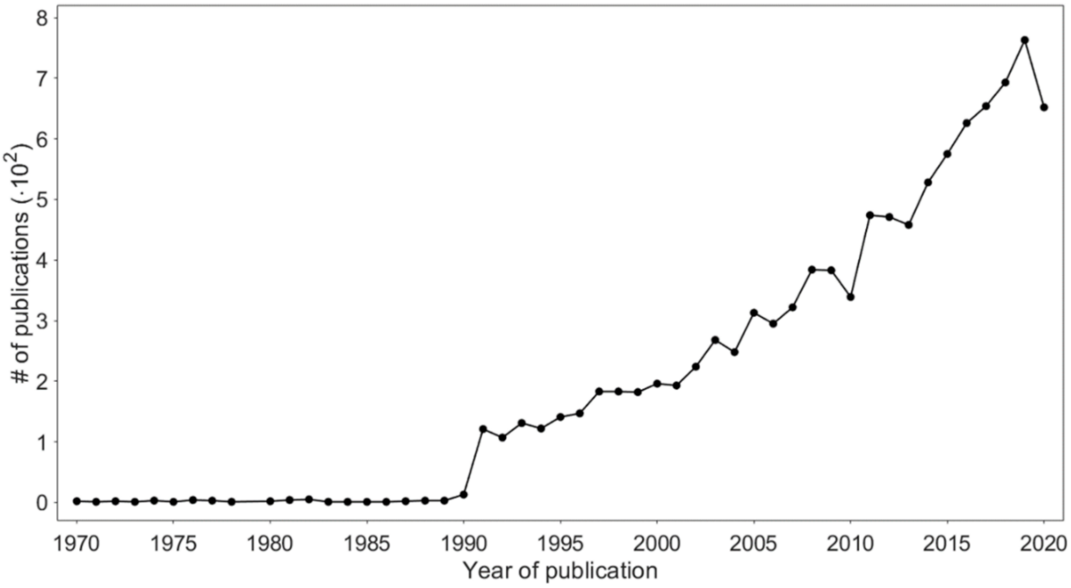

Fig. 6.3. A plot of the number of publications during the last fifty years related to *antibacterial glasses*. Data are taken from the *Web of Science* online database.

Bellantone et al. [41] discuss the bioactivity and bacteriostatic properties of a silver-doped calcium-phosphate-silicate glass produced following a sol-gel route. Due to the high surface area of sol-gel derived glass, compared to the standard melt-quenched bulk glass, the bioactivity of the former is increased. The addition of silver does not affect the bioactivity of the glasses but produces a marked bacteriostatic action against *Escherichia coli* [41]. Some recent works on the effect of the addition of MgO [32] or ZrO_2 [33] in place of CaO to a standard 58S bioactive glass or a Cu-doped 58S bioactive glass suggest the beneficial effect of these compositions in fighting methicillin-resistant *Staphylococcus aureus*. These glasses were synthesised via a sol-gel technique and their biocompatibility with an osteoblast-like cell line is also demonstrated [32], [33].

This brief overview of some aspects of bioactive glasses with antibacterial properties allows understanding the extent of this research sector. Fig. 6.3 shows the trend in publications regarding the topic of antibacterial glass, according to the *Web of Science* online database. In the last four years, more than 2500 papers have been published on this topic. The slope of the curve also highlights the growing interest of the scientific community in the research on the antibacterial behaviour of glasses. In the next paragraphs, we will concentrate on a specific subset of bioactive glasses, i.e. phosphate glasses, which are the main subject of the present work and can be engineered to offer antibacterial properties.

6.2.2 Phosphate glasses

The main network former of phosphate glasses, i.e. phosphorus ion, is also one of the main nutrients that bacteria need to proliferate. Indeed, the use of phosphate glass particles in feeding bacteria culture has been demonstrated [42]. Yet, due to the unique property of bioresorbable glasses that can easily carry and dissolve antibacterial ions, phosphate glasses have been widely employed for antibacterial applications for many years

The employment of phosphate glasses has been proposed for fighting the infections of the urinary tract, by using a Na-Ca-P glass doped with Ag^+ for the realisation of catheters [43]. The antibacterial properties of Ag^+ are often exploited with phosphate glasses [44]–[51]. In detail, Mulligan et al. [44] describe the formation of a biofilm on the surface of Na_2O-CaO-P_2O_5 glasses doped with different concentrations of Ag_2O, pointing out how, upon immersion in artificial saliva, the formed biofilm hinders the dissolution of therapeutic ions. Thus, the bacteria viability of *Streptococcus sanguinis* decreases in the first hours after exposure with the glass samples and then starts to increase again. After a few hours, the dead bacteria form a compact layer on the surface of the glass, through which the silver ions cannot diffuse. Furthermore, a similar composition with a high amount of silver (up to 20 mol%) was studied by Valappil et al. [46], reaching comparable results. The same behaviour was demonstrated also with other antibacterial ions, like copper [52]. Other studies, conducted with similar glasses but with a lower amount of Ag^+ ions and with different culture medium, demonstrate the effective antibacterial action of silver against a Gram-positive bacterium (*Staphylococcus aureus*), a Gram-negative bacterium (*Escherichia coli*), and a pathogenic yeast (*Candida albicans*) [45]. The composition with 3 mol% of Ag_2O gave an excellent long-term release of silver ions that fostered a powerful antibacterial effect against the tested organisms. Another work from the same research group was aimed at investigating the effect of a lower concentration of silver on different bacteria species [47]. Furthermore, the pH variation upon glass dissolution causes some inhibition in the growth of bacteria even in the absence of silver. Tests were conducted with different bacteria (*Staphylococcus aureus*, *Pseudomonas aeruginosa*, and *Escherichia coli*) and with different concentrations of Ag^+ ions (from silver-free up to 2 mol% of Ag_2O), and all the samples showed a marked inhibition zone. A paper by Mishra et al. [48] describes the effect of silver on the structural and optical properties as well as the dissolution rates for a strontium-containing Na-Ca-P glass. In terms of optical absorbance, the presence of Ag^+ causes a shift in the UV-edge towards higher wavelengths. In other words, the transparency of the glass in the UV region is reduced in the presence of silver. Similar behaviour was also denoted for Ag-doped Zn-Na-P glasses with molar compositions in the range 42% P_2O_5 – 42% ZnO – (16-x)% Na_2O, where $x = 0 – 1.6$ mol% is the amount of Ag_2O [49]. As in the previous case, the shift in the cut-off wavelength was correlated with the amount of silver.

Invert glasses with molar compositions 60% CaO – 30% P_2O_5 – (10-x)% Nb_2O_5 – x Ag_2O, with $x = 0 – 5$ mol%, were also studied by Lee et al. [50]. These glasses, intended for bone tissue regeneration, showed good cytocompatibility with primary osteoblast cells isolated from newborn mouse calvariae, regardless of the amount of silver. Finally, recent work has been published on the performances of a glass with molar composition 20% ZnO – 10% Li_2O – 10% Na_2O – 60% P_2O_5, doped both with 0.5 mol% of Dy_2O_3 and with 0 – 5 mol% of Ag_2O [51]. These glasses have potential applications in tissue regeneration, where the presence of luminescent Dy^{3+} ions can allow using them as phosphors [51]. Antibacterial tests were conducted against *Escherichia coli*, *Staphylococcus aureus*, and *Listeria monocytogenes*, while antifungal tests were performed with the yeasts *Candida albicans* and *Cryptococcus neoformans*. The results show how Ag^+ ions can be effective in the prevention of the growth of pathogenic microorganisms, but the heavily-doped specimens showed traces of agglomeration of Ag^+ nanoparticles that resulted in reduced transparency [51].

Another ion, well-studied for its antibacterial properties, is copper. In one study, the effect of an increasing amount of Cu^{2+} added to different Na-Ca-P glass compositions is investigated [52]. In this paper, the authors demonstrate how for high-copper content (10 – 15 mol%), the antibacterial effect against *Streptococcus sanguinis* is negligible, except for a small decrease in bacteria viability visible within the first 24 h of contact with the glass, followed by a complete recovery. This reduced effect is due to the formation of a biofilm on the surface already described for silver. In other tests, Abou Neel et al. [53] demonstrated the efficacy of glasses with molar composition 50% P_2O_5 – 30% CaO – (20-x)% Na_2O – x CuO, in fighting the growth of *Staphylococcus epidermidis*. The authors claim that the most effective composition is the one containing a 10 mol% of CuO, testing the glass in fibre form. The declared aim of the work is to employ such glasses in wound healing applications. However, the authors only performed the count of colony-forming units (CFU) over a period of 20 h. Longer test periods may be needed to exclude the possibility of recovery described by Mulligan et al. [52]. A similar glass family has been also studied to detect the oxidation state and the coordination environment of copper ions in the phosphate glass network [54]. The authors proposed that the antibacterial effect was mainly related to the amount of copper rather than to differences in the structural environment. Copper ions are coordinated within the phosphate glass network without any sign of phase separation and being mainly in the form of Cu^{2+}, regardless of the type of oxide employed, i.e. copper(II) oxide (cupric oxide, with chemical formula CuO) or copper(I) oxide (cuprous oxide, with chemical formula Cu_2O) [54].

All the above-mentioned Cu-doped glasses are obtained with the conventional melt-quenching technique, using glass precursors in the form of high-purity oxides, carbonates, or sulphates. In recent years, Foroutan et al. [31] produced Cu-doped calcium-phosphate glasses using a technique based on room temperature precipitation reaction in aqueous solution. This method allows avoiding both the high-temperature melting and the use of organic solvent required for the sol-gel technique. The glass is designed to be used in bone-tissue regeneration applications, thus both antibacterial tests with *Staphylococcus aureus* and cytocompatibility tests with osteosarcoma cells are conducted. Both tests revealed the good performances of the glass. The previously reported reduction in the antibacterial effect due to biofilm formation is here neglected since the tests are conducted using glass powder. Nevertheless, the proposed glasses are considered as a promising candidate for bone-tissue regeneration applications, since a marked contraction in the number of CFU/ml of bacteria is reported especially for glasses with 6 mol% Cu^{2+}, and osteoblast-like cell viability increased during the 5-days lasting experiments.

Jiménez & Sendova [55] described the behaviour of a nanodiamond (ND)-doped barium-phosphate glass. In some samples, also a small percentage (0.5 mol%) of CuO was added. The authors did not perform any biological test, but they studied the optical behaviour as well as the structural characteristic of the glasses. The results showed how the simultaneous presence of CuO and ND fostered the complete reduction of copper in the glass matrix to metallic Cu^0, enhancing the optical transparency of the glass and promoting the plasmonic transformation to Cu-nanocomposites [55].

In recent years, also other antibacterial ions have been added to phosphate glasses and tested against different pathogenic organisms. For example, Babu et al. [56] developed a set of glasses with molar compositions 8% ZnO – 22% Na_2O – (24-x)% CaO – 46% P_2O_5 – x TiO_2 (with x = 0.2 – 1 mol%). These glasses showed enhanced cytocompatibility with rat mesenchymal stem cells without any sign of toxicity. The glasses also stimulated the formation of a rich crystalline hydroxyapatite layer upon immersion in Simulated Body Fluid (SBF). Furthermore, the antimicrobial tests performed with *Escherichia coli* showed a reduced number of bacteria after exposure with the glasses, suggesting that the combined effect of ZnO and an optimum value of 0.6 mol% of TiO_2 may be effective in fighting this microorganism [56]. In another work by Raja et al. [57], the effect of the addition of a different amount of CoO to the molar composition 50% P_2O_5 – 20% Na_2O – (30-x)% CaO – x CoO is studied. The glass powders showed good cytocompatibility with both human monocytic and osteosarcoma cell lines. Also, angiogenesis assays were conducted using human umbilical vein endothelial cells. The results demonstrated how these glasses may have significant potential for angiogenic applications. Furthermore, antimicrobial tests were performed with *Escherichia coli*, *Staphylococcus aureus*, and *Candida albicans*. The experiments revealed good performances when the bacterial cultures were placed in direct contact with the glass samples: an increasing antibacterial activity was visible against all the microorganisms, with an enhanced effect for the specimens with high-cobalt content. Furthermore, the paper also reports the effect of the dissolution products of the glass with an indirect antibacterial assay. In this latter case, no significative antimicrobial effect was visible for any of the tested pathogens. The authors remark that the dissolution rate of all the ions is decreased with an increasing amount of cobalt, thus the number of dissolved ions is not proportional to the mol% of CoO present in the glass. The authors suggested that the difference between direct-contact and indirect experiments may be explained with the mechanism of antibacterial action [57]. When the bacteria get into contact with the glass surface, their outer membrane may easily break, while, in the case of indirect contact assays, the ions present in the solution may enter the cells via non-specific ion channels. In the latter case, the metal ions may then affect the metabolism of the cells in secondary ways, eventually leading them to death. The nutrient broth may also provide a complex environment in which the presence of free metal ions may be reduced because of precipitation or the formation of soluble complexes. Finally, two different papers appeared in the last two years by Łapa et al. [28], [58], investigating the behaviour of glasses composed of P_2O_5-MgO-Na_2O-CaO doped with different amount of CeO_2 and/or Ga_2O_3. The authors tested the glasses both in bulk and fibre forms and demonstrated the possible application for wound healing by showing the wound closure in vitro of mice embryonic fibroblast cells in the presence of Ce-doped glass fibres [58]. The glasses also showed good cytocompatibility with human epidermal keratinocytes [58]. Furthermore, antimicrobial tests were conducted with different samples against both *Escherichia coli* and *Staphylococcus carnosus* showing effective antibacterial action, for Ce-doped, Ga-doped, and co-doped glasses containing both Ce and Ga [28]. The samples with the highest gallium content proved to be toxic for mice bone marrow stromal cells [28]. On the contrary, all the glasses containing cerium proved to be non-toxic for the tested cells, improving at the same time the cell viability. The proposed co-doped samples also showed promising results against bacteria without being harmful for mammalian cells [28]. In conclusion, an interesting review, also written by Łapa et al., was published in 2020, containing a thorough description of degradable phosphate glasses [59]. The review analyses the different production techniques for phosphate glasses and for phosphate glass fibres, providing also a focus on the effects of doping phosphate glasses with different ions for specific biomedical applications [59].

A wide range of application has been reported so far, examining different aspects of the production of antibacterial phosphate glasses. The cited papers represent only a selection of the available literature on the topic, but they allow understanding some of the choices that we made during the preparation of our own ion-doped phosphate glass compositions, which is described in the next paragraphs.

6.3 Ion-doped bioresorbable glasses with antibacterial properties

Doping a phosphate glass with ions featuring antibacterial activity enables the production of bioresorbable glasses with antibacterial properties. The main process is analogous to the one described in Chapter 4 for light amplification when we added active ions to the phosphate glass composition. Yet, in the present case, the doped glass is intended to be used as the external layer, or the coating of a bioresorbable fibre, to prevent biofilm formation.

As several cited works demonstrate [44], [46], [52], the formation of a biofilm on the surface of phosphate glass may hinder the glass from further dissolution into the aqueous medium. A bioresorbable glass that does not fully dissolve after the formation of the biofilm presents chemical and technological limitations. Bioresorbable devices are designed to be completely soluble inside the body. Yet, if the biofilm formation blocks the glass dissolution, the whole functionality of the device is compromised. Also, bioresorbable devices capable of releasing antibacterial ions may be effective against antibiotic-resistant bacteria.

For these reasons, the idea of adding a few antibacterial ions to the bioresorbable glass composition already studied seems to offer great potential in different situations. The number of antibacterial ions must be small since a huge amount would substantially affect the thermo-mechanical and optical properties of the glass, as well as its dissolution rate. Indeed, in several works [44], [52] it is reported how above a certain amount the antibacterial ions become useless and their presence may even alter the dissolution properties of the glass and/or be toxic for the surrounding tissues [28]. Yet, the antibacterial effect of these ions must be powerful, to produce the desired results.

To investigate all these aspects, we fabricated different glasses doped with different ions and we performed preliminary tests on the obtained compositions.

Starting from a bioresorbable phosphate glass composition belonging to the same family as the one described in Chapter 5, we added several ions to study the antibacterial behaviour. We decided to pick a slightly different glass as the base composition: we reduced the amount of MgO and added the same quantity of CaO compared to the glass employed for microstructured bioresorbable fibre. This variation in the composition leads to an increase in the glass refractive index and dissolution rate, as well as the temperature working window [60]. Thus, the starting molar composition of the bioresorbable glass employed for antibacterial tests is 50% P_2O_5 – 8% MgO – 11.5% Na_2O – 25% CaO – 3% SiO_2 – 2.5% B_2O_3. Perhaps the most important aspect of this composition is that, according to Ceci-Ginistrelli et al. [60], the glass crystallisation temperature is increased, i.e. the glass is more stable. This is a good condition to perform the addition of new components, that may alter the crystallisation kinetics. Moreover, the content of MgO may be still reduced to obtain a higher-refractive index composition. This means that our starting glass may be used as cladding or coating for optical fibres, by coupling it with a core glass, i.e. a glass with lower MgO content. This latter aspect is important since we aim at testing the glass for extrusion, i.e. for the production of tubes usually employed as claddings or coatings.

For the addition of antibacterial properties, we chose five antibacterial ions, i.e. Ce^{4+}, Cu^{2+}, Ga^{3+}, Sn^{4+}, Zn^{2+}. We analysed the variation of the bioresorbable phosphate glass properties after the addition of 1 mol% of antibacterial oxides, respectively CeO_2, CuO, Ga_2O_3, SnO_2, and ZnO. We scaled the amount of the reagents in the starting glass composition to accommodate for the presence of the additional 1 mol% of the different dopants. In this way, the actual proportion between the reagents does not vary.

As will be illustrated in the next paragraphs, the thermal properties of the glasses are not so sensitive to this amount of doping agent, but the optical properties showed to be affected especially by some of these metal ions, that present specific absorption bands. Exploratory antimicrobial tests are conducted with different pathogenic organisms. Preliminary results of these measurements are presented in the following sections.

6.3.1 Antibacterial phosphate glass preparation

Antibacterial glasses have been prepared using the conventional melt-quenching technique starting from high-purity oxides and carbonates powders. The reagents were weighed and mixed in a controlled atmosphere to minimise the presence of impurities and reduce the content of OH^- groups in the glass. The powders were also mixed overnight using an automatic mixing machine, to ensure the proper homogeneity of the reagents. The powder mixture was then poured into a silica crucible and melted at 1200 °C under a N_2 flux.

Fig. 6.4. Different samples of bioresorbable phosphate glasses doped with antibacterial ions. On the left, from the top to the bottom, the polished slab containing CuO and the unpolished slabs containing Ce_2O, Ga_2O_3, Sn_2O and ZnO, respectively. On the right, the rods made with Cu-doped and undoped glasses. The different degree of transparency of the rods is related to the incidental contamination of one glass batch, that was not employed for subsequent tests.

The molar composition of the antibacterial glasses is 49.5% P_2O_5 – 7.92% MgO – 11.38% Na_2O – 24.75% CaO – 2.97% SiO_2 – 2.48% B_2O_3 – 1 % x, where x is either CeO_2, CuO, Ga_2O_3, SnO_2, or ZnO. The glass samples have been prepared in different shapes, i.e. rods and slabs, to perform both the material characterisation and the antibacterial tests. Some of the obtained glasses are shown in Fig. 6.4.

6.3.2 Bulk glass characterisation: the effect of antibacterial ions

The base material has been characterised through conventional thermal analysis: DTA has been performed on bulk annealed glass samples, to determine the glass transition temperature and the eventual onset of crystallisation. The second quantity was not detectable on the tested samples, since the crystallisation phenomenon was probably not completed at the maximum testing temperature. Contact profilometry was also conducted on both polished and unpolished samples, to determine the roughness of the surfaces and correlate this quantity with the antibacterial properties of the glass. Furthermore, the glasses were also characterised in terms of optical properties such as the refractive index and the UV-vis absorption spectroscopy. The effect of the presence of different ions on the properties of the glass is briefly discussed in the following paragraphs.

Thermal properties

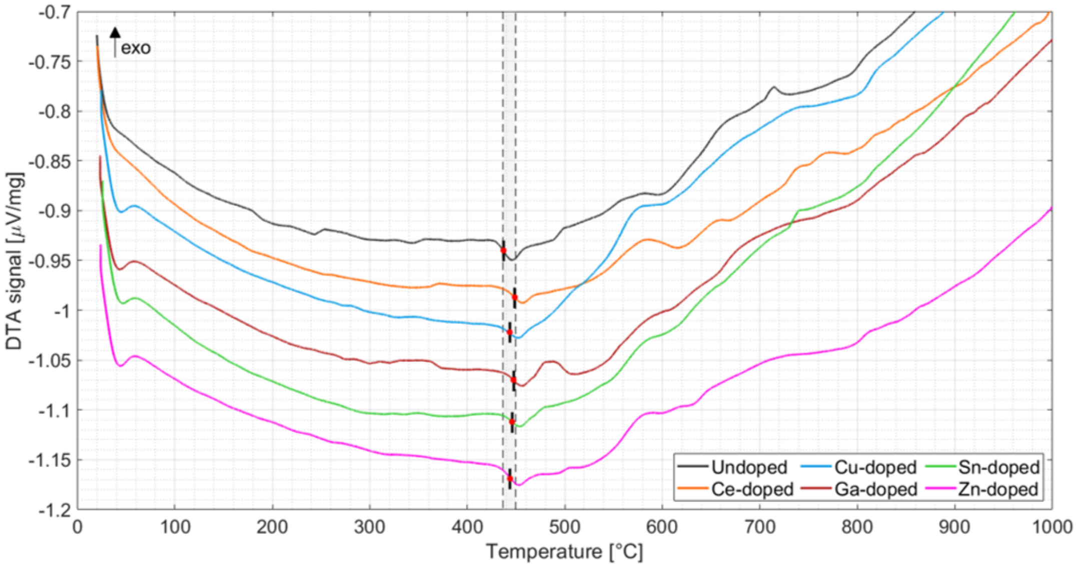

Fig. 6.5. DTA curves of antibacterial-doped bioresorbable phosphate glasses. The curves are shifted for visualisation purpose. The T_g of the different glasses are measured and are comprised between ± 10 °C as shown by the shaded area.

The DTA measurement allowed demonstrating the small influence of the antibacterial ions on the temperature behaviour of the glass. The T_g of the doped glasses has increased compared to the T_g of the undoped one. The maximum increment in the glass transition temperatures between the undoped and the doped glasses is kept within nearly 10 °C, as reported in Table 6.1. Furthermore, Fig. 6.5 shows the DTA curves of all the samples. The curves have been shifted to facilitate the comparison. The inflexion of the curve at the T_g was detected for all samples by looking at the null values of the second derivative of the curves.

Table 6.1. The glass transition temperatures T_g of the doped and undoped glasses.

Sample	**Ce**	**Cu**	**Ga**	**Sn**	**Zn**	**Undoped**
T_g [°C] ±1	449	443	447	446	444	437

Optical properties

Doping the glasses with antibacterial ions may also influence their optical properties. The effect of the addition of the different ions may be observed by analysing the UV-vis-NIR absorption coefficient and the refractive index of all the glasses. The measurements have been performed with the instruments described in Chapter 2. For both the measurements, flat samples, with dimensions 10x10x1 mm, were cut and polished from the glass slabs shown in Fig. 6.4.

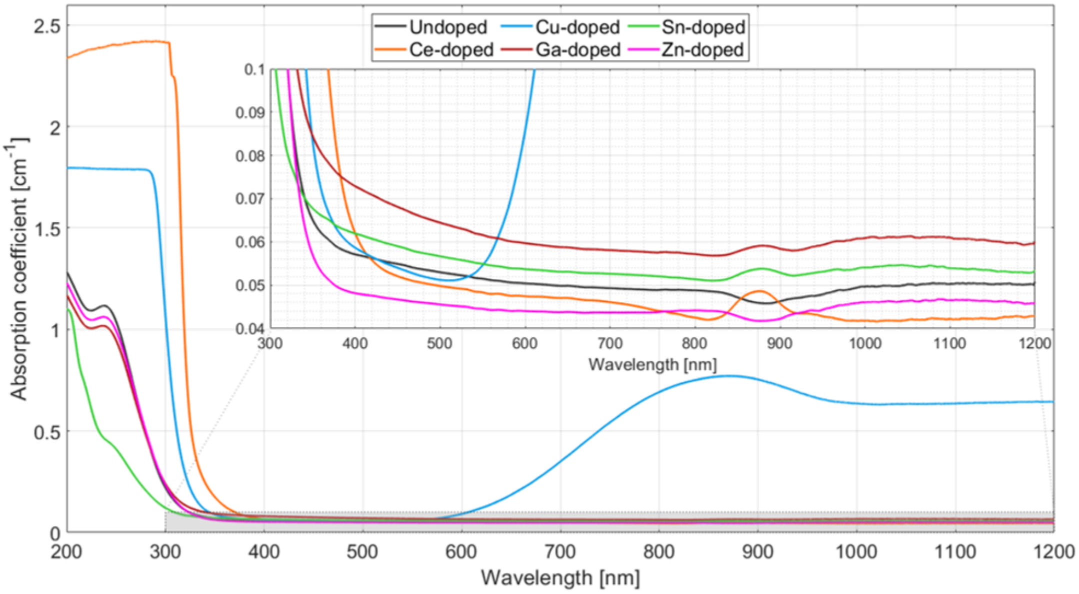

Fig. 6.6. The UV-vis-NIR absorption spectrum for the undoped bioresorbable glass and the glasses doped with antibacterial ions.

In Fig. 6.6, the UV-vis-NIR absorbance spectrum is reported for wavelengths in the range between 200 and 1200 nm. The calculation of the absorption coefficient is performed with the equation $\alpha = \frac{1}{d} \cdot \log(\frac{100}{T\%})$, where d is the specimen thinkness and $T\%$ is the transmittance, i.e. the per cent of transparency.

It is possible to observe the different areas of this plot. In the UV region, we can look at the cut-off wavelength, λ_{50}, i.e. the wavelength at which the glass transmittance drops below 50%. The λ_{50} values are reported in Table 6.2. The Ce-doped glass is the least transparent in the UV. On the contrary, the Sn-doped glass shows the lowest cut-off wavelength, followed by the undoped glass and by Ga- and Zn-doped samples all below 300 nm; the Cu- and the Ce-doped glasses have $\lambda_{50} > 300$ nm. In the NIR, the Cu-doped glass is the least transparent, since it shows a broad absorption peak centred at 870 nm. In the same wavelength region, the most transparent is the Ce-doped one, and the other glasses show similar values.

Table 6.2. The cut- off wavelengths, at which the glass transparency drops below 50%.

Sample	**Ce**	**Cu**	**Ga**	**Sn**	**Zn**	**Undoped**
λ_{50} [nm]	333.8	318.2	290.6	263.2	291.2	290.2

In the visible region, the Zn-doped glass is the most transparent, followed by the other glasses that have all values of transparency around 90% in the whole wavelength range. Except for the Cu-doped glass, which has only a deep penetration in the blue region, i.e. below 400 nm, but its transparency is reduced below 320 and above 610 nm. This explains the blue colouration of this latter glass.

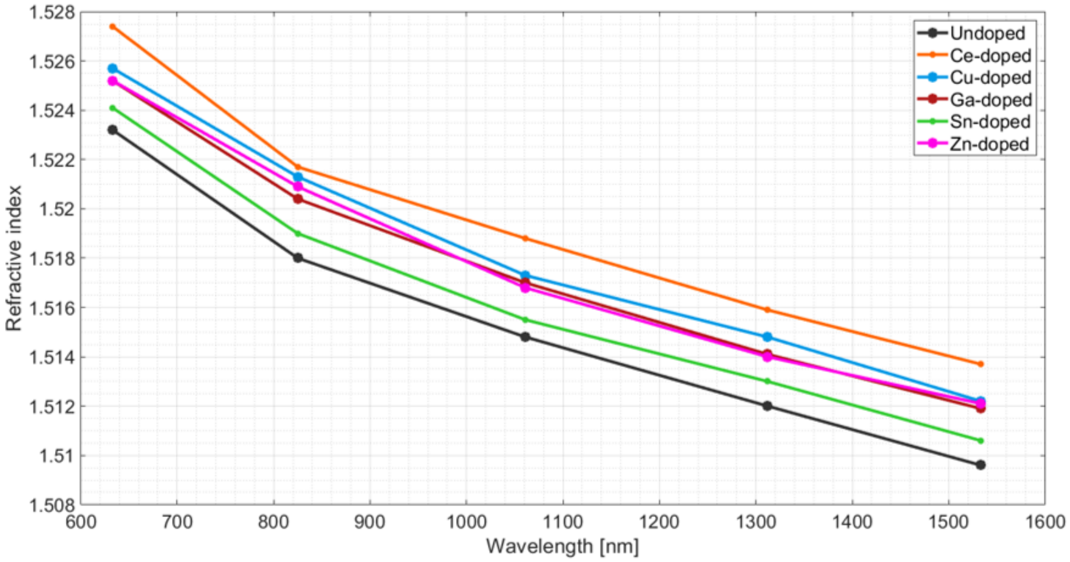

Fig. 6.7. The dependence of the refractive index on the incident wavelength in the presence of antibacterial ions doping.

Fig. 6.7 shows the influence of the different ions on the refractive index of the glasses. Overall, the addition of antibacterial metal ions seems to increase the refractive index of the glasses at all wavelengths. Cerium, a lanthanide, is the most influent on the refractive index. On the contrary, tin offers only a small increment to the refractive index at the tested wavelengths.

Ion release and surface properties

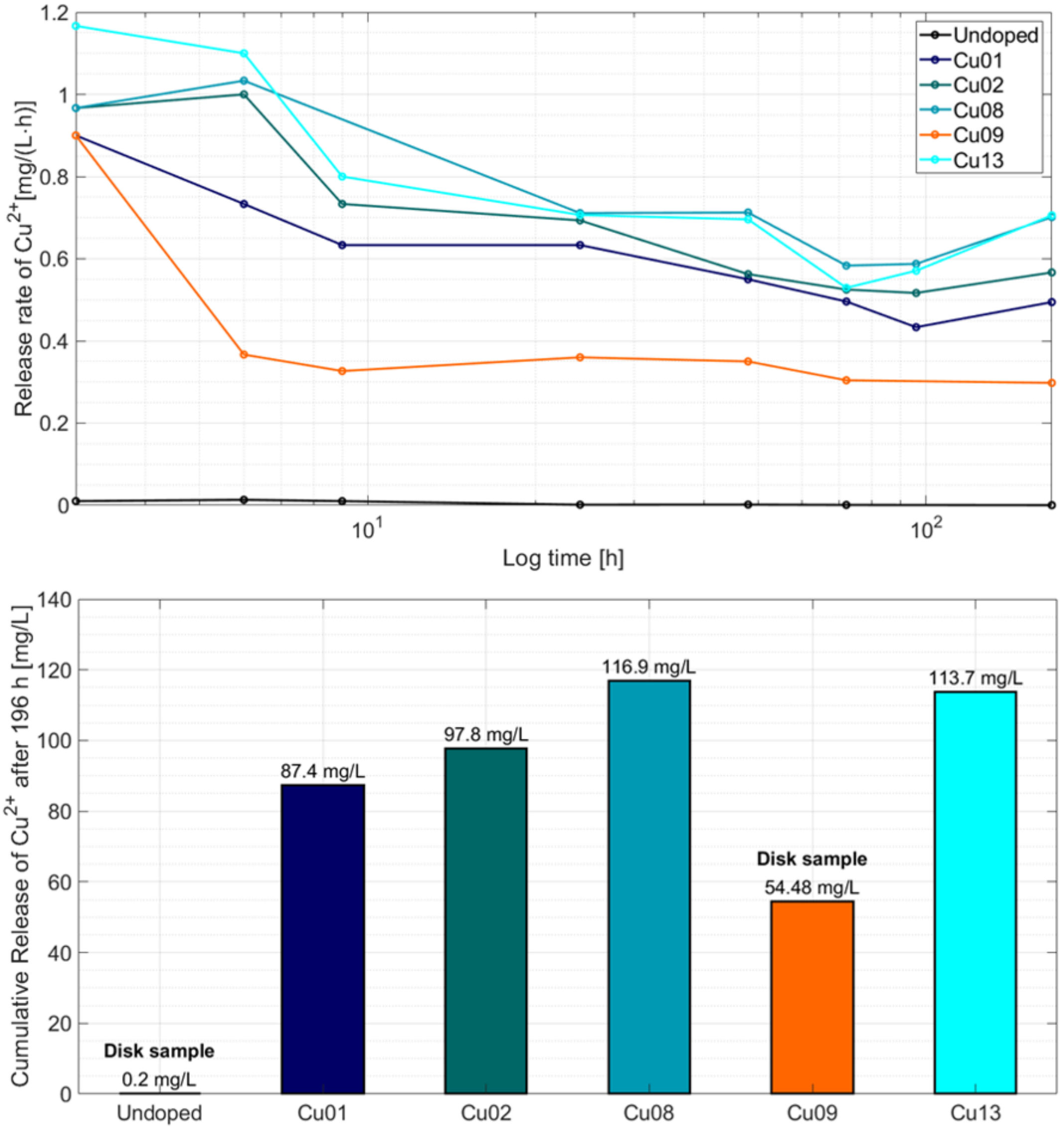

Fig. 6.8. Analysis of the release of Cu^{2+} ions with the data acquired with ICP-OES. The upper plot shows the release rate of Cu vs. logarithmic time. For all the doped samples, the release rate resulted to be higher in the first hours of dissolution. The lower bar graph represents the overall cumulative released Cu after 196 h for all the samples. The differences between the samples in these graphs are also related to the different shape and surface finishing of the samples. Details and normalised values are reported in Table 6.3.

The dissolution of the bioresorbable phosphate glass has been already studied. After the addition of the antibacterial ions, the dissolution kinetics may show small changes. Indeed, we do not aspect to see big differences in the dissolution time since the compositional variation is limited. The dissolution time is mainly related to the ratio Mg/Ca and to the shape and roughness of the samples. Tests could be performed with the glasses either in bulk or as fibres (or even in powder form), to analyse the kinetics of dissolution in different conditions. Furthermore, different dissolution media could also be tested, like water (MilliQ water or double-distilled water, ddH$_2$O), phosphate-buffered saline solution (PBS), or other biological fluids.

Before performing both these dissolution test campaign and the antimicrobial tests, which are the subject of the next paragraph, we wanted to know the effective amount of the specific antibacterial ion that is dissolved. We started with the study of the release rate of copper ions. Rather than investigating the overall weight reduction upon immersion, Inductively Coupled Plasma Optical Emission Spectroscopy (ICP-OES) was performed using an ICP-OES Optima 3300 DV Perkin Elmer instrument belonging to our collaborators in Pavia. The release of copper was evaluated in ddH2O water at 37 °C, in a static incubator with a 5% CO$_2$ atmosphere. In this way, the release in a simulated physiological condition is studied.

The release tests are carried out for several days and, at each time step, some water was withdrawn, and fresh sterile water was added to the sample. The results of the Cu^{2+} ions release over time is shown in Fig. 6.8 for different samples. The cumulative release after 196 h for the same samples is also reported with a bar graph in the same figure.

Table 6.3. The cumulative release of Cu^{2+} is normalised with the weight of Cu^{2+} present in each sample.

Sample name	**Undoped**	**Cu01**	**Cu02**	**Cu08**	**Cu09**	**Cu13**
Sample shape	Disk	Cube	Cube	Cube	Disk	Cube
Polishing	Not polished	Polished	Polished	Polished	Not polished	Polished
Weight [mg]	182.80	463.30	511.90	581.40	185.80	558.70
Cumulative Cu release after 196 h [mg/L]	0.20	87.40	97.80	116.90	54.48	113.70
Weight of Cu in each sample [mg] ± 0.02	0.00	2.98	3.30	3.74	1.20	3.60
Normalised release [(mg/L)/mg] ± 0.2	-	29.30	29.67	31.23	45.54	31.61

While evaluating the difference of released Cu among the samples we recall that both the weight and the shape of the samples are slightly different. We summarised all the details in Table 6.3. The measured amount of released Cu has also been normalised to the weight of Cu present in each sample. This latter value was evaluated by knowing the weight of the sample and the amount of CuO added to the glass batch, also considering the small weight loss (around 2%) that occurred during melting. It is possible to see that the lower amount of the cumulative released Cu after 196 h of sample Cu09, i.e. the orange one in Fig. 6.8, is related to the lower effective weight of Cu in the sample. However, considering the higher surface area of the disk-shaped sample and the absence of surface polishing, the normalised release value of sample Cu09 is higher than the others. Instead, all the polished cube-shaped samples, i.e. the ones reported in Fig. 6.8 with different blue colours, showed a similar normalised release value.

The roughness of the surface of the glass samples before and after polishing was measured with a contact profilometer. The unpolished samples showed a value of R_a ranging between 1.2 – 1.7 μm. After the polishing, the R_a dropped between 17.8 – 25.2 nm.

6.4 In vitro tests of fabricated glasses

The microbiological tests have been conducted in collaboration with different institutions: the Department of Molecular Medicine (DMM) and Centre for Health Technologies (CHT) of Università di Pavia, the Department of Occupational Medicine, Toxicology and Environmental Risks of Istituti Clinici Scientifici Maugeri, Pavia, and Scuola Universitaria Superiore IUSS, Pavia. Thanks to Prof. Livia Visai and all her collaborators involved in the conduction of the tests during the last years, we started to perform a deep investigation about the interaction between the bioresorbable phosphate glasses doped with antibacterial ions and several bacterial species. The tested samples were all prepared in our laboratories in Politecnico di Torino and subsequently sent to Pavia, where the microbiological tests were performed, within the different laboratories.

We performed two main kinds of tests, namely *direct* and *indirect* contact test. In the former, the bacterial culture is directly put into contact with the glass surface, while in the latter the bacteria culture is inoculated into a solution in which part of the glass was dissolved. The results of the two kinds of tests in terms of bacterial viability are different. We could foresee this behaviour since the two mechanisms of interaction of the bacteria either with the surface of the glass or with the metal ions dissolved in a solution are substantially different as explained by [57]. Further details about the performed tests will be presented in the following paragraphs.

We decided to start the evaluation of the antibacterial properties of our bioresorbable phosphate glasses with one of the most studied antibacterial ions, i.e. copper. The viability data presented result from the comparison between the effect of Cu-doped and undoped glasses with a tissue culture plate (TCP). Some of these data have been presented at the 11th World Biomaterial Congress in late 2020.

6.4.1 Sample preparation

Fig. 6.9. Disk-shaped samples of undoped (white) and Cu-doped (bluish) glasses, obtaining by slicing glass rods.

To perform antibacterial tests, we needed some small samples of glass with and without antibacterial ions. We started to perform these trials by using a glass slab, like the ones shown in Fig. 6.4. To perform the tests, we cut the slab into small parallelepipeds with an approximate edge of 5 mm. Afterwards, this shape resulted to be difficult to manage and the procedure to obtain the sample is also laborious. Furthermore, the dimensions were slightly different from sample to sample, and this could alter the results of the tests.

For this reason, we moved to a different sample shape: we cast the glasses into a rod mould with a diameter of 8 mm. The glass rods were then cut into slices with a thickness of 1 mm. The procedure for cutting the rod is simple since the rod is mounted on the cutting machine and the slices are cut in sequence with a micrometre screw moving system. This allowed producing several glass disks, all featuring the same thickness (± 0.1 mm), shown in Fig. 6.9.

After the shipment, the glass samples resulted to have some sort of dust or filth on the surface, as can be visible by the spots in the autofluorescence tests performed on the glass surface (see Fig. 6.10). This image resulted from the investigation with a Confocal Laser Scanning Microscopy (model Leica TCS SP8 DLS – Wetzlar, Germany). The presence of the fluorescent spots highlighted the necessity of a sterilisation step.

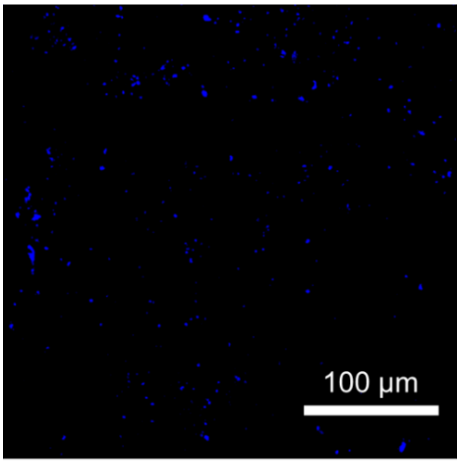

Fig. 6.10. Autofluorescence of the glass samples. Almost the same spots were visible for different samples also in green and red channels. The spots are attributed to filth on the glass surface.

A standard cleaning procedure was adopted to sterilise the glass samples before each experiment. This procedure consisted of the following steps: *(i)* the samples were wiped with a double-distilled water (ddH$_2$O) solution containing 10% sodium dodecyl sulfate (SDS), *(ii)* abundantly rinsed with MilliQ water, and *(iii)* sterilised for 3 h at 180 °C. After the sterilisation process, the spots were no longer present in the fluorescence measurement.

An interesting aspect was detected using Energy Dispersive X-ray Spectroscopy (EDS) (Oxford Scientific, OXFORD INCA Energy 350 X-Max 50, Oxford, United Kingdom) associated with Scanning Electron Microscopy (SEM) (Zeiss, EVO MA10-HR “dual gun”, Oberkochen, Germany). Maps of the distribution of P and Cu on the surface of the samples have been acquired and are reported in Fig. 6.11. The pictures demonstrate the homogeneous distribution of the different elements on the surface of Cu-doped and undoped glasses.

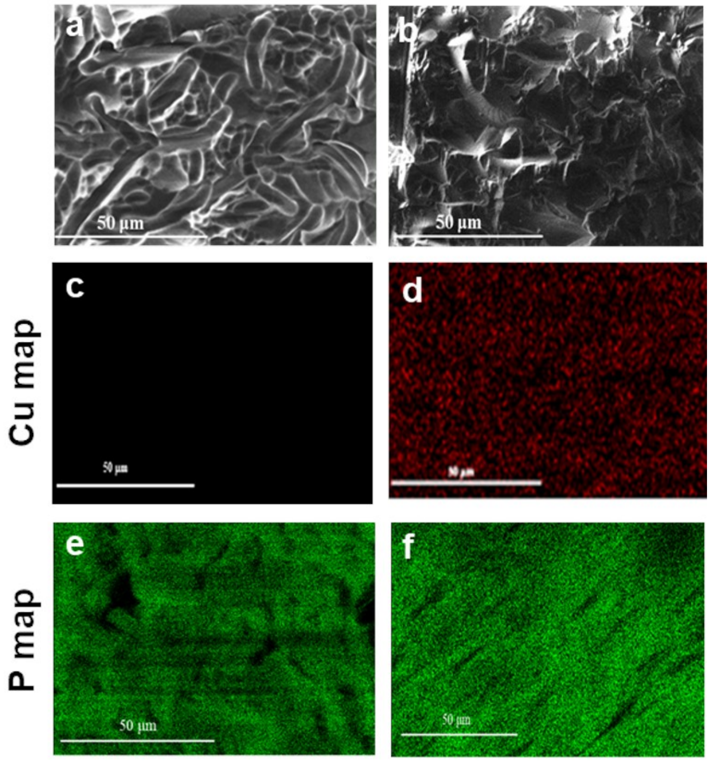

Fig. 6.11. Pictures and SEM-EDS images of undoped (a, c, e) and Cu-doped CPG (b, d, f) samples. (a) and (b) are SEM images obtained through EDS analysis (20kV, 1000X magnification); (c) and (d) are maps of Cu while (e) and (f) are maps of P on the surface of undoped and Cu-doped glasses, respectively. All the scale bars are equal to 50µm.

6.4.2 Interaction between bacteria and bulk glass

The direct interaction between bacteria and glass samples was tested by the evaluation of bacterial viability using the quantitative *MTT assay*. This colourimetric test has been firstly described by Mosmann [61] to assess cellular growth and survival. After a few years, it has also been demonstrated for the in vitro evaluation of cell/biomaterial interaction [62]. Nowadays it has become a standard colourimetric assay for measuring cellular proliferation. The MTT assay takes advantage of a tetrazolium salt, (3-(4,5-dimethylthiazol-2-yl)-2,5-diphenyltetrazolium bromide), or MTT, which is reduced to an insoluble formazan by the mitochondria of living cells. The latter salt has a strong purple colouration. The colour determination allows determining the number of living cells in a cell culture or, in our case, a bacterial culture.

Different bacterial strains were selected to perform the antimicrobial tests of our glasses. Details about the employed bacteria and the related culture medium are given in Table 6.4. Each bacterial strain was grown in its culture medium overnight under aerobic conditions at 37 °C using a shaker incubator. Then, the bacterial cultures were reduced to the final densities of either 10^5 cells/mL or 10^2 cells/mL.

Table 6.4. The bacteria employed for the present study, with an indication of the culture medium employed for bacterial growth before testing.

Bacterium name	**Code**	**Culture medium**
Escherichia coli	ATCC 25922	Luria Bertani broth
Staphylococcus Aureus	ATCC 25923	Brain Heart Infusion
Pseudomonas aeruginosa	PAO1	Mueller Hinton broth
Klebsiella pneumoniae	Clinical isolate	Mueller Hinton broth

The MTT assay was then performed using 5 mg/mL of MTT solution dissolved in PBS as a stock solution. The final working concentration was 0.5 mg/mL. The test was performed at 37 °C for 3 h avoiding light exposure. Then, the MTT reaction was stopped by adding an equal volume of acidified 2-propanol (2-propanol, HCl 0.04 N) and incubated for other 15 minutes. Upon the presence of viable cells, the reduction of the MTT salt results in purple insoluble formazan granules that are dissolved in acidified 2-propanol. Bacterial plates were read using a CLARIOstar (BMG Labtech, Germany). Results were normalised to tissue culture plate (TCP) set as 100%. The experiments were performed in duplicates three times.

The results of the MTT assay are compared also with another quantitative test that monitors the viability of bacterial populations as a function of the membrane integrity of the cells. This test allows detecting the different fluorescence of dead and viable cells. The measurement required the following steps. A portion of bacterial suspensions (200 μL of the 10^5 cells/mL culture) was inoculated for 24 h at 37 °C. Then, suspensions were gently removed, and the viability of adherent cells was estimated with the BacLight Live/Dead viability kit (Molecular Probes, Eugene, OR, United States). The kit includes two fluorescent nucleic acid stains: SYTO 9 and propidium iodide. The former penetrates both viable and non-viable cells, while propidium iodide penetrates only cells with damaged membranes and quenches SYTO 9 fluorescence. Dead cells, which take up propidium iodide, fluoresce red, while viable cells fluoresce green. For assessing viability, 1 μL of the stock solution of each stain was added to 3 mL of PBS and, after being mixed, 200 μL of the solution was dispensed into 48-well microplates containing the glass samples and incubated at room temperature for 10 minutes in the dark. Cells on the surface were then observed under the confocal microscope. For each sample, images from three randomly selected positions were acquired by using an oil immersion objective.

Furthermore, SEM analysis of the surface of the glasses was performed to visualise the bacterial adhesion and the surface quality of the samples. These analyses are conducted after incubation of 10^5 cells/mL bacterial culture on the glass samples for 24 h at 37 °C. Then, the samples were washed carefully with PBS and fixed with 2.5% (v/v) glutaraldehyde in 0.1 M Na-cacodylate buffer (pH 7.2), for 1 h at 4 °C. After two washes with Na-cacodylate to remove the excess of glutaraldehyde, Gram-positive and Gram-negative bacteria were treated in different ways: *S. aureus* samples were dehydrated using increasing concentrations of ethanol (25, 50, 75%) for 5 min and two washes of 96% ethanol for 10 min. On the other hand, Gram-negative samples were only dehydrated with two washes of 96% ethanol for 10 min. Subsequently, the samples were lyophilised for 3 h using an Emitech (Ashford, UK) K-850 apparatus and placed on a mounting base. Finally, the samples were sputter-coated with gold and investigated using a Zeiss EVO-MA10 SEM (Carl Zeiss, Oberkochen, Germany), with 20 kV acceleration voltage.

6.4.3 Interaction between bacteria and dissolved glass

The direct contact tests just described allowed only to assess the antibiofouling effect, i.e. the capability of the glasses to prevent or inhibit the growth of a living bacterial biofilm on the surface. Yet, we were also interested in investigating the effect on the bacteria of the solution in which the glass has been dissolved. Thus, we performed also *indirect contact* tests to determine the antibacterial effect of the dissolution product of Cu-doped bioresorbable glasses. Luria Bertani broth and ddH2O were inoculated separately onto the glass samples contained in a 48-well plate, for 24 h at 37 °C. Serial dilutions of the solutions were performed in a 96-well plate starting from a volume of 100 μL of solution. Then, 100 μL of 10^2 cells/mL bacterial culture were inoculated overnight, at 37 °C. Finally, after incubation with MTT solution, performed as already described, the reaction was stopped, and the plates were read using a microplate reader.

The results of the indirect contact tests are expected to be less effective than the direct contact ones. As described in [57] the interaction of bacteria with the surface of a biomaterial may induce the direct death of the microorganism because of a physical rupture of the external cell membrane. On the contrary, the ions present in a solution may interact with the cells in different ways, affect their metabolism, and eventually lead to cell death as a secondary effect. With the employed antibacterial-ions concentration, most of the bacteria may be able to survive in these latter conditions.

6.4.4 Bacteria viability

The results of the preliminary tests are reported in Fig. 6.12, for each bacterial species. An average value of the two bacterial strains concentrations is reported.

The direct contact tests highlight a different effect of Cu-doped glasses on *S. Aureus*, i.e. the only Gram-positive bacterium tested, and all the other Gram-negative bacteria.

The Gram-positive *S. Aureus* seems almost insensible to the presence of Cu in the glass, while *E. Coli*, *P. Aeruginosa*, and *K. Pneumoniae* all show a marked viability reduction when put into contact with the Cu-doped glasses.

All the data are obtained using TCP as control. This behaviour is not fully confirmed by the existing literature. In the extensive literature available about the antibacterial action of copper, both Gram-positive and Gram-negative bacteria seems to be affected by the presence of Cu. Further investigations are needed to find a proper explanation for this behaviour.

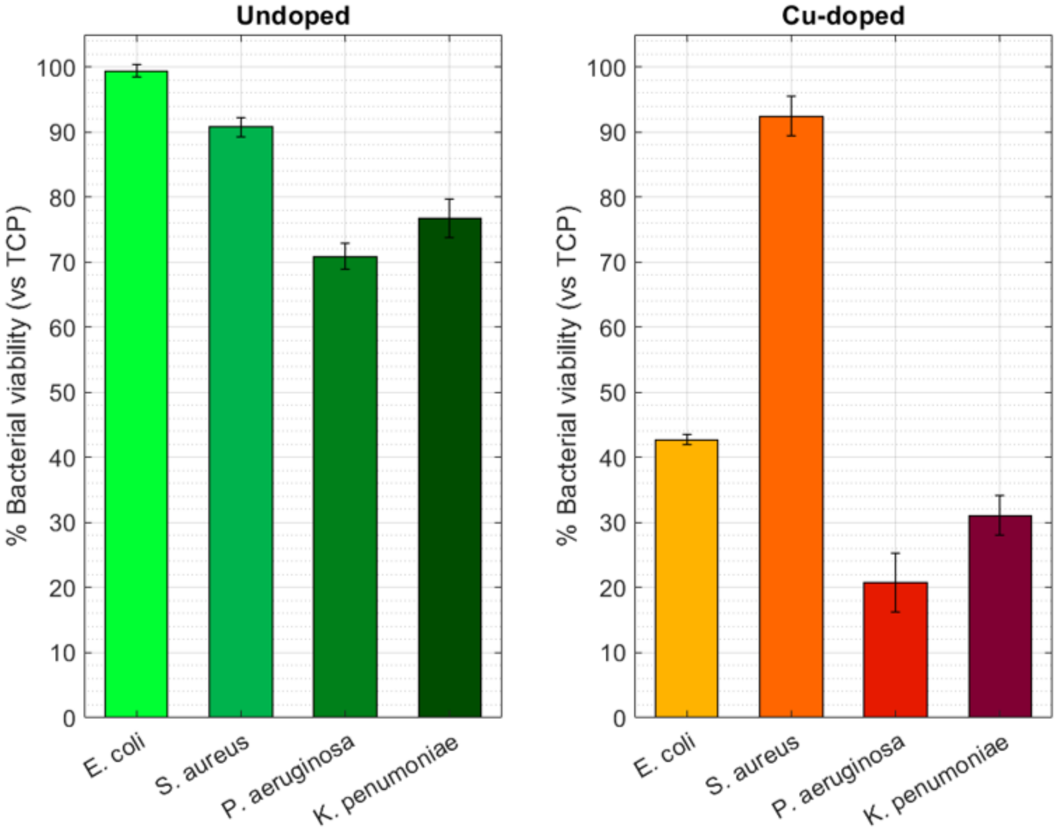

Fig. 6.12. Percentage of bacterial viability after 24 h incubation with undoped (left) and Cu-doped (right) samples; TCP (tissue culture plate) used as a positive control.

The fluorescence images acquired for the BacLight Live/Dead viability test are shown in Fig. 6.13. The inspection of these images confirms the results of the MTT assays, highlighting both the high viability of *S. Aureus* and the strong antibacterial effect against *E. Coli*, *P. Aeruginosa*, and *K. Pneumoniae* in the presence of Cu-doped glasses.

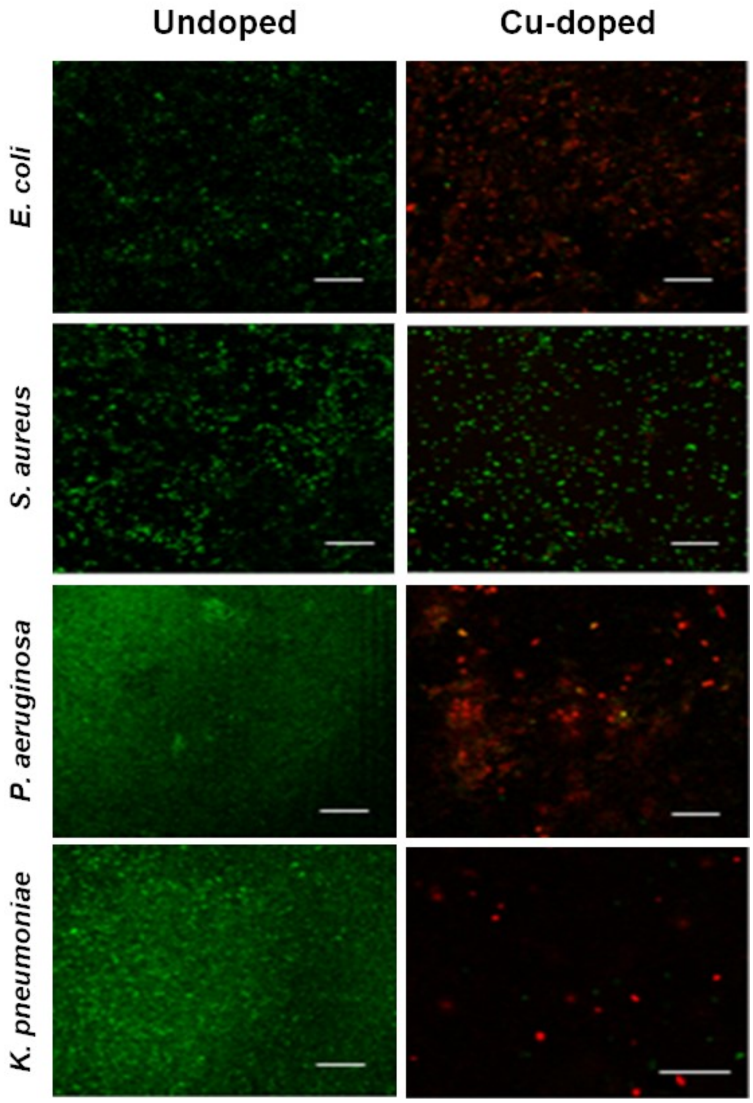

Fig. 6.13. BacLight staining kit. Live bacteria show green fluorescence because are stained with SYTO 9 dye, whereas dead ones are red because of propidium iodide. The scale bars are equal to 10 µm.

Regarding the SEM analyses, reported in Fig. 6.14, it was difficult to see any difference between the Cu-doped and undoped glasses since, upon dissolution, the glass surface resulted to be full of cracks. Further investigation, performed after different dissolution times, may be needed to compare this behaviour to the values of the release rate of Cu reported in Fig. 6.8.

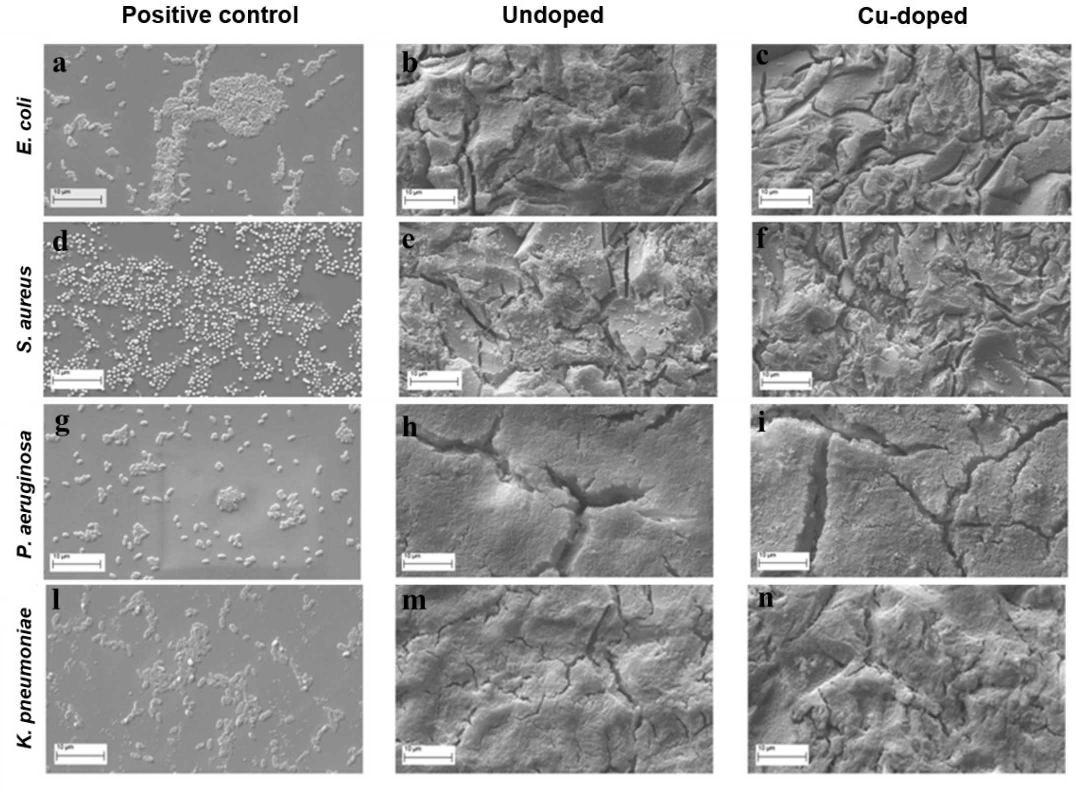

Fig. 6.14. SEM images showing Bacterial adhesion on undoped (b, e, h, m) and Cu-doped (c, f, i, n) compared to positive controls (a, d, g, l). 5kX magnification, 10 µm scale bar.

As expected, indirect contact tests did not show any effect in terms of variation of the bacterial viability. As Fig. 6.15 highlights, no particular response can be detected on the bacterial viability for any of the studied bacterial species upon inoculation of the solution containing ions dissolved by the glass samples.

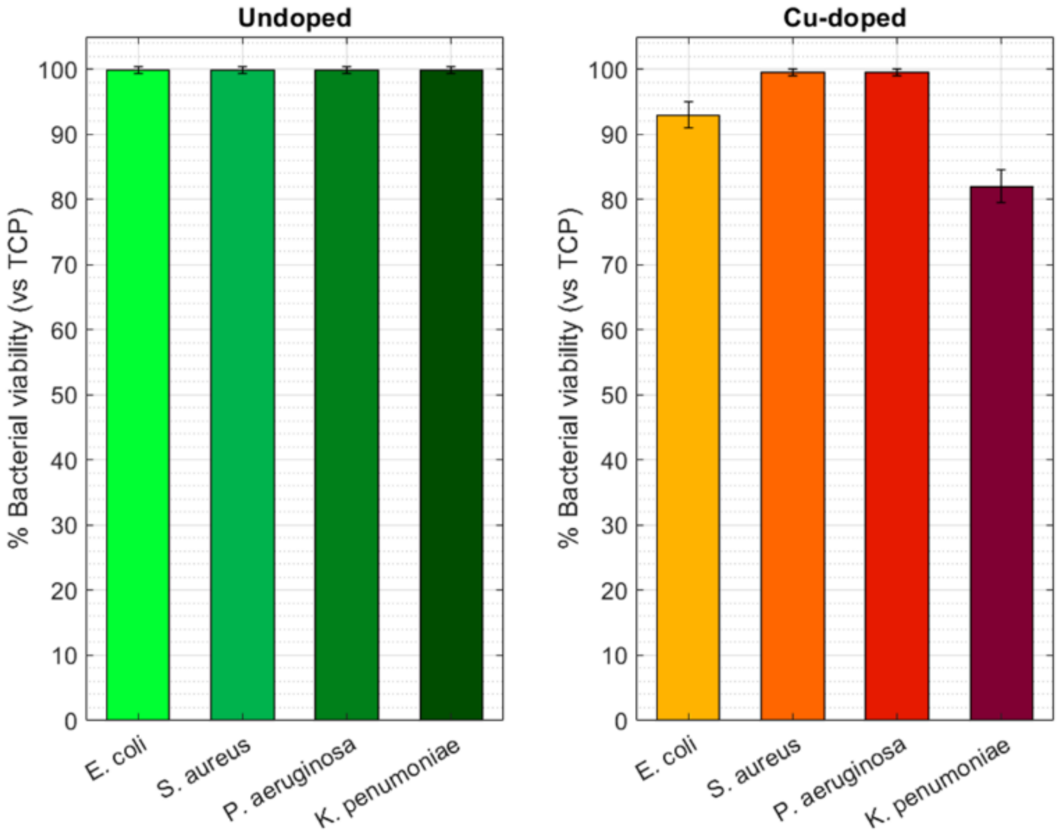

Fig. 6.15. Percentage of bacterial viability at 10^2 concentration, after 24 h of incubation of the undoped (left) and Cu-doped (right) samples with ddH2O; TCP (tissue culture plate) used as a positive control.

6.4.5 Cytotoxicity

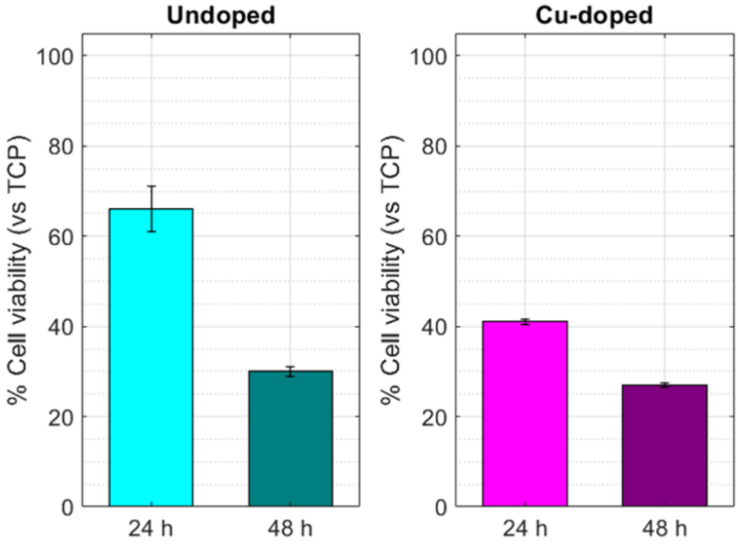

Fig. 6.16. Percentage of the viability of 3T3 cells at 24 h and 48 h on undoped and Cu-doped glasses; TCP set as 100%.

Finally, cytotoxicity assays must also be conducted to determine the interaction of the glasses with different cells. Preliminary tests have been performed through direct and indirect contact. NIH-3T3 cell line from ATCC was tested. This is a cell-line commonly used in microbiology derived from mice embryo fibroblast cells. The cells were cultured in Dulbecco's modified Eagle's medium (DMEM) with 4.5 g L^{-1} glucose, supplemented with 10% Bovine Calf Serum and 1% p/v L-glutamine. The cell line was incubated at 37 °C with 5% CO_2, routinely trypsinised after confluence, then counted, and seeded into wells on the phosphate glass samples. After 24 h and 48 h, the culture medium was replaced by MTT solution and incubated for 3 h, at 37 °C, 5% CO_2. The reactions were stopped with acidified 2-propanol and the absorbance was measured with a microplate reader (Bio-Rad Laboratories, Hercules, CA). As visible in Fig. 6.16, the cellular adhesion was reduced for both undoped and Cu-doped glasses compared with tissue culture plate (TCP used as positive control). Indeed, after 48h the difference in cellular viability between Cu-doped and undoped glasses was negligible.

Furthermore, to visualise the cells on the surface of the samples, $5 \cdot 10^4$ cells/well were seeded on the phosphate glasses, and incubated for 48 h, at 37 °C, 5% CO_2. Then the medium was gently removed and after one washing with ddH2O the samples have been stained. Cells were observed using either 20x or 40x objectives. The resulting images are reported in Fig. 6.17.

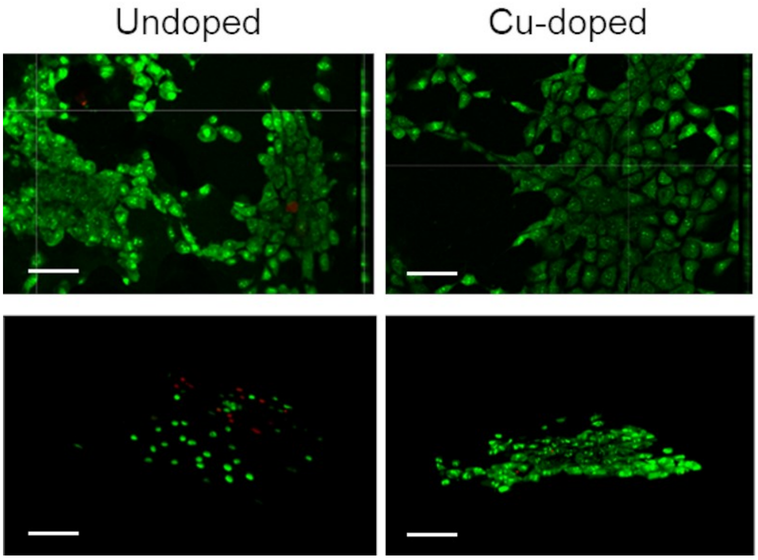

Fig. 6.17. BacLight staining kit. After 48h of incubation, live cells are green because are stained with SYTO 9 dye, whereas dead ones show red fluorescence because of propidium iodide. (a) and (b) are orthogonal projections of 3T3 cells at 40x magnification (the scale bars are equal to 10 µm);(c) and (d) are 3D projections at 20x magnification (the scale bars are equal to 100 µm).

In indirect contact, DMEM medium (without bovine calf serum) was incubated at 37 °C with 5% CO_2 on the phosphate glasses for 24 h and 48 h to see if the scaffolds released cytotoxic compounds. At the end of the incubation time, serial dilutions of inoculated solutions were performed in a 96-well plate starting from a volume of 100 µL of solution. They were then incubated with 3T3 cells. With indirect contact experiments, the cells do not seem to be affected by the presence of either the Cu-doped or undoped glasses dissolution products.

These preliminary results allow being optimistic since the tested cells show good viability both in direct and indirect contact tests. Yet, more tests must be performed, and different cells lines have to be tested to confirm the non-cytotoxic behaviour of the produced glasses.

6.5 Conclusions

While antibiotic-resistant bacteria keep evolving, the need for other solutions to limit or prevent the growth of bacteria is every day more urgent. Bacteria related infections, also developed during hospitalisation, are a well-known cause of disease. We reported on several ways to fight bacteria colonisation and we adopted one of these, i.e. doping a bioresorbable phosphate glass with antibacterial ions. In this way, a bioresorbable optical device, as the ones described in Chapter 5, can be designed to show also therapeutic properties since, while it dissolves, it can release antibacterial ions. Details about the glass manufacturing are provided and the characterisation of the first set of antibacterial-doped glasses is reported. Furthermore, thanks to a collaboration with prof. Livia Visai and her research group from Università di Pavia, we performed different antibacterial assays. The first results demonstrate the efficacy of the Cu-doped bioresorbable phosphate glasses in fighting the proliferation of Gram-negative bacteria. The antibacterial effect was indeed almost absent with Gram-positive bacteria. Also, a mice fibroblast cell line showed only a small interaction with both Cu-doped and undoped glasses.

The interesting properties of the glasses and the results of antimicrobial tests performed on Cu-doped glasses encourage further studies with the different antibacterial ions. Since the glass properties are well controlled, also the synergistic effect of different ions may be investigated. Furthermore, the variation of the antibacterial ion concentration can be also studied. The glass properties may be affected by an increasing concentration of different elements. Also, the effect against different species of bacteria may be an interesting aspect to investigate, as well as the analysis of the interaction with different cells.

References

[1] J. R. Porter, ‘Antony van Leeuwenhoek: tercentenary of his discovery of bacteria.’, *Bacteriological Reviews*, vol. 40, no. 2, pp. 260–269, Jun. 1976.

[2] S. Haensch *et al.*, ‘Distinct clones of Yersinia pestis caused the black death’, *PLoS Pathogens*, vol. 6, no. 10, 2010, doi: 10.1371/journal.ppat.1001134.

[3] *Global Tubercolosis Report 2020*. Geneva: World Health Organization, 2020.

[4] E. P. Ivanova and R. J. Crawford, *Antibacterial surfaces*. Springer International Publishing Switzerland, 2015.

[5] L. Gaetke, ‘Copper toxicity, oxidative stress, and antioxidant nutrients’, *Toxicology*, vol. 189, no. 1–2, pp. 147–163, Jul. 2003, doi: 10.1016/S0300-483X(03)00159-8.

[6] J. W. Bennett and K.-T. Chung, ‘Alexander Fleming and the discovery of penicillin’, *Advances in Applied Microbiology*, vol. 49, pp. 163–184, Jan. 2001, doi: 10.1016/S0065-2164(01)49013-7.

[7] C. F. Amabile-Cuevas, *Antibiotics and Antibiotic Resistance in the Environment*. Leiden, The Netherlands: CRC Press/Balkema, 2016.

[8] D. Pittet *et al.*, ‘Effectiveness of a hospital-wide programme to improve compliance with hand hygiene’, *The Lancet*, vol. 356, no. 9238, pp. 1307–1312, Oct. 2000, doi: 10.1016/S0140-6736(00)02814-2.

[9] J.-L. Vincent, ‘The Prevalence of Nosocomial Infection in Intensive Care Units in Europe: Results of the European Prevalence of Infection in Intensive Care (EPIC) Study’, *JAMA*, vol. 274, no. 8, p. 639, Aug. 1995, doi: 10.1001/jama.1995.03530080055041.

[10] T. G. Emori and R. P. Gaynes, ‘An overview of nosocomial infections, including the role of the microbiology laboratory.’, *Clinical Microbiology Reviews*, vol. 6, no. 4, pp. 428–442, Oct. 1993, doi: 10.1128/cmr.6.4.428.

[11] W. Bereket *et al.*, ‘Update on bacterial nosocomial infections’, *European Review for Medical and Pharmacological Sciences*, vol. 16, no. 8, pp. 1039–1044, Aug. 2012.

[12] H. Vlamakis, C. Aguilar, R. Losick, and R. Kolter, ‘Control of cell fate by the formation of an architecturally complex bacterial community’, *Genes & Development*, vol. 22, no. 7, pp. 945–953, Jan. 2008, doi: 10.1101/gad.1645008.

[13] P. S. Stewart and J. William Costerton, ‘Antibiotic resistance of bacteria in biofilms’, *The Lancet*, vol. 358, no. 9276, pp. 135–138, Jul. 2001, doi: 10.1016/S0140-6736(01)05321-1.

[14] S. Ferraris and S. Spriano, ‘Antibacterial titanium surfaces for medical implants’, *Materials Science and Engineering C*, vol. 61, pp. 965–978, 2016, doi: 10.1016/j.msec.2015.12.062.

[15] E. P. Ivanova *et al.*, ‘Natural bactericidal surfaces: Mechanical rupture of pseudomonas aeruginosa cells by cicada wings’, *Small*, vol. 8, no. 16, pp. 2489–2494, 2012, doi: 10.1002/smll.201200528.

[16] O. Akhavan and E. Ghaderi, ‘Cu and CuO nanoparticles immobilized by silica thin films as antibacterial materials and photocatalysts’, *Surface and Coatings Technology*, vol. 205, no. 1, pp. 219–223, 2010, doi: 10.1016/j.surfcoat.2010.06.036.

[17] M. Raffi *et al.*, ‘Investigations into the antibacterial behavior of copper nanoparticles against Escherichia coli’, *Annals of Microbiology*, vol. 60, no. 1, pp. 75–80, 2010, doi: 10.1007/s13213-010-0015-6.

[18] A. K. Chatterjee, R. K. Sarkar, A. P. Chattopadhyay, P. Aich, R. Chakraborty, and T. Basu, ‘A simple robust method for synthesis of metallic copper nanoparticles of high antibacterial potency against E. coli’, *Nanotechnology*, vol. 23, no. 8, 2012, doi: 10.1088/0957-4484/23/8/085103.

[19] A. P. Ingle, N. Duran, and M. Rai, ‘Bioactivity, mechanism of action, and cytotoxicity of copper-based nanoparticles: A review’, *Applied Microbiology and Biotechnology*, vol. 98, no. 3, pp. 1001–1009, 2014, doi: 10.1007/s00253-013-5422-8.

[20] N. R. Dhineshbabu, V. Rajendran, N. Nithyavathy, and R. Vetumperumal, ‘Study of structural and optical properties of cupric oxide nanoparticles’, *Applied Nanoscience*, vol. 6, no. 6, pp. 933–939, 2016, doi: 10.1007/s13204-015-0499-2.

[21] K. Chaloupka, Y. Malam, and A. M. Seifalian, ‘Nanosilver as a new generation of nanoproduct in biomedical applications’, *Trends in Biotechnology*, vol. 28, no. 11, pp. 580–588, 2010, doi: 10.1016/j.tibtech.2010.07.006.

[22] L. Wang, C. Hu, and L. Shao, ‘The antimicrobial activity of nanoparticles: Present situation and prospects for the future’, *International Journal of Nanomedicine*, vol. 12, pp. 1227–1249, 2017, doi: 10.2147/IJN.S121956.

[23] S. M. Amininezhad, A. Rezvani, M. Amouheidari, S. M. Amininejad, and S. Rakhshani, 'The Antibacterial Activity of SnO2 Nanoparticles against Escherichia coli and Staphylococcus aureus', *Zahedan Journal of Research in Medical Sciences*, vol. 17, no. 9, 2015, doi: 10.17795/zjrms-1053.

[24] S. Rehman *et al.*, 'Biocompatible Tin Oxide Nanoparticles: Synthesis, Antibacterial, Anticandidal and Cytotoxic Activities', *ChemistrySelect*, vol. 4, no. 14, pp. 4013–4017, 2019, doi: 10.1002/slct.201803550.

[25] M. Akram and R. Hussain, 'Antibacterial Properties of Bioactive Glasses', in *Clinical Applications of Biomaterials: State-of-the-Art Progress, Trends, and Novel Approaches*, Springer International Publishing AG, 2017, pp. 357–382.

[26] P. Naresh, N. Narsimlu, C. Srinivas, M. Shareefuddin, and K. Siva Kumar, 'Ag2O doped bioactive glasses: An investigation on the antibacterial, optical, structural and impedance studies', *Journal of Non-Crystalline Solids*, vol. 549, no. May, 2020, doi: 10.1016/j.jnoncrysol.2020.120361.

[27] D. Zhang *et al.*, 'Antibacterial effects and dissolution behavior of six bioactive glasses', *Journal of Biomedical Materials Research - Part A*, vol. 93, no. 2, pp. 475–483, 2010, doi: 10.1002/jbm.a.32564.

[28] A. \Lapa *et al.*, 'Gallium- and Cerium-Doped Phosphate Glasses with Antibacterial Properties for Medical Applications', *Advanced Engineering Materials*, vol. 22, no. 9, 2020, doi: 10.1002/adem.201901577.

[29] B. A. Kyffin *et al.*, 'Antibacterial silver-doped phosphate-based glasses prepared by coacervation', *Journal of Materials Chemistry B*, vol. 7, no. 48, pp. 7744–7755, 2019, doi: 10.1039/c9tb02195g.

[30] C. Wu *et al.*, 'Copper-containing mesoporous bioactive glass scaffolds with multifunctional properties of angiogenesis capacity, osteostimulation and antibacterial activity', *Biomaterials*, vol. 34, no. 2, pp. 422–433, 2013, doi: 10.1016/j.biomaterials.2012.09.066.

[31] F. Foroutan *et al.*, 'Antibacterial Copper-Doped Calcium Phosphate Glasses for Bone Tissue Regeneration', *ACS Biomaterials Science and Engineering*, vol. 5, no. 11, pp. 6054–6062, 2019, doi: 10.1021/acsbiomaterials.9b01291.

[32] A. Moghanian *et al.*, 'Novel antibacterial Cu/Mg-substituted 58S-bioglass: Synthesis, characterization and investigation of in vitro bioactivity', *International Journal of Applied Glass Science*, vol. 11, no. 4, pp. 685–698, 2020, doi: 10.1111/ijag.14510.

[33] A. Moghanian, M. Zohourfazeli, and M. H. M. Tajer, 'The effect of zirconium content on in vitro bioactivity, biological behavior and antibacterial activity of sol-gel derived 58S bioactive glass', *Journal of Non-Crystalline Solids*, vol. 546, no. June, p. 120262, 2020, doi: 10.1016/j.jnoncrysol.2020.120262.

[34] E. Vernè *et al.*, 'Surface characterization of silver-doped bioactive glass', *Biomaterials*, vol. 26, no. 25, pp. 5111–5119, 2005, doi: 10.1016/j.biomaterials.2005.01.038.

[35] L. L. Hench, 'The story of Bioglass®', *Journal of Materials Science: Materials in Medicine*, vol. 17, no. 11, pp. 967–978, 2006, doi: 10.1007/s10856-006-0432-z.

[36] S. Hu, J. Chang, M. Liu, and C. Ning, 'Study on antibacterial effect of 45S5 Bioglass®', *Journal of Materials Science: Materials in Medicine*, vol. 20, no. 1, pp. 281–286, 2009, doi: 10.1007/s10856-008-3564-5.

[37] Z. P. Xie, C. G. Zhang, C. G. Yi, J. J. Qiu, J. G. Wang, and J. Zhou, 'Failure of particulate bioglass to prevent experimental staphylococcal infection of open tibial fractures', *Journal of Antimicrobial Chemotherapy*, vol. 62, no. 5, pp. 1162–1163, 2008, doi: 10.1093/jac/dkn336.

[38] Z. P. Xie, C. Q. Zhang, C. Q. Yi, J. J. Qiu, J. Q. Wang, and J. Zhou, 'In vivo study effect of particulate Bioglass® in the prevention of infection in open fracture fixation', *Journal of Biomedical Materials Research - Part B Applied Biomaterials*, vol. 90, no. 1, pp. 195–201, 2009, doi: 10.1002/jbm.b.31273.

[39] S. Begum, W. E. Johnson, T. Worthington, and R. A. Martin, 'The influence of pH and fluid dynamics on the antibacterial efficacy of 45S5 Bioglass', *Biomedical Materials*, vol. 11, no. 1, 2016, doi: 10.1088/1748-6041/11/1/015006.

[40] C. Heras, J. Jiménez-Holguín, A. L. Doadrio, M. Vallet-Regí, S. Sánchez-Salcedo, and A. J. Salinas, 'Multifunctional antibiotic- and zinc-containing mesoporous bioactive glass scaffolds to fight bone infection', *Acta Biomaterialia*, vol. 114, pp. 395–406, 2020, doi: 10.1016/j.actbio.2020.07.044.

[41] M. Bellantone, N. J. Coleman, and L. L. Hench, 'Bacteriostatic action of a novel four-component bioactive glass', *Journal of Biomedical Materials Research*, vol. 51, no. 3, pp. 484–490, 2000, doi: 10.1002/1097-4636(20000905)51:3<484::AID-JBM24>3.0.CO;2-4.

[42] C. Curless, J. Baclaski, and R. Sachdev, 'Phosphate glass as a phosphate source in high cell density Escherichia coli fermentations', *Biotechnology Progress*, vol. 12, no. 1, pp. 22–25, 1996, doi: 10.1021/bp9500369.

[43] A. G. Avent, C. N. Carpenter, J. D. Smith, D. M. Healy, and T. Gilchrist, 'The dissolution of silver-sodium-calcium-phosphate glasses for the control of urinary tract infections', *Journal of Non-Crystalline Solids*, vol. 328, no. 1–3, pp. 31–39, 2003, doi: 10.1016/S0022-3093(03)00476-9.

[44] A. M. Mulligan, M. Wilson, and J. C. Knowles, 'Effect of increasing silver content in phosphate-based glasses on biofilms of Streptococcus sanguis', *Journal of Biomedical Materials Research - Part A*, vol. 67, no. 2, pp. 401–412, 2003, doi: 10.1002/jbm.a.10052.

[45] I. Ahmed, D. Ready, M. Wilson, and J. C. Knowles, 'Antimicrobial effect of silver-doped phosphate-based glasses', *Journal of Biomedical Materials Research Part A*, vol. 79A, no. 3, pp. 618–626, 2006, doi: 10.1002/jbm.a.30808.

[46] S. P. Valappil *et al.*, 'Effect of silver content on the structure and antibacterial activity of silver-doped phosphate-based glasses', *Antimicrobial Agents and Chemotherapy*, vol. 51, no. 12, pp. 4453–4461, 2007, doi: 10.1128/AAC.00605-07.

[47] A. A. Ahmed, A. A. Ali, D. A. R. Mahmoud, and A. M. El-Fiqi, ‘Study on the preparation and properties of silver-doped phosphate antibacterial glasses (Part I)’, *Solid State Sciences*, vol. 13, no. 5, pp. 981–992, 2011, doi: 10.1016/j.solidstatesciences.2011.02.004.

[48] A. Mishra, J. Rocherulle, and J. Massera, ‘Ag-doped phosphate bioactive glasses: Thermal, structural and in-vitro dissolution properties’, *Biomedical Glasses*, vol. 2, no. 1, pp. 38–48, 2016, doi: 10.1515/bglass-2016-0005.

[49] M. S. Abdel-Gayed, Y. H. Elbashar, M. H. Barakat, and M. R. Shehata, ‘Optical spectroscopic investigations on silver doped sodium phosphate glass’, *Optical and Quantum Electronics*, vol. 49, no. 9, pp. 1–12, 2017, doi: 10.1007/s11082-017-1132-2.

[50] S. Lee, T. Nakano, and T. Kasuga, ‘Structure, dissolution behavior, cytocompatibility, and antibacterial activity of silver-containing calcium phosphate invert glasses’, *Journal of Biomedical Materials Research - Part A*, vol. 105, no. 11, pp. 3127–3135, 2017, doi: 10.1002/jbm.a.36173.

[51] T. K. Pathak, B. Viljoen, H. C. Swart, and R. E. Kroon, ‘Luminescence and biological properties of Ag doped Dy:(ZnO–Li2O–Na2O–P2O5) glass’, *Advances in Applied Ceramics*, vol. 119, no. 3, pp. 144–149, 2020, doi: 10.1080/17436753.2019.1707392.

[52] a Mulligan, ‘The effect of increasing copper content in phosphate-based glasses on biofilms of Streptococcus sanguis’, *Biomaterials*, vol. 24, no. 10, pp. 1797–1807, 2003, doi: 10.1016/S0142-9612(02)00577-X.

[53] E. A. Abou Neel, I. Ahmed, J. Pratten, S. N. Nazhat, and J. C. Knowles, ‘Characterisation of antibacterial copper releasing degradable phosphate glass fibres’, *Biomaterials*, vol. 26, no. 15, pp. 2247–2254, 2005, doi: 10.1016/j.biomaterials.2004.07.024.

[54] D. M. Pickup *et al.*, ‘X-ray absorption spectroscopy and high-energy XRD study of the local environment of copper in antibacterial copper-releasing degradable phosphate glasses’, *Journal of Non-Crystalline Solids*, vol. 352, no. 28–29, pp. 3080–3087, 2006, doi: 10.1016/j.jnoncrysol.2006.02.094.

[55] J. A. Jiménez and M. Sendova, ‘Nanodiamond-induced UV transparency in phosphate glasses and development of plasmonic Cu nanocomposites’, *Journal of Non-Crystalline Solids*, vol. 544, no. April, p. 120193, 2020, doi: 10.1016/j.jnoncrysol.2020.120193.

[56] M. M. Babu *et al.*, ‘Titanium incorporated Zinc-Phosphate bioactive glasses for bone tissue repair and regeneration: Impact of Ti4+on physico-mechanical and in vitro bioactivity’, *Ceramics International*, vol. 45, no. 17, pp. 23715–23727, 2019, doi: 10.1016/j.ceramint.2019.08.087.

[57] F. N. S. Raja *et al.*, ‘The Antimicrobial Efficacy of Hypoxia Mimicking Cobalt Oxide Doped Phosphate-Based Glasses against Clinically Relevant Gram Positive, Gram Negative Bacteria and a Fungal Strain’, *ACS Biomaterials Science and Engineering*, vol. 5, no. 1, pp. 283–293, 2019, doi: 10.1021/acsbiomaterials.8b01045.

[58] A. \Lapa *et al.*, ‘Ga and Ce ion-doped phosphate glass fibres with antibacterial properties and their composite for wound healing applications’, *Journal of Materials Chemistry B*, vol. 7, no. 44, pp. 6981–6993, 2019, doi: 10.1039/c9tb00820a.

[59] A. \Lapa, M. Cresswell, P. Jackson, and A. R. Boccaccini, ‘Phosphate glass fibres with therapeutic ions release capability–a review’, *Advances in Applied Ceramics*, vol. 119, no. 1, pp. 1–14, 2020, doi: 10.1080/17436753.2018.1564413.

[60] E. Ceci-Ginistrelli *et al.*, ‘Novel Biocompatible and Resorbable UV-Transparent Phosphate Glass Based Optical Fiber’, *Optical Materials Express*, vol. 6, no. 6, pp. 2040–2051, 2016, doi: 10.1364/OME.6.002040.

[61] T. Mosmann, ‘Rapid colorimetric assay for cellular growth and survival: Application to proliferation and cytotoxicity assays’, *Journal of Immunological Methods*, vol. 65, no. 1–2, pp. 55–63, Dec. 1983, doi: 10.1016/0022-1759(83)90303-4.

[62] G. Ciapetti, E. Cenni, L. Pratelli, and A. Pizzoferrato, ‘In vitro evaluation of cell/biomaterial interaction by MTT assay’, *Biomaterials*, vol. 14, no. 5, pp. 359–364, Apr. 1993, doi: 10.1016/0142-9612(93)90055-7.

Chapter 7.

Conclusions

7.1 Main contributions and achievements

Two enabling technologies have been addressed throughout the present work: the synthesis of phosphate glasses and the extrusion technique employed to reshape these glasses into preforms for the production of optical fibres. Results in different fields are reported such as laser light generation and amplification, multifunctional biomedical fibres, and antibacterial materials.

Phosphate glasses have proved to be excellent candidates as either host for active ions or bioresorbable optically transparent materials used for light/drug delivery as well as biochemical sensing; also, these latter bioresorbable glass compositions may be further engineered by embedding therapeutic agents directly into the glass matrix, thus using transparent glass as a carrier for antimicrobial ions. The successful synthesis and processing of all these compositions is a demonstration of the tailorability of phosphate glasses. A fine control on the glass synthesis is needed since small variations in the glass composition can lead to substantial differences in the properties of the material. Despite these differences, the processing of the various glass compositions is carried out in similar ways. Indeed, the results reported within the present work may be directly adapted to other applications, as we demonstrate in the case of antibacterial bioresorbable glasses.

Furthermore, the extrusion technique has shown to be a powerful tool for reshaping the soft phosphate glasses into different kinds of preforms. In comparison with other preform production methods, extrusion offers enhanced flexibility since it can be adapted to the most diverse preform shapes. In the glass field, the potential impacts of this process have not been fully explored yet. We have demonstrated one of the most powerful aspects of the extrusion technique, i.e. the possibility of producing non-symmetrical preforms. Indeed, this aspect opens new scenarios for the research in applied biomedicine as well as in other technological sectors such as biochemical sensing. The multifunctionality of complex devices, such as the ones proposed within the present work, is a powerful concept that may promote the development of brand-new applications. In the case of these multifunctional preforms, the extrusion die design can be very complex. Thus, we gave special attention to the design of different dies, during all the current thesis. For highly-complex and non-symmetrical preforms, the distortions may play a substantial role. For this reason, we also developed a Computational Fluid Dynamic (CFD) tool to be able to predict the glass distortions by observing the glass flow inside the die. Some of the distortions that can arise in the case of complex non-symmetric preforms are related to the non-homogeneous distribution of the glass flow inside the die. We successfully built a simple and robust CFD model to account for the glass flow distribution within the extrusion die. The interpretation of the results of the CFD simulations allows predicting some of the distortions that may affect the preform. With this tool, the process of designing, producing, and testing the extrusion die may be more effective. This is one of the main outcomes of the present work since it allows a great advancement in the extrusion die design. As described in Chapter 5, this tool allowed optimising the double-channel extrusion die, thus obtaining a non-symmetrical extruded glass preform featuring reduced distortions. Indeed, the proposed tool, which may be easily adapted to different designs, can guide the choice of the designer towards the best solution for the production of the die. The whole prototyping process is reduced to the realisation of a computer-aided 3D model of the die followed by the simulation of its behaviour using dedicated CFD software. This is a great improvement for the design of the die and allows to dramatically reduce the time and energy consumptions otherwise required for the die optimisation. In the case of the presented device, the results of the simulations have demonstrated to be reliable, since the shapes of the double-channel extruded preforms are in good agreement with the simulation results.

By combining the potentialities of phosphate glasses with the flexibility of the extrusion process we achieved interesting results, and the bright performances demonstrated by the devices produced within the present work may become a stimulus for further research in this field. By summarising the whole work carried out during the present PhD, we may identify three main achievements:

(i) the design and realisation of a compact fibre laser;
(ii) the design and production of multifunctional bioresorbable fibres;
(iii) the synthesis and characterisation of drawable antibacterial bioresorbable optical glasses.

In the case of active fibre production, the choice of phosphate glasses has already demonstrated its advantages and fibre lasers made with phosphate glasses are already employed in several industrial applications. Nevertheless, we addressed some specific aspects that are at the forefront of research, the most important of which is a systematic procedure to obtain a single-mode fibre by preform extrusion. Indeed, this technique supported by the proposed tools (e.g. CFD analysis among the others) to predict the distortions of the extrudate is a fast and reliable way of obtaining custom preforms with a high level of flexibility in terms of possible preform dimensions. Thus, we demonstrated herein that extrusion is a promising alternative, compared to other hollow-preform production techniques. Together with the Interdepartmental Centre PhotoNext of Politecnico di Torino and LINSK Foundation, and thanks to the collaboration with other research institutions such as the Laser Zentrum of Hannover e.V. (LZH), the Tampere University of Technology (TUT), the Ben-Gurion University of the Negev (BGU), and the United States Army Research Laboratory (U.S.ARL), we successfully produced different single-mode fibres. Part of these works has also been supported by the NATO – *Science for Peace and Security Programme*. Some results of the characterisation of these fibres, together with the achievement of a high-power amplification (maximum peak power 8.25 kW with 0.7 ns pulse duration and 40 kHz repetition rate) within a small device (14 cm of active fibre), have been reported in a publication appeared in September 2020 on *Optics Letters* entitled "Characterization of sub-nanosecond pulsed laser amplification with Er:Yb co-doped phosphate glass fibers" [1].

The second achievement leverages a developed bioresorbable glass composition along with extrusion to obtain multifunctional bioresorbable microstructured fibres. We successfully demonstrated the possibility of producing two different kinds of preforms for microstructured fibres production: a double-channel preform and a solid-core photonic crystal fibre (SC-PCF) preform. The former may be employed for a multifunctional device, i.e. a fibre for simultaneous light and drug delivery. The latter fibre may be used as a multifunctional sensor since the light that travels inside the solid core of the fibre is affected by the presence of different fluids contained in the hollow cladding structure. This microstructured fibre was successfully drawn with a standard diameter of 125 μm or with other less conventional dimensions (75-200 μm). The preliminary result showed promising light-guiding properties. This part of the work has been conducted between Politecnico di Torino and LINKS Foundation, also thanks to the Interdepartmental Centre PhotoNext, and partially supported by Compagnia di S. Paolo through the Starting Grant Program. The results of the work have been published in a Special Issue of the *International Journal of Applied Glass Science* [2].

The third achievement is related to antibacterial bioresorbable glasses. The combination of antibacterial properties with bioresorbability may offer intriguing opportunities for the biomedical sector. Bioresorbable glasses are intended to dissolve in physiological conditions within a reasonable amount of time. During this time, a bacterial colony may grow on the surface of the glass and eventually affects its dissolution kinetic or, in the worst case, produce a point of origin for sepsis which is a serious issue for nosocomial infections in both developing and developed countries. The presence among the glass components of a few ions that may act as bacterial killers can help to control the biofilm formation on the surface of the implant. This is the main idea driving the addition of antibacterial ions to the bioresorbable glass composition. To determine the behaviour of the proposed glass compositions we investigated the thermophysical and optical properties of the glasses doped with different antibacterial ions: Ce^{4+}, Cu^{2+}, Ga^{3+}, Sn^{4+}, and Zn^{2+}. We demonstrated that the addition of a 1 mol% of these metal oxides slightly increased the glass transition temperature and the refractive index of the glasses. The optical transparency was mainly affected by the presence of Cu^{2+}, which presents a strong absorption in the red-infrared region. Small variations in the absorbance spectrum are visible also with the other ions. As an example, the addition of Sn^{4+} extended the transparency of the glass in the UV portion of the spectrum. After glass fabrication, ion release tests, bacterial viability, and cytotoxicity tests were performed to analyse the behaviour of the antibacterial ions. We started with Cu-doped glasses and, thanks to the collaboration with Università di Pavia, with Scuola Universitaria Superiore IUSS, Pavia, and with Istituti Clinici Scientifici Maugeri, Pavia we performed preliminary studies of bacterial adhesion, antibiofouling effect, and bactericidal action of the dissolution products of the bioresorbable phosphate glass doped with copper. The Gram-negative bacteria tested (*E. Coli*, *P. Aeruginosa* and *K. Pneumoniae*) appeared to be very sensitive to contact with Cu-doped glasses since more than 50% of bacteria died within the first 24 h of incubation. On the contrary, the Gram-positive *S. Aureus* resulted to be not affected by copper. Also, the indirect contact tests have demonstrated a reduced impact of the dissolution product of the glass against bacteria. Finally, explorative tests have been performed with a common mammalian cell-line to determine the absence of cytotoxicity of both doped and undoped glasses. Some of the results achieved with these antibacterial compositions have been presented at the 11th World Biomaterial Congress in late 2020 [3].

7.2 Outlook and perspectives

In this paragraph, we present the possible lines of work and research stemming from this thesis that, in our opinion, deserve attention and can potentially lead to scientific and technological advancements. These lines can be summarised as follows:

- *(i)* synthesis of new glass compositions and assessment of their properties and performances;
- *(ii)* optimisation/automation of the extrusion system and realisation of more complex preforms;

- *(iii)* thorough validation of the CFD models adopted and advanced die design strategies (e.g. machine learning);
- *(iv)* scaling up of the extrusion process, that must also take into account technical and economic aspects as well as the environmental impact of the extrusion process and the evaluation of possible improvements in terms of energy and material consumption.

Regarding the glass compositions, we produced and tested different mixes of reagents that provided stable glasses all featuring enhanced optical transparency and other special properties. We tested different aspects of the employed glasses and we varied the starting compositions to match the specific requirement of each project. While some of the adopted compositions have already been partially studied, the antibacterial glasses presented in Chapter 6 are novel. Several aspects can be further investigated in this regard, like the surface properties of the glass, the chemical structure, and the ion-release kinetics. Some of them are already the subject of ongoing experiments. Yet, the glass compositions can be further varied to allow for different content of antibacterial ions. A study of the variation of the properties of these bioresorbable glasses upon the addition of different quantities of antibacterial ions could lead to interesting results. One aspect that must be deeply investigated is how the dissolution behaviour may vary in the presence of different dopants. Furthermore, antibacterial tests must be performed in different situations, either with direct or indirect contact antibacterial assays. Also, the antibacterial performances of the glass should be assessed for different types of substrates, i.e. either polished bulk glass, rough bulk glass, glass powder, or fibres. Finally, the extrusion and drawing ability of these glasses may be inferred by their thermo-mechanical properties, but proper extrusion and drawing tests must be conducted.

Concerning the extrusion system, several aspects have been already addressed. Yet, further optimisation of the control unit and enhanced automation of the process would be desirable since a substantial part of the work is still deeply linked to the skills of the operator and this aspect may limit the evolution as well as the scaling up of the process. The CFD-based method that we proposed for the optimisation of the extrusion dies goes in this direction. Indeed, only a basic understanding of the physics underneath the extrusion process is needed, to be able to set up the main boundary conditions and discuss the outputs of the calculations. Moreover, close monitoring of the glass properties may also offer new potentialities. To this aim, a tool that may introduce a great improvement is an in-line viscosity measurement system, that would go at the same pace as an enhanced capability of temperature measuring and control. This may give a precise estimation of the actual behaviour of the glass inside the extrusion chamber, which is of primary interest for the success of the extrusion. In a scale-up phase scenario, further improvements may require to re-design the whole extruder allowing to deal with bigger preforms and directly extrude core-cladding as well as stacking structure. The ultimate stage of this system may be a *draw-trusion* device, in which the extrusion may be directly followed by drawing into fibre form. This improvement may allow for the reduction of the contamination of the preform and may also be effective in the reduction of time and energy consumption.

The support of analytical and computational tools used for modelling the extrusion process has proven its importance in the realisation of preforms with complex shapes. Yet, the models that we proposed may be improved in terms of: *(i)* the quality of the mesh and the computational performances, *(ii)* an extended implementation of the dependence of glass viscosity from temperature variations, that could allow deriving a more realistic behaviour of the system in the presence of any eventual temperature difference across the die; *(iii)* the introduction of the glass/air interface and the computation of the free surface shape of the extrudate. All these aspects may introduce substantial improvements, making CFD simulations closer and closer to the reality of the experiments. Moreover, another technology may be introduced in the simulation-aided design of the extrusion die, i.e. machine learning. The concept of *surrogate models* is already extensively employed in design engineering [4]. In the design of the die, surrogates or metamodels may be used as well, to reduce computational costs and apply design optimisation techniques to the extrusion die. In our case, either the overall optimisation of the glass flow or only the enhanced homogeneity of the flow at the die exit may be the variables to optimise [5]. A s*imulated annealing* algorithm (i.e. a probabilistic technique used to find an approximation of the global optimum of a function) may be used to promote the selection of the best configuration that optimise the glass flow [6]. Furthermore, a multivariable or multidisciplinary approach may be used too, considering also pressure and temperature variations [7]. All these steps may enhance the performances of the die and allow for a reduction of the preform distortions. Furthermore, testing the developed simulations with other geometries may provide more data to further confirm the robustness of the code.

The final remarks are related to a fundamental topic, i.e. the scaling up of the extrusion process. Technical considerations are needed to design a robust system able to withstand more extended heating and loading. The CFD as well as thermomechanical simulation described within the present work may be a good starting point to find optimal solutions. Even though the thesis was partially directed towards the development of standard procedures to process either the glass before or the extrudate after extrusion and also to design or even to clean and polish the extrusion dies, more complex and comprehensive methods are needed to scale up the process. In the case of a semi-continuous production of preforms, the margin of error must be minimised and the dwelling time between two productions must be reduced as much as possible. From the economic point of view, a detailed business plan of the whole process is beyond the scope of an academic study. Yet, some steps can be made at a research level, starting with a market analysis, to determine the demand for multifunctional optical fibres. Then, a comparative study between different production techniques has to be set up. Furthermore, some considerations can be made dealing both with the economic aspects and the environmental impact since nowadays there is an urgent need for giving the right attention to the environmental issue. Even in an advanced and sectorial topic like glass extrusion, one of the aims of the designer must be related to the reduction of energy consumption, which could affect both the economic and environmental costs of the process. Also, the production of waste material must be controlled and possibly avoided, as well as the production of polluting agents, either solid, liquid, or gaseous. Some of these aspects have been addressed during the present work. For example, the re-usage of the extrusion dies, which can be polished and re-employed without affecting the quality of the extrudates, is a step forward in the right direction. Also, the control and reduction of the heat dispersed by the extruder may limit energy consumption. The simulation-aided approach also allowed to dramatically reduce the consumption of materials and energy. This has favoured a lighter approach in the design of the extrusion die that lowered both the time required for the optimisation of the extrusion die and the waste of material and energy. Moreover, this method gave good results in terms of the quality of the extrusion product. Especially in the scaling-up phase, the system must be optimised by design to allow for a continuous improvement of the performances, in terms of quality of the results as well as concerning the possibility of promoting new ideas that may reduce the impact of the whole process. Preliminary research may be performed such as the Environmental Impact Assessment (EIA) of the extrusion technique in comparison with other production technique. For example, the extrusion of a tube compared to the rotational casting technique may reduce the processing temperature and the energy and material consumption related to the polishing of the preform. Yet, a proper study, e.g. a Life-Cycle Assessment (LCA), must be conducted to precisely determine the environmental impact of extrusion compared to other techniques.

References

[1] O. Moschovitz *et al.*, ‘Characterization of sub-nanosecond pulsed laser amplification with Er : Yb co-doped phosphate glass fibers’, *Optics Letters*, vol. 45, no. 18, pp. 5291–5294, 2020, doi: https://doi.org/10.1364/OL.402575.

[2] D. Gallichi-Nottiani, D. Pugliese, N. Giovanna Boetti, D. Milanese, and D. Janner, ‘Toward the fabrication of extruded microstructured bioresorbable phosphate glass optical fibers’, *International Journal of Applied Glass Science*, no. June, pp. 1–9, 2019, doi: 10.1111/ijag.14652.

[3] D. Gallichi-Nottiani *et al.*, ‘Calcium-phosphate glass-based bioresorbable fibre optics for light and drug delivery’, presented at the 11th World Biomaterial Congress, Glasgow, Dec. 2020.

[4] P. Jiang, Q. Zhou, and X. Shao, *Surrogate Model-Based Engineering Design and Optimization*. Singapore: Springer International Publishing, 2020.

[5] G. M. Uddin *et al.*, ‘Artificial intelligence-based Monte-Carlo numerical simulation of aerodynamics of tire grooves using computational fluid dynamics’, *Artificial Intelligence for Engineering Design, Analysis and Manufacturing*, vol. 33, no. 03, pp. 302–316, Aug. 2019, doi: 10.1017/S0890060419000039.

[6] L. Zimmermann, T. Chen, and K. Shea, ‘A 3D, performance-driven generative design framework: automating the link from a 3D spatial grammar interpreter to structural finite element analysis and stochastic optimization’, *Artificial Intelligence for Engineering Design, Analysis and Manufacturing*, vol. 32, no. 2, pp. 189–199, May 2018, doi: 10.1017/S0890060417000324.

[7] D. Hulse, K. Tumer, C. Hoyle, and I. Tumer, ‘Modeling multidisciplinary design with multiagent learning’, *Artificial Intelligence for Engineering Design, Analysis and Manufacturing*, vol. 33, no. 1, pp. 85–99, Feb. 2019, doi: 10.1017/S0890060418000161.